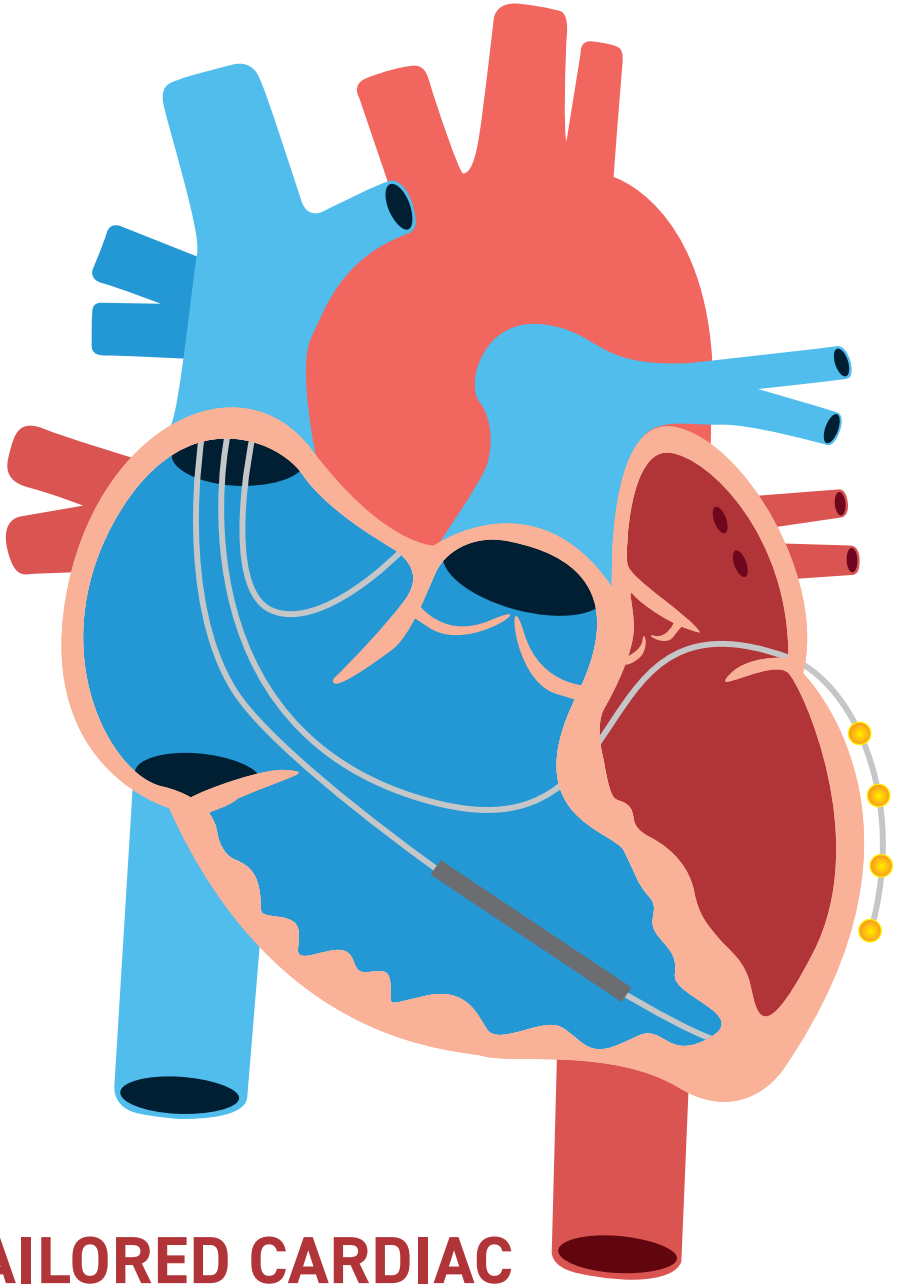


TAILORED CARDIAC RESYNCHRONIZATION THERAPY

CARDIAC IMAGING BEFORE IMPLANT AND DEVICE OPTIMIZATION AFTERWARDS

ALWIN ZWEERINK

Tailored Cardiac Resynchronization Therapy

Cardiac imaging before implant and device optimization afterwards

Alwin Zweerink

Tailored Cardiac Resynchronization Therapy - Cardiac imaging before implant and device optimization afterwards
Thesis, VU University, Amsterdam, the Netherlands

Cover design: Bregje Jaspers
Layout: Mathilde H. Verbrugge
Printing: Proefschriftmaken.nl
ISBN: 978-94-6380-761-6

Copyright © 2020 A. Zweerink

All rights reserved. No parts of this thesis may be reproduced or transmitted in any form or by any means, without the prior permission of the author.

Additional financial support was provided by Abbott, AstraZeneca, Bayer, Biotronik, Boston Scientific, Chipsoft, CART-Tech B.V., CD Leycom, Fysiologic ECG services, Guerbet, Johnson&Johnson, Medis Medical Imaging Systems B.V., Microport, Novartis, VU University Amsterdam

VRIJE UNIVERSITEIT

Tailored Cardiac Resynchronization Therapy
Cardiac imaging before implant and device optimization afterwards

ACADEMISCH PROEFSCHRIFT

ter verkrijging van de graad Doctor
aan de Vrije Universiteit Amsterdam,
op gezag van de rector magnificus
prof.dr. V. Subramaniam,
in het openbaar te verdedigen
ten overstaan van de promotiecommissie
van de Faculteit der Geneeskunde
op vrijdag 24 april 2020 om 11.45 uur
in de aula van de universiteit,
De Boelelaan 1105

door

Alwin Zweerink

geboren te Steenderen

Promotor:	prof.dr. A.C. van Rossum
Copromotoren:	dr. C.P. Allaart
	prof.dr. R. Nijveldt

Leescommissie: prof.dr. C. Boer (voorzitter)
prof.dr. M.J. Schalij
prof. dr. H. Burri
dr. M.J.W. Götte
prof.dr. J. Stoker

Financial support by the Dutch Heart Foundation for the publication of this thesis is gratefully acknowledged

TABLE OF CONTENTS

Chapter 1	General Introduction and Outline of the Thesis	9
PART IA	**PATIENT SELECTION: NORMALIZATION OF QRS DURATION TO LEFT VENTRICULAR DIMENSION**	
Chapter 2	Improved Patient Selection for Cardiac Resynchronization Therapy by Normalization of QRS Duration to Left Ventricular Dimension *Europace 2017;19:1508-1513*	27
Chapter 3	Size Matters: Normalization of QRS Duration to Left Ventricular Dimension Improves Prediction of Long-term Cardiac Resynchronization Therapy Outcome *Circ Arrhythmia Electrophysiology 2018;11:e006767*	43
PART IB	**PATIENT SELECTION: STRAIN IMAGING**	
Chapter 4	Prediction of Acute Response to Cardiac Resynchronization Therapy by Means of the Misbalance in Regional Left Ventricular Myocardial Work *J Card Fail 2016;22:133-42*	73
Chapter 5	Comparison of Strain Imaging Techniques in CRT Candidates: CMR Tagging, CMR Feature Tracking and Speckle Tracking Echocardiography *Int J Cardiovasc Imaging 2018;34:443-456*	95
Chapter 6	Strain Imaging to Predict Response to Cardiac Resynchronization Therapy: a Systematic Comparison of Strain Parameters Using Multiple Imaging Techniques *ESC Heart Failure 2018;5:1130-1140*	121

Chapter 7 Strain Analysis in CRT Candidates Using the Novel Segment Length in Cine (SLICE) Post-processing Technique on Standard CMR Cine Images
Eur Radiology 2017;27:5158-5168 155

Chapter 8 Segment Length in Cine (SLICE) Strain Analysis: a Practical Approach to Estimate Potential Benefit from Cardiac Resynchronization Therapy
Submitted 181

Chapter 9 Septal Mechanics by Segment Length in Cine (SLICE) Strain Analysis Predicts Clinical Outcome After Cardiac Resynchronization Therapy
Submitted 205

PART II DEVICE OPTIMIZATION

Chapter 10 Can We Use the Intrinsic Left Ventricular Delay (QLV) to Optimize the Pacing Configuration for Cardiac Resynchronization Therapy with a Quadripolar Left Ventricular Lead?
Circ Arrhythmia Electrophysiology 2018;11:e005912 225

Chapter 11 Hemodynamic Optimization in Cardiac Resynchronization Therapy: Should We Aim For dP/dt_{max} or Stroke Work?
JACC Clinical Electrophysiology 2019;5:1013-1025 251

Chapter 12 Chronotropic Incompetence in Chronic Heart Failure: A State-of-the-Art Review
Circ Heart Failure 2018;11:e004969 279

Chapter 13 Summary and Future Perspectives 311

APPENDIX

Appendix I Nederlandse Samenvatting 329
Appendix II Dankwoord 337
Appendix III Curriculum Vitae 345
Appendix IV List of Publications 347

Chapter 1

General Introduction and Outline of the Thesis

GENERAL INTRODUCTION

Heart failure epidemic

Chronic heart failure (HF) is a clinical syndrome characterized by typical symptoms (e.g. breathlessness, peripheral edema and fatigue) caused by a structural and/or functional cardiac abnormality.(1) Cardiac dysfunction originates from a variety of underlying disorders including coronary artery disease, inflammation, infiltration, toxic damage, genetic disorders, or abnormal loading conditions. Chronic HF has been singled out as an epidemic with an overall prevalence that ranges from 1 to 12% based on available data from the USA and Europe.(2) These figures are likely to increase in the near future, as a result of progressive ageing of the population. At present, the reported lifetime risk of developing HF ranges from 20% to 33%.(3) Moreover, the prognosis of HF is worse than that of most cancers with an estimated survival of 50% and 10% at 5 and 10 years, respectively.(2,4) Treatment of HF includes management of contributing conditions, lifestyle modification, medication, and device therapy as will be discussed later.

Approximately one-quarter of patients presenting with HF demonstrates a left bundle branch block (LBBB) on the electrocardiogram (ECG).(5) LBBB results when rapid conduction over the specialized Purkinje fibers is interrupted. Most often, this is due to ventricular remodeling in patients with underlying heart disease. Slow cell-to-cell conduction results in a septal-to-lateral activation delay. The ensuing uncoordinated contraction results in reduced LV pump function efficiency as illustrated in figure 1.(6) Inefficient LBBB contraction in patients with HF further reduces LV function, leading to emerging HF and prematurely death.(5,7)

Cardiac Resynchronization Therapy

Cardiac resynchronization therapy (CRT) emerged 2 decades ago as a new form of device therapy for patients with heart failure and LBBB. Biventricular pacing is delivered using two leads, one placed in the right ventricular (RV) apex and one targeted via the epicardial coronary sinus onto the LV lateral wall. Ventricular stimulation is synchronized with atrial activation by placing a third lead in the right atrium.

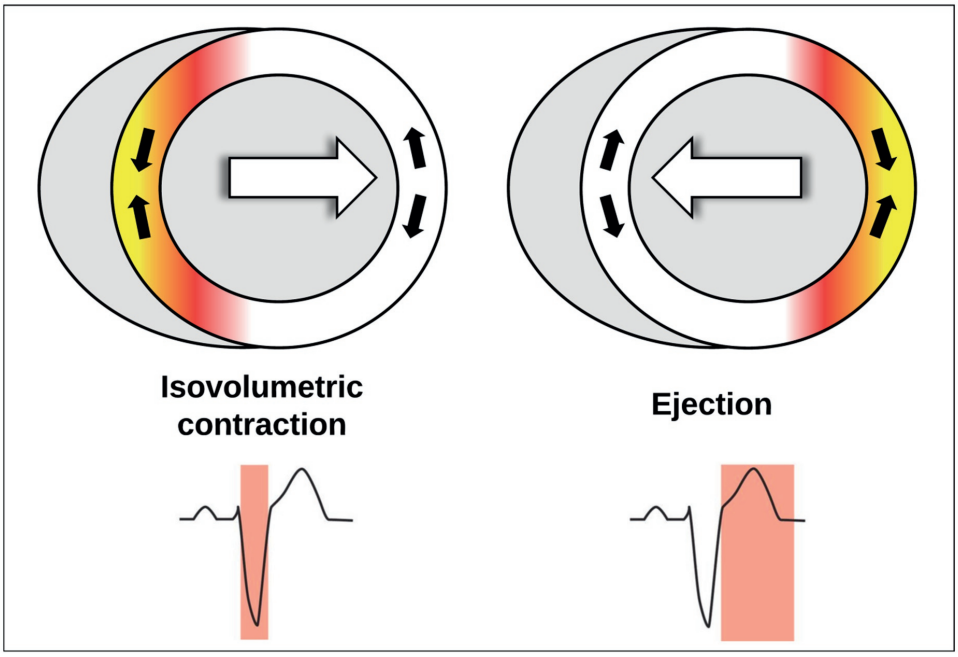


Figure 1: Electrical activation and contraction during LBBB. Schematic illustration of LBBB activation where the septum becomes activated first and starts contracting. Due to LBBB, the lateral wall is still passive and becomes stretched during the isovolumetric contraction phase. After delayed activation, contraction of the lateral wall pushes the septum back throughout the ejection phase. Back and forth movement of the blood-pool between segments reduces LV pump function efficiency.

Simultaneous LV and RV pacing reduces the septal-to-lateral activation delay, restoring LV pump function efficiency as illustrated in figure 2.(8) Several landmark trials showed that CRT markedly reduces morbidity and mortality in selected patients, and has led to the acceptance of CRT as a non-pharmalogical treatment option for patients with HF and LV conduction delay.(9-12) The beneficial effects of CRT are mediated by attenuation of disease progression and LV reverse remodeling with a decrease in LV volumes and increase in LV function.(13) Landmark CRT trials enrolled a select group of patients being those with symptomatic HF, LV dysfunction and QRSd ≥120 or ≥130ms.(14,15) Current European Society of Cardiology (ESC) guidelines recommend CRT in chronic HF patients with LV ejection fraction (LVEF) ≤35% who remain symptomatic (NYHA function class II, III and ambulatory IV) despite optimal medical treatment, and who have prolonged QRSd ≥130ms with strict LBBB morphology, or QRSd

≥150ms irrespective of QRS morphology.(1) Notwithstanding CRT being a very efficacious and cost-effective treatment, not all patients respond favorably to this therapy. Following guideline criteria, approximately one-third of the patients become non-responders.(16) These patients lack relief of symptoms or slowing of disease progression, and remain at risk for HF hospitalization or cardiac death. Meanwhile, these patients are exposed to unnecessary risks during device implantation with a reported peri-procedural complication rate of 6.1%.(17) These include pneumothorax, pocket hematoma, cardiac perforation, infection, thrombo-embolic events and death. Therefore, not every patient should be given CRT due to its high costs and substantial complication rate.

Two strategies that can potentially increase effectiveness of cardiac resynchronization are (i) improved selection of potential responders prior to implantation using cardiac imaging techniques and (ii) optimized device settings afterwards in order to maximize hemodynamic benefits. Both strategies will now be discussed.

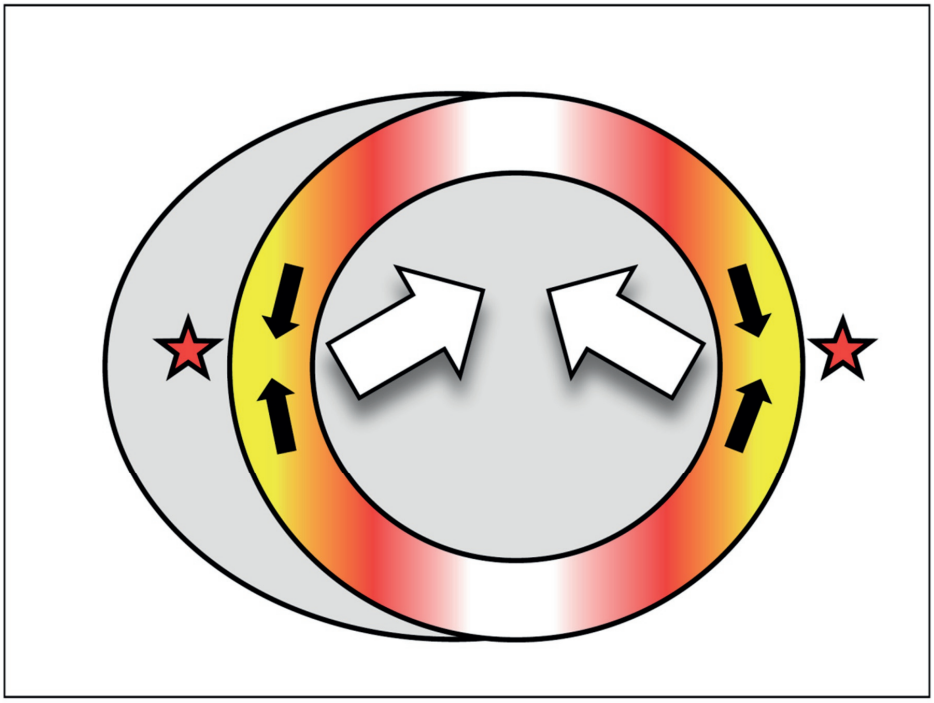


Figure 2: Electrical activation and contraction during CRT. CRT pacing sites are located at the RV apex and on top off the LV lateral wall (red stars). Biventricular stimulation reduces the septal-to-lateral activation delay and re-coordinated contraction subsequently restores LV pump function efficiency.

Electrocardiogram

Patient selection for CRT is primarily guided by the presence of a wide QRS complex with LBBB morphology on the 12-lead surface ECG.(1,14,18) Prolonged QRSd indicates an electrical conduction delay through the ventricular myocardium, resulting in a higher class of recommendation for CRT. However, QRSd shows large interpatient variability and is dependent on various parameters including conduction pattern, functional lines of block, presence of scar tissue, and structural factors such as LV hypertrophy and LV size.(19) These factors are likely to contribute to the large heterogeneity in CRT response between patients. Women, for example, demonstrate up to 20% smaller LV size compared to men and have relatively shorter QRSd.(20) In order to reach an identical QRSd value for men and women, female hearts will have more conduction delay compared to male hearts. This could partly explain the present underrepresentation of women with CRT when using an identical QRSd cut-off value for both sexes.(21) Moreover, progressive LV dilation during the HF course may influence QRSd and its predictive value for CRT response. Therefore, LV dimension may be considered an important confounder which should be corrected for in the assessment of LV dyssynchrony as will be discussed in the outline of the thesis. The role of Cardiovascular magnetic resonance (CMR) imaging is of special interest, since this technique is considered the 'gold standard' technique for quantification of LV size and function.(22)

Myocardial strain imaging

As the heart contracts, muscle shortens in the longitudinal and circumferential orientations, and thickens in the radial direction. Strain is defined as a measure of deformation representing the displacement between particles in the body relative to a reference length. More specifically, strain reflects whether the length L of a piece of tissue gets smaller or larger with respect to an initial reference state length L0. Based on this, strain can be defined by the Lagrangian formula:

$$\text{Strain} = \frac{\text{L} - \text{L0}}{\text{L0}}$$

Myocardial strain imaging is of special interest in CRT candidates as it enables quantification of the mechanical consequences of LBBB. Patients with a highly inefficient contraction pattern (previously illustrated in figure 1) leave more room for improvement after CRT compared to patients lacking mechanical substrate for LV pump function improvement. Therefore, myocardial strain analysis is considered a potential tool to improve patient selection for CRT. Local strain curves provide mechanical information on regional timing differences (also known as dyssynchrony) and inefficient contraction patterns (also known as discoordination). Traditionally, echocardiographic modalities have been used to measure regional timing differences throughout the LV. Echocardiographic dyssynchrony parameters, however, showed disappointing results in the PROSPECT study.(23) More recent single-center studies showed discoordination rather than dyssynchrony to be predictive for CRT response.(6,24-26) Most of these parameters were introduced in single-modality studies, but multiple imaging modalities are presently available as illustrated in figure 3. CMR imaging offers non-invasive assessment of myocardial strains by the implementation of myocardial taglines (CMR-TAG).(27) Tracing the displacement of the taglines throughout the cardiac cycle produces high quality measures of intramural shortening. Although CMR-TAG is often used as reference technique in scientific research, availability is limited in clinical practice. More recently, CMR feature tracking (CMR-FT) emerged as a post-processing technique on standard CMR cine images. The features that are tracked by CMR-FT are anatomic elements along the cavity-myocardial border. Despite large interest on this topic in recent years, further validation is warranted.(28) Lastly, speckle tracking echocardiography (STE) offers strain analysis by tracking specific grey scale speckle patterns in the myocardial wall throughout the cardiac cycle.(29) Although STE is widely available as a bedside tool and offers high-frequent strain sampling, analysis is highly dependent on the quality of the available acoustic windows. Due to the relative differences in strengths and weaknesses between techniques, predictive value of strain parameters may vary between modalities. Therefore, the implanting physician should be informed what strain parameter predicts CRT response best, and which imaging technique can be used for assessment. Moreover, identifying the key-element that underlies CRT response could enable a fast and simple strain measurement in clinical practice.

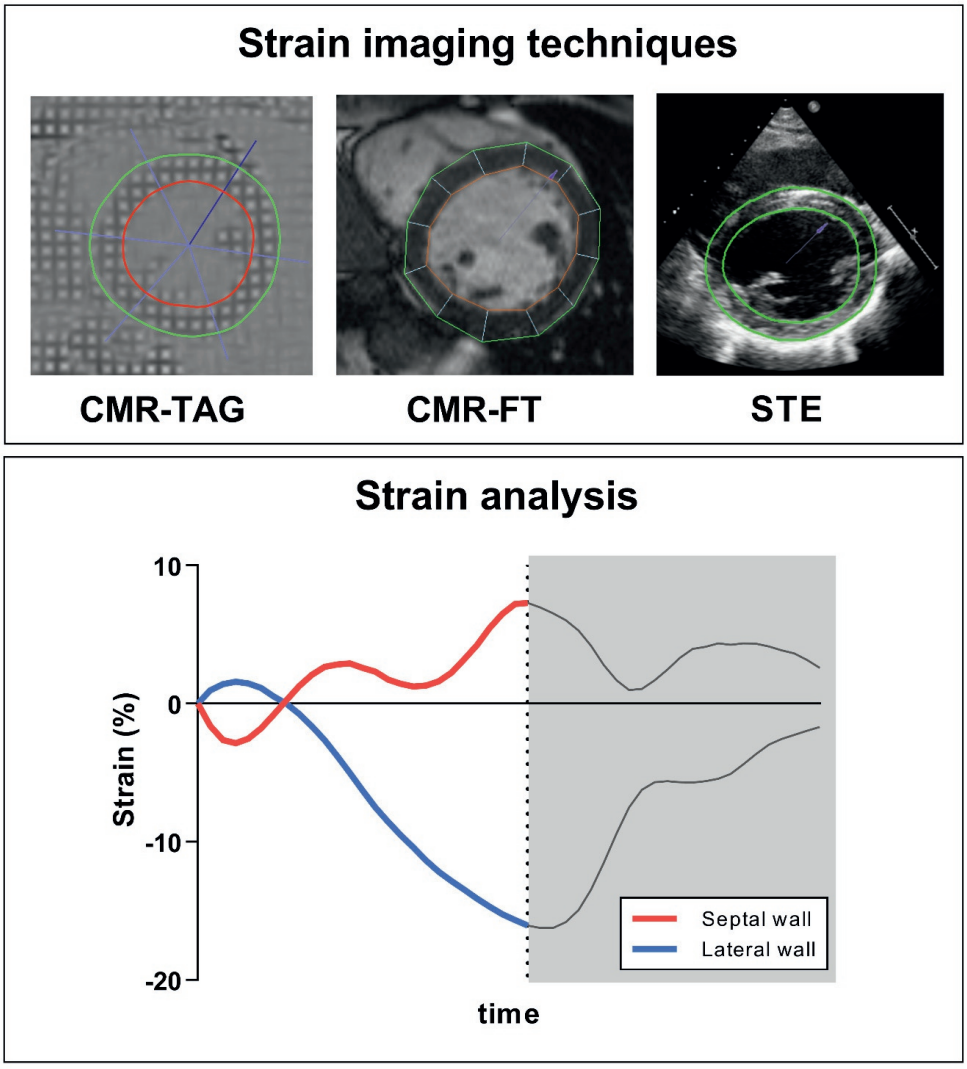


Figure 3: Myocardial strain imaging techniques. Multiple strain imaging techniques are presently available including CMR tagging (CMR-TAG), CMR feature tracking (CMR-FT) and speckle tracking echocardiography (STE). Circumferential strain curves of the septal (red) and lateral (blue) wall. Negative numbers indicate shortening, positive numbers indicate lengthening. In this typical example of a patient with LBBB delayed contraction of the lateral wall results in septal stretching during systole.

Device optimization

Device optimization includes tailored LV lead placement and individualized programming of the atrioventricular (AV) and interventricular (VV) delay in order to maximize hemodynamic benefits. Strategies to optimize LV lead placement must account for variations in coronary venous anatomy in an attempt to target the lead away from phrenic nerve stimulation or myocardial scarring and close to regions of late LV activation.(30,31) Quadripolar LV leads have been developed to overcome these challenges by incorporating 4 independent electrodes, spaced several centimeters along the distal end of the lead.(32) Electrical stimulation is offered in multiple pacing configurations in order to improve CRT efficiency during implant and at follow-up as illustrated in figure 4. Moreover, quadripolar LV leads provide the opportunity for multi-site LV stimulation using multiple electrodes (i.e. multipoint pacing). Although quadripolar leads increase the possible number of pacing sites compared to conventional leads, a robust optimization tool that helps the clinician select the most beneficial configuration is missing. Echocardiographic parameters (e.g. stroke volume; mitral flow) are most widely used in clinical practice although convincing scientific evidence for these methods is lacking. Alternatively, electrical optimization parameters incorporate local activation times derived from the intracardiac electrogram. The QLV interval is one of these electrical delays, defined by the delay between 'Q' on the surface ECG and local LV depolarization on the intracardiac electrogram at a given LV pacing site during intrinsic rhythm. Previous studies demonstrated a positive association between QLV and hemodynamic CRT response.(33,34) These studies, however, only compared QLV and hemodynamic measurements between different patients or between different venous branches. So far, it has not been investigated whether selecting the LV lead electrode of a quadripolar lead with the longest QLV (i.e. pacing the latest activated area within a venous branch) produces better results. This objective will be part of the aim of the thesis.

Alternatively, acute CRT response can be assessed by invasive hemodynamic testing in order to optimize device settings.(35) Typically, the maximum rate of LV pressure rise (dP/dtmax) is used as an index of ventricular performance. dP/dt_{max} is easily obtained using a pressure wire and is used as a surrogate for LV contractility. Alternatively, stroke work (SW) incorporates all pressure and volume changes throughout the cardiac cycle and provides a comprehensive

appraisal of LV pump function. A conductance catheter is positioned in the LV cavity and acquires simultaneous pressure-volume measurements throughout the cardiac cycle. Measuring LV volume changes using the conductance catheter, however, warrants careful data acquisition. At present, a direct comparison between hemodynamic CRT optimization strategies is lacking. Whether acute improvement in hemodynamics translates into beneficial effects from CRT in the longer term is also matter of debate.

Rate-adaptive pacing

Chronotropic incompetence (CI), the inability of the heart rate to increase adequately in response to exercise, is common in the heart failure population and contributes to a limited functional capacity and survival in these patients. During exercise the normal heart increases both stroke volume and heart rate, whereas in the failing heart contractility reserve is lost thus rendering increases in cardiac output primarily dependent on cardio-acceleration. Consequently, insufficient cardio-acceleration due to CI is considered to be a major limiting factor in the exercise capacity of HF patients. Despite the profound effects of CI in this specific population, the issue has drawn limited attention over the past years and is often overlooked in clinical practice. Cardiac implantable electronic devices (i.e. ICD; CRT) now offer a unique opportunity to study HR dynamics and provide treatment options for CI by rate-adaptive pacing using an incorporated sensor that measures physical activity. A critical appraisal of literature on the role of CI in HF patients is included in the last part of the thesis. This topic includes a special focus on new diagnostic and therapeutic options offered by the latest generation cardiac implantable electronic devices including CRT.

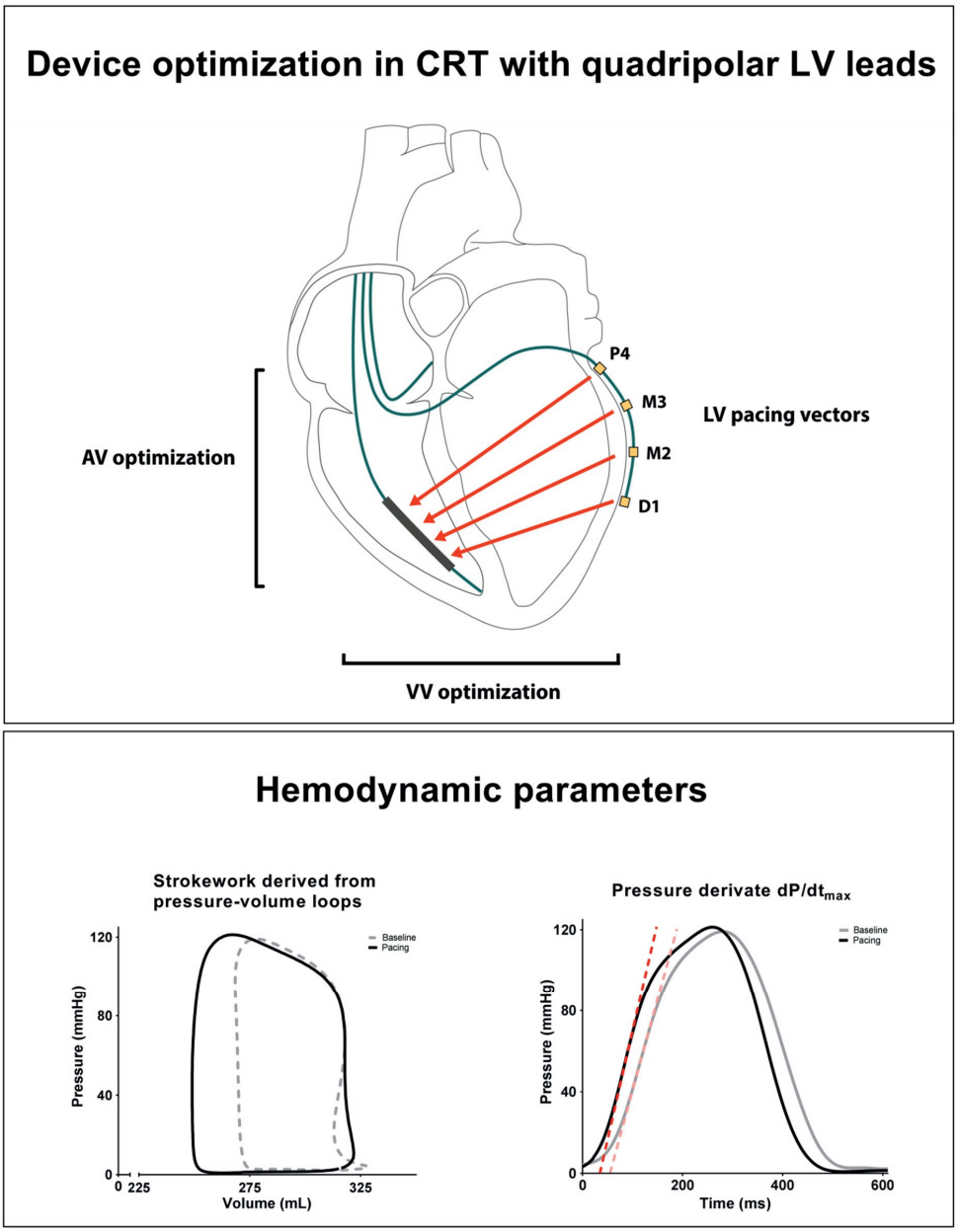


Figure 4: Hemodynamic optimization. Device optimization in CRT with quadripolar LV leads includes programming of the atrioventricular (AV) and interventricular (VV) delay, as well as LV pacing electrode. Hemodynamic parameters that may be used include stroke work (SW) derived from pressure-volume loops or the maximum rate of LV pressure rise (dP/dt_{max}).

OUTLINE OF THE THESIS

This thesis aims (i) to gain insights into the underlying mechanisms that enable LV pump function improvement after CRT, and (ii) to maximize CRT benefits by electrical and hemodynamic optimization strategies.

The first part of the thesis focuses on the use of cardiac imaging techniques to improve patient selection for CRT. Part IA evaluates the theoretical concept that adjusting QRSd to LV structural characteristics improves patient selection for CRT. As a first step, **chapter 2** provides a proof-of-concept study that illustrates the effect of QRSd normalization on the relation with acute hemodynamic CRT response. Subsequently, **chapter 3** extends the role of QRSd normalization to the prediction of clinical endpoints in a large cohort of CRT patients. Part IB explores the role of myocardial strain imaging to improve patient selection for CRT. First, regional strain measurements are combined with LV pressure curves to calculate the distribution of myocardial work throughout the LV, as presented in **chapter 4**. It is hypothesized that the lower the septal contribution to total myocardial work (or the higher the septal waste) during LBBB, the higher the achievable improvement in LV pump function during CRT. CMR-TAG is used for strain assessment in this study. In clinical practice, however, multiple strain imaging techniques are presently available. **Chapter 5** provides a comparison of strain values between 'gold standard' CMR-TAG and more widely available alternatives CMR-FT and STE. This study is part of the markers and response to CRT (MARC) study, a prospective multi-center study in six medical centers in the Netherlands.(36) Lastly, **chapter 6** provides follow-up data in these patients to compare predictive performance of different strain parameters using multiple imaging techniques for echocardiographic CRT response after one year. Subsequently, the novel segment length in cine (SLICE) strain analysis technique is introduced to derive segmental strains from standard CMR cine images without the need for commercial software. **Chapter 7** provides a validation study that compares SLICE strain values to CMR-TAG in a subset of patients of the MARC study who underwent CMR examination including additional tagging. Subsequently, SLICE strain analysis was performed in all MARC patients who underwent standard CMR examination to relate different SLICE strain parameters to echocardiographic CRT response after one year (**chapter 8**). In **chapter 9**, the predictive value of SLICE for clinical outcome after CRT implantation is evaluated in a large population of CRT candidates.

Part two of the thesis presents a series of studies evaluating the value of different device optimization strategies to maximize benefit from CRT. The first two studies are part of the OPTICARE-QLV (Optimization of Cardiac Resynchronization Therapy With a Quadripolar Left Ventricular Lead) study, a multicenter, observational study performed in three university medical centers throughout the Netherlands. **Chapter 10** investigates whether electrical parameters (QLV; QLV/QRSd) can be used to identify the most beneficial pacing electrode of a quadripolar lead. It is hypothesized that pacing the electrode with the latest activation (i.e. longest QLV), results in the largest hemodynamic improvement as measured by pressure-volume loops. Subsequently, **chapter 11** evaluates the effect of dP/dt_{max} versus SW guided optimization on acute response to CRT. Furthermore, acute changes in hemodynamic parameters are related to echocardiographic CRT response after six months. Lastly, the latest generation cardiac implantable electronic devices (ICD; CRT) offer a unique opportunity to study HR dynamics and provide treatment options for CI by rate-adaptive pacing using an incorporated sensor that measures physical activity. **Chapter 12** provides a review paper with an overview of disease mechanism, diagnostic strategies, clinical consequences and state-of-the-art device therapy for CI in HF.

REFERENCES

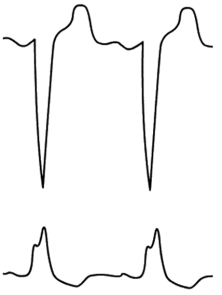
1. Ponikowski P, Voors AA, Anker SD, Bueno H, Cleland JG, Coats AJ, et al. 2016 ESC Guidelines for the diagnosis and treatment of acute and chronic heart failure: The Task Force for the diagnosis and treatment of acute and chronic heart failure of the European Society of Cardiology (ESC). Developed with the special contribution of the Heart Failure Association (HFA) of the ESC. Eur J Heart Fail. 2016;18(8):891-975.
2. Roger VL. Epidemiology of heart failure. Circ Res. 2013;113(6):646-59.
3. Lloyd-Jones DM, Larson MG, Leip EP, Beiser A, D'Agostino RB, Kannel WB, et al. Lifetime risk for developing congestive heart failure: the Framingham Heart Study. Circulation. 2002;106(24):3068-72.
4. Braunwald E. The war against heart failure: the Lancet lecture. Lancet. 2015;385(9970):812-24.
5. Zannad F, Huvelle E, Dickstein K, van Veldhuisen DJ, Stellbrink C, Kober L, et al. Left bundle branch block as a risk factor for progression to heart failure. Eur J Heart Fail. 2007;9(1):7-14.
6. Prinzen FW, Vernooy K, De Boeck BW, Delhaas T. Mechano-energetics of the asynchronous and resynchronized heart. Heart Fail Rev. 2011;16(3):215-24.
7. Hawkins NM, Wang D, McMurray JJ, Pfeffer MA, Swedberg K, Granger CB, et al. Prevalence and prognostic impact of bundle branch block in patients with heart failure: evidence from the CHARM programme. Eur J Heart Fail. 2007;9(5):510-7.
8. Vernooy K, van Deursen CJ, Strik M, Prinzen FW. Strategies to improve cardiac resynchronization therapy. Nat Rev Cardiol. 2014;11(8):481-93.
9. Bristow MR, Saxon LA, Boehmer J, Krueger S, Kass DA, De Marco T, et al. Cardiac-resynchronization therapy with or without an implantable defibrillator in advanced chronic heart failure. N Engl J Med. 2004;350(21):2140-50.
10. Cleland JG, Daubert JC, Erdmann E, Freemantle N, Gras D, Kappenberger L, et al. The effect of cardiac resynchronization on morbidity and mortality in heart failure. N Engl J Med. 2005;352(15):1539-49.
11. Moss AJ, Hall WJ, Cannom DS, Klein H, Brown MW, Daubert JP, et al. Cardiac-resynchronization therapy for the prevention of heart-failure events. N Engl J Med. 2009;361(14):1329-38.
12. Tang AS, Wells GA, Talajic M, Arnold MO, Sheldon R, Connolly S, et al. Cardiac-resynchronization therapy for mild-to-moderate heart failure. N Engl J Med. 2010;363(25):2385-95.
13. Gold MR, Thebault C, Linde C, Abraham WT, Gerritse B, Ghio S, et al. Effect of QRS duration and morphology on cardiac resynchronization therapy outcomes in mild heart failure: results from the Resynchronization Reverses Remodeling in Systolic Left Ventricular Dysfunction (REVERSE) study. Circulation. 2012;126(7):822-9.
14. Cleland JG, Abraham WT, Linde C, Gold MR, Young JB, Claude Daubert J, et al. An individual patient meta-analysis of five randomized trials assessing the effects of cardiac resynchronization therapy on morbidity and mortality in patients with symptomatic heart failure. Eur Heart J. 2013;34(46):3547-56.
15. Ruschitzka F, Abraham WT, Singh JP, Bax JJ, Borer JS, Brugada J, et al. Cardiac-resynchronization therapy in heart failure with a narrow QRS complex. N Engl J Med. 2013;369(15):1395-405.

16. Daubert C, Behar N, Martins RP, Mabo P, Leclercq C. Avoiding non-responders to cardiac resynchronization therapy: a practical guide. Eur Heart J. 2017;38(19):1463-72.
17. Hosseini SM, Moazzami K, Rozen G, Vaid J, Saleh A, Heist KE, et al. Utilization and in-hospital complications of cardiac resynchronization therapy: trends in the United States from 2003 to 2013. Eur Heart J. 2017;38(27):2122-8.
18. Yancy CW, Jessup M, Bozkurt B, Butler J, Casey DE, Jr., Drazner MH, et al. 2013 ACCF/AHA guideline for the management of heart failure: a report of the American College of Cardiology Foundation/American Heart Association Task Force on Practice Guidelines. J Am Coll Cardiol. 2013;62(16):e147-239.
19. Chan DD, Wu KC, Loring Z, Galeotti L, Gerstenblith G, Tomaselli G, et al. Comparison of the relation between left ventricular anatomy and QRS duration in patients with cardiomyopathy with versus without left bundle branch block. Am J Cardiol. 2014;113(10):1717-22.
20. Kawel-Boehm N, Maceira A, Valsangiacomo-Buechel ER, Vogel-Claussen J, Turkbey EB, Williams R, et al. Normal values for cardiovascular magnetic resonance in adults and children. J Cardiovasc Magn Reson. 2015;17:29.
21. Randolph TC, Hellkamp AS, Zeitler EP, Fonarow GC, Hernandez AF, Thomas KL, et al. Utilization of cardiac resynchronization therapy in eligible patients hospitalized for heart failure and its association with patient outcomes. Am Heart J. 2017;189:48-58.
22. Grothues F, Smith GC, Moon JC, Bellenger NG, Collins P, Klein HU, et al. Comparison of interstudy reproducibility of cardiovascular magnetic resonance with two-dimensional echocardiography in normal subjects and in patients with heart failure or left ventricular hypertrophy. Am J Cardiol. 2002;90(1):29-34.
23. Chung ES, Leon AR, Tavazzi L, Sun JP, Nihoyannopoulos P, Merlino J, et al. Results of the Predictors of Response to CRT (PROSPECT) trial. Circulation. 2008;117(20):2608-16.
24. De Boeck BW, Teske AJ, Meine M, Leenders GE, Cramer MJ, Prinzen FW, et al. Septal rebound stretch reflects the functional substrate to cardiac resynchronization therapy and predicts volumetric and neurohormonal response. Eur J Heart Fail. 2009;11(9):863-71.
25. Kirn B, Jansen A, Bracke F, van Gelder B, Arts T, Prinzen FW. Mechanical discoordination rather than dyssynchrony predicts reverse remodeling upon cardiac resynchronization. Am J Physiol Heart Circ Physiol. 2008;295(2):H640-6.
26. Lumens J, Tayal B, Walmsley J, Delgado-Montero A, Huntjens PR, Schwartzman D, et al. Differentiating Electromechanical From Non-Electrical Substrates of Mechanical Discoordination to Identify Responders to Cardiac Resynchronization Therapy. Circ Cardiovasc Imaging. 2015;8(9):e003744.
27. Shehata ML, Cheng S, Osman NF, Bluemke DA, Lima JA. Myocardial tissue tagging with cardiovascular magnetic resonance. J Cardiovasc Magn Reson. 2009;11:55.
28. Schuster A, Hor KN, Kowallick JT, Beerbaum P, Kutty S. Cardiovascular Magnetic Resonance Myocardial Feature Tracking: Concepts and Clinical Applications. Circ Cardiovasc Imaging. 2016;9(4):e004077.
29. Tanaka H, Hirata K. Is speckle tracking actually helpful for cardiac resynchronization therapy? J Echocardiogr. 2016;14(2):53-60.

30. de Roest GJ, Wu L, de Cock CC, Hendriks ML, Delnoy PP, van Rossum AC, et al. Scar tissue-guided left ventricular lead placement for cardiac resynchronization therapy in patients with ischemic cardiomyopathy: an acute pressure-volume loop study. Am Heart J. 2014;167(4):537-45.
31. Pastromas S, Manolis AS. Cardiac resynchronization therapy: Dire need for targeted left ventricular lead placement and optimal device programming. World J Cardiol. 2014;6(12):1270-7.
32. van Everdingen WM, Cramer MJ, Doevendans PA, Meine M. Quadripolar Leads in Cardiac Resynchronization Therapy. JACC: Clinical Electrophysiology. 2015;1(4):225-37.
33. Gold MR, Birgersdotter-Green U, Singh JP, Ellenbogen KA, Yu Y, Meyer TE, et al. The relationship between ventricular electrical delay and left ventricular remodelling with cardiac resynchronization therapy. Eur Heart J. 2011;32(20):2516-24.
34. Zanon F, Baracca E, Pastore G, Fraccaro C, Roncon L, Aggio S, et al. Determination of the longest intrapatient left ventricular electrical delay may predict acute hemodynamic improvement in patients after cardiac resynchronization therapy. Circ Arrhythm Electrophysiol. 2014;7(3):377-83.
35. Clark JE, Marber MS. Advancements in pressure-volume catheter technology - stress remodelling after infarction. Exp Physiol. 2013;98(3):614-21.
36. Maass AH, Vernooy K, Wijers SC, van 't Sant J, Cramer MJ, Meine M, et al. Refining success of cardiac resynchronization therapy using a simple score predicting the amount of reverse ventricular remodelling: results from the Markers and Response to CRT (MARC) study. Europace. 2018;20(2):e1-e10.

PART IA

PATIENT SELECTION: NORMALIZATION OF QRS DURATION TO LEFT VENTRICULAR DIMENSION



Chapter 2

Improved Patient Selection for Cardiac Resynchronization Therapy by Normalization of QRS Duration to Left Ventricular Dimension

Europace 2017;19:1508-1513

Alwin Zweerink
LiNa Wu
Gerben J. de Roest
Robin Nijveldt
Carel C. de Cock
Albert C. van Rossum
Cornelis P. Allaart

ABSTRACT

Aims: This study evaluates the relative importance of two components of QRS prolongation, myocardial conduction velocity and travel distance of the electrical wave front (i.e. path length), for the prediction of acute response to Cardiac Resynchronization Therapy (CRT) in left bundle branch block (LBBB) patients.

Methods: Thirty-two CRT candidates (ejection fraction <35%, LBBB) underwent Cardiac Magnetic Resonance (CMR) imaging to provide detailed information on left ventricular (LV) dimensions. LV end-diastolic volume (LVEDV) was used as primary measure for path length, subsequently QRSd was normalized to LV dimension (i.e. QRSd divided by LVEDV) to adjust for conduction path length. Invasive pressure-volume loop analysis at baseline and during CRT was used to assess acute pump function improvement, expressed as LV stroke work (SW) change.

Results: During CRT, SW improved by +38±46% ($p<0.001$). Baseline LVEDV was positively related to QRSd (R 0.36, $p=0.044$). Despite this association, a paradoxical inverse relation was found between LVEDV and SW improvement during CRT (R -0.40; $p=0.025$). Baseline unadjusted QRSd was found to be unrelated to SW changes during CRT (R 0.16; $p=0.383$), whereas normalized QRSd (QRSd/LVEDV) yielded a strong correlation with CRT response (R 0.49; $p=0.005$). Other measures of LV dimension, including LV length, LV diameter and LV end-systolic volume, showed similar relations with normalized QRSd and SW improvement.

Conclusion: Since normalized QRSd reflects myocardial conduction properties, these findings suggest that myocardial conduction velocity rather than increased path length mainly determines response to CRT. Normalizing QRSd to LV dimension might provide a relatively simple method to improve patient selection for CRT.

BACKGROUND

Current guidelines recommend Cardiac Resynchronization Therapy (CRT) for patients with drug refractory symptomatic heart failure (HF), reduced ejection fraction (EF) and left bundle branch block (LBBB). Using these criteria, patient selection remains suboptimal with QRS duration (QRSd) being the strongest predictor of CRT response.(1) In the presence of LBBB, prolongation of QRSd is determined by both myocardial conduction velocity and travel distance of the wave front over the left ventricle (LV).(2-5) In HF patients, LV dilatation is typically present causing increased conduction path length and thus QRS lengthening. Increased QRSd is expected to result in improved CRT response. On the other hand, however, progressive LV dilatation per se is known to limit CRT response.(6-9) We therefore hypothesize that decreased myocardial conduction velocity rather than increased path length determines the response to CRT.
This study evaluates the relative importance of two components of QRS prolongation, myocardial conduction velocity and travel distance of the electrical wave front (i.e. conduction path length), for the prediction of acute response to CRT in LBBB patients.

METHODS

Subjects

Data for this retrospective study were extracted from the Temporary Biventricular Stimulation (TBS) database. The original TBS-based studies evaluated the acute hemodynamic effects of CRT using conductance catheter measurements in heart failure patients. In brief, biventricular stimulation using several temporary LV leads was applied to study effects of QRS duration, lead location, scar size and location, and pacing configurations. The studies corroborated the importance of QRS duration and scar evaluation in selection for CRT (10,11) and showed that optimal LV lead placement should be guided by late mechanical activation, which obviates the need for multisite LV stimulation.(12) Moreover, it was clearly shown that acute pump function improvement using stroke work (SW) assessment rather than dP/dt measurements strongly predicts long term outcome.(13,14) Inclusion criteria were sinus rhythm, drug refractory heart failure (NYHA class II-III) and severely depressed systolic LV function with EF ≤35%. In the original studies, patients with

different QRSd and QRS morphologies were included. For the present analysis additional inclusion criteria were 1. stable pressure-volume (PV) loop measurements at baseline and during conventional biventricular pacing with pacing leads in the RV apex and located at the LV mid lateral/posterolateral wall (for details see section on Temporary Biventricular Pacing); 2. complete LBBB as judged by two independent specialists using the criteria for complete LBBB according the ESC guidelines.(15) and 3. a pre-implantation CMR examination including delayed contrast enhancement (LGE) to evaluate scar tissue. All subjects gave informed consent and the local medical ethics committee (VU University Medical Center, Amsterdam) approved data collection and management. The study conforms with the principles outlined in the Declaration of Helsinki.(16)

Cardiac Magnetic Resonance Imaging

CMR imaging was performed on a 1.5T whole body system (Sonata, Siemens, Erlangen, Germany) using a phased-array cardiac receiver coil. Functional imaging was performed using retrospectively ECG-gated steady-state free precession cine imaging with breath-holding. Per patient, 8-12 contiguous short-axis slices were obtained every 10mm covering the entire LV. Endocardial and epicardial borders were manually traced on the short axis cine images using MASS software (version 5.1b, MEDIS, Leiden, the Netherlands). Papillary muscles and trabeculae were included in the LV cavity, and LV volumes and mass were calculated using the summation of disks method. LV length was determined from the four chamber long-axis view measuring the length between the apex and the middle of the mitral valve annulus in end-diastole. The LV diameter was measured in the mid short-axis slice in end-diastole. Conduction path length is derived from LV dimensions with left ventricular end-diastolic volume (LVEDV) as its primary measure. Secondary LV dimension indices are left ventricular end-systolic volume (LVESV), LV length, LV diameter and LV mass. QRSd was normalized to LV dimension (i.e. QRSd divided by LV dimension) to adjust for conduction path length. Myocardial scar territory was assessed by late gadolinium enhancement (LGE) imaging using the full width at half maximum method.(17) Patients were classified having an ischemic cardiomyopathy (ICMP) in case of a history of myocardial infarction accompanied by associated LGE findings.

Temporary Biventricular Pacing

Within the same week of the CMR scan, all patients underwent temporary biventricular stimulation as described previously.(11) In brief, biventricular pacing was performed either in VDD mode or DDD mode with a lower rate set at 5-10 beats per minute above the intrinsic rate. In case of arrhythmias interfering with analyzable PV loops, atrial pacing was performed with a rate of 5-10% above the intrinsic rhythm (DDD mode). Patients were stimulated using a fixed atrioventricular delay set to 100ms or lower ensuring full ventricular capture, and a VV interval of 0 ms. AV- and VV-optimization was not performed. Patients were included in the present study when the LV lead was located at the mid-lateral or mid-posterolateral segment. The anatomic position of the LV lead tip was assessed on biplane fluoroscopy using LAO 40° and RAO 30° projections as proposed by Boogaard et al.(18) In brief, in the LAO projection the heart contour was divided into five equal parts of 40° from anterior to posterior with the LV lead located at the lateral or posterolateral segment. In the RAO projection the heart contour was divided into three equal parts from base to apex with the LV lead positioned at the mid segment. A conductance catheter (CD Leycom, Zoetermeer, The Netherlands) was placed in a stable position in the LV apex to obtain a series of PV loops at baseline (no ventricular pacing) and during biventricular pacing. PV loops were constructed using Conduct NT software (version 3.18.1). Each measurement was obtained after a stabilization period of 30 seconds and consisted of a minimum of 30 representative cardiac cycles disregarding all inappropriate beats (i.e. extra-systoles and two subsequent beats), which were subsequently averaged. By averaging PV loops throughout multiple respiratory cycles, respiratory influences were minimized.(19) Baseline measurements were taken before and after the pacing run. Prior to biventricular stimulation, the initial series of baseline PV-loops were calibrated to the CMR derived LV volumes (LVEDV and LVESV) obtained by CMR examination the day before. Subsequently, PV loops during biventricular stimulation and a post-pacing baseline measurement (no ventricular stimulation) were obtained. LV pump function was quantified by Stroke work (SW), calculated as the area of the PV loop. The effect of biventricular pacing was calculated as the relative SW change compared with the mean of the two flanking baseline measurements.(11)

Patients with a SW increase of >20% compared with baseline were classified as CRT responders as this cut-off accurately predicted reverse remodeling at 6 months.(13)

Statistics

The commercially available Statistical Package for Social Sciences software (IBM SPSS Statistics for Windows, Version 20.0. Armonk, NY, USA) was used for statistical analysis. Continuous variables are expressed as mean ± SD. Categorical variables are presented as absolute numbers and percentages. A Student t-test (independent or paired) or non-parametric test was used to compare groups when appropriate. Correlations were assessed using the Pearson's correlation coefficient or when normal distribution was absent, the Spearman's Rho correlation coefficient. Associations between baseline QRSd indices (unadjusted QRSd and QRSd normalized to LV dimension) and hemodynamic response during CRT were analyzed by linear regression analysis. Receiver Operating Characteristics (ROC) curve analysis was used to determine the predictive value of the parameters. Multivariate linear regression analysis was performed for the primary measure, normalized QRSd, combined with gender and scar size being determinants of response. A P-value of <0.05 was considered statistically significant.

RESULTS

Thirty-two CRT candidates (age 66±9 years, 20 men, 16 IMCP) were included in the present study. The original TBS database consists of 88 subjects. Fifteen patients were excluded because of non-analyzable PV loops at baseline, or during conventional biventricular stimulation. Furthermore, 16 patients with QRSd <120ms and 3 patients with right bundle branch block (RBBB) were excluded. From the resulting 54 subjects, a total of 32 patients fulfilled the requirements of CMR with LGE and ECG criteria for complete LBBB according the ESC guidelines.(15) Baseline patient characteristics are listed in table 1.

Table 1 Patient characteristics

Parameter	N = 32
Clinical	
Age (years)	66 ± 9
Sex (male/female)	20/12
NYHA (II/III)	7/25
Aetiology (ICMP/NICMP)	16/16
Med: ACE-inhibitors (n, %)	28 (82%)
Med: aldosterone-inhibitors (n, %)	9 (28%)
Med: beta-blockers (n, %)	25 (78%)
Med: diuretics (n, %)	21 (66%)
ECG	
QRS duration (ms)	155 ± 18
CMR	
LVEDV (ml)	291 ± 84
LVESV (ml)	223 ± 81
EF (%)	24 ± 9
LV length (mm)	104 ± 8
LV diameter (mm)	68 ± 10
LV mass (gr)	137 ± 38
Scar present (n, %)	16 (50%)
Scar size (%)	12 ± 8
Hemodynamics	
Heart rate (bpm)	81 ± 12
dP/dt_{max} (mmHg/s)	831 ± 180
dP/dt_{min} (mmHg/s)	-832 ± 163
τ (ms)	43 ± 7
Maximal pressure (mmHg)	121 ± 23
Minimal pressure (mmHg)	10 ± 7
EDP (mmHg)	17 ± 9
SW (L • mmHg)	4.8 ± 2.3

ICMP, ischemic cardiomyopathy; NICMP, non-ischemic cardiomyopathy; CMR, cardiac magnetic resonance imaging; LVEDV, end-diastolic volume; LVESV, end-systolic volume; EF, ejection fraction; τ, tau; EDP, end-diastolic pressure; SW, stroke work.

LV dimension and QRS duration

CMR derived volumetric parameters LVEDV and LVESV showed large variation (LVEDV 291±84; LVESV 223±81). LVEDV was positively correlated with QRSd (R 0.36; p=0.044, figure 1A), whereas LVESV showed a positive trend (R 0.33; p=0.064). LV length was not related to QRSd (R 0.23; p=0.213), while LV diameter showed a positive correlation (R 0.36; p=0.046). Both LV mass and scar size were not significantly related to QRSd (R 0.26; p=0.157 and R -0.21; p=0.911, respectively).

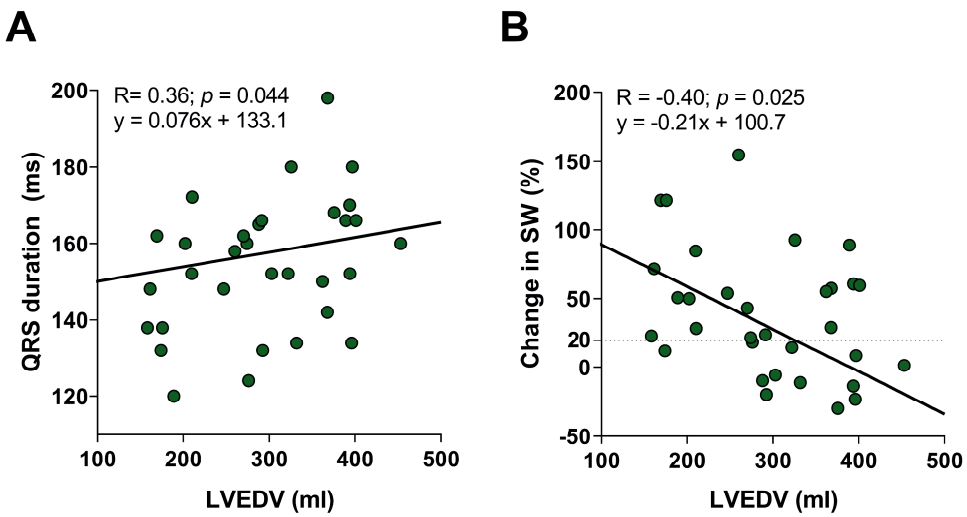


Figure 1 shows scatter plots illustrating (A) the positive correlation between left ventricular end-diastolic volume (LVEDV) and baseline QRS duration; and (B) the negative correlation between LVEDV and acute strokework (SW) changes during CRT.

LV dimension and acute response to CRT

During biventricular pacing overall LV pump function improved significantly (SW change +38±46%; p<0.001). Based on the 20% cut-off value, 20 patients (63%) were classified as SW responder. Both LVEDV and LVESV were inversely related to SW improvement during CRT (R -0.40; p=0.025 see figure 1B, and R -0.52; p=0.002, respectively). LV length was not significantly related to SW improvement (R -0.34; p=0.054), while LV diameter was inversely related (R -0.40; p=0.025). LV mass was unrelated to SW changes during CRT (R -0.27; p=0.143).

QRS duration and acute response to CRT

Unadjusted baseline QRSd was unrelated to SW changes during CRT, as illustrated in figure 2A, and yielded no predictive value for SW response (AUC 0.61; p=0.302). Although SW benefit was higher in patients with QRSd≥150ms than with QRSd<150ms, this did not reach significance (+43±47% vs. +30±43%, p=0.435). Normalizing baseline QRSd relative to the following measures of conduction path length resulted in a significant correlation with SW change during CRT: QRSd/LVEDV (R 0.49; p=0.005, see figure 2B); QRSd/LVESV (R 0.57; p=0.001); QRSd/LV length (R 0.38; p=0.034) and QRSd/LV diameter (R 0.52; p=0.002). Although QRSd/LV mass showed a positive trend with SW change, it did not reach significance (R 0.33; p=0.063). ROC curve analysis revealed that all adjusted measures were significant predictors of SW response. QRSd/LVEDV (AUC 0.79; p=0.006), predicted SW response with a 80% sensitivity and 83% specificity at a cut-off value of 0.52.

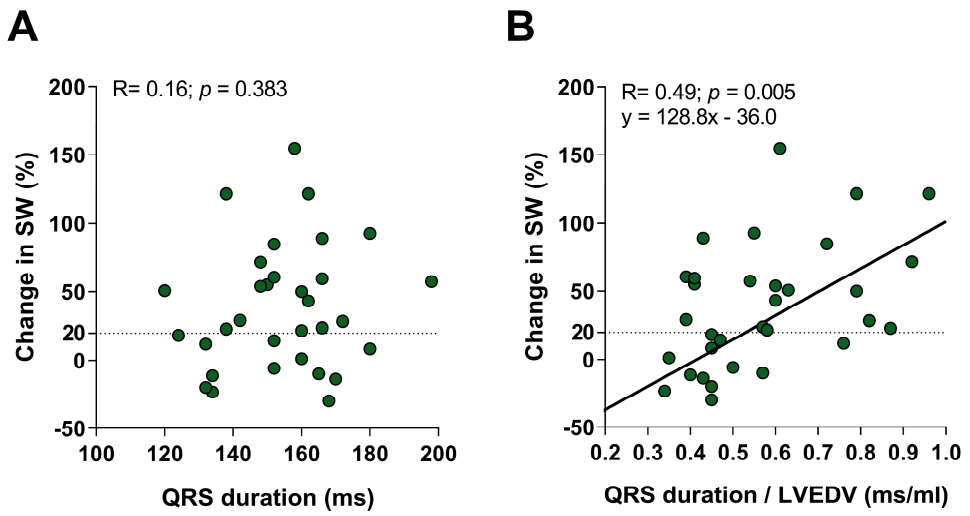


Figure 2 shows scatter plots illustrating (A) no significant correlation between unadjusted QRS duration and acute strokework (SW) changes during CRT; and (B) the positive correlation between QRS duration normalized to left ventricular end-diastolic volume (QRS/LVEDV), and acute SW changes during CRT.

Determinants of CRT response

In the present study, NIMCP patients achieved a non-significant higher SW change compared to ICMP patients (+49±44% vs. +28±46%; p=0.206, figure 3A). In seven (44%) ICMP patients scar was located in the posterolateral wall, these

patients showed less SW gain compared to ICMP patients without posterolateral scar although this did not reach significance in this small subgroup (+7±29% vs. +45±51%, p=0.079). ICMP patients with posterolateral scar, however, showed significantly less SW improvement compared to NICMP patients (+7±29% vs. +49±44%, p=0.032). Furthermore, scar size was significantly correlated with acute SW response (R -0.36; p=0.041, figure 3B). Subgroup analysis by gender did show a statistically significant difference in acute response to CRT with a higher SW gain in women compared to men (+62±49% vs. +24±38%; p=0.019, figure 3C). Multivariate regression analysis including QRSd/LVEDV, aetiology, scar size and gender in the model revealed QRSd/LVEDV to be the only independent predictor of SW response. The same results were found for QRSd/LVESV; QRSd/LV length and QRSd/LV diameter.

DISCUSSION

The present study demonstrates that in CRT candidates LV dimensions are positively correlated with QRSd, but also inversely related to acute pump function improvement during CRT (i.e. larger LV dimensions result in lower response to CRT). Moreover, in the present study baseline QRSd was not found to be related to acute response to CRT. Normalization of QRSd to LV dimension, however, yielded a strong correlation with CRT response.

In line with previous reports, a large variation in LV size was found in our group of CRT patients.(2-4,6-9,20) Chan and colleagues found several CMR-derived LV anatomical measurements (including LVEDV) to be positively related with QRSd, both in LBBB and narrow QRS complex patients.(4) Their findings agree with ours, showing that differences in LV size (i.e. differences in conduction path length) significantly contribute to the variation in QRSd among HF patients with LBBB. Despite this positive correlation, an inverse relation was found between LV dimensions and acute response to CRT which is also in line with earlier reports.(6,8,9) This paradox of dimension mediated increase in QRSd resulting in decreased CRT response suggests conduction path length to be an important confounder in the assessment of electrical dyssynchrony which should be corrected for.

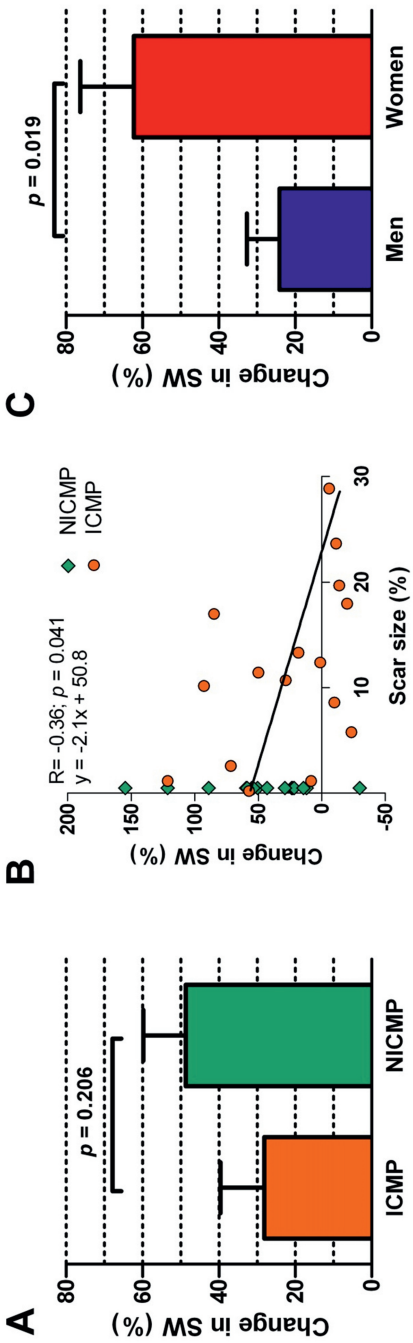


Figure 3 shows bar charts and scatter plot illustrating that (A) non-ischemic cardiomyopathy (NICMP) patients achieve higher SW changes compared to ischemic cardiomyopathy (ICMP) patients although this did not reach statistical significance; (B) scar size itself was negatively correlated with acute strokework (SW) changes during CRT; (C) CRT results in significant more strokework (SW) increase in women than in men.

In contrast to unadjusted baseline QRSd, baseline QRSd normalized to LV dimension (i.e. QRSd divided by LV dimension) strongly correlates with acute pump function improvement by CRT. Similar outcomes were found irrespective of the measure chosen for LV dimension (LV length, LV diameter, LVEDV, LVESV). Normalization of QRSd for conduction path length results in a measure of myocardial conduction velocity, with higher values indicating lower conduction velocity. These findings therefore suggest that myocardial conduction velocity rather than increased path length mainly determines response to CRT. Typically, measures of conduction velocity are expressed as distance over time but we chose time over distance to provide a modification of the traditional QRSd marker and to overcome the issue of volume over time not being an actual measure of velocity.

Several other parameters for prediction of response to CRT have been reported, including scar size, etiology of CMP and gender.(21-23) Although the present study is fairly small, both scar size and gender were found to be significantly related to CRT response, and NICMP patients showed a larger but not statistically significant response to CRT compared to ICMP patients (figure 3). Scar size and etiology of CMP might relate to the same mechanism of non-recruitable tissue, rendering patients with ICMP/larger scar size less amenable to the effects of CRT.(21) Gender differences in response to CRT might also be partly attributed to underlying etiology, since females included in CRT studies predominantly suffer from NICMP whereas males more often have a history of ICMP.(24) This was also found in the present study with 63% of patients in the NICMP group being female, in contrast to only 13% in the ICMP group. However, conduction velocity and conduction path length might also play a role since heart size is generally smaller in females. Assuming a normal conduction velocity independent of gender,(25) smaller (female) hearts will typically lead to shorter QRS duration. In patients eligible for CRT, however, using an identical QRSd cut-off value (120 ms) for men and women will lead to selection of female hearts in poorer conduction. In other words, female (smaller) hearts with a QRS duration of >120 ms will have slower conduction velocity (i.e. those hearts are sicker) compared to male hearts, and might therefore more amenable for successful treatment with CRT.

In the present study, analysis in a multivariate model of aetiology, scar size and gender together with QRSd/LVEDV showed the latter to be the only independent predictor of SW response. This finding suggests QRSd/LVEDV to be a rather robust marker, underlining the possible importance of conduction velocity as a pivotal marker of CRT response.

There are several limitations that have to be considered. First, this is a retrospective study with a small number of patients and future studies with larger patient numbers and with standardized long-term follow up will be needed to confirm our present findings. Secondly, several measures of the LV are used as surrogate markers for travel distance of the wave front over the LV. Although these measures do not reflect actual travel distance, they all show similar results suggesting the normalization to be rather robust. Further, for definition of complete LBBB the criteria according to the ESC guidelines were used whereas the stricter Strauss criteria for true-LBBB currently receive increasing interest.(26) In the present study 22 patients fulfilled the Strauss criteria. This subset showed a trend towards higher SW increase compared to non-Strauss LBBB patients, and similar effects of normalizing QRSd were found as for the entire study group. Finally, measuring pump function (SW) changes during CRT using the conductance catheter warrants careful data acquisition as extensively discussed elsewhere.(11) Nevertheless, using this technique acute changes in SW have proven to be strongly related to long-term outcome.(13)

CONCLUSION

In conclusion, the present study suggests that myocardial conduction velocity rather than increased path length mainly determines response to CRT. Thus, normalization of QRS duration for LV dimension might result in improved patient selection for CRT. This hypothesis will have to be addressed in future studies, including assessment of long term response to CRT.

REFERENCES

1. Kang SH, Oh IY, Kang DY, Cha MJ, Cho Y, Choi EK, et al. Cardiac resynchronization therapy and QRS duration: systematic review, meta-analysis, and meta-regression. J Korean Med Sci 2015 Jan;30(1):24-33.
2. De Winter O., Van de Veire N, Van Heuverswijn F., Van Pottelberge G., Gillebert T.C., De Sutter J. Relationship between QRS duration, left ventricular volumes and prevalence of nonviability in patients with coronary artery disease and severe left ventricular dysfunction. Eur J Heart Fail 2006 May;8(3):275-7.
3. Stewart RA, Young AA, Anderson C, Teo KK, Jennings G, Cowan BR. Relationship between QRS duration and left ventricular mass and volume in patients at high cardiovascular risk. Heart 2011 Nov;97(21):1766-70.
4. Chan DD, Wu KC, Loring Z, Galeotti L, Gerstenblith G, Tomaselli G, et al. Comparison of the relation between left ventricular anatomy and QRS duration in patients with cardiomyopathy with versus without left bundle branch block. Am J Cardiol 2014 May 15;113(10):1717-22.
5. Hakacova N, Steding K, Engblom H, Sjogren J, Maynard C, Pahlm O. Aspects of left ventricular morphology outperform left ventricular mass for prediction of QRS duration. Ann Noninvasive Electrocardiol 2010 Apr;15(2):124-9.
6. Antonio N, Teixeira R, Coelho L, Lourenco C, Monteiro P, Ventura M, et al. Identification of 'super-responders' to cardiac resynchronization therapy: the importance of symptom duration and left ventricular geometry. Europace 2009 Mar;11(3):343-9.
7. Carluccio E, Biagioli P, Alunni G, Murrone A, Pantano P, Biscottini E, et al. Presence of extensive LV remodeling limits the benefits of CRT in patients with intraventricular dyssynchrony. JACC Cardiovasc Imaging 2011 Oct;4(10):1067-76.
8. Diaz-Infante E, Mont L, Leal J, Garcia-Bolao I, Fernandez-Lozano I, Hernandez-Madrid A, et al. Predictors of lack of response to resynchronization therapy. Am J Cardiol 2005 Jun 15;95(12):1436-40.
9. Gradaus R, Stuckenborg V, Loher A, Kobe J, Reinke F, Gunia S, et al. Diastolic filling pattern and left ventricular diameter predict response and prognosis after cardiac resynchronisation therapy. Heart 2008 Aug;94(8):1026-31.
10. de Roest GJ, Wu L, de Cock CC, Hendriks ML, Delnoy PP, van Rossum AC, et al. Scar tissue-guided left ventricular lead placement for cardiac resynchronization therapy in patients with ischemic cardiomyopathy: an acute pressure-volume loop study. Am Heart J 2014 Apr;167(4):537-45.
11. de Roest GJ, Allaart CP, de Haan S, Hendriks ML, Bronzwaer JGF, van Rossum AC, et al. Effects of QRS Duration and Pacing Location on Pressure-Volume Loop Evaluation of Cardiac Resynchronization Therapy in End-Stage Heart Failure. The American Journal of Cardiology 2011 Dec 1;108(11):1581-8.
12. de Roest GJ, Wu L, de Cock CC, Delnoy PP, Hendriks ML, van Rossum AC, et al. Bifocal left ventricular stimulation or the optimal left ventricular stimulation site in cardiac resynchronization therapy: a pressure-volume loop study. Europace 2016 Jul;18(7):1030-7.
13. de Roest GJ, Allaart CP, Kleijn SA, Delnoy PP, Wu L, Hendriks ML, et al. Prediction of long-term outcome of cardiac resynchronization therapy by acute pressure-volume loop measurements. European Journal of Heart Failure 2012 Nov 25.

14. de Roest G, Knaapen P, Götte M, Hendriks T, Allaart C, de Cock C, et al. Stroke work or systolic dP/dt_{max} to evaluate acute response to cardiac resynchronization therapy: are they interchangeable? European Journal of Heart Failure 2009 Jul 1;11(7):706-8.
15. Brignole M, Auricchio A, Baron-Esquivias G, Bordachar P, Boriani G, Breithardt OA, et al. 2013 ESC Guidelines on cardiac pacing and cardiac resynchronization therapy. European Heart Journal 2013 Aug 1;34(29):2281-329, Web Table 11.
16. Rickham P.P. Human experimentation. Code of ethics of the world medical association. Declaration of Helsinki. Br Med J 1964 Jul 18;2(5402):177.
17. Flett AS, Hasleton J, Cook C, Hausenloy D, Quarta G, Ariti C, et al. Evaluation of techniques for the quantification of myocardial scar of differing etiology using cardiac magnetic resonance. JACC Cardiovasc Imaging 2011 Feb;4(2):150-6.
18. Bogaard MD, Doevendans PA, Leenders GE, Loh P, Hauer RN, van WH, et al. Can optimization of pacing settings compensate for a non-optimal left ventricular pacing site? Europace 2010 Sep;12(9):1262-9.
19. Thibault B, Dubuc M, Karst E, Andrade J, Dyrda K, Guerra PG, et al. Design of an acute dP/dt hemodynamic measurement protocol to isolate cardiac effect of pacing. J Card Fail 2014 May;20(5):365-72.
20. van Bommel RJ, Borleffs CJ, Ypenburg C, Marsan NA, Delgado V, Bertini M, et al. Morbidity and mortality in heart failure patients treated with cardiac resynchronization therapy: influence of pre-implantation characteristics on long-term outcome. Eur Heart J 2010 Nov;31(22):2783-90.
21. Chalil S, Foley PW, Muyhaldeen SA, Patel KC, Yousef ZR, Smith RE, et al. Late gadolinium enhancement-cardiovascular magnetic resonance as a predictor of response to cardiac resynchronization therapy in patients with ischaemic cardiomyopathy. Europace 2007 Nov;9(11):1031-7.
22. Cheng YJ, Zhang J, Li WJ, Lin XX, Zeng WT, Tang K, et al. More favorable response to cardiac resynchronization therapy in women than in men. Circ Arrhythm Electrophysiol 2014 Oct;7(5):807-15.
23. van Bommel RJ, Bax JJ, Abraham WT, Chung ES, Pires LA, Tavazzi L, et al. Characteristics of heart failure patients associated with good and poor response to cardiac resynchronization therapy: a PROSPECT (Predictors of Response to CRT) sub-analysis. Eur Heart J 2009 Oct;30(20):2470-7.
24. Martinez-Selles M, Doughty RN, Poppe K, Whalley GA, Earle N, Tribouilloy C, et al. Gender and survival in patients with heart failure: interactions with diabetes and aetiology. Results from the MAGGIC individual patient meta-analysis. Eur J Heart Fail 2012 May;14(5):473-9.
25. Taneja T, Mahnert BW, Passman R, Goldberger J, Kadish A. Effects of sex and age on electrocardiographic and cardiac electrophysiological properties in adults. Pacing Clin Electrophysiol 2001 Jan;24(1):16-21.
26. Migliore F, Baritussio A, Stabile G, Reggiani A, D'Onofrio A, Palmisano P, et al. Prevalence of true left bundle branch block in current practice of cardiac resynchronization therapy implantation. J Cardiovasc Med (Hagerstown) 2016 Jul;17(7):462-8.

Chapter 3

Size Matters: Normalization of QRS Duration to Left Ventricular Dimension Improves Prediction of Long-term Cardiac Resynchronization Therapy Outcome

Circ Arrhythmia Electrophysiology 2018;11:e006767

Alwin Zweerink
Daniel J. Friedman
Igor Klem
Peter M. van de Ven
Caitlin Vink
P. Stefan Biesbroek
Steen M. Hansen
Kasper Emerek
Raymond J. Kim
Albert C. van Rossum
Brett D. Atwater
Robin Nijveldt
Cornelis P. Allaart

ABSTRACT

Aims: In patients with left bundle branch block (LBBB), QRS duration (QRSd) depends on left ventricular (LV) dimension. Previously, we demonstrated that normalizing QRSd to LV dimension, to adjust for variations in LV size, improved prediction of hemodynamic response to cardiac resynchronization therapy (CRT). In addition, sex specific differences in CRT outcome have been attributed to normalized QRSd. The present study evaluates the effect of normalization of QRSd to LV dimension on prediction of survival after CRT implantation.

Methods: In this two-center study, we studied two-hundred-fifty heart failure patients with LV ejection fraction ≤35% and QRSd ≥120ms who underwent cardiac magnetic resonance (CMR) imaging before CRT implantation. LV end-diastolic volumes (LVEDV) were used for QRSd normalization (i.e. QRSd/LVEDV). The primary endpoint was a combined endpoint of death, LV assist device or heart transplantation.

Results: During a median follow-up of 3.9 years, 79 (32%) patients reached the primary endpoint. Using univariable Cox regression, unadjusted QRSd was unrelated to CRT outcome (p=0.116). In contrast, normalized QRSd was a strong predictor of survival (HR 0.81 per 0.1 ms/ml, p=0.008). Women demonstrated higher normalized QRSd than men (0.62±0.17 ms/ml vs. 0.55±0.17 ms/ml; p=0.003) and showed better survival after CRT (HR 0.52; p=0.018). A multivariable prognostic model included normalized QRSd together with age, atrial fibrillation, renal function and heart failure etiology whereas sex, diabetes mellitus, strict LBBB morphology and LVEDV were expelled from the model.

Conclusions: Normalization of QRSd to LV dimension improves prediction of survival after CRT implantation. In addition, sex-specific differences in CRT outcome might be attributed to the higher QRSd/LVEDV ratio that was found in selected women, indicating more conduction delay.

INTRODUCTION

Cardiac Resynchronization Therapy (CRT) improves survival of patients with heart failure and left bundle branch block (LBBB).(1-3) Guideline recommendations for CRT primarily depend on QRS duration (QRSd) and QRS morphology, with a higher class of recommendation for patients with QRSd ≥150ms and LBBB morphology.(4,5) Patient selection by guideline criteria, however, is imperfect as a substantial portion of the patients with a class I indication for CRT derive little to no benefit from the therapy.(6) Despite substantial efforts to improve patient selection for CRT, QRSd remains a pivotal predictor of the effect of CRT on clinical outcome.(7) Both in narrow QRS complex and LBBB, however, LV size influences QRSd with more extensive LV dilation leading to longer QRSd.(8) Although this LV dimension induced increase in QRSd is expected to result in improved CRT benefit, advanced LV dilation is actually associated with poor CRT outcome.(9,10)

Previously, we demonstrated that normalizing QRSd to LV dimension improved prediction of CRT response measured by pressure-volume loops.(11) In this proof-of-concept study, unadjusted QRSd was unrelated to hemodynamic changes during CRT whereas normalization of QRSd to LV dimension resulted in a good correlation with acute hemodynamic CRT response. In addition, women achieved more pump function improvement during CRT compared to men since heart size is generally smaller in women. In a subsequent study by Varma et al., sex-specific differences in the QRSd-response relationship resolved after QRSd normalization for LV dimension.(12) The present study evaluates the effect of QRSd normalization to LV dimension on the prediction of survival after CRT implantation.

METHODS

Study population

Patients who underwent CMR examination within twelve months prior to CRT implantation between 2005 and 2017 were retrospectively included in this two-center observational study (VU University Medical Center, Amsterdam, the Netherlands; Duke University Hospital, Durham, North Carolina, USA). Inclusion criteria were moderate to severe heart failure (NYHA class II-IV), LV ejection fraction (LVEF) ≤35% measured by CMR and QRSd ≥120ms (strict LBBB or

intraventricular conduction delay (IVCD)). Exclusion criteria were age under 18 years, right bundle branch block (RBBB) and upgrade procedures from other implanted non-CRT devices. Clinical data were collected from medical records. The electrocardiogram (ECG) before CRT implantation was used for manual QRSd measurements and assessment of QRS morphology. The presence of strict LBBB morphology was assessed by two independent specialists using the Strauss criteria: QRSd ≥130ms (women) or ≥140ms (men), QS or rS in V1-V2, mid-QRS notching or slurring in at least two contiguous leads (V1, V2, V5, V6, I and aVL).(13) Included patients who did not meet Strauss criteria were classified as IVCD. LV volumes, mass, diameter and length were measured on short-axis CMR cine images and left ventricular end-diastolic volume (LVEDV) was used as primary measure for LV dimension since this is the most comprehensive measure of LV size without influence of contraction. QRSd was normalized to LV dimension (i.e. QRSd divided by LVEDV). The primary endpoint was a combined endpoint of all-cause mortality, left ventricular assist device (LVAD) or heart transplantation (HTx). The local medical ethics committee of the VU University Medical Center and Duke University Medical Center approved the study protocol. The investigation conforms to the principles outlined in the Declaration of Helsinki. As the data of this study is also used for future publications, the data, analytic methods, and study materials will not be made available to other researchers for purposes of reproducing the results or replicating the procedure.

Image acquisition: CMR imaging

Patients underwent CMR examination at VU University Medical Center (Amsterdam, the Netherlands) or at Duke Cardiovascular Magnetic Resonance Center (Durham, North Carolina, USA), on a clinical 1.5 Tesla MR scanner (Magnetom Sonata/Avanto, Siemens, Erlangen, Germany) with dedicated phased array cardiac receiver coil. Standard CMR cine images were acquired using a retrospectively ECG-gated balanced steady-state free-precession (SSFP) sequence during end-expiratory breath holding. A stack of 8-12 consecutive short-axis cine images was acquired covering the full LV. Typical imaging parameters were: slice thickness 5mm, slice gap 5mm, voxel size 1.3*1.6mm and temporal resolution <50ms. Subsequently, LV dimensions, function and mass were quantified. LVEDV, LV end-systolic volume (LVESV), LVEF and LV mass were derived from the short-axis images using commercially available software on

locally available workstations. LV length was determined from the four chamber long-axis view between the apex and the middle of the mitral valve annulus in end-diastole. LV diameter was measured in the mid short-axis slice in end-diastole. Patients were classified as having ischemic cardiomyopathy (ICMP) in case of a history of myocardial infarction, percutaneous coronary intervention (PCI), or coronary artery bypass grafting (CABG) accompanied by associated findings on CMR.

Image acquisition: echocardiography

Part of the patients underwent additional echocardiographic examination before CRT implantation. LV quantification was performed by experienced operators in accordance with the guidelines of the American Society of Echocardiography and European Association of Echocardiography.(14) Typically, echocardiographic volumes were obtained using the biplane Simpson's method. If image quality of the apical two chamber view was deemed unsuitable for reliable biplane volume assessment, solely the apical four chamber view was used instead.

Statistics

Continuous variables are expressed as mean ± standard deviation (SD) in case normally distributed or median and interquartile range otherwise. Categorical variables are presented as absolute numbers and percentages. The independent-samples t-test and a Mann-Whitney test were used to compare means and distributions of continuous variables between groups. Pearson's and Spearman correlations were calculated as a measure of association depending on whether distribution was normal or not. Time to occurrence of the combined endpoint was compared between groups using Kaplan-Meier curve analysis and a log-rank test. The association between baseline parameters and time to the combined endpoint was tested using univariable Cox regression analysis with strength expressed by hazard ratios (HR). Parameters that showed a statistically significant effect on survival in univariable analysis were entered in a multivariable Cox proportional hazards models, using a backward elimination procedure. Assumptions of the Cox model were tested by the visual assessment of log-minus-log plots. Beta-coefficients of the remaining predictors in the model were used to calculate a composite risk score. Internal validation of the predictive model was performed by bootstrap analysis of 50 samples with

variable selection repeated for each bootstrap sample. Discriminative ability of the model was quantified by the receiver operating characteristic (ROC) estimated on the original dataset on which the model was build and an ROC corrected for over-optimism calculated as part of the internal validation procedure. A correction factor for the beta-coefficients in the final risk score model was applied to prevent over-optimism when used in new patients. Patients were then divided in quartiles based on their risk score to estimate the HR of each quartile relative to the first quartile (reference group). The commercially available Statistical Package for Social Sciences software (IBM SPSS Statistics for Windows, Version 20.0. Armonk, NY, USA) was used for statistical analysis and internal validation was done using the 'rms'-package version 5.1-2 in R version 3.4.2 (R Foundation for Statistical Computing, Vienna, Austria). A P-value of <0.05 was considered statistically significant.

RESULTS

Two-hundred-fifty patients (34% female, median age 67 years) were included. After screening a total of 372 patients who underwent a pre-implantation CMR examination, 26 patients were excluded from the present analysis based on a LVEF >35%, 41 patients because of RBBB, 42 patients with QRSd <120ms, 9 patients who were asymptomatic (NYHA class 1), and 4 patients because of missing data. A detailed description of the patient characteristics is given in table 1. Median time between CMR examination and CRT implantation was 43 (5–114) days. Over a median follow-up time of 3.9 (1.8–6.3) years, 79 (32%) patients reached the combined endpoint of all-cause mortality, LVAD or HTx.

Table 1. Patient characteristics

Variables	Total group (n=250)	QRSd/LVEDV <0.52ms/ml (n=100)	QRSd/LVEDV ≥0.52ms/ml (n=150)	p-value
Age (years)	67 (59–74)	64 (57–72)	69 (59–75)	0.105
Sex (n, % female)	86 (34%)	24 (24%)	62 (41%)	0.005
NYHA class (n, %)				
Class II	74 (30%)	26 (26%)	48 (32%)	
Class III	172 (69%)	73 (73%)	99 (66%)	
Class IV	4 (2%)	1 (1%)	3 (2%)	0.465
Device				
ICD function (CRT-D) (n, %)	240 (96%)	96 (96%)	144 (96%)	1.000
Quadripolar LV lead (n, %)	47 (19%)	19 (19%)	28 (19%)	0.947
Medical history (n, %)				
Atrial fibrillation	49 (20%)	18 (18%)	31 (21%)	0.603
Diabetes Mellitus	58 (23%)	22 (22%)	36 (24%)	0.714
Hypertension	67 (27%)	27 (27%)	40 (27%)	0.954
Medication (n, %)				
Beta-blockers	209 (84%)	83 (83%)	126 (84%)	0.834
Diuretics	195 (78%)	78 (78%)	117 (78%)	1.000
ACE / ATII inhibitors	218 (87%)	89 (89%)	129 (86%)	0.487
Aldosterone antagonist	102 (41%)	40 (40%)	62 (44%)	0.934
ECG				
QRS duration (ms)	158 ± 22	156 ± 22	159 ± 21	0.342
QRS duration ≥150ms (n, %)	151 (60%)	54 (54%)	97 (65%)	0.091
Strict LBBB (Strauss) (n, %)	165 (66%)	58 (60%)	107 (73%)	0.034
Laboratory results				
creatinine (µmol/L)	97 (78–118)	101 (78–128)	97 (79–115)	0.198
Echocardiography*				
LVEDV (ml)	221 ± 81	284 ± 79	181 ± 52	<0.001
LVESV (ml)	168 ± 76	225 ± 74	131 ± 49	<0.001
LVEF (%)	25 ± 9	21 ± 7	28 ± 9	<0.001
CMR				
LVEDV (ml)	298 ± 93	379 ± 78	244 ± 55	<0.001
LVESV (ml)	234 ± 87	307 ± 77	185 ± 51	<0.001
LVEF (%)	23 ± 7	19 ± 6	25 ± 6	<0.001
LV diameter (mm)	74 ± 9	80 ± 8	69 ± 7	<0.001
LV length (mm)	105 ± 10	112 ± 8	100 ± 9	<0.001
LV mass (g)	155 ± 45	184 ± 45	136 ± 33	<0.001
Ischemic CMP (n, %)	84 (34%)	37 (37%)	47 (32%)	0.353
ECG + CMR				
LVEDV normalized QRS duration (ms/ml)	0.57 ± 0.18	0.42 ± 0.07	0.68 ± 0.15	<0.001

NYHA, New York Heart Association class; CRT-D, cardiac resynchronization therapy with defibrillator function; LBBB, left bundle branch block; LVEDV, left ventricular end-diastolic volume; LVESV, left ventricular end-systolic volume; LVEF, left ventricular ejection fraction; CMP, cardiomyopathy;

* incompletely recorded, n=176

Normalization of QRS duration to LV dimension

Mean QRSd was 158±22ms, 151 (60%) patients had QRSd ≥150ms. CMR-derived measures of LV dimension showed large variation (LVEDV 298±93ml; LVESV 234±87ml; LV diameter 74±9mm; LV length 105±10mm; LV mass 155±45g) and were positively correlated with QRSd (LVEDV and LVESV, R 0.32; LV diameter, R 0.29; LV length, R 0.25; LV mass, R 0.36; all p<0.001). An inverse relationship was found between LV volumes and CRT survival (HR 1.03 per 10ml increase in either LVEDV or LVESV; p=0.019 for both analyses). Both LV diameter and length were also inversely related with CRT outcome (HR 1.03 per mm; p=0.015 and HR 1.03 per mm; p=0.034, respectively). LV mass, however, was unrelated with CRT survival (HR 1.04 per 10g; p=0.121). Univariable Cox regression analysis showed that QRSd on a continuous scale was unrelated to the combined endpoint, see table 2. Normalization of QRSd to LVEDV, on the other hand, resulted in a significant association with the primary endpoint (HR 0.81 per 0.1 ms/ml; p=0.008). ROC curve analysis revealed an optimal cut-off value (by maximizing the Youden's index) of 0.52ms/ml for predicting survival free of LVAD or HTx. Patients with QRSd/LVEDV <0.52ms/ml demonstrated a two-fold higher likelihood of death, LVAD, or HTx after CRT implantation compared to patients with QRSd/LVEDV ≥0.52ms/ml (HR 2.13; p=0.001) as illustrated in figure 1A. Patient stratification by unadjusted QRSd using the 150ms criterion, incorporated into CRT implantation guideline recommendations, showed weaker discriminative value for CRT survival (HR 1.64; p=0.030) as illustrated in figure 1B. Similar results were found for QRSd/LVESV, QRSd/LV diameter, QRSd/LV length and QRSd/LV mass, see table 3.

Table 2. Univariable and multivariable Cox regression analysis for the primary endpoint: death / LVAD / HTx

Variables (n=250)	Univariable analysis		Multivariable analysis		
	HR (95% CI)	P-value	HR (95% CI)	ß	P-value
Age (per year)	**1.05 (1.02–1.07)**	**<0.001**	**1.03 (1.00–1.06)**	**0.0304**	**0.026**
Sex (female)	0.52 (0.30–0.89)	0.018	-	-	-
NYHA class (per class)	1.10 (0.66–1.82)	0.714			
Device					
ICD function (i.e. CRT-D)	0.51 (0.20–1.25)	0.142			
Quadripolar LV lead	0.91 (0.36–2.30)	0.842			
Medical history					
Atrial fibrillation	**2.07 (1.27–3.35)**	**0.003**	**1.74 (1.05–2.90)**	**0.5549**	**0.033**
Diabetes Mellitus	1.72 (1.08–2.75)	0.024	-	-	-
Hypertension	1.25 (0.77–2.03)	0.372			
Medication					
Beta-blockers	0.94 (0.54–1.65)	0.830			
Diuretics	0.83 (0.50–1.39)	0.481			
ACE / ATII inhibitors	0.76 (0.41–1.41)	0.381			
Aldosteron antagonist	1.00 (0.63–1.60)	0.987			
ECG					
QRS duration (per 10ms)	0.91 (0.82–1.02)	0.116			
Strict LBBB (Strauss)	0.54 (0.34–0.86)	0.009	-	-	-
Laboratory results					
creatinine (per 10µmol/L)	**1.06 (1.04–1.08)**	**<0.001**	**1.06 (1.04–1.08)**	**0.0057**	**<0.001**
CMR					
LVEDV (per 10ml)	1.03 (1.00–1.05)	0.019	-	-	-
LVESV (per 10ml)	1.03 (1.00–1.05)	0.019			
LVEF (per %)	0.97 (0.94–1.00)	0.062			
LV diameter (per mm)	1.03 (1.01–1.06)	0.015			
LV length (per mm)	1.03 (1.00–1.05)	0.034			
LV mass (per 10g)	1.04 (0.99–1.09)	0.121			
Ischemic CMP (n, %)	**2.15 (1.38–3.34)**	**0.001**	**2.12 (1.29–3.47)**	**0.7437**	**0.003**
ECG + CMR					
LVEDV normalized QRS duration (per 0.1 ms/ml)	**0.81 (0.70–0.95)**	**0.008**	**0.83 (0.71–0.97)**	**1.8703**	**0.016**

The "-" sign indicates that parameters were included as candidate predictors in multivariable analysis but removed in the backward elimination procedure and therefore do not appear in the final model (i.e. non-significant). For other abbreviations, see table 1.

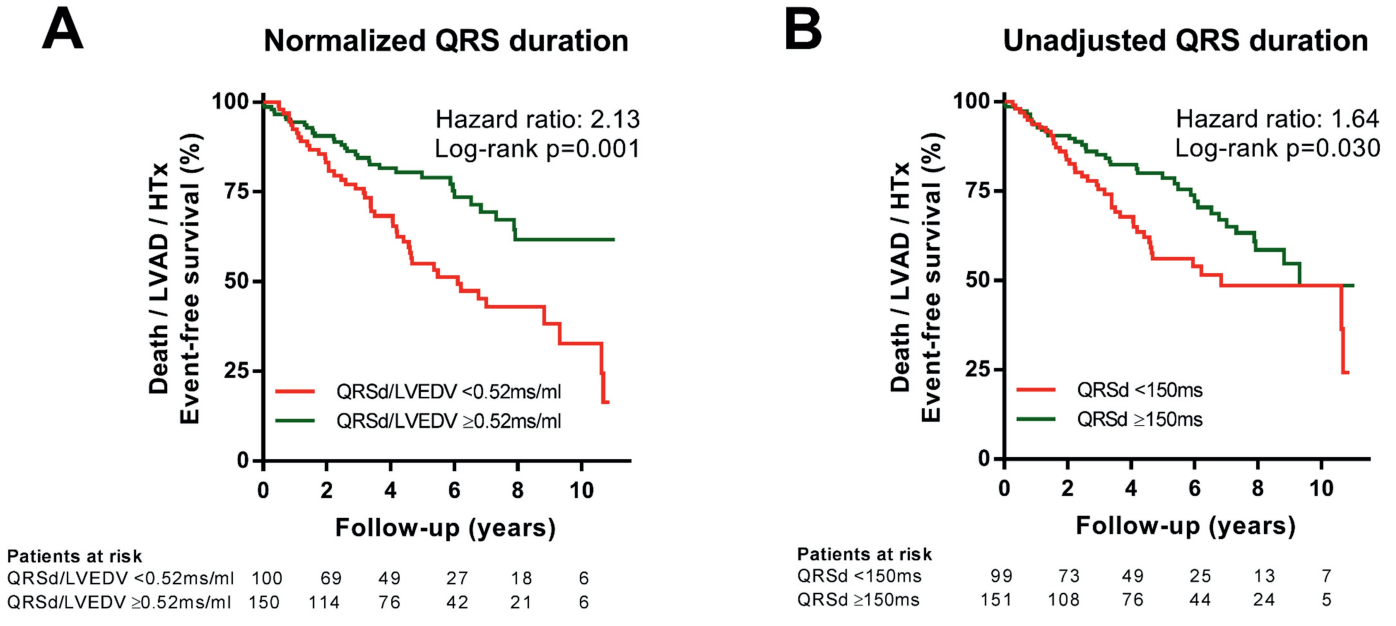


Figure 1: Kaplan-Meier curve analysis for patient stratification by LVEDV normalized QRS duration using CMR imaging and unadjusted QRS duration. Kaplan-Meier curves showing (A) stronger differentiation in outcome between groups stratified by normalized QRS duration at a cut-off value of 0.52ms/ml compared to (B) patients stratified by unadjusted QRSd at a cut-off value of 150ms.

Table 3. Normalization of QRSd to LVEDV and other metrics of LV size

Variables	Cox regression HR (95% CI)	p-value	Cut-off	# pos/neg	HR	p-value
Unadjusted QRSd (10 ms)	0.91 (0.82–1.02)	p=0.116	≥150	151/99	0.61	0.030
QRSd/LVEDV (0.1 ms/ml)	0.81 (0.70–0.95)	p=0.008	≥0.52	150/100	0.47	0.001
QRSd/LVESV (0.1 ms/ml)	0.88 (0.80–0.97)	p=0.008	≥0.69	141/109	0.53	0.006
QRSd/LV diameter (0.1 ms/mm)	0.89 (0.83–0.96)	p=0.002	≥2.01	176/74	0.48	0.001
QRSd/LV length (0.1 ms/mm)	0.87 (0.78–0.96)	p=0.007	≥1.40	175/75	0.52	0.004
QRSd/LV mass (0.1 ms/g)	0.91 (0.83–0.99)	p=0.028	≥0.90	191/59	0.57	0.021

Abbreviations, see table 1.

Patient stratification by unadjusted and normalized QRS duration

Normalization of QRSd to LVEDV resulted in a mean QRSd/LVEDV of 0.57±0.18ms/ml, 150 (60%) patients had QRSd/LVEDV ≥0.52ms/ml. Patients with QRSd/LVEDV ≥0.52ms/ml had similar QRSd compared to <0.52ms/ml patients (159±21ms vs. 156±22ms; p=0.342), but significantly smaller LVEDV (244±55ml vs. 379±78ml; p<0.001). These patients more often had strict LBBB morphology on their ECG (73% vs. 60%; p=0.034) whereas no differences in etiology were found between the groups (ICMP in 31% vs. 37%; p=0.353). Furthermore, patients with QRSd/LVEDV ≥0.52ms/ml were relatively more often women (41% vs. 24%; p=0.005). The stratification of patients by normalized QRSd compared to unadjusted QRSd is illustrated in figure 2. A total of 107 (43%) patients showed incongruent classification between both definitions. The percentage of positive test results per definition, however, remained identical (60%, both).

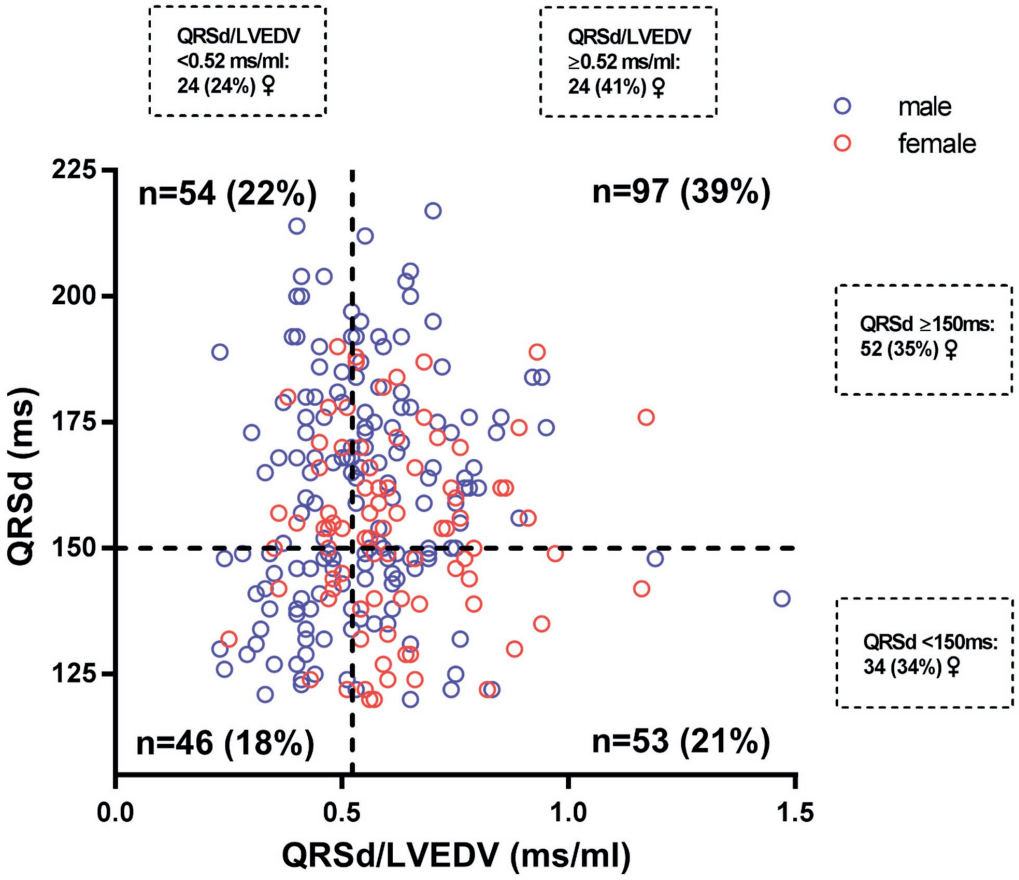


Figure 2: Scatter plot illustrating patient classification by unadjusted QRSd and QRSd normalized to LV dimension. A total of 107 (43%) patients showed incongruent classification (lower right and upper left section) between both definitions. The percentage of positive test results per definition, however, remained identical (60%, both). Female proportion was similar between QRSd ≥150ms and <150ms (35% vs. 34%, respectively), but relatively higher in QRSd/LVEDV ≥052.ms/ml compared to <052.ms/ml (41% vs. 24%, respectively).

Sex-specific differences

Comparing groups by sex, women demonstrated shorter QRSd compared to men (153±18ms vs. 160±23ms; p=0.016), but also had significantly smaller LVEDV (266±78ml vs. 315±95ms; p<0.001), see table S1 in the supplemental material. As a result, the QRSd/LVEDV ratio was higher in women than in men (0.62±0.17ms/ml vs. 0.55±0.17ms/ml; p=0.003), see figure 3. This finding was accompanied by a trend towards more frequent strict LBBB morphology in women (72% vs. 63%; p=0.058). Furthermore, women more often had NICMP than men (84% vs. 57%; p<0.001). Univariable analysis showed women to have a more favorable outcome compared to men (HR 0.52; p=0.018). In multivariable analysis, however, sex was no longer a predictor of the combined endpoint as shown in the next paragraph.

Prognostic model

Significant predictors in univariable Cox regression analysis were normalized QRSd as well as age, sex, atrial fibrillation, diabetes mellitus, strict LBBB morphology, creatinine level, LV dimensions (LVEDV; LVESV; LV diameter; LV length) and heart failure etiology. Multivariable Cox regression analysis revealed that normalized QRSd was an independent predictor of the combined endpoint together with age, atrial fibrillation, creatinine level and heart failure etiology whereas sex, diabetes mellitus, strict LBBB morphology and LVEDV were expelled from the model (table 2). Of the 250 patients included in the multivariable model, 16 cases (6%) were dropped due to missing values. Based on the standard errors, confidence intervals and beta-coefficients there were no signs of multi-collinearity. A composite risk score was calculated based on the ß-coefficients of all independent predictors. Discriminative ability of the model was good with an area under the ROC curve of 0.71. Internal validation using a bootstrap procedure showed that the area under the ROC curve remained fairly stable (0.67).

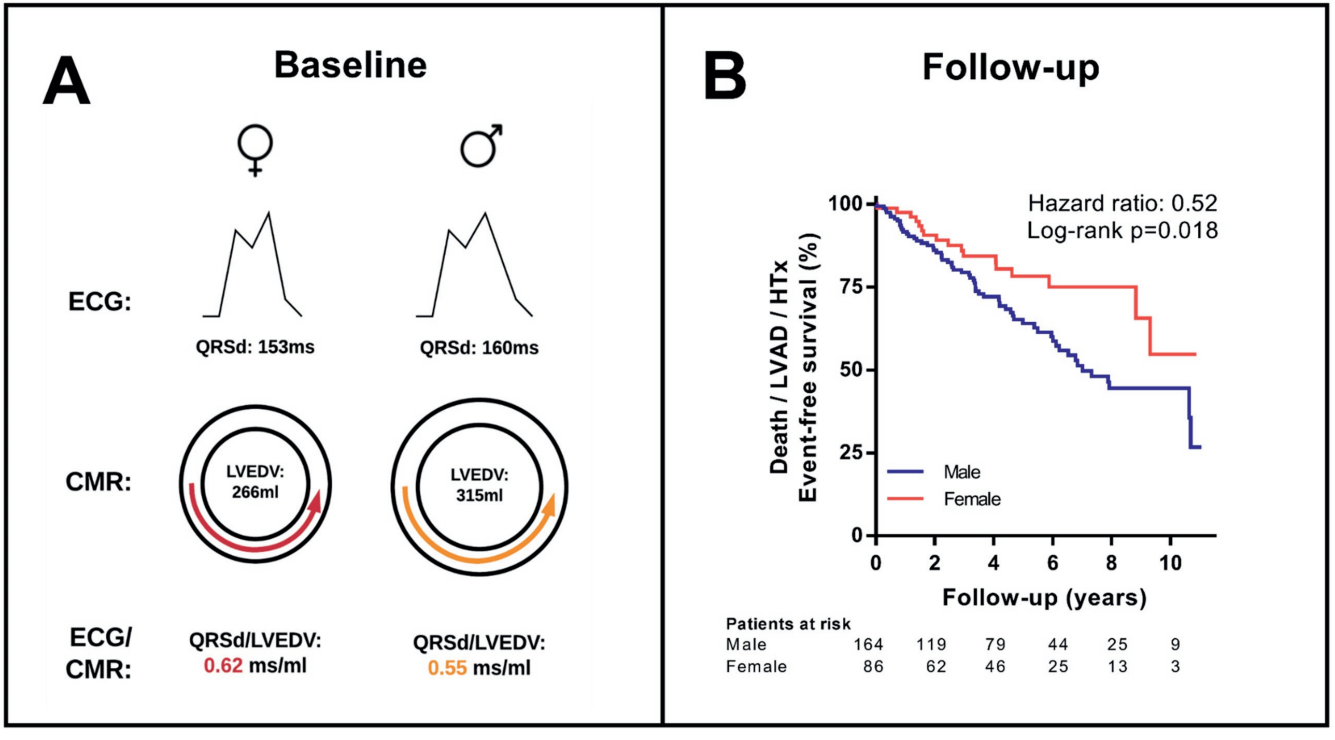
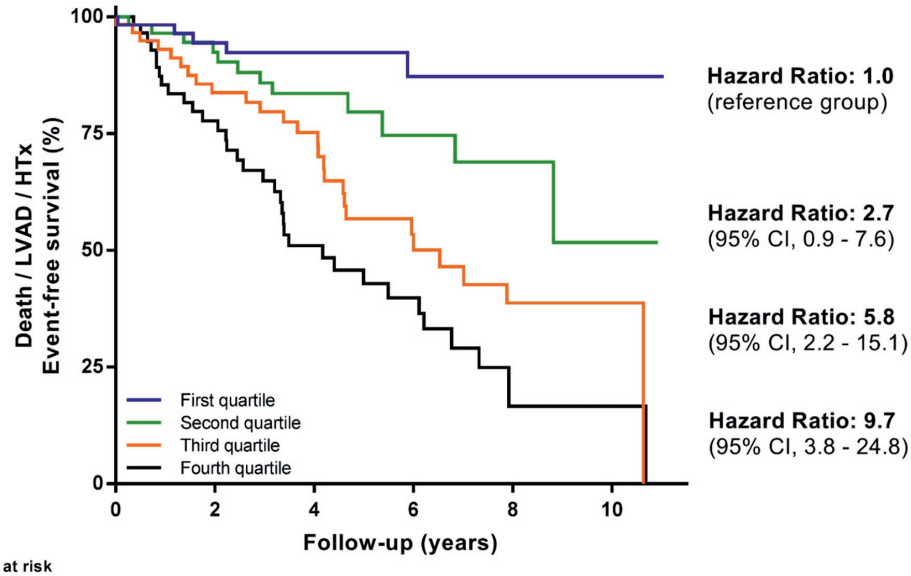


Figure 3: Sex differences and survival after CRT implantation. Women demonstrate shorter QRS duration (QRSd) than men, but also have substantially smaller left ventricular end-diastolic volumes (LVEDV). As a result, the QRSd/LVEDV ratio is higher in women.(A). Kaplan-Meier curves illustrating better survival after CRT implantation for women (red curve) compared to men (blue curve) (B).

Subsequently, a correction factor of 0.7491 was applied to all ß-coefficients to prevent over-optimism in an external cohort, resulting in the following final risk score: (0.02274 x age) + (0.41569 x atrial fibrillation) + (0.00429 x creatinine level) + (0.55707 x ischemic heart failure etiology) - (1.4010 x QRSd/LVEDV). Patients were divided in quartiles (first quartile: <0.97; second quartile 0.97–1.37; third quartile 1.38–1.86; fourth quartile >1.86) and survival rates were compared as illustrated in figure 4. Although there was no statistical difference in survival between the first and second quartile (HR 2.7; 95% CI, 0.9–7.6), patients in the third and fourth quartile showed significant higher mortality rates compared to the first quartile (HR 5.8; 95% CI, 2.2–15.1 and HR 9.7; 95% CI, 3.8–24.8, respectively).



Patients at risk

First quartile	60	46	37	18	10	5
Second quartile	60	44	28	16	10	3
Third quartile	60	45	32	16	11	3
Fourth quartile	59	38	21	13	2	2

Figure 4: Kaplan-Meier curve analysis for patient stratification by the composite risk score. Kaplan-Meier curves illustrating patient stratification by a composite risk score including normalized QRSd, age, atrial fibrillation, creatinine level and heart failure etiology. Patients in the first quartile yield the most favorable CRT survival (blue curve) whereas patients in the fourth quartile demonstrate the worst survival rates (black curve).

Echocardiography

Echocardiography within twelve months prior to CRT implantation was available in 176 (70%) patients. Median time between echocardiography and CRT implantation was 20 (1–77) days. Similar to CMR, echocardiographic measurements of LV dimension showed large variation (LVEDV 221±81ml) and were positively correlated with QRSd (R 0.34; p<0.001). An inverse relationship was found between LVEDV and CRT survival (HR 1.04 per 10ml increase; p=0.044). Whereas unadjusted QRSd was unrelated to CRT outcome (HR 0.89 per 10ms; p=0.087), normalization of QRSd to echocardiographic LVEDV resulted in a significant relation with CRT outcome (HR 0.88 per 0.1 ms/ml; p=0.043). Patients with QRSd/LVEDV <0.69ms/ml demonstrated two-fold higher likelihood of death, LVAD, or HTx after CRT implantation compared to patients with QRSd/LVEDV ≥0.69ms/ml (HR 2.11; p=0.008) as illustrated in figure 5.

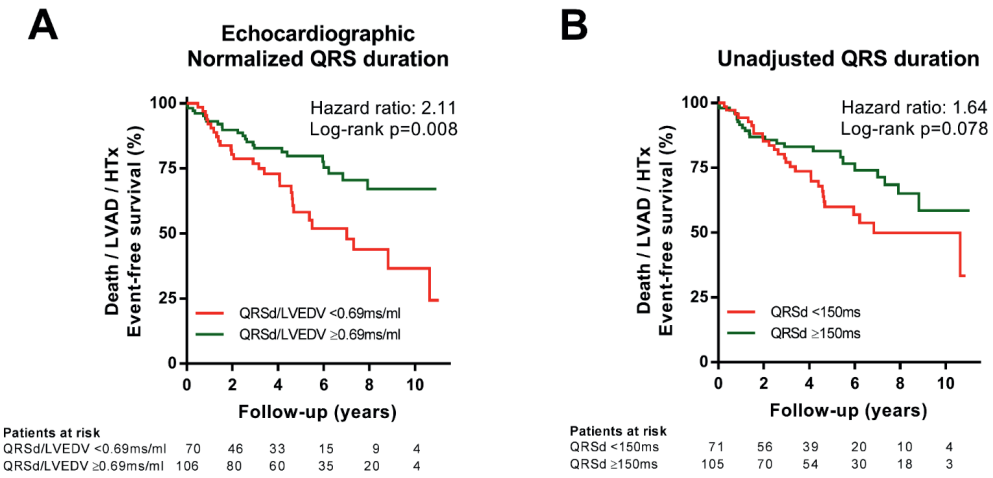


Figure 5: Kaplan-Meier curve analysis for patient stratification by LVEDV normalized QRS duration using echocardiography and unadjusted QRS duration. Echocardiography was used for QRSd normalization in a subset of 176 patients. Similar results were found compared to CMR with Kaplan-Meier curves showing (A) stronger differentiation in outcome between groups stratified by normalized QRS duration at a cut-off value of 0.69ms/ml compared to (B) patients stratified by unadjusted QRSd at a cut-off value of 150ms.

Additional statistical analyses

To test whether LVEDV was an effect modifier of QRSd, an interaction term was created and entered into a multivariable Cox model together with LVEDV and QRSd. The effect modifier term did not reach statistical significance, although a trend could be observed: interaction term HR 1.10 [1.00 – 1.21] per 1000 units increase in QRSd*LVEDV, p=0.051. In order to assess the marginal predictive value of normalized QRSd over LV size and unadjusted QRSd, change in chi-square (X^2) was observed after addition of normalized QRSd to a model with each of its components. Addition of normalized QRSd to a model with unadjusted QRSd significantly improved fit of the model (change X^2: 6.72; df=1; p=0.010). Addition of normalized QRSd to a model with LVEDV also increased fit of the model although this did not reach statistical significance (change X^2: 1.52; df=1; p=0.217). Normalization to other LV size metrics showed similar results with addition of normalized QRSd increasing the overall fit of the model (i.e. the ratio of QRSd relative to LV dimension adding new information).

DISCUSSION

The present study demonstrates that normalization of QRSd to LV dimension (LVEDV) improves prediction of survival free of LVAD or HTX after CRT implantation. Whereas QRSd was unrelated to CRT outcome in univariable regression analysis, normalization of QRSd to LVEDV showed to be a strong predictor of the combined endpoint. Using the ROC-curve derived optimal cut-off point, patients with shorter normalized QRSd (<0.52ms/ml) showed a two-fold higher mortality rate compared to patients with longer normalized QRSd (≥0.52ms/ml). Similar results were found for normalization to other CMR-derived metrics of LV size (diameter, length, mass) as well as echocardiographic LV quantification. Furthermore, sex-specific differences in CRT outcome may be attributed to the higher QRSd/LVEDV ratio that was found in selected women, indicating more conduction delay. Finally, normalized QRSd yielded prognostic value in a prognostic model together with age, atrial fibrillation, renal function and heart failure etiology. This model showed good discriminative ability with patients in the highest quartile demonstrating a nearly ten-fold higher likelihood to reach the combined endpoint compared to the lowest quartile.

Normalization of QRS duration to LV dimension

CRT aims to lower morbidity and mortality in patients with symptomatic heart failure and LBBB.(1-3) Although QRSd is incorporated into guideline recommendations for CRT patient selection, in the present study this parameter failed to predict LVAD, HTx or death after CRT implant. In line with previous findings, LV dimension influenced QRSd with more extensive LV dilation leading to longer QRSd.(8,11) Although QRSd prolongation is expected to result in increased CRT benefit, we found LV dimension to be inversely related to CRT survival, also in line with previous studies.(9-11) This paradox of dimension-mediated increase in QRSd, resulting in decreased CRT survival, suggests LV dimension to be an important confounder which should be corrected for in the assessment of LV dyssynchrony. This notion is supported by the main finding of the present study that normalization of QRSd to LVEDV resulted in a strong association with the combined endpoint (HR 0.81 per 0.1 ms/ml; p=0.008).

LV size quantification

Different metrics of LV size (volumes; diameter; length; mass) all showed similar results in relation to QRSd and CRT outcome. Moreover, normalization of QRSd to any metric of LV size improved correlation with CRT outcome. These results are completely in line with our proof-of-concept study measuring acute hemodynamic CRT response with pressure-volume loops.(11) In addition, we showed that echocardiographic volumes can be used for QRSd normalization (figure 5). Echocardiography holds the advantage of being more widely available in clinical practice compared to CMR imaging. Of note, cut-off values differed between modalities since LV volumes are generally underestimated by echocardiography.(15) In summary, normalization of QRSd to LV dimension improves prediction of CRT outcome irrespective of the choice of LV size metric or imaging modality used for quantification.

Patient stratification by unadjusted and normalized QRS duration

Previous studies showed that CRT candidates with narrow QRS complexes yield no benefit (or derived harm) from CRT.(16,17) Therefore, international guidelines use a QRSd entry criterion of 120ms (U.S.) or 130ms (European) before considering CRT.(4,5). The recommendation for CRT depends on QRS morphology and QRSd with a higher class of recommendation (i.e. class I

indication) for patients with LBBB morphology and QRSd ≥150ms. Although CRT landmark trials showed better outcome in patients with QRSd ≥150ms compared to patients with QRSd between 120 and 149 ms,(18) other studies could not reproduce these findings.(19,20) Our results indicate that there was a significant difference in CRT outcome between patients with QRSd <150ms and patients with QRSd ≥150ms (figure 1B). However, QRSd on a continuous scale was unrelated to the combined endpoint in univariable Cox regression analysis (table 2). After QRSd normalization, ROC curve analysis revealed an optimal cut-off value of 0.52ms/ml for predicting survival free of LVAD or HTx. This cut-off value is identical to the optimal cut-off value that we found previously to predict hemodynamic CRT response.(11) Since normalized QRSd reflects myocardial conduction properties with higher values indicating poorer conduction, patients with QRSd/LVEDV ≥0.52ms/ml are thought to have more delayed LV activation compared to patients with QRSd/LVEDV <0.52ms/ml. In line with this concept, patients with QRSd/LVEDV ≥0.52ms/ml more often had strict LBBB morphology (73 vs. 60%; p=0.034). QRSd/LVEDV ≥0.52ms/ml patients showed a more than two-fold better survival after CRT implantation compared to QRSd/LVEDV <0.52ms/ml patients as illustrated in figure 1A.

Mechanisms of activation delay

Different mechanisms may be accountable for delayed LV activation in LBBB. Theoretically, QRSd is dependent upon two components: myocardial conduction velocity and conduction path length. In case of a homogenous activation front, a high QRSd/LVEDV ratio indicates low conduction speed (i.e. slow cell-to-cell conduction) resulting from poor His-Purkinje conduction (i.e. true LBBB). However, increased QRSd/LVEDV ratio may also arise from functional lines of block causing inhomogeneous propagation of the activation front. A heterogeneous activation pattern increases conduction path length (and therefore activation delay) independent of LV size or conduction velocity. Auricchio et al. was the first to describe different LV activation patterns in patients with LBBB.(21) A ‘U-shaped’ conduction pattern with a line of conduction block between the septum and lateral wall was associated with favorable response to CRT when compared to a homogenous activation pattern.(22,23) Both mechanisms of slow conduction and functional block

support the concept of a greater substrate of electrical dyssynchrony that may be corrected by CRT.

Sex-specific differences

Although female sex is associated with favorable outcome after CRT implantation, the underlying mechanisms for this association remain largely unclarified.(24) A first contributing factor might be that women are more likely to have NICMP, which is associated with larger CRT response than ICMP.(25) Secondly, women more often demonstrate strict LBBB, also associated with favorable CRT outcome.(26) Perhaps the most striking difference between the male and female heart, is the difference in size with women demonstrating up to 20% smaller LV dimensions.(27) As a result, women have shorter QRSd compared to men.(28) In order to reach an identical QRSd value for men and women, female hearts will have more conduction delay compared to male hearts as illustrated in figure 3. This was reflected by a higher QRSd/LVEDV ratio that was found in women compared to men (0.62 vs. 0.55 ms/ml, respectively). In other words, using the same QRSd cut-off value for men and women might lead to under treatment of women whereas men might be subject to overtreatment. This might (partly) explain the present underrepresentation of women with CRT,(29) also demonstrated in the present study as women accounted for only 34% of the total population. Multivariable analysis demonstrated that normalized QRSd, rather than sex itself, was independently related to CRT survival. These results are in line with results from Varma et al. who demonstrated that sex-specific differences in echocardiographic CRT response resolved after normalization of QRSd to LV dimension in a population of one-hundred-thirty NICMP patients.(12) Our study confirms these findings and extends the role of QRSd normalization to (i) prediction of clinical endpoints (i.e. mortality, LVAD, HTx), and (ii) a larger population including both ischemic and non-ischemic patients. Moreover, all patients in our study underwent CMR imaging for QRSd normalization since this technique is preferred to echocardiography for LV quantification.(30) This provides a significant addition to the growing body of evidence that QRSd normalization could potentially improve patient selection for CRT.(11,12,31)

The role of normalized QRS duration in a prognostic model

Using various (clinical, laboratory, electrocardiographic and CMR) pre-implantation variables, we derived a five-parameter risk score that was able to identify high-risk patients in our cohort (figure 4). Parameters in the final model were normalized QRSd, age, atrial fibrillation, creatinine level and heart failure etiology. Most of these parameters were also included in prior prognostic CRT models (age, atrial fibrillation, creatinine). However, this is the first study to demonstrate that normalized QRSd is an independent predictor of survival whereas prior studies found no value of (unadjusted) QRSd in multivariable analysis.(32-34) Assessment of strict LBBB (compared to IVCD) morphology of the QRS complex also showed to be associated with favorable CRT outcome in univariable analysis (HR 0.54; p=0.009). In multivariable analysis, however, QRS morphology was expelled from the model whereas normalized QRSd remained statistical significant. These findings indicate that normalized QRSd provides predictive value over QRS morphology. Measures of LV dimension may be obtained by either CMR or echocardiography (although cut-off values differ between modalities). However, CMR is considered to be the 'gold standard' technique for LV quantification and offers late gadolinium enhancement (LGE) imaging for etiology assessment as well (also included in the final model).(30) In clinical practice, the role of CMR is of interest as CMR is increasingly used to screen candidates by measuring LVEF combined with LGE imaging to guide LV lead placement.(35)

Limitations

Due to the observational and retrospective nature of the study, some selection bias may have occurred during patient inclusion. The study protocol was designed to relate baseline characteristics (a.o. QRSd/LVEDV) to survival after CRT implantation. However, it should be considered that survival after CRT implantation is dependent on (i) pre-implantation characteristics, and (ii) the effect of CRT. Therefore, pre-implantation characteristics that determine CRT survival are not necessarily indicators of CRT benefit. Conversely, factors associated with poor CRT survival do not exclude benefit from CRT. Previously we demonstrated that QRSd/LVEDV <0.52ms/ml patients lacked hemodynamic response to CRT.(11)

In line with these findings, patients with QRSd/LVEDV <0.52ms/ml showed relatively poor survival after CRT implantation. Nevertheless, it cannot be excluded that these patients derived benefit from CRT since there was no control group without CRT. Secondly, although normalization of QRSd showed incremental value over QRSd itself, marginal predictive value over LVEDV did not reach statistical significance. From a clinical perspective, however, the value of normalized QRSd over unadjusted QRSd may be considered most relevant since present patient selection for CRT is based on QRSd (and not LVEDV). Lastly, backwards stepwise modeling was used to derive a simple model that only included key predictors of CRT outcome.

CONCLUSION

Normalization of QRSd to LV dimension improves prediction of survival after CRT implantation. In addition, sex-specific differences in CRT outcome were found to be explained by normalized QRSd and other prognostic factors (i.e. HF etiology). QRSd normalization is a relatively simple method that might improve patient selection for CRT.

REFERENCES

1. Bristow MR, Saxon LA, Boehmer J et al. Cardiac-resynchronization therapy with or without an implantable defibrillator in advanced chronic heart failure. N Engl J Med 2004;350:2140-50.
2. Cleland JG, Daubert JC, Erdmann E et al. The effect of cardiac resynchronization on morbidity and mortality in heart failure. N Engl J Med 2005;352:1539-49.
3. Tang AS, Wells GA, Talajic M et al. Cardiac-resynchronization therapy for mild-to-moderate heart failure. N Engl J Med 2010;363:2385-95.
4. Ponikowski P, Voors AA, Anker SD et al. 2016 ESC Guidelines for the diagnosis and treatment of acute and chronic heart failure: The Task Force for the diagnosis and treatment of acute and chronic heart failure of the European Society of Cardiology (ESC)Developed with the special contribution of the Heart Failure Association (HFA) of the ESC. Eur Heart J 2016;37:2129-200.
5. Yancy CW, Jessup M, Bozkurt B et al. 2013 ACCF/AHA guideline for the management of heart failure: a report of the American College of Cardiology Foundation/American Heart Association Task Force on Practice Guidelines. J Am Coll Cardiol 2013;62:e147-239.
6. Daubert C, Behar N, Martins RP, Mabo P, Leclercq C. Avoiding non-responders to cardiac resynchronization therapy: a practical guide. Eur Heart J 2017;38:1463-1472.
7. Cleland JG, Abraham WT, Linde C et al. An individual patient meta-analysis of five randomized trials assessing the effects of cardiac resynchronization therapy on morbidity and mortality in patients with symptomatic heart failure. Eur Heart J 2013;34:3547-56.
8. Chan DD, Wu KC, Loring Z et al. Comparison of the relation between left ventricular anatomy and QRS duration in patients with cardiomyopathy with versus without left bundle branch block. Am J Cardiol 2014;113:1717-1722.
9. Carluccio E, Biagioli P, Alunni G et al. Presence of extensive LV remodeling limits the benefits of CRT in patients with intraventricular dyssynchrony. JACC Cardiovasc Imaging 2011;4:1067-1076.
10. Vidal B, Delgado V, Mont L et al. Decreased likelihood of response to cardiac resynchronization in patients with severe heart failure. Eur J Heart Fail 2010;12:283-287.
11. Zweerink A, Wu L, de Roest GJ et al. Improved patient selection for cardiac resynchronization therapy by normalization of QRS duration to left ventricular dimension. Europace 2017;19:1508-1513.
12. Varma N, Lappe J, He J, Niebauer M, Manne M, Tchou P. Sex-Specific Response to Cardiac Resynchronization Therapy. JACC: Clinical Electrophysiology 2017;3:844-853.
13. Strauss DG, Selvester RH, Wagner GS. Defining left bundle branch block in the era of cardiac resynchronization therapy. Am J Cardiol 2011;107:927-34.
14. Lang RM, Badano LP, Mor-Avi V et al. Recommendations for cardiac chamber quantification by echocardiography in adults: an update from the American Society of Echocardiography and the European Association of Cardiovascular Imaging. Eur Heart J Cardiovasc Imaging 2015;16:233-70.

15. Aurich M, Andre F, Keller M et al. Assessment of left ventricular volumes with echocardiography and cardiac magnetic resonance imaging: real-life evaluation of standard versus new semiautomatic methods. J Am Soc Echocardiogr 2014;27:1017-24.
16. Ruschitzka F, Abraham WT, Singh JP et al. Cardiac-resynchronization therapy in heart failure with a narrow QRS complex. N Engl J Med 2013;369:1395-405.
17. Wang G, Zhao Z, Zhao S, Ding S, Shen S, Wang L. Effect of cardiac resynchronization therapy on patients with heart failure and narrow QRS complexes: a meta-analysis of five randomized controlled trials. J Interv Card Electrophysiol 2015;44:71-9.
18. Poole JE, Singh JP, Birgersdotter-Green U. QRS Duration or QRS Morphology: What Really Matters in Cardiac Resynchronization Therapy? J Am Coll Cardiol 2016;67:1104-17.
19. Gervais R, Leclercq C, Shankar A et al. Surface electrocardiogram to predict outcome in candidates for cardiac resynchronization therapy: a sub-analysis of the CARE-HF trial. Eur J Heart Fail 2009;11:699-705.
20. Khidir MJ, Delgado V, Ajmone Marsan N, Schalij MJ, Bax JJ. QRS duration versus morphology and survival after cardiac resynchronization therapy. ESC Heart Fail 2017;4:23-30.
21. Auricchio A, Fantoni C, Regoli F et al. Characterization of left ventricular activation in patients with heart failure and left bundle-branch block. Circulation 2004;109:1133-9.
22. Jackson T, Sohal M, Chen Z et al. A U-shaped type II contraction pattern in patients with strict left bundle branch block predicts super-response to cardiac resynchronization therapy. Heart Rhythm 2014;11:1790-7.
23. Sohal M, Shetty A, Duckett S et al. Noninvasive assessment of LV contraction patterns using CMR to identify responders to CRT. JACC Cardiovasc Imaging 2013;6:864-73.
24. Cheng YJ, Zhang J, Li WJ et al. More favorable response to cardiac resynchronization therapy in women than in men. Circ Arrhythm Electrophysiol 2014;7:807-815.
25. Goldenberg I, Moss AJ, Hall WJ et al. Predictors of response to cardiac resynchronization therapy in the Multicenter Automatic Defibrillator Implantation Trial with Cardiac Resynchronization Therapy (MADIT-CRT). Circulation 2011;124:1527-36.
26. Zusterzeel R, Curtis JP, Canos DA et al. Sex-specific mortality risk by QRS morphology and duration in patients receiving CRT: results from the NCDR. J Am Coll Cardiol 2014;64:887-94.
27. Kawel-Boehm N, Maceira A, Valsangiacomo-Buechel ER et al. Normal values for cardiovascular magnetic resonance in adults and children. J Cardiovasc Magn Reson 2015;17:29.
28. MacFarlane PPP. Appendix 1: Adult normal limits. Comprehensive Electrocardiology 2011:2057-2126.
29. Randolph TC, Hellkamp AS, Zeitler EP et al. Utilization of cardiac resynchronization therapy in eligible patients hospitalized for heart failure and its association with patient outcomes. Am Heart J 2017;189:48-58.
30. Grothues F, Moon JC, Bellenger NG, Smith GS, Klein HU, Pennell DJ. Interstudy reproducibility of right ventricular volumes, function, and mass with cardiovascular magnetic resonance. Am Heart J 2004;147:218-23.

31. Varma N, Sogaard P, Bax JJ et al. Interaction of Left Ventricular Size and Sex on Outcome of Cardiac Resynchronization Therapy Among Patients With a Narrow QRS Duration in the EchoCRT Trial. J Am Heart Assoc 2018;7.
32. Gasparini M, Klersy C, Leclercq C et al. Validation of a simple risk stratification tool for patients implanted with Cardiac Resynchronization Therapy: the VALID-CRT risk score. Eur J Heart Fail 2015;17:717-24.
33. Hoke U, Mertens B, Khidir MJH et al. Usefulness of the CRT-SCORE for Shared Decision Making in Cardiac Resynchronization Therapy in Patients With a Left Ventricular Ejection Fraction of </=35. Am J Cardiol 2017;120:2008-2016.
34. Khatib M, Tolosana JM, Trucco E et al. EAARN score, a predictive score for mortality in patients receiving cardiac resynchronization therapy based on pre-implantation risk factors. Eur J Heart Fail 2014;16:802-9.
35. Sommer A, Kronborg MB, Norgaard BL et al. Multimodality imaging-guided left ventricular lead placement in cardiac resynchronization therapy: a randomized controlled trial. Eur J Heart Fail 2016;18:1365-1374.

SUPPLEMENTAL MATERIAL

Table S1. Patient characteristics compared by sex

Variables	Total group (n=250)	Male (n=164)	Female (n=86)	p-value
Age (years)	67 (59 – 74)	67 (59 – 74)	69 (57 – 75)	0.943
NYHA class (n, %)				
Class II	74 (30%)	53 (32%)	21 (24%)	
Class III	172 (69%)	110 (67%)	62 (72%)	
Class IV	4 (2%)	1 (1%)	3 (4%)	0.115
Device				
ICD function (CRT-D) (n, %)	240 (96%)	158 (96%)	82 (95%)	0.704
Quadripolar LV lead (n, %)	47 (19%)	34 (21%)	13 (15%)	0.280
Medical history (n, %)				
Atrial fibrillation	49 (20%)	39 (24%)	10 (12%)	0.021
Diabetes Mellitus	58 (23%)	42 (26%)	16 (19%)	0.213
Hypertension	67 (27%)	44 (27%)	23 (27%)	0.988
Medication (n, %)				
Beta-blockers	209 (84%)	135 (82%)	74 (86%)	0.449
Diuretics	195 (78%)	128 (78%)	67 (78%)	0.979
ACE / ATII inhibitors	218 (87%)	145 (88%)	73 (85%)	0.427
Aldosterone antagonist	102 (41%)	64 (39%)	38 (44%)	0.479
ECG				
QRS duration (ms)	158 ± 22	160 ± 23	153 ± 18	0.016
Strict LBBB (Strauss) (n, %)	165 (66%)	103 (63%)	62 (72%)	0.058
Laboratory results				
creatinine (µmol/L)	97 (78 – 118)	106 (87 – 132)	80 (70 – 97)	<0.001
Echocardiography*				
LVEDV (ml)	221 ± 81	235 ± 85	199 ± 68	0.004
LVESV (ml)	168 ± 76	181 ± 80	147 ± 62	0.004
LVEF (%)	25 ± 9	24 ± 9	25 ± 9	0.473
CMR				
LVEDV (ml)	298 ± 93	315 ± 95	266 ± 78	<0.001
LVESV (ml)	234 ± 87	248 ± 90	206 ± 73	<0.001
LVEF (%)	23 ± 7	22 ± 7	23 ± 7	0.352
LV diameter (mm)	74 ± 9	75 ± 9	71 ± 8	<0.001
LV length (mm)	105 ± 10	108 ± 10	99 ± 8	<0.001
LV mass (g)	155 ± 45	166 ± 46	135 ± 35	<0.001
Ischemic CMP (n, %)	84 (34%)	70 (43%)	14 (16%)	<0.001
ECG + CMR				
LVEDV normalized QRS duration (ms/ml)	0.57 ± 0.18	0.55 ± 0.17	0.62 ± 0.17	0.003

NYHA, New York Heart Association class; CRT-D, cardiac resynchronization therapy with defibrillator function; LBBB, left bundle branch block; LVEDV, left ventricular end-diastolic volume; LVESV, left ventricular end-systolic volume; LVEF, left ventricular ejection fraction; CMP, cardiomyopathy; * incompletely recorded, n=176

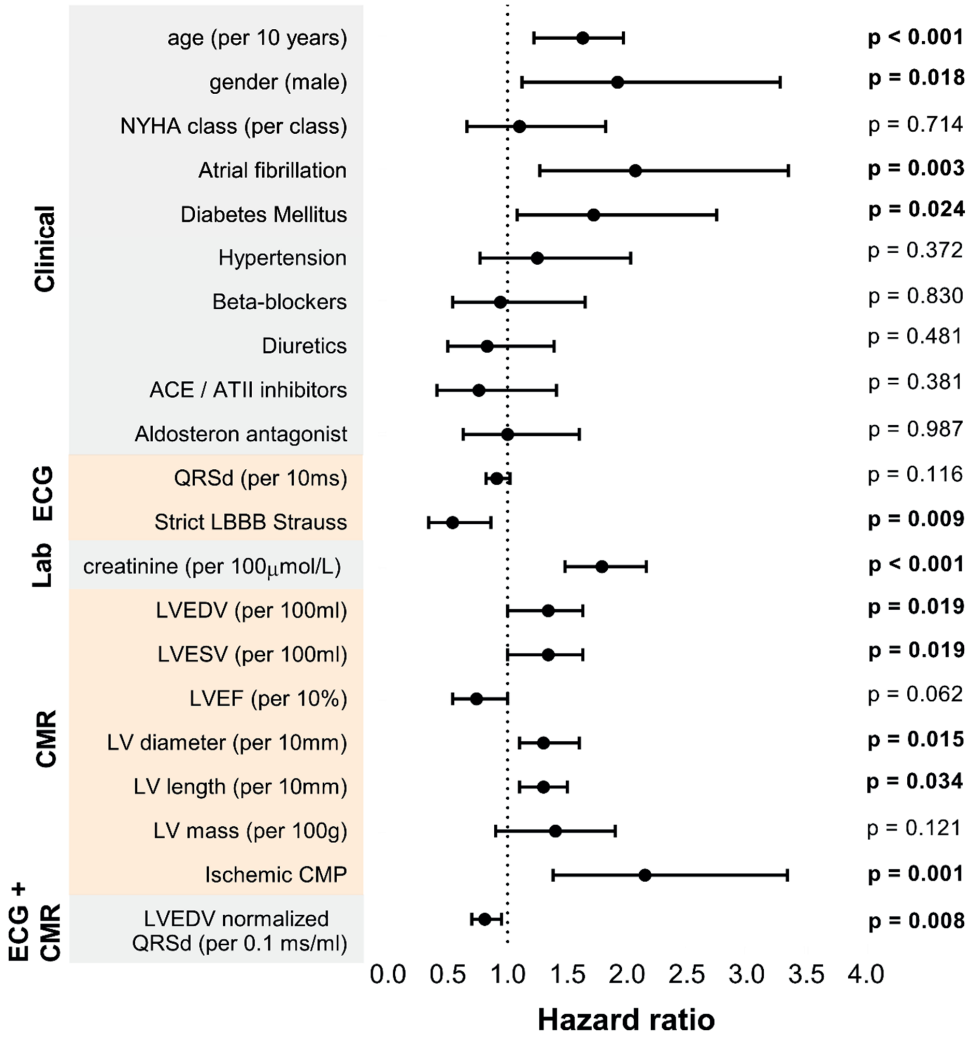


Figure S1: Forest plot of univariable Cox regression analysis for the primary endpoint: death / LVAD / HTx

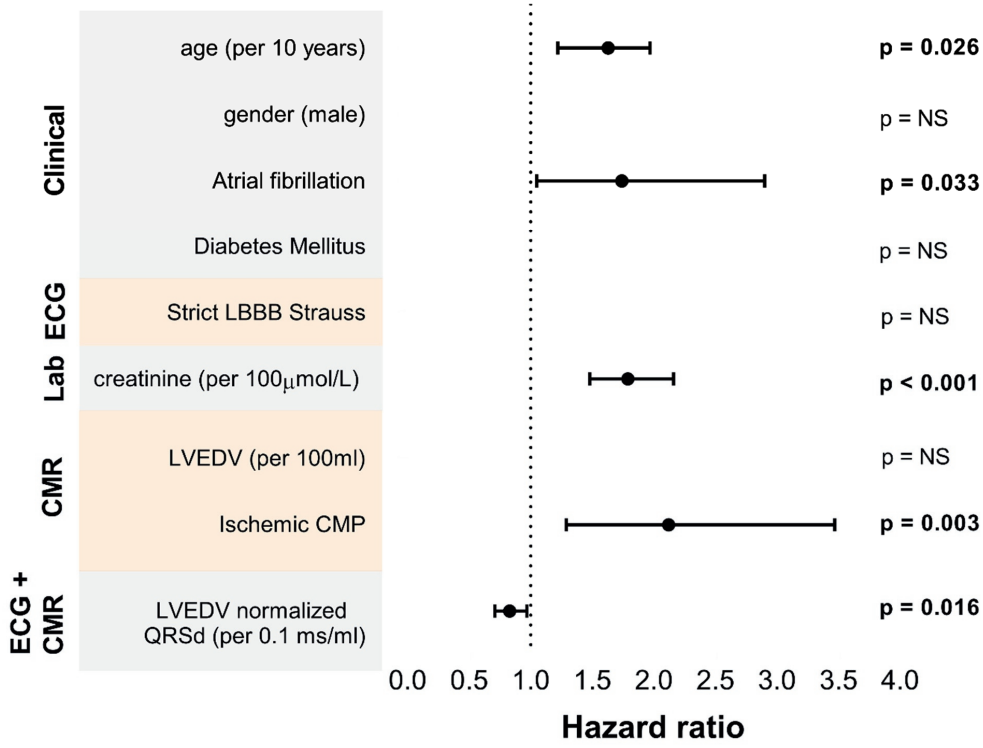
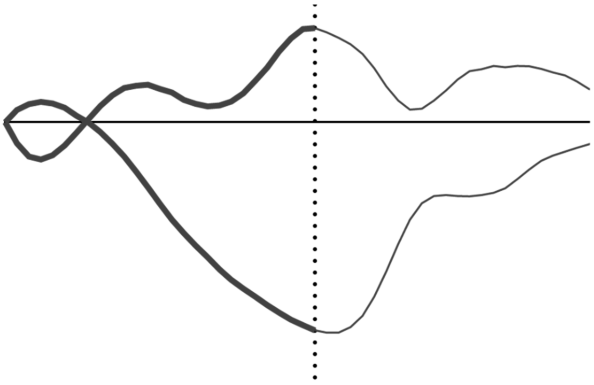


Figure S2: Forest plot of multivariable Cox regression analysis for the primary endpoint: death / LVAD / HTx

PART IB

PATIENT SELECTION:
MYOCARDIAL STRAIN IMAGING



Chapter 4

Prediction of Acute Response to Cardiac Resynchronization Therapy by Means of the Misbalance in Regional Left Ventricular Myocardial Work

J Card Fail 2016;22:133-42

Alwin Zweerink*
Gerben J. de Roest*
LiNa Wu
Robin Nijveldt, MD, PhD
Carel C. de Cock
Albert C. van Rossum
Cornelis P. Allaart

* Both authors contributed equally to this work

ABSTRACT

Background: Patients with left ventricular (LV) dyssynchrony have a marked misbalance in LV myocardial work distribution with wasted work in the septum and increased work in the lateral wall. We hypothesized that a low septum to lateral wall (SL) myocardial work ratio at baseline predicts acute LV pump function improvement during Cardiac Resynchronization Therapy (CRT).

Methods: Twenty patients (age 65±10years, 15 men) underwent CMR tagging for regional LV circumferential strain assessment, and invasive pressure-volume loop assessment at baseline and during biventricular pacing. Segmental work at baseline was calculated from regional strain rate and LV pressure. Subsequently, the SL work ratio was calculated and related to acute pump function (SW) improvement during CRT.

Results: During biventricular pacing, SW increased by +33% ($p<0.001$). SL work ratio at baseline was found to be significantly related to SW improvement by CRT (R -0.54; $p=0.015$). Moreover, it proved to be the only marker that was significantly related to acute response to CRT whereas QRS duration and other measures of dyssynchrony or discoordination were not.

Conclusion: The contribution of the septum to LV work varies widely in CRT candidates with LBBB. The lower the septal contribution to myocardial work at baseline, the higher the acute pump function improvement that can be achieved during CRT.

INTRODUCTION

Cardiac Resynchronization Therapy (CRT) is an established therapy for patients with drug refractory heart failure (HF) and left bundle branch block (LBBB). CRT, however, does not always lead to improvement in ventricular function and clinical symptoms. Rates of non-response to CRT are still reported to be 20-50%, despite substantial efforts to derive predictive parameters from both electrical and mechanical dyssynchrony assessment.(1-4) Several studies found mechanical discoordination (opposing shortening and stretch within the LV) to be a more powerful tool to predict CRT response than timing indices.(5-9) In 1974 Dillon was the first to described a unique abnormal septal motion in LBBB patients using echocardiographic techniques.(10) In these patients the septum typically demonstrates a substantial pre-ejection inward motion causing stretch of the LV lateral wall. Subsequently a paradoxical outward motion of the septum is observed during contraction of the late-activated LV lateral wall.(11) Indices that reflect this discoordination such as Systolic Rebound Stretch (SRS) and Internal Stretch Factor (ISF) are based on regional fiber strain and were found to be significantly related to CRT response in single center studies.(6-8,12) Nonetheless, these indices of regional fiber strain are load-dependent and therefore may not reflect actual regional myocardial work.(13,14) Regional myocardial work can be determined by combining regional fiber strain with instantaneous LV pressure as shown by Delhaas (15) and Urheim.(14) Recently, Russell et al validated this approach by demonstrating that the area of regional LV pressure – strain loops reflects regional myocardial metabolism.(16)

Previous studies have shown that CRT candidates have a marked misbalance in regional myocardial work resulting in an inefficient LV pump function and a significant waste of work in the septum.(17) Moreover, CRT was shown to increase the contribution of septal work thus restoring a more homogeneous septal to lateral myocardial work distribution.(16) Based on the finding that CRT can recruit myocardial work that is wasted by LBBB, we hypothesized that the amount of misbalance in regional myocardial work determines response to CRT. For that purpose, we investigated the relation between the misbalance in regional myocardial work and acute LV pump function improvement during CRT.

METHODS

Subjects

Twenty patients (age 65±10 years, 15 male (75%)) referred for CRT system implantation were selected from the Temporary Biventricular Stimulation (TBS) database, containing data on the acute hemodynamic effects of temporary multisite pacing in patients with advanced heart failure as previously described.(18,19) Inclusion criteria for the original TBS study were sinus rhythm, moderate to severe heart failure (New York Heart Association class II and III), severely depressed LV function (LV ejection fraction ≤35%) and at least 3 months stable optimal tolerated medical therapy. QRS duration was not an inclusion criterion. Patients with myocardial infarction or acute coronary syndrome within 3 months prior to study inclusion, previous pacemaker implantation, aortic valve stenosis, mechanical aortic valve replacement, or the presence of LV thrombus were excluded. For the present analysis patients were selected from this database with (i) typical LBBB (according to AHA/ACC/HRS recommendations, ref 20), and with both (ii) pressure-volume (PV) loop measurements and (iii) cardiac magnetic resonance imaging (CMR) derived myocardial strain data of sufficient quality (see below). The study complies with the Declaration of Helsinki and the local research ethics committee approved conduction of this study. Informed consent was obtained in all patients prior to the study procedures.

Cardiac magnetic resonance imaging

CMR imaging was performed on a 1.5T whole body system (Magnetom Sonata, Siemens, Erlangen, Germany) using a phased-array cardiac receiver coil. Functional imaging was performed using retrospectively ECG-gated steady-state free precession cine imaging with breath-holding (temporal resolution <50ms, repetition time 3.2ms, echo time 1.6ms). Per patient, 8-12 short-axis slices were obtained every 10mm covering the entire left ventricle. From these images, LV volumes were measured and ejection fraction (EF) was calculated. Myocardial scar territory was assessed by late gadolinium enhancement (LGE) imaging. Complementary tagged myocardial images were acquired using steady state free precession imaging and a multiple brief expiration scheme (temporal resolution 15ms, repetition time 3.6ms, echo time 1.8ms).(21) Images for 2D strain analysis were acquired in three short-axis planes, evenly distributed over the LV. Further, high temporal resolution (temporal resolution ~15ms, repetition time 3.4ms,

echo time 1.7ms) cine imaging of the LV in the three-chamber view was performed to assess the opening and closure times of the mitral and aortic valve. From the tagged images, circumferential strain (CS) curves were obtained from the 50% mid-myocardial wall by in-house developed software using the harmonic phase method, as previously reported.(22) Segmental strain curves were calculated for every slice (base, mid and apex).(23) The CS reflects the percentage change in length of a small line segment in the circumferential direction, with respect to the end-diastolic length. Septal strain was calculated as the averaged strain from the antero-septal and infero-septal segments from the 3 slices. Lateral wall strain was calculated as the averaged strain from the antero-lateral and infero-lateral segments from the 3 slices. The strain curves were discarded in case of low signal-to-noise ratio as judged by two independent investigators. The strain-rate was calculated as the change in strain per time frame.

Temporary Biventricular Pacing

Within the same week of the CMR, all patients underwent temporary biventricular stimulation as described previously.(19) In brief, after infusion of 5000IE of heparin two temporary bipolar pacing leads were placed, one in the right atrium and the other in the right ventricular apex (RVA). An unipolar pacing lead (Visionwire, Biotronik, Berlin, Germany) was targeted at the mid posterolateral (PL) position. A conductance catheter (CD Leycom, Zoetermeer, The Netherlands) was placed in a stable position in the LV apex to obtain PV loops. Baseline PV loops were recorded during intrinsic rhytm before and after each biventricular run. Approximately 30 representative cardiac cycles were averaged, disregarding all inappropriate beats (i.e. extra-systoles) using Conduct NT software (version 3.18.1). Biventricular pacing was performed in VDD mode using a fixed atrioventricular delay set to <100ms ensuring full ventricular capture, and a VV interval of 0 ms. CMR derived LV volumes were used for the calibration. Left ventricular function was quantified by end-diastolic volume (EDV), end-systolic volume (ESV), stroke volume (SV), and EF. Also, end-systolic pressure (ESP), end-diastolic pressure (EDP) and maximum rate of systolic and diastolic pressure change (dP/dt_{max}, dP/dt_{min}) were determined. Stroke work (SW) was directly calculated as the area of the pressure-volume loop. The effect of biventricular pacing was calculated as the relative SW change compared with

the mean of the two flanking baseline measurements. Patients with a SW increase of >20% compared with baseline were classified as CRT responders as this cut-off value accurately predicted longterm response to CRT in a previous study.(24)

Data analysis

Mechanical dyssynchrony was defined as the delay in onset of contraction between the septum and the lateral wall (SL delay).(6) Analysis of mechanical discoordination was assessed in both the systolic and diastolic phase of the cardiac cycle. Systolic discoordination was assessed by measuring the amount of SRS, defined as the cumulative amount of systolic stretch of the septum after initial shortening.(6) The internal stretch factor (ISF) was calculated by dividing the total systolic stretch of the septum and the lateral wall by the total systolic shortening of the septum and the lateral wall.(25) Diastolic discoordination was assessed by measuring diastolic rebound shortening (DRS), defined as the cumulative amount of septal shortening during the isovolumic relaxation (IVR) phase. Myocardial work of the septal and lateral wall was calculated separately using the regional strain recordings and measured LV pressure, as previously described.(26) In brief, instantaneous segmental strain rates were calculated from strain differences between successive strain images (CMR tagging imaging temporal resolution 15 ms) and multiplied by -1 causing positive values to indicate shortening. Subsequently, this inverted strain-rate was multiplied by instantaneous LV pressure to obtain a measure of power. Integration of this measure of power over time gives a measure of regional work, expressed as mmHg•% (Fig 1A). Regional myocardial work was calculated for five phases of the cardiac cycle: isovolumic contraction (IVC) phase, ejection phase, IVR phase, passive filling phase and active filling phase. The latter two phases were discarded for calculation of the SL work ratio, since filling is a largely passive process and contributes for a small part to myocardial work.(26) During systole, useful work was defined as positive work (indicating circumferential shortening) whereas waste was defined as negative work (indicating circumferential lengthening).

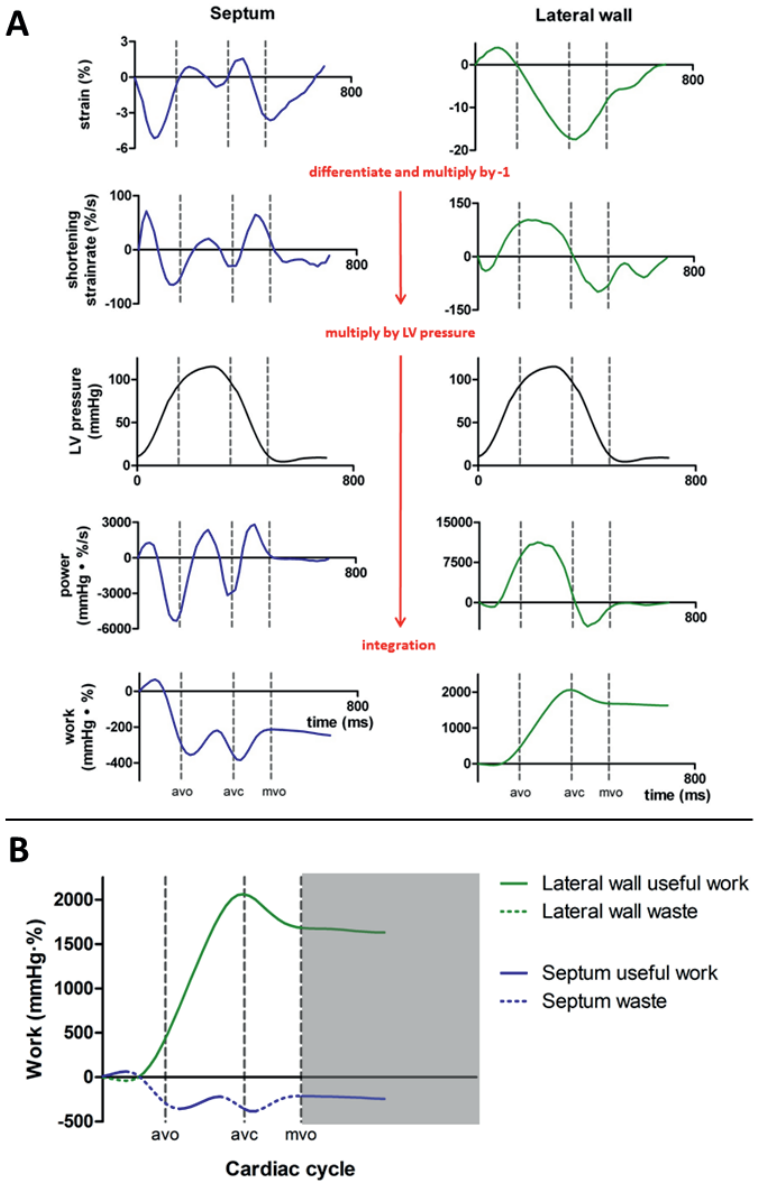


Figure 1 diagram A demonstrates the calculation process of segmental myocardial work by combining regional strain of the septum (blue) and lateral wall (green) with global LV pressure changes throughout the cardiac cycle. Diagram B shows segmental work as a function of time. Useful work is illustrated by a solid line while waste is illustrated by a dotted line. During systole positive work (indicating shortening) is considered useful and negative work (indicating lengthening) waste. In diastole this is vice versa. avo, aortic valve opening; avc, aortic valve closure; mvo, mitral valve opening.

During diastole, useful work was defined as negative myocardial work (indicating circumferential lengthening) whereas waste was defined as positive work (indicating circumferential shortening), as depicted in figure 1B. Subsequently, the ratio between the septal and lateral work was calculated by dividing the net result of useful work and wasted work of the septum by the net result of useful work and wasted work of the lateral wall.

$$\text{SL work ratio} = \frac{(\text{useful work septum} - \text{waste septum})}{(\text{useful work lateral wall} - \text{waste lateral wall})}$$

Statistics

The commercially available Statistical Package for Social Sciences software (IBM SPSS Statistics for Windows, Version 20.0. Armonk, NY, USA) was used for statistical analysis. Continuous variables are expressed as mean ± SD. Categorical variables are presented as absolute numbers and percentages. A Student t-test (independent or paired) or non-parametric test was used to compare groups when appropriate. Correlations were assessed using the Pearson's correlation coefficient or when normal distribution was absent, the Spearman's Rho correlation coefficient. Receiver Operating Characteristics (ROC) curve analysis was used to determine the predictive value of the parameters. Associations between baseline dyssynchrony-, discoordination-, myocardial work- indices and hemodynamic response during CRT were analyzed by linear regression analysis. A p-value of <0.05 was considered statistically significant.

RESULTS

Twenty patients (mean age 65±10 years, 15 (75%) men) were enrolled in this study. Patient characteristics are listed in table 1.

Systolic and diastolic pump function

Baseline hemodynamic measurements and acute response to biventricular pacing are summarized in table 2. At baseline both systolic and diastolic function were severely depressed (dP/dt_{max} 876±19 mmHg/s, dP/dt_{min} -845±16 mmHg/s, τ 44±7 ms) resulting in a reduced overall pump function (SW 5.1±2.2 L•mmHg).

Table 1 Patient characteristics

Parameter	N = 20
Clinical	
Age (years)	65 ± 10
Sex (male/female)	15/5
QRS duration (ms)	151 ± 14
NYHA (II/III)	4/16
Aetiology (ICMP/NICMP)	11/9
Conduction delay (LBBB/LBBB-like)	18/2
Med: diuretics (%)	60
Med: beta-blockers (%)	75
Med: Ace-inhibitors (%)	95
CMR	
EF (%)	22 ± 9
EDV (ml)	284 ± 97
ESV (ml)	225 ± 92
Scar mass (%)	10 ± 11
Peak strain septum (%)	-5.9 ± 3.7
Peak strain lateral wall (%)	-14.2 ± 4.2
Systolic strain rate septum (%/s)	-6.8 ± 13.3
Systolic strain rate lateral wall (%/s)	-37.3 ± 13.0
Septum to lateral shortening delay (ms)	53.1 ± 29.1
Systolic Rebound Stretch (%)	3.7 ± 2.9
Diastolic Rebound Stretch (%)	-2.3 ± 1.9
Internal Stretch Factor (%)	0.23 ± 0.18

ICMP, ischemic cardiomyopathy; NICMP, non-ischemic cardiomyopathy; LBBB, left bundle branch block; CMR, cardiac magnetic resonance imaging; EF, ejection fraction; EDV, end-diastolic volume; ESV, end-systolic volume. No significant differences were found between responders and non-responders for the baseline clinical parameters.

During biventricular pacing systolic LV function significantly improved, reflected by an increase in dP/dt_{max} (+11±14%, p=0.003) and shortening of the systolic time period (-4±7%, p=0.025). Also diastolic LV function improved, reflected by a significant decrease in dP/dt_{min} (-5±10%, p=0.025) and increase in diastolic time period (+6±9%, p=0.003). In addition, LV preload improved, reflected by an increased EDV (+3±5%, p=0.036) under equal loading conditions (EDP 0±19%, p=0.571). These changes resulted in an overall pump function improvement reflected by a SW increase of +33±38% compared with baseline (p<0.001).

Table 2 Hemodynamic measurements at baseline and during pacing

Parameter	Baseline	Pacing	Δ%	p-value
Heart rate (bpm)	81 ± 14	80 ± 12	-1 ± 3	0.174
dP/dt_{max} (mmHg/s)	875 ± 190	967 ± 205	+11 ± 14	0.003
dP/dt_{min} (mmHg/s)	-845 ± 164	-883 ± 162	-5 ± 10	0.025
Maximal pressure (mmHg)	120 ± 23	122 ± 23	+2 ± 5	0.164
Minimal pressure (mmHg)	11 ± 8	10 ± 8	-11 ± 20	0.056
τ (ms)	43 ± 5	42 ± 5	-3 ± 9	0.140
EDV (ml)	284 ± 97	290 ± 96	+3 ± 5	0.036
EDP (mmHg)	19 ± 10	19 ± 11	0 ± 19	0.517
EF (%)	22 ± 9	23 ± 9	+4 ± 13	0.236
SW (L • mmHg)	5.1 ± 2.2	6.7 ± 3.3	+33 ± 38	0.003
Systolic time: T at EDP- T at max pressure (ms/RR-interval)	35 ± 4	34 ± 4	-4 ± 7	0.016
Diastolic time: T at dP/dt_{min} – T at EDP (ms/RR-interval)	48 ± 8	51 ± 6	+6 ± 9	0.003

T, tau; EDV, end-diastolic volume; EDP, end-diastolic pressure; EF, ejection fraction; SW, stroke work; T, time

Regional myocardial work

All patients underwent successful CMR imaging with LV tissue tagging. Per patient a mean of 4.6±1.5 (77%) of the septal segments and 3.6±1.4 (60%) of the lateral segments were suitable for analysis resulting in a total inclusion of 163 out of 240 segments (68%). Baseline strain parameters are shown in table 1. Both averaged peak strain and systolic strain rate were significantly higher in the lateral wall compared with the septum (-14.2±4.2% vs. -5.9±3.7%; p<0.001 and -37.3±13.0%/s vs. -6.8±13.3%/s; p=0.033, respectively). Overall, a high systolic negative strain rate in the lateral wall was associated with a low negative or positive strain rate of the septum (R 0.48; p=0.033). Conversely, a high positive strain rate in the lateral wall during diastole was correlated with a low positive or negative strain rate of the septum (R -0.62; p=0.004). Systolic strain rate was also significantly related to diastolic strain rate in the septum (R -0.93; p<0.001), and the lateral wall (R -0.82; p<0.001). Calculation of myocardial work showed net regional work (positive work minus waste) to be significantly higher in the lateral wall compared with the septum during systole (1444±619 mmHg•% vs. 123±358 mmHg•%; p<0.001) and diastole (-289±267 mmHg•% vs. 53±211 mmHg•%; p<0.001; table 3).

Table 3 Regional myocardial work during systolic and diastolic phase

		septum			lateral wall		
		positive work (mmHg·%)	negative work (mmHg·%)	**net work** (mmHg·%)	positive work (mmHg·%)	negative work (mmHg·%)	**net work** (mmHg·%)
Total (N=20)	systolic	427±256‡	304±193‡	123±358‡	1472±626	28±38	1444±619
	diastolic	126±132‡	73±113‡	53±211‡	33±54	322±236	-289±267
NR (N=7)	systolic	524±292	187±168*	337±364*	954±447‡	0±0‡	954±447‡
	diastolic	33±73‡	170±150‡	-138±197‡	36±35	193±168	-158±185
R (N=13)	systolic	374±229	368±181	7±309	1751±530	43±41	1708±540
	diastolic	176±130	21±21	156±136	33±64	392±243	-360±284

NR, non-responder; R, responder, significant differences between the septum and the lateral wall for the total group (upper row), and NR compared with R (lower two rows) marked by * P = <0.05 or ‡ P = <0.02

During systole, positive work exceeded negative work (i.e. waste) significantly in the lateral wall (1472±626 mmHg•% vs. 28±38 mmHg•%; p<0.001), whereas septal positive systolic work was counterbalanced by a relative high negative systolic work (427±256 mmHg•% vs. 304±193 mmHg•%; p=0.142). The SL work ratio was 0.17±0.48. Eleven (55%) patients were classified with ischemic cardiomyopathy (ICMP) based on LGE imaging. Averaged amount of scar was 10±11% and scar was evenly distributed over the myocardium. The amount of scar was not significantly correlated with SL work ratio (R 0.28, p=0.248) within ICMP patients. Also SL work ratio between ICMP patients and non-ischemic (NICMP) patients did not significantly differ (0.34±0.51 vs. 0.0±0.37; p=0.077), although a trend towards higher SL work ratio's in the ICMP group was visible. For the total group of both ICMP and NICMP patients, correlation of scar with SL work ratio did reach significance (R 0.49, p=0.030).

Prediction of response

The SL work ratio was found to be significantly related to acute SW improvement during CRT (R -0.54; p=0.015; figure 2). In contrast, QRS duration, SL delay and mechanical discoordination parameters SRS, ISF and DRS showed no significant correlation with acute SW improvement in this small group although a trend was suggestive in each case.

Multiple regression analysis revealed that regressing SW change only on QRS duration yields a R-square of 0.16 (p=0.080; figure 2A), adding SL work ratio to this model doubles the R-square to 0.33 (p=0.033). This substantial change in R-square however, is not statistically significant although a trend is observed (p=0.054). The correlation of SL work ratio with other dyssynchrony and discoordination parameters is given in table 4. The measures SRS, DRS and ISF show close correlation with SL work ratio, which is expected since SL work ratio calculation includes each of them. Regressing SW in a model that includes QRS duration, SL delay, SRS, DRS and ISF yields a R-square of 0.23 (p=0.536), adding SL work ratio to this model results in a R-square of 0.43 (p=0.221). This change in R-square is also not statistically significant although once again a trend is observed (p=0.056). Interpretation of this latter model, however, should be done with great caution because of the small sample size. Thirteen (65%) patients were classified as SW-responder and 7 (35%) as SW non-responder assuming a SW improvement cut-off value of 20%.(24) Regional myocardial work of the different phases of the cardiac cycle in both responders and non-responders is displayed in figure 3. Responders and non-responders demonstrated predominantly positive work in the lateral wall during the systolic phase but responders showed a significant higher net work compared with non-responders (1708±540mmHg·% vs. 954±447mmHg·%; p=0.006). In contrast, in the septum the responders showed a significant lower net work compared with non-responders (7±309mmHg·% vs. 337±364mmHg·%; p=0.046), mainly based on a significantly higher waste of work during the isovolumic contraction phase (-368±181mmHg•% vs. -187±168mmHg•%; p=0.042). A typical patient is shown in figure 1. During diastole both responders and non-responders demonstrated predominantly negative work (relaxation) in the lateral wall resulting in a comparable net negative work (-360±284mmHg·% vs. -158±185mmHg·%; p=0.108). However, the net septal work during diastole was positive in responders while negative in non-responders (156±136mmHg·% vs. -138±197mmHg·%; p=0.001), due to higher septal wasting in responders. This is reflected by a significant lower SL work ratio in responders compared with non-responders (-0.07±0.24 vs. 0.62±0.49; p=0.001). ROC curve analysis demonstrated the SL work ratio to be significantly predictive for response (AUC 0.87; p=0.008). A cut-off value of 0.43 predicted response with a 100% sensitivity and 86% specificity.

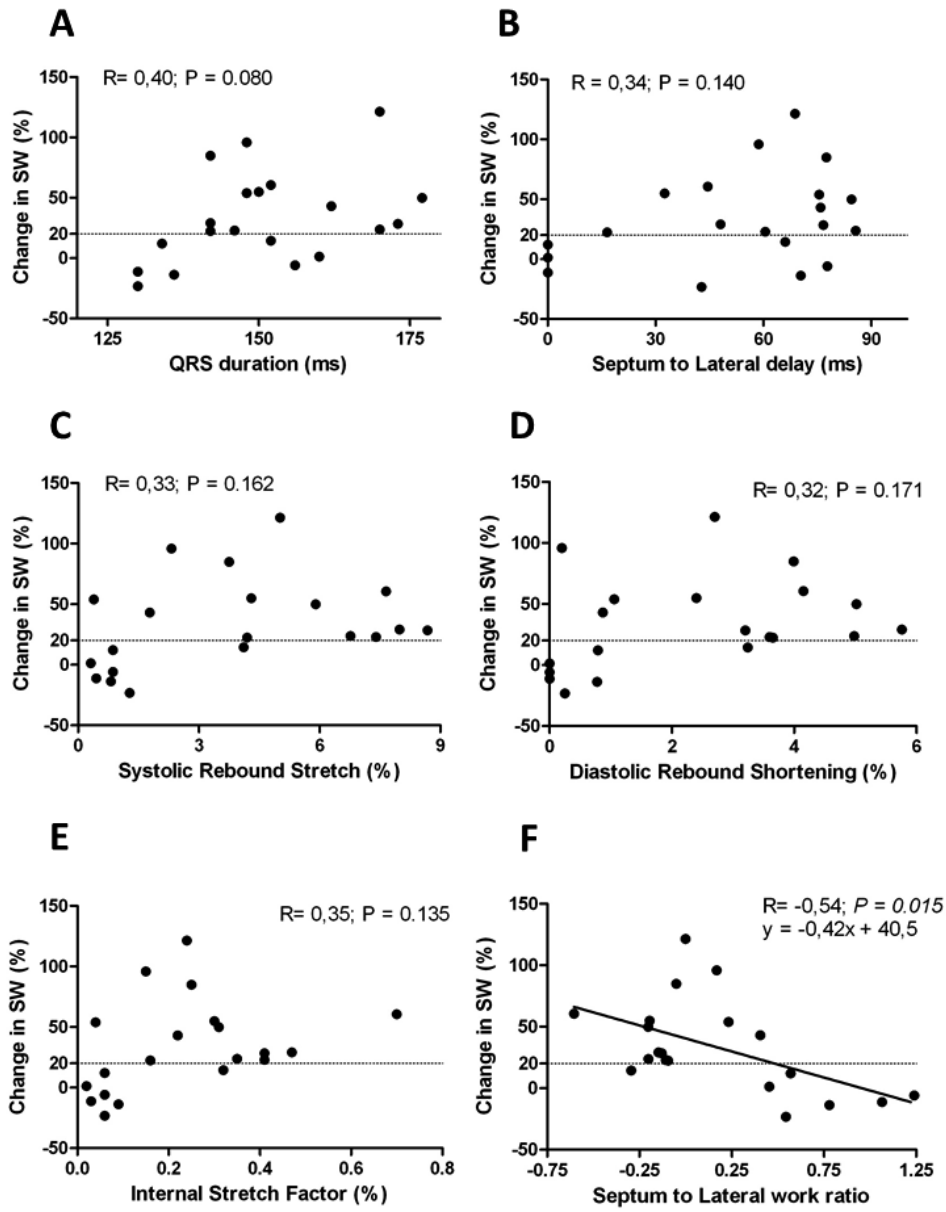


Figure 2 shows scatter plots illustrating the relationships between acute improvement in SW during CRT (Y axis) and baseline QRS width (A), mechanical dyssynchrony reflected by the septum to lateral (SL) delay (B), mechanical discoordination reflected by systolic rebound stretch (SRS) of the septum (C); diastolic rebound shortening (DRS) of the septum (D); the internal stretch factor (ISF) of the septum and the lateral wall (E) and the septum to lateral work ratio (F).

Table 4 Correlation of SL work ratio with dyssynchrony and discoordination parameters

Parameter	QRS duration	SL delay	SRS	DRS	ISF
SL work ratio	R -0.40; p=0.084	R -0.25; p=0.294	R -0.80; p<0.001	R 0.81; p<0.001	R -0.81; p<0.001

SL work ratio, septal to lateral work ratio; SL delay, septal to lateral delay onset contraction; SRS, systolic rebound stretch of the septum; DRS, diastolic rebound shortening of the septum; ISF, internal stretch factor

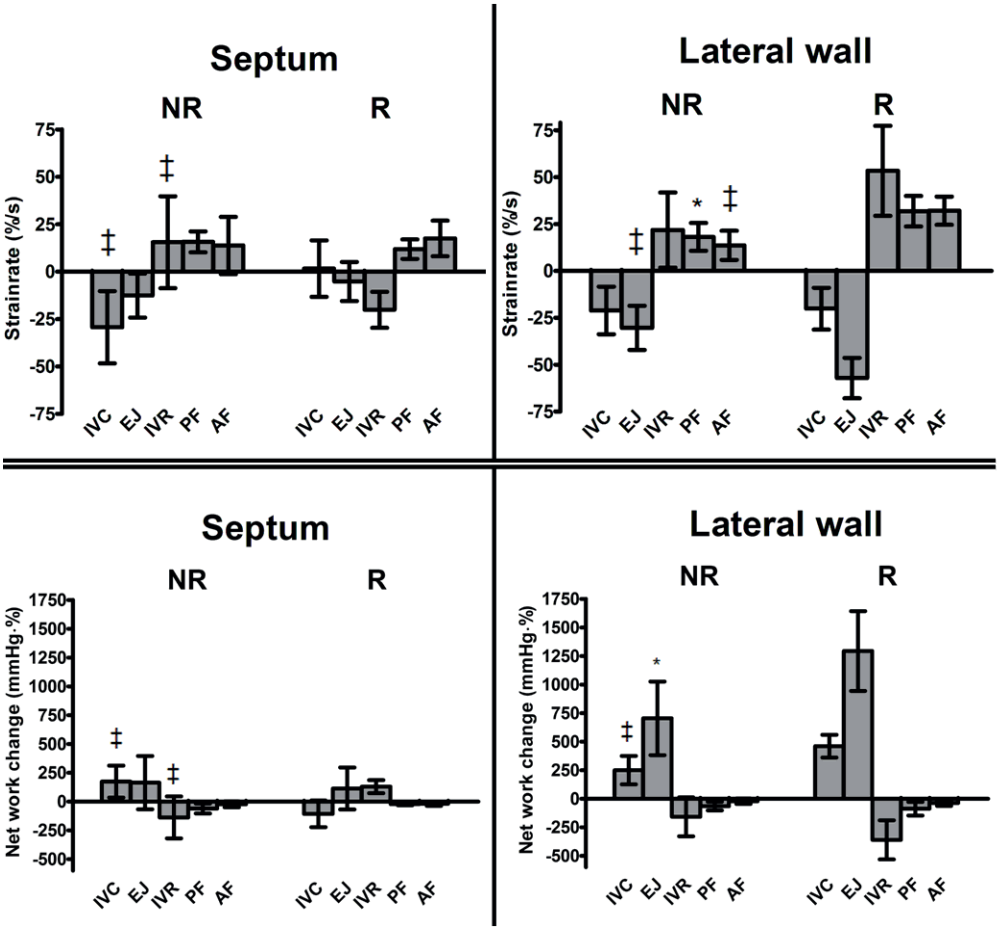


Figure 3 shows segmental strain rate (upper diagrams) and net change in work (lower diagrams) of the septum and the lateral wall throughout the phases of the cardiac cycle (IVC, isovolumic contraction; EJ, ejection; IVR, isovolumic relaxation; PF, passive filling; AF, active filling). Significant difference between non-responder (NR) compared with responder (R) marked by * p<0.05 or ‡ p<0.02.

DISCUSSION

The present proof-of-principle study shows that the misbalance in regional myocardial work varies substantially between CRT candidates with LBBB. Moreover, our results indicate that the amount of misbalance (expressed as the SL work ratio) is significantly related to acute SW improvement during CRT, with lower septal contribution to myocardial work (or higher the septal waste) at baseline leading to higher pump function improvement. In contrast, QRS duration and other measures of dyssynchrony or discoordination were not significantly related to acute CRT response. Future developments towards fully non-invasive assessment of regional myocardial work using estimated LV pressure curves as validated by Russell et al.(16) need to be explored and will ultimately improve clinical applicability. After the disappointing results of the PROSPECT study, several single center studies have proposed discoordination as a promising parameter to predict response to CRT.(3,6,7) From a theoretical point of view, however, myocardial motion parameters do not fully describe myocardial function since the stress at which a particular motion is accomplished is lacking. Recently, Russell et al elegantly showed the consequences of involving stress (LV pressure) in myocardial function analysis in both animal experiments and nine LBBB patients receiving CRT. Their results demonstrate a substantial septal waste of myocardial work during LBBB as well as recruitment of the septum during CRT leading to a more balanced distribution of work over the LV. Applying a similar method, the present study corroborates their findings and in addition demonstrates that the amount of septal waste is related to the magnitude of CRT benefit. To our knowledge this is the first study demonstrating that the amount of wasted myocardial work at baseline predicts LV pump function improvement during CRT in patients.

Further analysis showed that comparable lateral wall motion occurred in responders and non-responders, although absolute values of strain, strain rate and work were significantly higher in responders. In contrast, major differences were found in septal wall motion. Comparing responders and non-responders during IVC, ejection and IVR phases opposite septal motion was observed (figure 4, panel B), very similar to observations reported in previous echocardiographic studies.(6,8,10)

The typical pre-ejection inward motion of the septum displayed in the responder group, reflecting the early onset of active septal contraction(11), amount to limited myocardial work as it takes place under low LV pressure. This (positive) work is absorbed by pre-stretching the LV lateral wall. Subsequently, the pre-stretched lateral wall starts contracting and the septum demonstrates a rebound stretch phenomenon under rising LV pressure, thus absorbing a substantial amount of myocardial work during IVC and ejection. Gjesdal et al. elegantly illustrated in their LBBB dog model that the septum in LBBB patients demonstrates a late systolic lengthening (stretch) while the lateral wall is still contracting. This is likely due to earlier onset relaxation of the early activated septum under a high global LV pressure (high wall stress) generated by the lateral wall. During this stretch elastic energy is stored in the septum. During the IVR phase, this energy is released again (rebound phenomenon) without contribution to external work, and the septum again significantly wastes myocardial work by shortening under high LV pressures.(11) Thus, the opposite septal strain pattern throughout the cardiac cycle results in a highly inefficient septum contribution. In our relatively small study population the motion differences (or discoordination) per se were not significantly related to acute SW improvement by CRT as indicated by linear regression analysis (figure 2, panel C-E). Combining of instantaneous pressure data with strain rate to obtain work, however, did result in a significant relation with acute SW improvement suggesting additive value of this approach in selection of CRT candidates. Regional myocardial function has been previously studied in heart failure patients with LBBB by using functional imaging modalities such as PET in which oxygen consumption, glucose uptake and myocardial perfusion reflect regional cardiac metabolism. Impaired septal glucose metabolism, oxygen consumption and myocardial blood flow were demonstrated, as well as the improvement upon CRT.(27-30) Birnie et al. found that reduction in septal glucose metabolism relative to perfusion as a surrogate for reduced regional myocardial work predicted response to CRT, further supporting the results of the present study.(31)

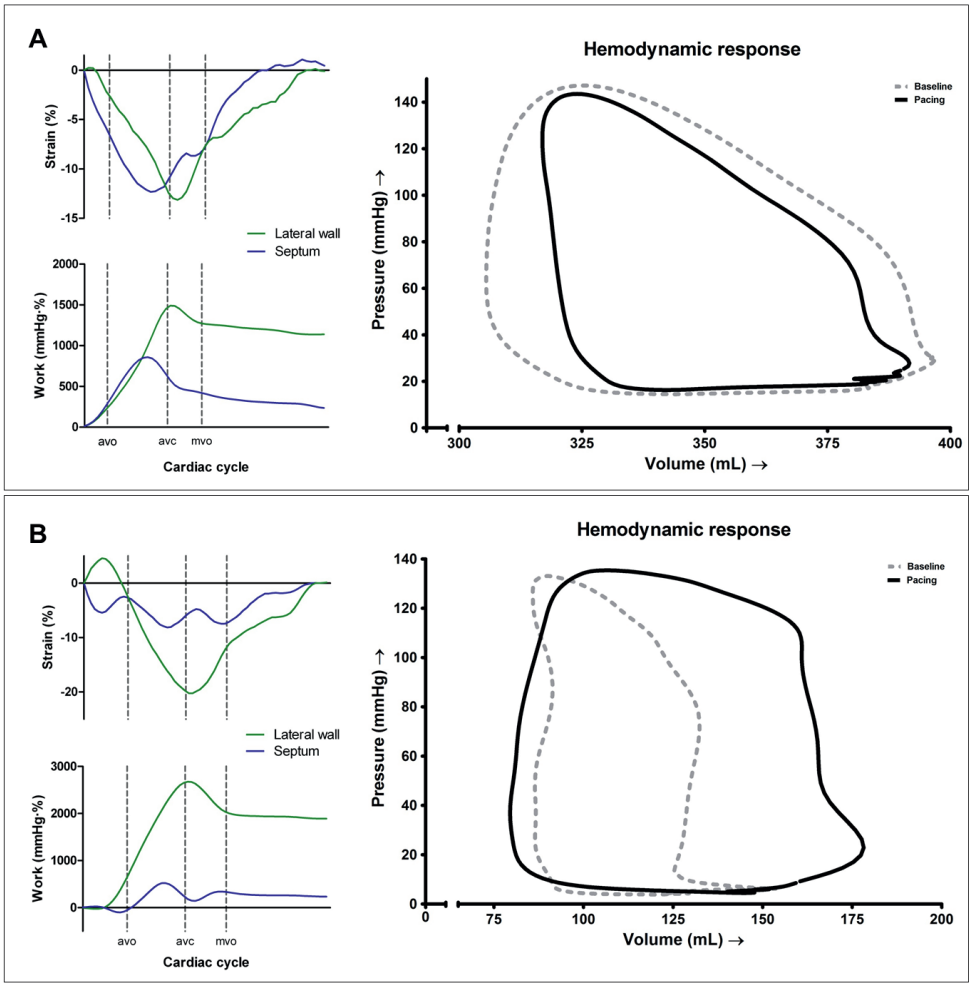


Figure 4 shows two typical examples of a non-responder (A) and responder (B). Regional strain (upper) and work (lower) curves of the septum (blue) and the lateral wall (green) are demonstrated on the left. The vertical lines indicate valve opening and closure (avo, aortic valve opening; avc, aortic valve closure; mvo, mitral valve opening). Right-sided figures show the pressure-volume (PV) loops during baseline conditions (dotted line) and during biventricular pacing (solid line). Both patients have dyssynchrony with a septal to lateral (SL) contraction delay of 42.8ms (A) and 68.8ms (B). However, patient A demonstrates a normal contraction pattern of the septum as compared with the lateral wall, resulting in a relative high SL work ratio of 0.54. As shown in the PV diagram, pump function decreased (ΔSW -23%) during CRT. Patient B demonstrated an opposing contraction pattern of the septum relative to the lateral wall resulting in a low SL work ratio of 0.00. During CRT, acute pump function dramatically increased as depicted in the PV diagram (ΔSW: +121%).

Moreover, several studies showed CRT to increase cardiac efficiency.(32,33) It is generally believed that improvement of efficiency leads to improved survival.(34,35) The approach of the present paper, focusing on reduction of wasted work, might therefore be of additional value in patient selection for CRT, and should be addressed in future studies.

Study limitations

Several limitations need to be addressed. First, the use of conductance catheter measurements warrants both careful data acquisition and analysis, as extensively discussed elsewhere.(19) However, SW (calculated as the area of the pressure-volume loop) is readily assessed and independent of arbitrarily determined LV volumes. Moreover, the acutely obtained SW has proven to be strongly related to long term outcome(24) from the same study the SW improvement cut-off value of 20% was obtained to separate responders from non-responders. Secondly, strain and strain rate analysis based on CMR tagging is strongly dependent on image quality. In the present study a significant amount of segments could not be analyzed due to poor image quality. However, per patient a sufficient number of segments of septum and lateral wall remained suitable for analysis. In the present study, anterior and posterior segments were excluded from analysis. Thirdly, we used ECG R-wave triggered CMR acquisition. As a consequence, contraction of the septum might have started just before the first image was acquired. However, LV pressure is still low at the beginning of contraction, and calculation of work will therefore be minimally affected. Fourthly, the measure of regional myocardial work (mmHg•%) used in this paper is calculated from strain rate and instantaneous pressure, as introduced by Russell et al.(26) Since it is not a measure of absolute work, comparison of different LV's might not be valid. However, the SL work ratio should be valid within the same LV since this relative measure compensates for differences in LV geometry. Finally, Left ventricular pressure and strain data were not acquired simultaneously, which might have introduced small errors as heart rates were found to be higher during invasive PV measurements compared to the CMR procedure (81±14 bpm vs. 71±13 bpm).

The observed relation with acute SW improvement strongly suggests an important role for the SL work ratio in patient selection for CRT, but in this small study only 20 patients were retrospectively analyzed. As a consequence, both the relevance of this new parameter and its relation to other known determinants of CRT response need to be established in future prospective studies.

CONCLUSION

The present study demonstrated that (i) baseline contribution of the septum to total LV work varies widely in CRT candidates with LBBB and that (ii) the lower the septal contribution to total myocardial work (or the higher the septal waste) at baseline, the higher the acute improvement in pump function that was achieved during CRT. The baseline septal-to-lateral work ratio was found to be strongly associated with acute CRT response, whereas dyssynchrony and discoordination parameters were not. These findings warrant further research in larger patient populations.

REFERENCES

1. McAlister FA, Ezekowitz J, Hooton N. Cardiac resynchronization therapy for patients with left ventricular systolic dysfunction: A systematic review. JAMA 2007;297(22):2502-2514.
2. Abraham WT, Fisher WG, Smith AL, Delurgio DB, Leon AR, Loh E et al. Cardiac Resynchronization in Chronic Heart Failure. N Engl J Med 2002;346(24):1845-1853.
3. Chung ES, Leon AR, Tavazzi L, Sun JP, Nihoyannopoulos P, Merlino J et al. Results of the Predictors of Response to CRT (PROSPECT) Trial. Circulation 2008;117(20):2608-2616.
4. Mollema SA, Bleeker GB, van der Wall EE, Schalij MJ, Bax JJ. Usefulness of QRS Duration to Predict Response to Cardiac Resynchronization Therapy in Patients With End-Stage Heart Failure. The American Journal of Cardiology 2007;100(11):1665-1670.
5. Bilchick KC, Dimaano V, Wu KC, Helm RH, Weiss RG, Lima JA et al. Cardiac Magnetic Resonance Assessment of Dyssynchrony and Myocardial Scar Predicts Function Class Improvement Following Cardiac Resynchronization Therapy. JACC: Cardiovascular Imaging 2008;1(5):561-568.
6. De Boeck BWL, Teske AJ, Meine M, Leenders GE, Cramer MJ, Prinzen FW et al. Septal rebound stretch reflects the functional substrate to cardiac resynchronization therapy and predicts volumetric and neurohormonal response. European Journal of Heart Failure 2009;11(9):863-871.
7. Leenders GE, De Boeck BWL, Teske AJ, Meine M, Bogaard MD, Prinzen FW et al. Septal Rebound Stretch is a Strong Predictor of Outcome After Cardiac Resynchronization Therapy. Journal of Cardiac Failure 2012;18(5):404-412.
8. Kirn B, Jansen A, Bracke F, van Gelder B, Arts T, Prinzen FW. Mechanical discoordination rather than dyssynchrony predicts reverse remodeling upon cardiac resynchronization. American Journal of Physiology-Heart and Circulatory Physiology 2008;295(2):H640-H646.
9. Lumens J, Leenders GE, Cramer MJ, De Boeck BWL, Doevendans PA, Prinzen FW et al. Mechanistic Evaluation of Echocardiographic Dyssynchrony Indices Patient Data Combined With Multiscale Computer Simulations. Circulation-Cardiovascular Imaging 2012;5(4):491-499.
10. Dillon JC, Chang S, Feigenbaum H. Echocardiographic manifestations of left bundle branch block. Circulation 1974;49(5):876-880.
11. Gjesdal O, Remme EW, Opdahl A, Skulstad H, Russell K, Kongsgaard E et al. Mechanisms of Abnormal Systolic Motion of the Interventricular Septum During Left Bundle-Branch Block. Circulation-Cardiovascular Imaging 2011;4(3):264-U109.
12. Chan YH, Wu LS, Kuo CT, Wang CL, Yeh YH, Ho WJ et al. Incremental Value of Inefficient Deformation Indices for Predicting Response to Cardiac Resynchronization Therapy. Journal of the American Society of Echocardiography 2013;26(3):307-315.
13. Urheim S, Rabben SI, Skulstad H, Lyseggen E, Ihlen H, Smiseth OA. Regional myocardial work by strain Doppler echocardiography and LV pressure: a new method for quantifying myocardial function. American Journal of Physiology-Heart and Circulatory Physiology 2005;288(5):H2375-H2380.
14. Urheim S, Edvardsen T, Torp H, Angelsen B, Smiseth OA. Myocardial strain by Doppler echocardiography - Validation of a new method to quantify regional myocardial function. Circulation 2000;102(10):1158-1164.

15. Delhaas T, Arts T, Prinzen FW, Reneman RS. Regional Fiber Stress Fiber Strain Area As An Estimate of Regional Blood-Flow and Oxygen-Demand in the Canine Heart. Journal of Physiology-London 1994;477(3):481-496.
16. Russell K, Eriksen M, Aaberge L, Wilhelmsen N, Skulstad H, Remme EW et al. A novel clinical method for quantification of regional left ventricular pressure-strain loop area: a non-invasive index of myocardial work. Eur Heart J 2012;33(6):724-733.
17. Prinzen FW, Hunter WC, Wyman BT, McVeigh ER. Mapping of regional myocardial strain and work during ventricular pacing: experimental study using magnetic resonance imaging tagging. Journal of the American College of Cardiology 1999;33(6):1735-1742.
18. de Cock CC, Vos DHS, Jessurun EMIL, Allaart CP, Visser CA. Effects of Stimulation Site on Diastolic Function in Cardiac Resynchronization Therapy. Pacing and Clinical Electrophysiology 2007;30:S40-S42.
19. de Roest GJ, Allaart CP, de Haan S, Hendriks ML, Bronzwaer JGF, van Rossum AC et al. Effects of QRS Duration and Pacing Location on Pressure-Volume Loop Evaluation of Cardiac Resynchronization Therapy in End-Stage Heart Failure. The American Journal of Cardiology 2011;108(11):1581-1588.
20. Surawicz B, Childers R, Deal BJ, Gettes LS. AHA/ACCF/HRS Recommendations for the Standardization and Interpretation of the Electrocardiogram: Part III: Intraventricular Conduction Disturbances A Scientific Statement From the American Heart Association Electrocardiography and Arrhythmias Committee, Council on Clinical Cardiology; the American College of Cardiology Foundation; and the Heart Rhythm Society Endorsed by the International Society for Computerized Electrocardiology. Journal of the American College of Cardiology 2009;53(11):976-981.
21. Zwanenburg JJM, Kuijer JPA, Marcus JT, Heethaar RM. Steady-state free precession with myocardial tagging: CSPAMM in a single breathhold. Magnetic Resonance in Medicine 2003;49(4):722-730.
22. Tecelao SRR, Zwanenburg JJM, Kuijer JPA, Marcus JT. Extended harmonic phase tracking of myocardial motion: Improved coverage of myocardium and its effect on strain results. J Magn Reson Imaging 2006;23(5):682-690.
23. American Heart Association Writing Group on Myocardial Segmentation and Registration for Cardiac Imaging:, Cerqueira MD, Weissman NJ, Dilsizian V, Jacobs AK, Kaul S et al. Standardized Myocardial Segmentation and Nomenclature for Tomographic Imaging of the Heart: A Statement for Healthcare Professionals From the Cardiac Imaging Committee of the Council on Clinical Cardiology of the American Heart Association. Circulation 2002;105(4):539-542.
24. de Roest GJ, Allaart CP, Kleijn SA, Delnoy PP, Wu L, Hendriks ML et al. Prediction of long-term outcome of cardiac resynchronization therapy by acute pressure-volume loop measurements. European Journal of Heart Failure 2012;15:299-307.
25. Prinzen FW, Vernooy K, De Boeck BW, Delhaas T. Mechano-energetics of the asynchronous and resynchronized heart. Heart Fail Rev 2011;16(3):215-224.
26. Russell K, Eriksen M, Aaberge L, Wilhelmsen N, Skulstad H, Gjesdal O et al. Assessment of wasted myocardial work: a novel method to quantify energy loss due to uncoordinated left ventricular contractions. Am J Physiol Heart Circ Physiol 2013;305(7):H996-1003.

27. Neri G, Zanco P, Zanon F, Buchberger R. Effect of biventricular pacing on metabolism and perfusion in patients affected by dilated cardiomyopathy and left bundle branch block: evaluation by positron emission tomography. Europace 2003;5(1):111-115.
28. Nowak B, Sinha AM, Schaefer WM, Koch KC, Kaiser HJ, Hanrath P et al. Cardiac resynchronization therapy homogenizes myocardial glucose metabolism and perfusion in dilated cardiomyopathy and left bundle branch block. Journal of the American College of Cardiology 2003;41(9):1523-1528.
29. Lindner O, Vogt J, Kammeier A, Wielepp P, Holzinger J, Baller D et al. Effect of cardiac resynchronization therapy on global and regional oxygen consumption and myocardial blood flow in patients with non-ischaemic and ischaemic cardiomyopathy. European Heart Journal 2005;26(1):70-76.
30. Knaapen P, van Campen LMC, de Cock CC, Gotte MJW, Visser CA, Lammertsma AA et al. Effects of cardiac resynchronization therapy on myocardial perfusion reserve. Circulation 2004;110(6):646-651.
31. Birnie D, de Kemp RA, Tang AS, Ruddy TD, Gollob MH, Guo A et al. Reduced septal glucose metabolism predicts response to cardiac resynchronization therapy. Journal of Nuclear Cardiology 2012;19(1):73-83.
32. Nelson GS, Berger RD, Fetics BJ, Talbot M, Hare JM, Kass DA et al. Left ventricular or biventricular pacing improves cardiac function at diminished energy cost in patients with dilated cardiomyopathy and left bundle-branch block. Circulation 2000;102(25):3053-3059.
33. Mills RW, Cornelussen RN, Mulligan LJ, Strik M, Rademakers LM, Skadsberg ND et al. Left Ventricular Septal and Left Ventricular Apical Pacing Chronically Maintain Cardiac Contractile Coordination, Pump Function and Efficiency. Circulation: Arrhythmia and Electrophysiology 2009;2(5):571-579.
34. Knaapen P, Germans T, Knuuti J, Paulus WJ, Dijkmans PA, Allaart CP et al. Myocardial Energetics and Efficiency: Current Status of the Noninvasive Approach. Circulation 2007;115(7):918-927.
35. Prinzen F, Vernooy K, DeBoeck B, Delhaas T. Mechano-energetics of the asynchronous and resynchronized heart. Heart Fail Rev 2011;16(3):215-224.

Chapter 5

Comparison of Strain Imaging Techniques in CRT Candidates: CMR Tagging, CMR Feature Tracking and Speckle Tracking Echocardiography

Int J Cardiovasc Imaging 2018;34:443-456

Alwin Zweerink*
Wouter M. van Everdingen*
Robin Nijveldt
Odette A.E. Salden
Mathias Meine
Alexander H. Maass
Kevin Vernooy
Frederik J. de Lange
Albert C. van Rossum
Pierre Croisille
Patrick Clarysse
Bastiaan Geelhoed
Michiel Rienstra
Isabelle C. Van Gelder
Marc A. Vos
Maarten J. Cramer*
Cornelis P. Allaart*

* The first two and last two authors contributed equally to this work

ABSTRACT

Aims: Parameters using myocardial strain analysis may predict response to cardiac resynchronization therapy (CRT). As the agreement between currently available strain imaging modalities is unknown, three different modalities were compared.

Materials and methods: Twenty-seven CRT-candidates, prospectively included in the MARC study, underwent cardiac magnetic resonance (CMR) imaging and echocardiographic examination. Left ventricular (LV) circumferential strain was analysed with CMR tagging (CMR-TAG), CMR feature tracking (CMR-FT), and speckle tracking echocardiography (STE). Basic strain values and parameters of dyssynchrony and discoordination obtained with CMR-FT and STE were compared to CMR-TAG.

Results: Agreement of CMR-FT and CMR-TAG was overall fair, while agreement between STE and CMR-TAG was often poor. For both comparisons, agreement on discoordination parameters was highest, followed by dyssynchrony and basic strain parameters. For discoordination parameters, agreement on systolic stretch index (SSI) was highest, with fair intra-class correlation coefficients (ICC) (CMR-FT: 0.58, STE: 0.55). ICC of septal systolic rebound stretch (SRS_{sept}) was poor (CMR-FT: 0.41, STE: 0.30). Internal stretch factor of septal and lateral wall ($ISF_{sep-lat}$) showed fair ICC values (CMR-FT: 0.53, STE: 0.46), while the ICC of the total LV (ISF_{LV}) was fair for CMR-FT (0.55) and poor for STE (0.32). The CURE index had a fair ICC for both comparisons (CMR-FT: 0.49, STE: 0.41).

Conclusion: Although comparison of STE to CMR-TAG was limited by methodological differences, agreement between CMR-FT and CMR-TAG was overall higher compared to STE and CMR-TAG. CMR-FT is a potential clinical alternative for CMR-TAG and STE, especially in the detection of discoordination in CRT-candidates.

INTRODUCTION

Cardiac resynchronization therapy (CRT) is an established treatment for patients with heart failure, reduced left ventricular (LV) ejection fraction, and a prolonged QRS caused by a left bundle branch block (LBBB) or nonspecific intraventricular conduction delay.(1) CRT aims to restore LV mechanics and improve hemodynamic by resynchronization of LV electrical activation.(2) Unfortunately, the effect of CRT is limited in 30-40% of the patients, partly due to a lack of optimal criteria for patient selection.(2,3) In current international guidelines the selection criteria for CRT are limited to clinical parameters, ECG parameters and LV ejection fraction ≤35%.(1) Patient selection for CRT may be improved with additional parameters reflecting mechanical dyssynchrony or discoordination obtained with strain analysis on imaging.(4-7) These parameters reflect the LV mechanical consequences caused by an inhomogeneous electrical activation. Mechanical dyssynchrony parameters are based on timing differences between particular LV segments.(8,9) However, these mechanical dyssynchrony parameters showed disappointing results in large multi-centre trials.(9) More promising parameters focus on discoordination, reflecting a percentage or fraction of opposing (i.e. inefficient) deformation.(6,10-12) These parameters are determined using myocardial strain analysis, which can be obtained with several cardiac imaging techniques, including cardiac magnetic resonance imaging (CMR) with tagging (CMR-TAG), CMR cine images and a post-processing technique named feature tracking (CMR-FT), and speckle tracking echocardiography (STE).(13,14) Although CMR-TAG is regarded as the non-invasive 'gold-standard', it is generally limited to scientific applications, requiring specific imaging protocols, sequences, and dedicated post-processing software. Clinical application of CMR-FT and STE is more feasible compared to CMR-TAG, as both techniques are applicable to images obtained during standard clinical imaging protocols.(14-16) Nevertheless, both techniques (i.e. CMR-FT and STE) lack validation on strain parameters reflecting mechanical dyssynchrony and discoordination. Thus, no study has yet compared results obtained with all three techniques (i.e. CMR-TAG, CMR-FT and STE) in patients eligible for CRT. This study aims to compare circumferential strain parameters obtained with CMR-FT and STE versus gold-standard CMR-TAG in patients eligible for CRT. The comparison of indices reflecting mechanical dyssynchrony and discoordination are of specific interest.

MATERIALS AND METHODS

Study population

This sub study is part of the Markers of Acute Response to CRT (MARC) study (Cohfar, CTMM, The Netherlands, clinicaltrials.gov: NCT01519908), which was designed to investigate predictors for response on CRT. The MARC study included two-hundred-forty patients planned for CRT implantation in six medical centres in the Netherlands, using previously published in- and exclusion criteria.(17) Twenty-seven of the 240 patients were included in this sub-study, as these patients gave consent for an additional CMR examination including myocardial tagging in the VU university medical centre (Amsterdam, The Netherlands). All subjects gave written informed consent and the local medical ethics committees approved data collection and management. The investigation conforms to the principles outlined in the Declaration of Helsinki.

Echocardiography

Echocardiographic examinations were performed on either GE Vivid7, GE Vivid9 (General Electric Healthcare, Chicago, Illinois, USA), or Philips iE33 (Philips Medical Systems, Best, The Netherlands) ultrasound machines prior to CRT implantation by all participating centres and analysed by the echocardiographic core lab (WE and MC, UMC Utrecht, Utrecht, The Netherlands). Standard echocardiographic images were obtained, including a parasternal short axis view at the papillary muscle and at the mitral valve level.(18) Image quality and frame rate (50-100Hz) were optimized for offline speckle tracking analysis. Pulsed-wave Doppler images of the mitral valve inlet and LV outflow tract were obtained of mitral valve and aortic valve closure (AVC) to define systole. Echocardiographic images were exported as DICOM-files for vendor-independent strain analysis (TomTec 2D Cardiac Performance Analysis (2DCPA) version 1.2.1.2, TomTec Imaging Systems, Unterschleissheim, Germany). A region of interest was placed by user defined markers at the endocardial border. The epicardial border was excluded, as it often lacked a clear border zone. The region of interest was automatically separated into six segments. Segments were excluded if, even after repeated adjustment of the region of interest, adequate tracking was not achievable. The marker for reference length was placed at QRS onset. STE results were exported for analysis with author written scripts for Matlab 2014b (Mathworks, Natick, MA, USA). Segmental strain curves were

discarded in case of low signal-to-noise ratio as judged by two independent investigators (WE and AZ). At least two segments needed to be analysable per wall. Results of strain parameters of the septum were based on averages of maximal four septal segments (i.e. basal- and mid-level of inferoseptal and anteroseptal segments) while the lateral wall parameters were based on averages of maximal four lateral wall segments (i.e. basal- and mid-level of inferolateral and anterolateral segments). The post-processing and selection of analysable segments and averaging into one septal and one lateral wall strain curve, was similar for STE, CMR-TAG and CMR-FT.

Cardiac magnetic resonance imaging

CMR examinations were performed on a 1.5T system (Magnetom Avanto, Siemens, Erlangen, Germany) with the use of a phased array cardiac receiver coil. Although performed on a different moment compared to STE, both standard CMR cine images for the CMR-FT analysis and CMR tagging images were obtained in the same examination. Standard CMR cine images were acquired using a retrospectively ECG-gated balanced steady-state free-precession (SSFP) sequence during end-expiratory breath holding. A stack of 8-12 consecutive short axis cine images was acquired covering the entire LV. Typical image acquisition parameters were: slice thickness 5mm, slice gap 5mm, echo time (TE) 1.6ms, repetition time (TR) 3.2ms, temporal resolution <50ms, in-plane spatial resolution 1.5 by 2.1mm, flip angle 60 degrees. The number of reconstructed temporal phases within the cardiac cycle was set at 20. Subsequently, high temporal resolution (TE 1.7ms, TR 3.4ms, temporal resolution ~15ms) cine imaging of the LV in the three-chamber view was performed to assess the opening and closure times of the mitral and aortic valve. Before contrast injection, tagged images were acquired at three short-axis slices (basal, mid, apical) using a complementary spatial modulation of magnetization (CSPAMM) line tagging sequence with segmented ECG-gated acquisitions and serial breath holds.(16) Typical image acquisition parameters were: slice thickness 6mm, TE 1.7ms, TR 3.6ms, temporal resolution <15ms, in-plane spatial resolution 1.3 by 4.3mm, flip angle 20 degrees, tag spacing 7mm. The number of reconstructed temporal phases within the cardiac cycle was set at 55. Tagged CMR images were exported and analysed (AZ, RN) with the SinMod technique (inTag, v2.0, CREATIS lab, Lyon, France, run as a plug-in for OsiriX Imaging Software v6.5, Pixmeo,

Switzerland).(19) Apical slices were discarded, while basal and mid short-axis slices were used for analysis in order to match the STE slice positions. After selecting the area of interest, endocardial and epicardial contours were manually drawn in the end-systolic phase and automatically propagated. A template was placed dividing the LV in six equally sized regions, similar to STE. The myocardium was divided in three layers (i.e. endo-, mid-, epi-wall layer). Results of the mid-wall layer were used, as these results are independent of contour placement. Semi-automated FT analysis software (QStrain Research Edition evaluation version 1.3.0.10, Medis, Leiden, The Netherlands) was used to analyse short-axis cine images corresponding with the mid and basal slice-location of the CMR-TAG images (AZ and RN). Apical slices were discarded to match STE. First, endo- and epicardial contours were manually drawn in both end-diastolic and end-systolic frames and propagated automatically. Both endocardial and epicardial features were included for strain analysis, resulting in myocardial strain. The LV was divided in six regions, similar to the other techniques.

Strain parameters

The following basic strain parameters were obtained for the septal and lateral wall (figure 1). 1) Peak strain was the maximal negative peak strain during the cardiac cycle. 2) AVC strain was defined as the strain value at aortic valve closure. 3) Time to maximal peak (TTP_{max}) was the time difference between the start of the strain curve to most negative peak strain. Furthermore, 4) average systolic strain rate (i.e. average strain rate between mitral valve closure and AVC) and 5) average diastolic strain rate (i.e. average strain rate after AVC) were obtained. Three parameters of dyssynchrony were analysed. a) Onset-delay was determined as the absolute time delay between onset of shortening of the septal and lateral wall. b) Peak delay was calculated as the absolute difference between lateral and septal wall TTP_{max}. c) The TTP_{SD} was calculated as the standard deviation of TTP_{max} of all analysable segments of the total LV. Three regional discoordination parameters were analysed. d) Systolic rebound stretch of the septum (SRS_{sept}) was defined as the total amount of systolic stretch after initial shortening of the septum (figure 1). e) Systolic stretch index (SSI) was calculated by adding SRS_{sept} to all systolic stretch of the lateral wall.(11) f) Internal stretch factor (ISF) was calculated as the fraction of all systolic stretch compared to cumulative systolic shortening for the septal and lateral wall ($ISF_{sep\text{-}lat}$).

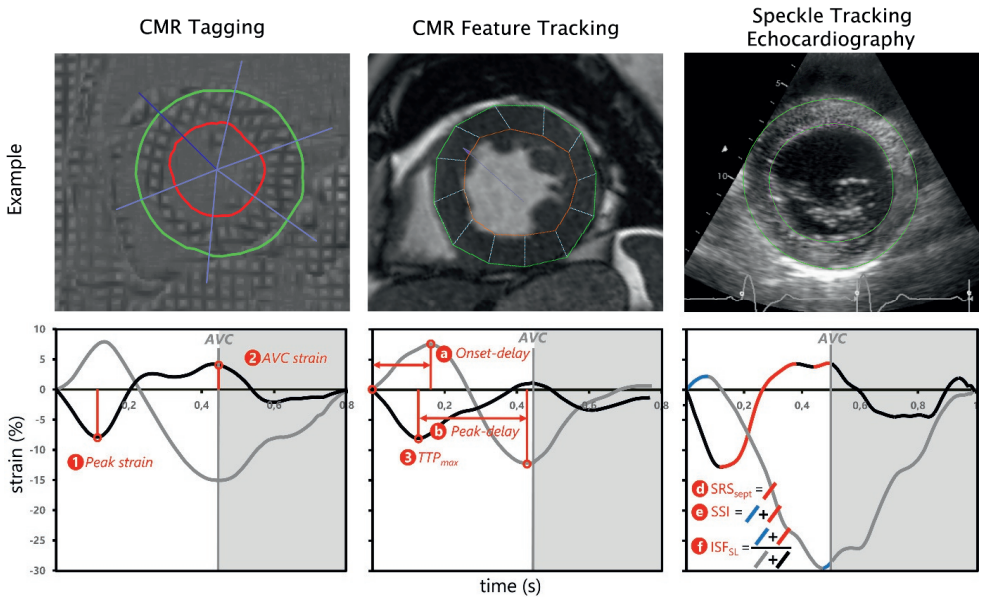


Figure 1: Overview of imaging techniques and corresponding myocardial strain analysis. Examples of imaging techniques (top row) and resulting strain signals (bottom row) of one specific patient. Each column represents a single technique with the corresponding strain results. Examples of derived parameters are shown per graph. Basic strain parameters are indicated with a number, dyssynchrony and discoordination parameters are indicated with a character. Strain signals of the septum (black line) and lateral wall (grey line) are given, with the aortic valve closure (grey vertical line) as end of systole. CMR, cardiac magnetic resonance imaging; AVC, aortic valve closure; AVC strain, strain value at aortic valve closure; TTP_{max}, time to maximal peak shortening; onset-delay, time delay between onset of shortening of septal and lateral wall; peak-delay, septal to lateral wall delay of TTP_{max}; $SRS_{sept,}$ systolic rebound stretch of the septum; SSI, systolic stretch index; $ISF_{sep-lat}$, internal stretch fraction of septal and lateral wall.

g) Septal strain curves were categorized in three types, determined by their shape, LBBB-1: double-peaked systolic stretch, LBBB-2: early pre-ejection shortening peak followed by prominent systolic stretching and LBBB-3: pseudo normal shortening with a late-systolic shortening peak, followed by less pronounced end-systolic stretch (figure 2).(12) Finally, two discoordination parameters reflecting the total LV were analysed. h) The internal stretch factor of the total LV (ISF_{LV}) was determined using all analysable segments. ISF_{LV} was determined as the total amount of stretch divided by the total amount of shortening during systole (supplemental figure 1).(20)

i) Lastly, the circumferential uniformity ratio estimates (CURE) was calculated, ranging from 0 (total dyssynchrony) to 1 (perfectly synchronous).(21)

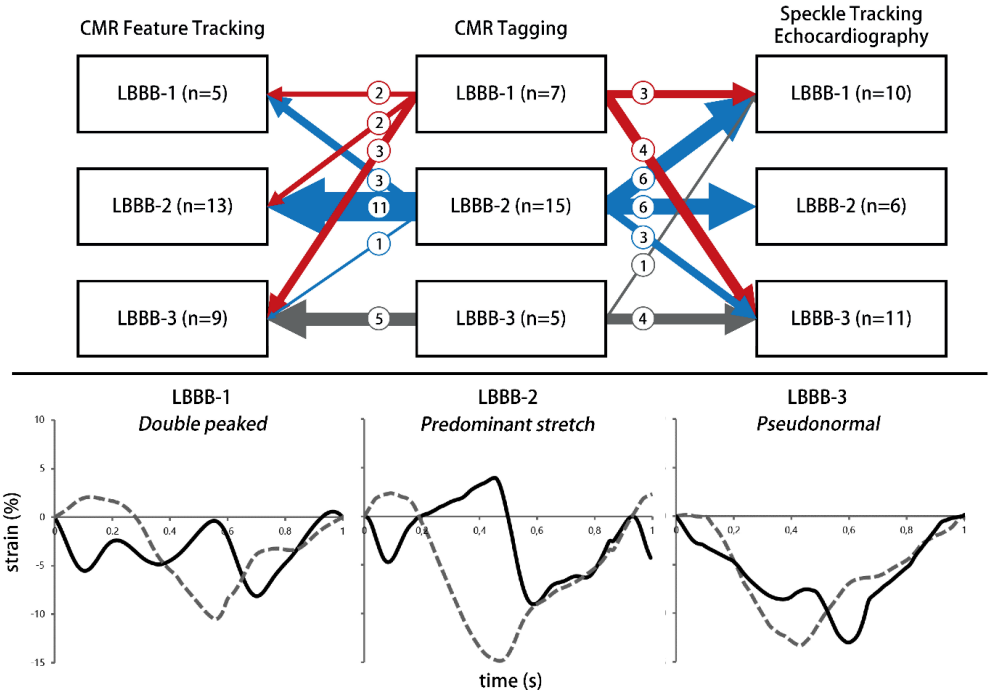


Figure 2: LBBB pattern categorization. Septal strain pattern categorization and distribution of strain patterns found by the three imaging techniques. The distribution per imaging technique is given vertical in the upper panel. The cross-over of patients from CMR tagging to speckle tracking echocardiography and CMR feature tracking is displayed by arrows. The thickness of the arrows matches the number of patients crossing over. The number of patients crossing over is also given by a number in each arrow. Specific examples of the three patterns are given in the lower panel. Black curve, septal strain; grey dashed curved, lateral wall strain. CMR, cardiac magnetic resonance imaging; LBBB-1, double peak shortening; LBBB-2, predominant stretch; LBBB-3, pseudo-normal shortening; n, number of patients.

Statistical analysis

Statistical analysis was performed (BG and MR) using R version 3.3.2 (The R foundation for Statistical Computing), and the R-packages psych version 1.5.8 (for calculation of Cohen's kappa coefficients, ICCs and their associated p-values). Results obtained with the three techniques were compared using the intra-class correlation coefficient (ICC) for absolute agreement between techniques (ICC2 according to Shrout and Fleiss) and Spearman rank or Pearson

correlation coefficient (R) depending on normality of data.(22) An ICC ≥0.75 was classified as excellent, 0.60-0.74 as good, 0.40-0.59 as fair, and <0.40 as poor.(23) Bland-Altman plots were made to observe the agreement between modalities. The mean difference and limits of agreement (±1.96 standard deviation) of the Bland-Altman plot were used a reference of agreement. Lastly, Cohen's kappa coefficient was calculated as the level of agreement between modalities on septal strain pattern categorization. A statistical result with a p-value <0.05 was deemed significant.

RESULTS

Study population

Twenty-seven patients with CMR tagging images were included, of which a detailed description is given in table 1. In these patients 94% of all segments were analysable with CMR-TAG, 87% with CMR-FT and 89% with STE. Frame rate of echocardiographic images was on average 65±11Hz, which corresponds to a temporal resolution of ~15ms. Temporal resolution of CMR-TAG was ~14ms, while it was ~40ms for CMR-FT.

Basic strain parameters

Overall, agreement of CMR-TAG and CMR-FT was higher compared to agreement of CMR-TAG and STE for basic strain parameters. This applied for ICC values, Bland-Altman characteristics and the correlation coefficient (R) (table 3). 1) For CMR-FT AVC strain of the septum was fair (ICC 0.55, R 0.67), while it was poor for STE (ICC 0.23, R 0.47). The ICC of AVC strain of the lateral wall was fair for CMR-FT (ICC 0.50, R 0.50) and poor for STE (ICC 0.08, R 0.10). 2) Peak strain of the septum had a fair ICC for CMR-FT (ICC 0.58, R 0.55) and a poor ICC for STE (ICC 0.155, 0.42). Lateral wall peak strain also had a fair ICC for CMR-FT (ICC 0.54, R 0.59) and a poor ICC for STE (ICC 0.01, R 0.02). 3) TTP_{max} of the septal and lateral wall showed an apparent wide distribution in the Bland-Altman plots for both comparisons (figure 3). Septal TTP_{max} caused a large spread in results, while the lateral wall TTP_{max} were more similar for both comparisons. Although ICC for TTP_{max} was poor for all comparisons, CMR-FT showed better agreement with CMR-TAG compared to STE for the septum (CMR-FT: ICC 0.17, R 0.11 and STE: ICC 0.00, R -0.16) and the lateral wall (CMR-FT: ICC 0.34, R 0.40 and STE: ICC 0.13, R 0.23).

Table 1. Baseline characteristics

Variable	Total cohort (n=27)
Age (years)	65.1 ± 9.7
Gender (n, male)	15 (56%)
BMI (kg/m^2)	26.3 ± 3.9
Aetiology (n, ischemic cardiomyopathy)	7 (26%)
QRS width (ms)	183 (167-194)
Sinus rhythm (%)	100%
QRS morphology (n)	
LBBB	21 (81%)
IVCD	6 (19%)
NYHA class (n)	
II	17 (63%)
III	10 (37%)
Medication (n)	
Beta-blockers	23 (85%)
Diuretics	22 (81%)
ACE / ATII inhibitors	17 (63%)
Aldosterone antagonists	10 (37%)
CMR - LVEDV (ml)	317 ± 100
CMR - LVESV (ml)	239 ± 99
CMR - LVEF (%)	26.7 ± 8.8
CMR - LV mass (gr)	131 (118-157)

Mean and standard deviation are given with ± symbol, median and interquartile range between brackets. BMI, body surface mass index; CMR, cardiac magnetic resonance imaging; LBBB, left bundle branch block; IVCD, intraventricular conduction delay; NYHA, New York Heart Association; ATII, angiotensin receptor II; LVEDV, left ventricular end-diastolic volume; LVESV, left ventricular end-systolic volume; LVEF, left ventricular ejection fraction; LV, left ventricular.

4) Systolic strain rate showed comparable results to AVC strain. For CMR-FT systolic strain rate of the septum was fair (ICC 0.56, R 0.66), while it was poor for STE (ICC 0.25, R 0.45). ICC of the systolic strain rate of the lateral wall was fair for CMR-FT (ICC 0.575, R 0.58) and poor for STE (ICC 0.05, R 0.05). 5) Diastolic strain rate showed good ICC for the septal (ICC 0.64, R 0.66) and excellent ICC for the lateral wall (ICC 0.82, 0.82) for CMR-TAG vs. CMR-FT. ICC of diastolic strain rate was poor for both walls comparing CMR-TAG and STE (septum: ICC 0.34, R 0.50, lateral wall: ICC 0.23, R 0.38).

Table 2. Strain parameters of each myocardial strain analysis modality

	CMR tagging	CMR feature tracking	STE
Basic strain septum			
1 - AVC strain septum (%)	2.4 ± 5.8	-1.1 ± 5.0	-6.8 ± 7.1
2 - Peak strain septum (%)	-4.0 ± 2.8	-5.1 ± 3.6	-10.4 ± 5.4
3 - TTP_{max} septum (ms)	195 ± 179	379 ± 211	459 ± 173
4 - Systolic strain rate septum (%/s)	5.4 ± 16.4	-3.0 ± 12.9	-15.9 ± 16.1
5 - Diastolic strain rate septum (%/s)	-1.1 ± 10.8	2.1 ± 10.9	-1.9 ± 29.0
Basic strain lateral wall			
1 - AVC strain lateral (%)	-12.6 ± 3.2	-12.0 ± 3.5	-14.5 ± 5.3
2 - Peak strain lateral (%)	-13.4 ± 2.7	-12.4 ± 3.6	-15.8 ± 5.5
3 - TTP_{max} lateral (ms)	424 ± 33	404 ± 31	474 ± 52
4 - Systolic strain rate lateral (%/s)	-32.2 ± 7.9	-30.8 ± 9.3	-32.8 ± 11.9
5 - Diastolic strain rate lateral (%/s)	29.7 ± 13.2	27.8 ± 13.7	12.5 ± 25.0
Dyssynchrony			
a - Onset-delay (ms)	55 ± 25	58 ± 46	57 ± 61
b - Peak-delay (ms)	268 ± 127	189 ± 104	144 ± 104
c - TTP_{SD} (ms)	149 ± 48	159 ± 44	149 ± 52
Discoordination septal / lateral wall			
d - SRS_{sept} (%)	7.2 ± 4.5	3.8 ± 2.6	3.6 ± 3.9
e - SSI (%)	8.7 ± 5.5	5.1 ± 3.8	5.0 ± 4.4
f – $ISF_{sep-lat}$	0.43 ± 0.25	0.29 ± 0.21	0.25 ± 0.16
g -Septal strain patterns (n, %)			
LBBB-1	7 (26)	5 (19)	10 (37)
LBBB-2	15 (56)	13 (48)	6 (22)
LBBB-3	5 (19)	9 (33)	11 (41)
Discoordination total LV			
h - ISF_{LV}	0.46 ± 0.22	0.35 ± 0.17	0.37 ± 0.13
i - CURE	0.81 ± 0.09	0.77 ± 0.09	0.78 ± 0.06

CMR, cardiac magnetic resonance imaging; TAG, tagging; FT, feature tracking; STE, speckle tracking echocardiography; AVC strain, strain value at aortic valve closure; TTP_{max}, time to maximal peak shortening; Onset-delay, time delay between onset of shortening of septal and lateral wall; Peak-delay, septal to lateral wall delay of TTP_{max}; TTP_{SD}, standard deviation if time to peak max of all segments; SRS_{sept}, septal systolic rebound stretch; SSI, systolic stretch index; $ISF_{sep-lat}$, internal stretch factor of septum and lateral wall; ISF_{LV}, internal stretch factor of all left ventricular segments; CURE, circumferential uniformity ratio estimates.

Table 3. Intra-class correlation and correlation of CMR tagging vs. CMR feature tracking and CMR tagging vs. speckle tracking echocardiography.

	CMR-TAG vs. CMR-FT (n=27)		CMR-TAG vs. STE (n=27)	
	ICC (95% CI)	R	ICC (95% CI)	R
Basic strain septum				
1 - AVC strain septum (%)	0.55 (0.09 - 0.79)	0.67‡	0.23 (-0.10 - 0.56)	0.47*
2 - Peak strain septum (%)	0.58 (0.26 - 0.78)	0.55†	0.155 (-0.10 - 0.45)	0.42*
3 - TTP_{max} septum (ms)	0.17 (-0.11 - 0.47)	0.11	0.00 (-0.15 - 0.22)	-0.16
4 - Systolic strain rate septum (%/s)	0.56 (0.16 - 0.79)	0.66‡	0.25 (-0.10 - 0.57)	0.45*
5 - Diastolic strain rate septum (%/s)	0.64 (0.35 - 0.82)	0.66‡	0.34 (-0.05 - 0.635)	0.50†
Basic strain lateral wall				
1 - AVC strain lateral (%)	0.50 (0.16 - 0.74)	0.50†	0.08 (-0.27 - 0.43)	0.10
2 - Peak strain lateral (%)	0.54 (0.22 - 0.76)	0.59†	0.01 (-0.31 - 0.36)	0.02
3 – TTP_{max} lateral (ms)	0.34 (0.00 - 0.63)	0.40*	0.13 (-0.12 - 0.41)	0.23
4 - Systolic strain rate lateral (%/s)	0.575 (0.26 - 0.78)	0.58†	0.05 (-0.35 - 0.42)	0.05
5 - Diastolic strain rate lateral (%/s)	0.82 (0.65 - 0.91)	0.82‡	0.23 (-0.08 - 0.53)	0.38
Dyssynchrony				
a - Onset-delay (ms)	0.42 (0.05 - 0.69)	0.23	0.024 (-0.37 - 0.40)	-0.08
b - Peak-delay (ms)	0.45 (0.045 - 0.715)	0.46*	0.23 (-0.09 - 0.53)	0.27
c - TTP_{SD} (ms)	0.46 (0.11 - 0.71)	0.49†	0.20 (-0.20 - 0.54)	0.19
Regional discoordination				
d - SRS_{sept} (%)	0.41 (-0.06 - 0.72)	0.65‡	0.30 (-0.05 - 0.60)	0.41*
e - SSI (%)	0.58 (0.00 - 0.83)	0.68‡	0.55 (0.02 - 0.81)	0.70‡
f – $ISF_{sep-lat}$	0.53 (0.10 - 0.77)	0.45*	0.46 (-0.06 - 0.76)	0.69‡
Discoordination total LV				
h - ISF_{LV}	0.55 (0.15 - 0.78)	0.66‡	0.32 (-0.02 - 0.61)	0.42*
i - CURE	0.49 (0.145 – 0.725)	0.37	0.41 (0.06 - 0.67)	0.36

CI, confidence interval; ICC, intra-class correlation coefficient; R, correlation coefficient; for other abbreviations see table 2. P-values for statistical significance of R-values are given with *, p-value <0.05; †, p-value <0.01; ‡, p-value <0.001.

Dyssynchrony parameters

a) Onset delay was quite similar for CMR-TAG and CMR-FT, with a mean difference in the Bland-Altman plot of -2.5ms (supplemental figure 2).

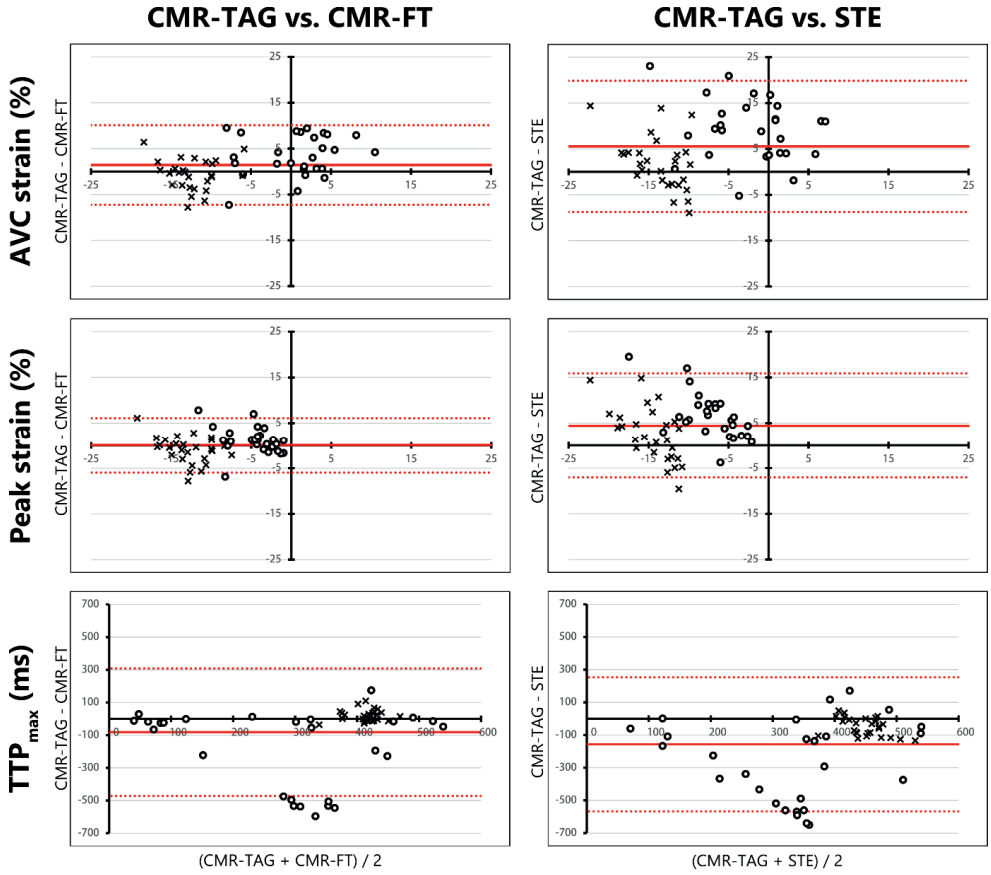


Figure 3: Bland-Altman plots of basic strain parameters. Bland-Altman plots for CMR-TAG vs. CMR-FT and CMR-TAG vs. STE of three basic strain parameters. The mean of two techniques is plotted on the x-axis and the difference on the y-axis. The mean difference is displayed as a solid red line, while the limits of agreement are displayed as dotted red lines. Septal values are given as dots, while lateral wall values are given as crosses. AVC strain, strain at aortic valve closure time; Peak strain, highest negative peak strain value; TTP_{max}, time to maximal peak strain; CMR, cardiac magnetic resonance imaging; TAG, tagging; FT, feature tracking; STE, speckle tracking echocardiography.

The corresponding ICC was fair (ICC 0.42, R 0.23). CMR-TAG vs. STE also had a low mean difference of -1.9ms, although the limits of agreement where larger, combined with a poor ICC (ICC 0.024, R -0.08). b) Peak delay of CMR-TAG was overall larger compared to CMR-FT and STE (supplemental figure 2). ICC was fair for CMR-FT (ICC 0.45, R 0.46), and poor for STE (ICC 0.23, R 0.27). TTP_{SD} (c) showed a fair ICC for CMR-FT (ICC 0.46, R 0.49), and poor ICC for STE (ICC 0.20, R 0.19).

Regional discoordination parameters

d) SRS_{sept} showed a fair ICC for CMR-FT (ICC 0.41, R 0.65), while agreement was poor for STE (ICC 0.30, R 0.41). CMR-TAG showed overall higher values for SRS_{sept} compared to both other imaging techniques. The difference of CMR-TAG to CMR-FT and STE were mostly positive, indicating an underestimation by CMR-FT and STE (figure 4). e) SSI also showed an overall underestimation by CMR-FT and STE compared to CMR-TAG. Agreement on SSI was fair for CMR-FT (ICC 0.58, R 0.68) and STE (ICC 0.55, R 0.70). f) $ISF_{sep-lat}$ was comparable between techniques, ICC's of both CMR-FT (ICC 0.53, R 0.45) and STE (ICC 0.46, R 0.69) were fair. Overall values were still lower by CMR-FT and STE compared to CMR-TAG (figure 4). For septal strain patterns (g) the kappa value of CMR-TAG vs. CMR-FT (0.465 $p<0.001$) was higher compared to the kappa of CMR-TAG vs. STE (0.265, $p<0.001$). The number of patients crossing over from LBBB-1 or LBBB-2 on the one hand, and LBBB-3 on the other, using CMR-TAG and CMR-FT is rather low (n=4, 15%), especially compared to CMR-TAG and STE (n=8, 30%) (figure 2).

Discoordination parameters of the total LV

ICC of ISF_{LV} (h) of CMR-FT (ICC 0.55, R 0.66) was the highest off all dyssynchrony and discoordination parameters. Both ICC and R values were lower for STE (ICC 0.32, R 0.42). The CURE index (i) showed rather comparable values between techniques (figure 5) with relative narrow limits of agreement in the Bland-Altman plot. Both CMR-FT (ICC 0.485, R 0.37) and STE (ICC 0.41, R 0.36) resulted in a fair ICC value for CURE compared to CMR-TAG (table 3).

DISCUSSION

This study explores the comparison of strain parameters in CRT candidates of two widely available strain analysis techniques, speckle tracking echocardiography and CMR feature tracking, with gold-standard CMR tagging. While most basic strain and dyssynchrony parameters differed substantially between techniques, there were apparent similarities found for discoordination parameters. This finding is promising, as discoordination parameters are potential predictors for CRT response.(10,11,20)

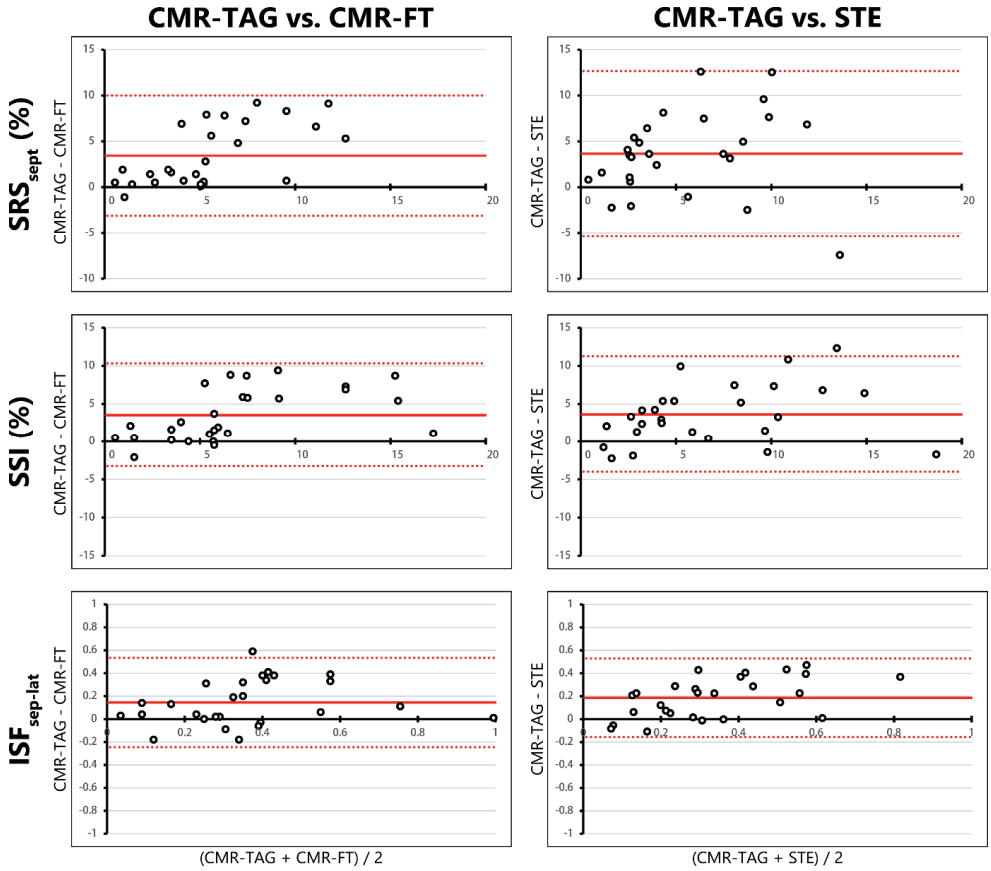


Figure 4: Bland-Altman plots of regional discoordination parameters. Bland-Altman plots for CMR-TAG vs. CMR-FT and CMR-TAG vs. STE of regional discoordination parameters (i.e. SRS_{sept}, SSI and $ISF_{sep-lat}$). The mean value of one patient analysed with the two techniques is plotted on the x-axis and the difference on the y-axis. The mean difference is displayed as a solid red line, while the limits of agreement are displayed as dotted red lines. SRS_{sept}, septal systolic rebound stretch; SSI, systolic stretch index; $ISF_{sep-lat}$, internal stretch factor of septum and lateral wall; CMR, cardiac magnetic resonance imaging; TAG, tagging; FT, feature tracking; STE, speckle tracking echocardiography.

The CMR-based techniques (i.e. CMR-TAG and CMR-FT) showed the highest agreement, shown in fair ICC values, higher R values, and relative narrow limits of agreement of the Bland-Altman plots. STE mostly had a poor agreement with CMR-TAG. CMR-FT may therefore be a valuable alternative to CMR-TAG for analysis of discoordination parameters in patients eligible for CRT.

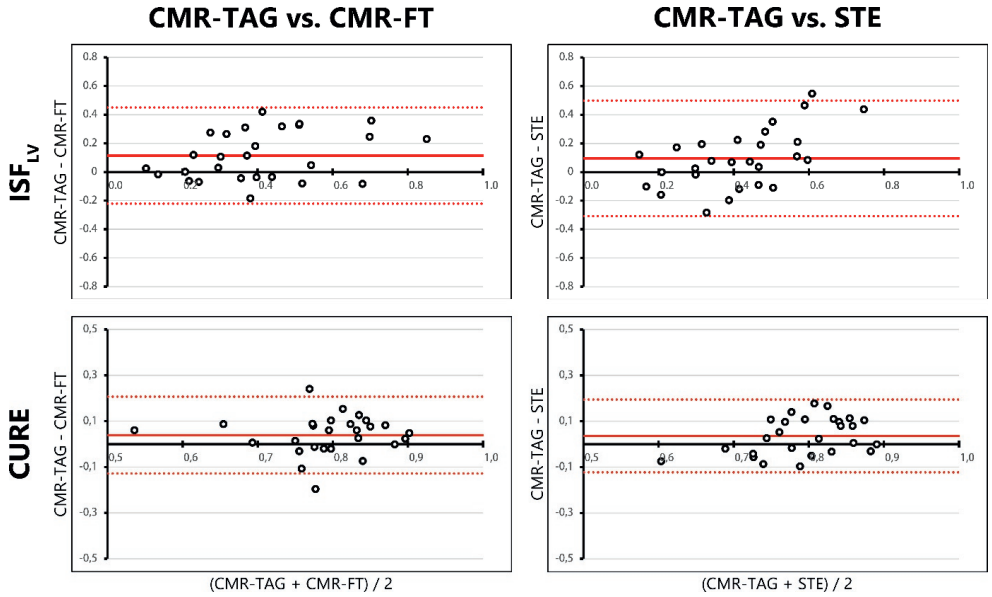


Figure 5: Bland-Altman plots of discoordination parameters of the total LV. Bland-Altman plots for CMR-TAG vs. CMR-FT and CMR-TAG vs. STE of two discoordination parameters, obtained from the total LV. The mean value of one patient analysed with the two techniques is plotted on the x-axis and the difference on the y-axis. The mean difference is displayed as a solid red line, while the limits of agreement are displayed as dotted red lines. ISF_{LV}, internal stretch factor of the total LV; CURE, circumferential uniformity ratio estimates; LV, left ventricle; CMR, cardiac magnetic resonance imaging; TAG, tagging; FT, feature tracking; STE, speckle tracking echocardiography.

Comparison of imaging techniques

To the best of our knowledge, this is the first study to compare strain parameters between different strain analysis techniques in a CRT patient population. The overall agreement between CMR-FT and CMR-TAG was higher compared to the agreement between STE and CMR-TAG. We would like to discuss three considerations to ascribe this difference. Firstly, STE uses a different imaging source, while both CMR-FT and CMR-TAG are obtained with the same imaging modality. Second, as part of the protocol, echocardiographic examinations and CMR scans were not performed on the same day. Therefore, physiological differences, such as loading conditions and heart rate, may have interfered with agreement of STE and CMR-TAG. Third, the imaging plane used for CMR and echocardiography is possibly different.

Echocardiographic parasternal short-axis views were obtained from a single intercostal position, angulating the echo probe to the mitral valve annulus plane and the papillary muscle plane. These imaging planes may thereby be partly oblique, while CMR imaging planes were 'true' short-axis views. Furthermore, CMR-FT and CMR-TAG images were acquired on the almost exact same slice position, while the anatomical plane of STE images may be different. Another factor causing discrepancies between techniques is the specific manufacturer used for strain analysis with either CMR-TAG, CMR-FT, or STE.(24) Results of CMR-TAG, CMR-FT, and STE are contemporary, as they are dependent on specific analysis algorithms which are constantly under development. Although earlier studies show less favourable agreement of CMR-TAG and CMR-FT,(25,26) recent developments are more promising.(27,28) This trend is in accordance with our results, as we found that CMR-FT had fair agreement with CMR-TAG. However, further improvements are necessary, as results obtained with different imaging techniques can still differ largely for the individual patient. These differences may have underestimated the agreement between STE and CMR-TAG, compared to CMR-TAG vs. CMR-FT. Nevertheless, echocardiography has its known limitations. High quality images are required for reliable strain analysis with STE,(29,30) but can be difficult in this selection of patients. Frame rate is directly related to the temporal resolution, which is often high in echocardiographic images, especially compared to the relative low frame rate of standard cine images used for CMR-FT. A low frame rate causes under sampling and may lead to misinterpretation of peak and time-to-peak values in strain signals.(29) The frame rate of CMR-TAG was relatively high and comparable to STE in our study. Therefore, CMR-TAG may be considered a true gold-standard technique in this study, as imaging quality and frame rate of the implemented tagging protocol were optimized.

Assessment of strain parameters

Peak strain parameters showed fair correlation, especially between CMR techniques, except for timing indices of the septum. The maximal peak of septal strain can shift easily in case of dyssynchrony, as there are often multiple peaks (e.g. LBBB-1 and -2 patterns). Changes in absolute strain values of these peaks can drastically change TTP_{max}. In previous studies, most dyssynchrony and discoordination parameters have been primarily analysed with a single imaging

technique. While some (i.e. CURE and ISF_{LV}) are predominantly used in CMR-based studies,(20) others (i.e. SRS_{sept}, peak-delay and septal strain patterns) are primarily derived with STE.(12) In our study, basic strain parameters, and more complex parameters of mechanical dyssynchrony showed apparent variations among the three techniques. However, the three techniques did show fair agreement on discoordination parameters. This indicates that these parameters adequately reflect mechanical discoordination and that they are detectable by multiple modalities. Discoordination parameters are promising as predictors for CRT response.(10,11,20) The predictive value of discoordination parameters is even known in combination with electrocardiographic parameters.(6,11) ISF_{LV} and CURE are predictors of CRT response and use information of all available LV segments,(31) therefore reflecting total LV discoordination.(20,21) These parameters are also less susceptible to outliers compared to basic strain parameters, as they contain information on all segments.(20,21) Parameters being calculated using averages of multiple segments (i.e. SRS_{sept}, SSI) also showed fair agreement between modalities. Obtaining deformation characteristics using averages of multiple segments may therefore reduce noise and measurement variability. Specific pre-specified septal strain patterns are known to predict CRT response, as LBBB-1 and LBBB-2 patterns are associated with volumetric response after CRT, while LBBB-3 is not.(12,32) The relative high agreement between CMR-TAG and CMR-FT on LBBB-1 and LBBB-2 on the one hand, and LBBB-3 on the other is therefore promising for further implementation of septal strain pattern categorization using CMR.(12)

Myocardial strain orientation

STE parameters are mainly validated with longitudinal strain,(33,34) while CMR is predominantly based on circumferential strain.(21) Circumferential strain is more intuitive, as mid-myocardial fibres are orientated in the circumferential direction and short-axis images represent all segments distributed around the LV at each level (i.e. basal, mid or apical).(35) The method of determining circumferential strain calculation differs between the three methods. Both the CMR-FT and STE software track specific myocardial details, respectively ‘features’ and ‘speckles’, of the endo- and epicardial border.(14) The specific wall layer used for strain analysis differed between techniques. The results of the endocardial layer were used for STE, as the epicardial layer often lacked an

appropriate border zone. Strain values of CMR-FT were a product of endocardial and epicardial strain. This is in contrast to CMR-TAG, of which strain of the mid-wall layer was used.(19) The difference between the approaches may have biased the overall level of agreement. Endocardial strain is known to give higher peak values compared to epicardial strain,(36) and might also be higher than midmyocardial values, which can be appreciated in the positive mean difference between CMR-TAG and STE on peak strain and AVC-strain in the Bland-Altman results. This difference may have also affected the agreement of dyssynchrony and discoordination parameters.

Limitations

CMR imaging with myocardial tagging was performed in a small subset of patients from the MARC study, which may have given outliers a relatively large effect on results. The patient population was moreover limited to patients eligible for CRT, reducing variability in measurements. These results should therefore be validated in a larger cohort. However, strain measurements are of particular interest in this specific population to improve patient selection for CRT. As mentioned, the study protocol has also influenced results, as echocardiographic and CMR examination were not performed on the same day. Moreover, differences in imaging plane between CMR and STE are possible and strain analysis was not performed on the same wall layers. ECG triggering differs between imaging techniques, as ECG electrodes were repositioned between examinations and a different lead may have been used. Moreover, ECG triggering of STE was placed at QRS onset, while the top of the R wave is used for CMR. ECG triggering affects the reference value and may have affected subsequent values of timing and absolute changes. While STE relied on end-diastolic region of interest placement, CMR-FT used both end-systolic and end-diastolic region of interests to determine myocardial strain. The reliability of CMR-FT may therefore be higher. Echocardiography was moreover obtained with ultrasound machines from two vendors, possibly introducing differences in source data. The overall lower agreement of CMR-TAG and STE should therefore be appreciated carefully. STE was performed with circumferential strain obtained from short axis images, for a more direct comparison between techniques. While circumferential strain is widely used in scientific publications, standardization of algorithms of STE has also mainly been done for longitudinal

strain.(5,34) Longitudinal strain assessed with STE may therefore have a higher reliability and reproducibility compared to circumferential strain. The effect of using longitudinal or circumferential strain derived with STE for prediction of CRT response deserves attention in future work.

Clinical application

The overall reasonable agreement between CMR-TAG and CMR-FT is promising for clinical application. CMR-FT might be a reasonable alternative for CMR-TAG and STE, as suitable CMR cine images are more easily available in clinical practice, compared to the highly specialized CMR-TAG protocols. Detection of mechanical discoordination with CMR-FT is a valuable addition to CMR, which already constitutes an important imaging tool in CRT-candidates for accurate determination of the LV ejection fraction and scar tissue localization.(31) On the other hand, a portable and bed-side tool like STE might have the highest clinical applicability, of which most discoordination parameters also showed fair agreement compared to the CMR-TAG. The reasonable agreement of the three techniques on mechanical discoordination parameters is moreover promising for the prediction of response to CRT. The implemented discoordination parameters were previously associated with CRT response in single centre studies.(10,11,20) However, previous markers of CRT response failed to take the final step to clinical application, partly because validation to gold-standard techniques was missing.(9) As the specific methods and modality may slightly differ from previous publications, further studies are needed for implementation into clinical practice. Future studies will focus on the predictive value of these parameters using follow-up data in this specific population.

CONCLUSION

In conclusion, comparison of strain analysis techniques showed that CMR-FT had an overall fair agreement with gold-standard CMR-TAG. Although agreement between STE and CMR-TAG was overall lower, direct comparison was limited by technical and methodological differences. The agreement was highest in parameters of mechanical discoordination, compared to basic strain or dyssynchrony parameters. CMR-FT is therefore a potentially valuable clinical alternative for CMR-TAG and STE, especially in the evaluation of mechanical discoordination in CRT-candidates.

REFERENCES

1. Brignole M, Auricchio A, Baron-Esquivias G, Bordachar P, Boriani G, Breithardt OA, et al. 2013 ESC Guidelines on cardiac pacing and cardiac resynchronization therapy. Eur Heart J. 2013;34:2281-2329.
2. Sweeney MO, Prinzen FW. Ventricular pump function and pacing: physiological and clinical integration. Circ Arrhythm Electrophysiol. 2008;1:127-39.
3. Daubert JC, Saxon L, Adamson PB, Auricchio A, Berger RD, Beshai JF, et al. 2012 EHRA/HRS expert consensus statement on cardiac resynchronization therapy in heart failure: implant and follow-up recommendations and management. Europace. 2012;14:1236-86.
4. Auricchio A, Prinzen FW. Non-responders to cardiac resynchronization therapy: the magnitude of the problem and the issues. Circ J. 2011;75:521-7.
5. van Everdingen WM, Schipper JC, van 't Sant J, Ramdat Misier K, Meine M, Cramer MJ. Echocardiography and cardiac resynchronisation therapy, friends or foes? Neth Heart J. 2016;24:25-38.
6. Risum N, Tayal B, Hansen TF, Bruun NE, Jensen MT, Lauridsen TK, et al. Identification of Typical Left Bundle Branch Block Contraction by Strain Echocardiography Is Additive to Electrocardiography in Prediction of Long-Term Outcome After Cardiac Resynchronization Therapy. J Am Coll Cardiol. 2015;66:631-41.
7. Wang CL, Wu CT, Yeh YH, Wu LS, Chan YH, Kuo CT, et al. Left bundle-branch block contraction patterns identified from radial-strain analysis predicts outcomes following cardiac resynchronization therapy. Int J Cardiovasc Imaging. 2017;33:869-877.
8. Leenders GE, Cramer MJ, Bogaard MD, Meine M, Doevendans PA, De Boeck BW. Echocardiographic prediction of outcome after cardiac resynchronization therapy: conventional methods and recent developments. Heart Fail Rev. 2011;16:235-50.
9. Chung ES, Leon AR, Tavazzi L, Sun JP, Nihoyannopoulos P, Merlino J, et al. Results of the Predictors of Response to CRT (PROSPECT) trial. Circulation. 2008;117:2608-16.
10. Leenders GE, De Boeck BW, Teske AJ, Meine M, Bogaard MD, Prinzen FW, et al. Septal rebound stretch is a strong predictor of outcome after cardiac resynchronization therapy. J Card Fail. 2012;18:404-12.
11. Lumens J, Tayal B, Walmsley J, Delgado-Montero A, Huntjens PR, Schwartzman D, et al. Differentiating Electromechanical From Non-Electrical Substrates of Mechanical Discoordination to Identify Responders to Cardiac Resynchronization Therapy. Circ Cardiovasc Imaging. 2015;8:e003744.
12. Leenders GE, Lumens J, Cramer MJ, De Boeck BW, Doevendans PA, Delhaas T, et al. Septal deformation patterns delineate mechanical dyssynchrony and regional differences in contractility: analysis of patient data using a computer model. Circ Heart Fail. 2012;5:87-96.
13. Revah G, Wu V, Huntjens PR, Piekarski E, Chyou JY, Axel L. Cardiovascular magnetic resonance features of mechanical dyssynchrony in patients with left bundle branch block. Int J Cardiovasc Imaging. 2016;32:1427-1438.
14. Pedrizzetti G, Claus P, Kilner PJ, Nagel E. Principles of cardiovascular magnetic resonance feature tracking and echocardiographic speckle tracking for informed clinical use. J Cardiovasc Magn Reson. 2016;18:51.

15. Harrild DM, Han Y, Geva T, Zhou J, Marcus E, Powell AJ. Comparison of cardiac MRI tissue tracking and myocardial tagging for assessment of regional ventricular strain. Int J Cardiovasc Imaging. 2012;28:2009-18.
16. Zwanenburg JJ, Gotte MJ, Kuijer JP, Heethaar RM, van Rossum AC, Marcus JT. Timing of cardiac contraction in humans mapped by high-temporal-resolution MRI tagging: early onset and late peak of shortening in lateral wall. Am J Physiol Heart Circ Physiol. 2004;286:H1872-80.
17. Maass AH, Vernooy K, Wijers SC, van 't Sant J, Cramer MJ, Meine M, et al. Refining success of cardiac resynchronization therapy using a simple score predicting the amount of reverse ventricular remodelling: results from the Markers and Response to CRT (MARC) study. Europace. 2017;euw445.
18. Lang RM, Badano LP, Mor-Avi V, Afilalo J, Armstrong A, Ernande L, et al. Recommendations for cardiac chamber quantification by echocardiography in adults: an update from the American Society of Echocardiography and the European Association of Cardiovascular Imaging. Eur Heart J Cardiovasc Imaging. 2015;16:233-70.
19. Miller CA, Borg A, Clark D, Steadman CD, McCann GP, Clarysse P, et al. Comparison of local sine wave modeling with harmonic phase analysis for the assessment of myocardial strain. J Magn Reson Imaging. 2013;38:320-8.
20. Kirn B, Jansen A, Bracke F, van Gelder B, Arts T, Prinzen FW. Mechanical discoordination rather than dyssynchrony predicts reverse remodeling upon cardiac resynchronization. Am J Physiol Heart Circ Physiol. 2008;295:H640-6.
21. Helm RH, Leclercq C, Faris OP, Ozturk C, McVeigh E, Lardo AC, et al. Cardiac dyssynchrony analysis using circumferential versus longitudinal strain: implications for assessing cardiac resynchronization. Circulation. 2005;111:2760-7.
22. Shrout PE, Fleiss JL. Intraclass correlations: uses in assessing rater reliability. Psychol Bull. 1979;86:420-8.
23. Castillo E, Osman NF, Rosen BD, El-Shehaby I, Pan L, Jerosch-Herold M, et al. Quantitative assessment of regional myocardial function with MR-tagging in a multi-center study: interobserver and intraobserver agreement of fast strain analysis with Harmonic Phase (HARP) MRI. J Cardiovasc Magn Reson. 2005;7:783-91.
24. van Everdingen WM, Paiman ML, van Deursen CJ, Cramer MJ, Vernooy K, Delhaas T, et al. Comparison of septal strain patterns in dyssynchronous heart failure between speckle tracking echocardiography vendor systems. J Electrocardiol. 2015;48:609-16.
25. Wu L, Germans T, Guclu A, Heymans MW, Allaart CP, van Rossum AC. Feature tracking compared with tissue tagging measurements of segmental strain by cardiovascular magnetic resonance. J Cardiovasc Magn Reson. 2014;16:10.
26. Onishi T, Saha SK, Ludwig DR, Marek JJ, Cavalcante JL, Schelbert EB, et al. Feature tracking measurement of dyssynchrony from cardiovascular magnetic resonance cine acquisitions: comparison with echocardiographic speckle tracking. J Cardiovasc Magn Reson. 2013;15:95.
27. Moody WE, Taylor RJ, Edwards NC, Chue CD, Umar F, Taylor TJ, et al. Comparison of magnetic resonance feature tracking for systolic and diastolic strain and strain rate calculation with spatial modulation of magnetization imaging analysis. J Magn Reson Imaging. 2015;41:1000-12.

28. Singh A, Steadman CD, Khan JN, Horsfield MA, Bekele S, Nazir SA, et al. Intertechnique agreement and interstudy reproducibility of strain and diastolic strain rate at 1.5 and 3 Tesla: a comparison of feature-tracking and tagging in patients with aortic stenosis. J Magn Reson Imaging. 2015;41:1129-37.
29. Rosner A, Barbosa D, Aarsaether E, Kjonas D, Schirmer H, D'Hooge J. The influence of frame rate on two-dimensional speckle-tracking strain measurements: a study on silico-simulated models and images recorded in patients. Eur Heart J Cardiovasc Imaging. 2015;16:1137-47.
30. D'Hooge J, Barbosa D, Gao H, Claus P, Prater D, Hamilton J, et al. Two-dimensional speckle tracking echocardiography: standardization efforts based on synthetic ultrasound data. Eur Heart J Cardiovasc Imaging. 2016;17:693-701.
31. Bilchick KC, Dimaano V, Wu KC, Helm RH, Weiss RG, Lima JA, et al. Cardiac magnetic resonance assessment of dyssynchrony and myocardial scar predicts function class improvement following cardiac resynchronization therapy. J Am Coll Cardiol Img. 2008;1:561-8.
32. Marechaux S, Guiot A, Castel AL, Guyomar Y, Semichon M, Delelis F, et al. Relationship between two-dimensional speckle-tracking septal strain and response to cardiac resynchronization therapy in patients with left ventricular dysfunction and left bundle branch block: a prospective pilot study. J Am Soc Echocardiogr. 2014;27:501-11.
33. De Boeck BW, Teske AJ, Meine M, Leenders GE, Cramer MJ, Prinzen FW, et al. Septal rebound stretch reflects the functional substrate to cardiac resynchronization therapy and predicts volumetric and neurohormonal response. Eur J Heart Fail. 2009;11:863-71.
34. Farsalinos KE, Daraban AM, Unlu S, Thomas JD, Badano LP, Voigt JU. Head-to-Head Comparison of Global Longitudinal Strain Measurements among Nine Different Vendors: The EACVI/ASE Inter-Vendor Comparison Study. J Am Soc Echocardiogr. 2015;28:1171-1181, e2.
35. de Simone G, Ganau A, Roman MJ, Devereux RB. Relation of left ventricular longitudinal and circumferential shortening to ejection fraction in the presence or in the absence of mild hypertension. J Hypertens. 1997;15:1011-7.
36. Leitman M, Lysiansky M, Lysyansky P, Friedman Z, Tyomkin V, Fuchs T, et al. Circumferential and longitudinal strain in 3 myocardial layers in normal subjects and in patients with regional left ventricular dysfunction. J Am Soc Echocardiogr. 2010;23:64-70.

SUPPLEMENTAL MATERIAL

Table S1. Bland-Altman characteristics of CMR tagging vs. feature tracking and CMR tagging vs. STE.

	CMR-TAG vs. CMR-FT (n=27)	**CMR-TAG vs. STE (n=27)**
Basic strain septum		
1 - AVC strain septum (%)	3.5 (-5.2 - 12.2)	9.2 (-4.0 - 22.5)
2 - Peak strain septum (%)	1.1 (-4.5 - 6.7)	6.4 (-3.4 - 16.2)
3 - TTP_{max} septum (ms)	-183 (-656 - 289)	-264 (-754 - 226)
4 - Systolic strain rate septum (%/s)	8.4 (-16.0 - 32.8)	21.3 (-11.9 - 54.6)
5 - Diastolic strain rate septum (%/s)	-3.1 (-20.7 - 14.4)	0.8 (-48.8 - 50.5)
Basic strain lateral wall		
1 - AVC strain lateral (%)	-0.6 (-7.2 - 5.9)	1.9 (-9.7 – 13.4)
2 - Peak strain lateral (%)	-1.0 (-6.8 - 4.9)	2.4 (-9.4 - 14.2)
3 – TTP_{max} lateral (ms)	19 (-49 - 88)	-50 (-158 - 58)
4 - Systolic strain rate lateral (%/s)	-1.4 (-17.0 - 14.3)	0.5 (-26.9 - 27.9)
5 - Diastolic strain rate lateral (%/s)	1.9 (-13.7 - 17.6)	17.2 (-28.9- 63.2)
Dyssynchrony		
a - Onset-delay (ms)	-3 (-81 - 76)	-2 (-130 - 126)
b - Peak-delay (ms)	80 (-138 - 297)	124 (-136 - 385)
c - TTP_{SD} (ms)	-9 (-103 - 85)	1 (-124 - 126)
Discoordination septal and lateral wall		
d - SRS_{sept} (%)	3.4 (-3.1 – 10.0)	3.7 (-5.3 - 12.7)
e - SSI (%)	3.5 (-3.2 - 10.3)	3.6 (-4.0 - 11.3)
f – $ISF_{sep\text{-}lat}$	0.14 (-0.245 - 0.53)	0.19 (-0.16 - 0.53)
Discoordination total LV		
h - ISF_{LV}	0.11 (-0.22 - 0.45)	0.10 (-0.31 - 0.50)
i - CURE	0.04 (-0.13 - 0.21)	0.04 (-0.12 - 0.195)

Mean difference of the two techniques is given for each comparison (CMR-TAG minus CMR-FT and CMR-TAG minus STE), with the 95% confidence interval within brackets. For abbreviations see table 2.

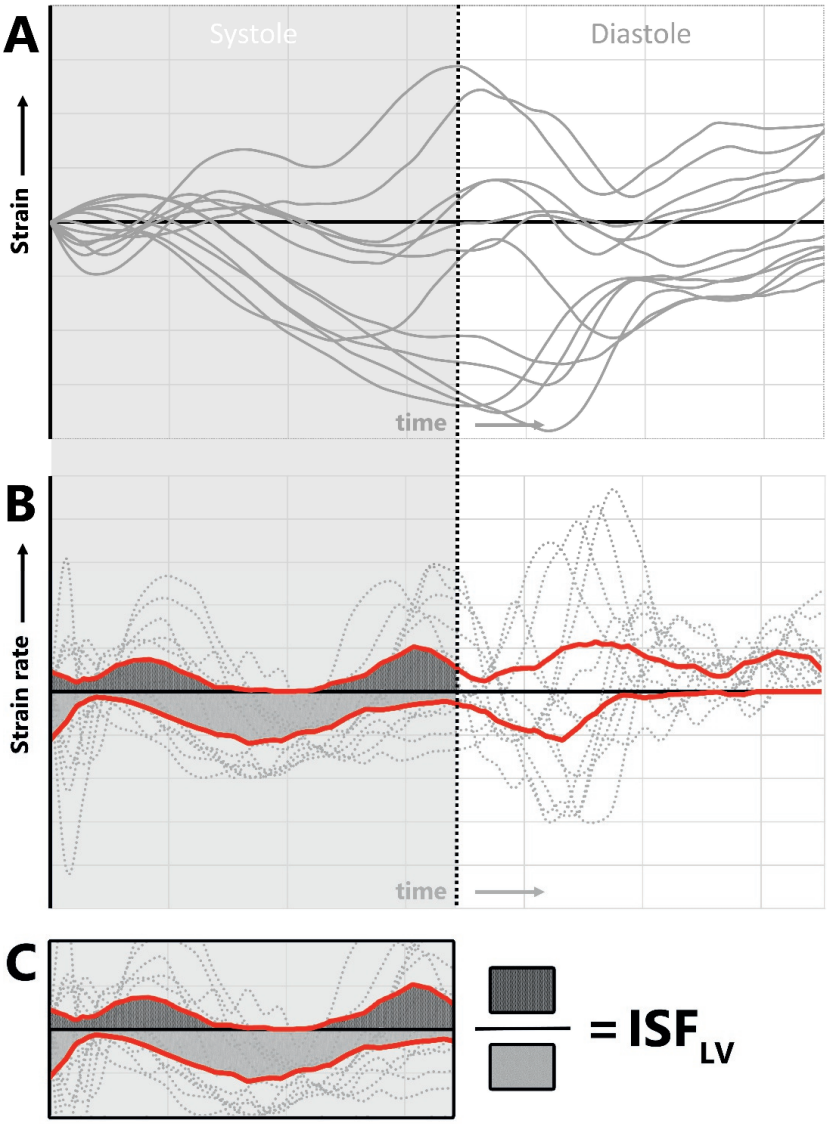


Figure S1: Method for calculation of $ISF_{LV.}$ After calculation of the first derivative of strain (panel A), positive and negative strain rate are averaged (red lines, panel B). The areas of positive (dark grey) and negative (light grey) average strain rate during systole are divided to obtain ISF_{LV} (panel C). The end of systole is marked by the black dotted line.

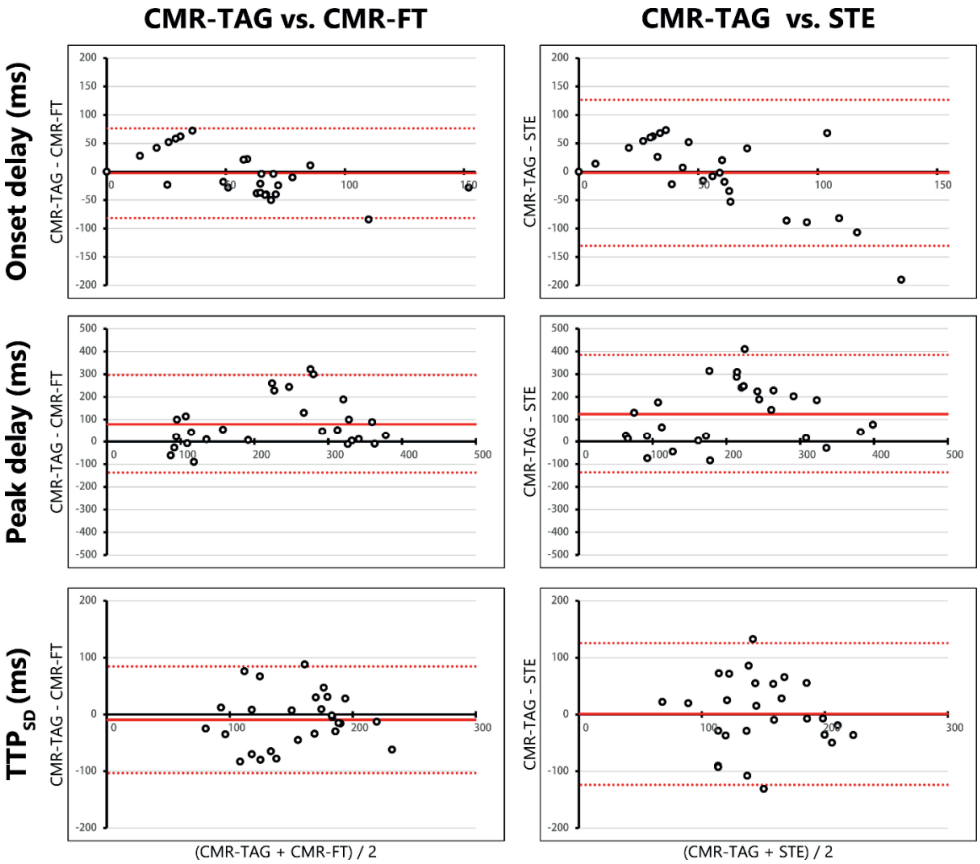


Figure S2: Bland-Altman plots of dyssynchrony parameters. Bland-Altman plots for CMR-TAG vs. CMR-FT and CMR-TAG vs. STE of remaining parameters, not displayed in the main manuscript. On the x-axis the mean of two techniques and on the y-axis the difference. The mean difference is displayed as a solid red line, while the limits of agreement are displayed as dotted red lines. Onset delay, delay between onset of shortening of septal and lateral wall. SSI, systolic stretch index; $TTP_{SD,}$ standard deviation of time to maximal peak of all segments; CMR, cardiac magnetic resonance imaging; TAG, tagging; FT, feature tracking; STE, speckle tracking echocardiography.

Chapter 6

Strain Imaging to Predict Response to Cardiac Resynchronization Therapy: a Systematic Comparison of Strain Parameters Using Multiple Imaging Techniques

ESC Heart Failure 2018;5:1130-1140

Alwin Zweerink*
Wouter M. van Everdingen*
Robin Nijveldt
Odette A.E. Salden
Mathias Meine
Alexander H. Maass
Kevin Vernooy
Frederik J. de Lange
Marc A. Vos
Pierre Croisille
Patrick Clarysse
Bastiaan Geelhoed
Michiel Rienstra
Isabelle C. Van Gelder
Albert C. van Rossum
Maarten J. Cramer*
Cornelis P. Allaart*

* The first two and last two authors contributed equally to this work

ABSTRACT

Aims: Various strain parameters and multiple imaging techniques are presently available including CMR tagging (CMR-TAG), feature tracking (CMR-FT) and speckle tracking echocardiography (STE). This study aims to compare predictive performance of different strain parameters and evaluate results per imaging technique to predict cardiac resynchronization therapy (CRT) response.

Methods and Results: Twenty-seven patients were prospectively enrolled and underwent CMR- and echocardiographic examination before CRT implantation. Strain analysis was performed in the circumferential (CMR-TAG, CMR-FT and STE-circ) and longitudinal (STE-long) orientation. Regional strain values, parameters of dyssynchrony and discoordination were calculated. After twelve months, CRT response was measured by the echocardiographic change in LV end-systolic volume (LVESV). Twenty-six patients completed follow-up, mean LVESV change was -29±27% with 17 (65%) patients showing ≥15% LVESV reduction. Measures of dyssynchrony (SD-TTP_{LV}) and discoordination (ISF_{LV}) were strongly related to CRT response when using CMR-TAG (R^2 0.61 and R^2 0.57, respectively), but showed poor correlations for CMR-FT and STE (all R^2 ≤0.32). In contrast, the end-systolic septal strain (ESS_{sep}) parameter showed a consistent high correlation with LVESV change for all techniques (CMR-TAG R^2 0.60; CMR-FT R^2 0.50; STE-circ R^2 0.43; and STE-long R^2 0.43). After adjustment for QRS duration and QRS morphology, ESS_{sep} remained an independent predictor of response per technique.

Conclusions: End-systolic septal strain was the only parameter with a consistent good relation to reverse remodeling after CRT, irrespective of assessment technique. In clinical practice, this measure can be obtained by any available strain imaging technique and provides predictive value on top of current guideline criteria.

INTRODUCTION

Guideline recommendations for cardiac resynchronization therapy (CRT) primarily depend on QRS duration and left bundle branch block (LBBB) morphology resulting in approximately one-third of patients becoming 'non-responders'.(1-3) Despite substantial efforts to improve patient selection for CRT, parameters that better predict CRT response are currently lacking. Myocardial strain imaging is a promising tool that quantifies the mechanical consequences of LBBB. Inhomogeneity of contraction during LBBB reduces left ventricular (LV) pump function efficiency,(4) and CRT subsequently improves LV pump function by restoring mechanical efficiency of the heart.(5,6) Therefore, a variety of strain parameters has been proposed to serve as markers for CRT response over the past years.(7-9) Most of these parameters were introduced using a single-imaging modality, but at present multiple imaging modalities are available. Cardiovascular magnetic resonance (CMR) imaging offers assessment of myocardial strains using feature tracking (CMR-FT) software on standard cine images,(10-12) or by the implementation of myocardial taglines (CMR-TAG).(8, 13-15) Although CMR-TAG is often used as reference technique in scientific research, availability is limited in clinical practice. Speckle tracking echocardiography (STE), on the other hand, is widely available as a bedside tool. Although STE analysis is highly dependent on the quality of the available acoustic windows, this technique also demonstrated predictive value for CRT outcome.(7,9,16) Despite promising results of multiple strain parameters used in single-modality studies, a direct comparison of parameters between available modalities is lacking. Relative differences in strengths and weaknesses between techniques may cause optimal strain parameters to vary between modalities. In addition, multiple strain imaging techniques may be available in clinical practice and the clinician should decide which technique to use. Therefore, this study aims to compare predictive performance of different strain parameters using multiple imaging techniques, in relation to CRT response.

METHODS

Study population

This pre-defined sub-study with focus on myocardial strain imaging techniques is part of the Markers And Response to CRT (MARC) study, designed to investigate predictors of CRT response. The MARC study included two-hundred-forty patients planned for CRT implantation in six medical centers in the Netherlands. Details on the original MARC study were published previously.(17) In this sub-study, twenty-seven patients were included for undergoing a comprehensive imaging protocol including CMR myocardial tagging. Since the dedicated CMR-tagging algorithm was only available in VU University Medical Center (Amsterdam, The Netherlands), patients included at this site and two near-by centers being Academic Medical Center (Amsterdam, The Netherlands) and University Medical Center Utrecht (Utrecht, The Netherlands) gave consent for additional CMR examination at VU University Medical Center. All patients gave written informed consent and all local medical ethics committees approved data collection and management. The investigation conforms to the principles outlined in the Declaration of Helsinki.

Image acquisition: CMR imaging

All patients underwent CMR examination at the VU University Medical Center (Amsterdam, the Netherlands) on a 1.5T whole body system (Magnetom Avanto, Siemens, Erlangen, Germany) with the use of a phased array cardiac receiver coil. Both CMR cine images for CMR-FT analysis and CMR-TAG images were obtained in the same examination. Standard CMR cine images were acquired using a retrospectively ECG-gated balanced steady-state free-precession (SSFP) sequence during end-expiratory breath holding. A stack of short axis cine images was acquired covering the full LV. Subsequently, high temporal resolution cine imaging of the LV in the three-chamber view was performed to assess the opening and closure times of the mitral and aortic valve. Tagged images were acquired at the basal and mid-LV short-axis slices using a complementary spatial modulation of magnetization (CSPAMM) line tagging sequence with segmented ECG-gated acquisitions and serial breath holds.(18) Typical image acquisition parameters are reported in the supplemental material.

Image acquisition: Echocardiography

Echocardiographic examinations were performed by participating centers and sent to the echocardiographic core lab (University Medical Center Utrecht, Utrecht, The Netherlands) for detailed analysis. Examinations were performed on GE Vivid7, GE Vivid9, or Philips iE33 ultrasound machines. Standard echocardiographic images were obtained, including a parasternal short axis (PSAX) view at the papillary muscle level and at the mitral valve level and an apical four chamber view (AP4CH) view, zoomed and focused on the LV. An additional zoomed and trimmed image of the interventricular septum in the AP4CH was recorded for septal single wall analysis with higher frame rates. Images were obtained of three consecutive beats. Image quality and frame rate of all images were optimized for offline speckle tracking analysis. Pulsed-wave Doppler images of the LV outflow tract and mitral valve inlet were obtained for definition of aortic valve and mitral valve closure, respectively.

Image post-processing

Strain analysis was performed in the circumferential (CMR-TAG, CMR-FT and STE-circ) and longitudinal (STE-long) orientation. Post-processing of CMR-TAG images was performed by dedicated software using the SinMod technique (inTag v2.0, CREATIS, Lyon, France),(19) as a plug-in for OsiriX (v6.5, Pixmeo, Switzerland). Semi-automated CMR-FT analysis software (QStrain Research Edition v1.3.0.10 evaluation version, Medis, Leiden, The Netherlands) was used to analyze short-axis cine images corresponding with the mid-LV and basal slice-location of the CMR-TAG images. Echocardiographic images of the two PSAX views (STE-circ), AP4CH view and septal single wall (STE-long) were used for offline speckle tracking analysis. Images were exported as DICOM-files for vendor independent strain analysis with TomTec 2D Cardiac Performance Analysis (2DCPA, version 1.2.1.2, TomTec Imaging Systems GmbH, Munich, Germany). A detailed description of the post-processing steps for the CMR-TAG, CMR-FT and STE analysis has been published previously and is given in the supplemental material.(20)

Strain parameters

Five subsets of strain parameters were evaluated. First, basic strain values were quantified by the septal and lateral peak negative strain (peak strain); and end-systolic strain (ESS) at aortic valve closure. Secondly, dyssynchrony was measured as septal to lateral delay in onset shortening (onset-delay); peak contraction (peak-delay)(21); and the standard deviation in time to peak of the total LV (SD-TTP_{LV})(22) Thirdly, discoordination of the septal and lateral wall was measured by: systolic rebound stretch of the septum (SRS_{sep})(7); systolic stretch index ($SSI_{sep-lat}$)(9); and the internal stretch index ($ISF_{sep-lat}$). Fourthly, discoordination parameters that include all LV segments were calculated by the: circumferential uniformity ratio estimate ($CURE_{LV}$) index(13); and the internal stretch index of the total LV (ISF_{LV}).(8) Lastly, septal strain patterns were visually categorized to the following pre-specified septal strain patterns: double peaked systolic shortening (LBBB-1); early pre-ejection shortening followed by prominent systolic stretch (LBBB-2); and pseudonormal shortening with a late-systolic shortening peak and less pronounced end-systolic stretch (LBBB-3).(23) Strain parameters are illustrated in figure 1 and further explained in the supplemental material.

Assessment of CRT response

Echocardiographic assessment of LV volumes was performed before and twelve months after CRT implantation. LV end-systolic volume (LVESV) was measured using the biplane Simpson's method by two experienced observers. Volumetric response was calculated as the percent change in LVESV between baseline and twelve month follow-up. Patients with ≥15% reduction in LVESV were classified CRT responders.

Statistical analysis

Statistical analysis was performed in the study core lab (University Medical Center Groningen, Groningen, The Netherlands) by statisticians (BG, MR) using the commercially available R software (R Foundation for Statistical Computing, Vienna, Austria). Continuous variables are expressed as mean ± standard deviation or in absence of a normal distribution as median and interquartile range.

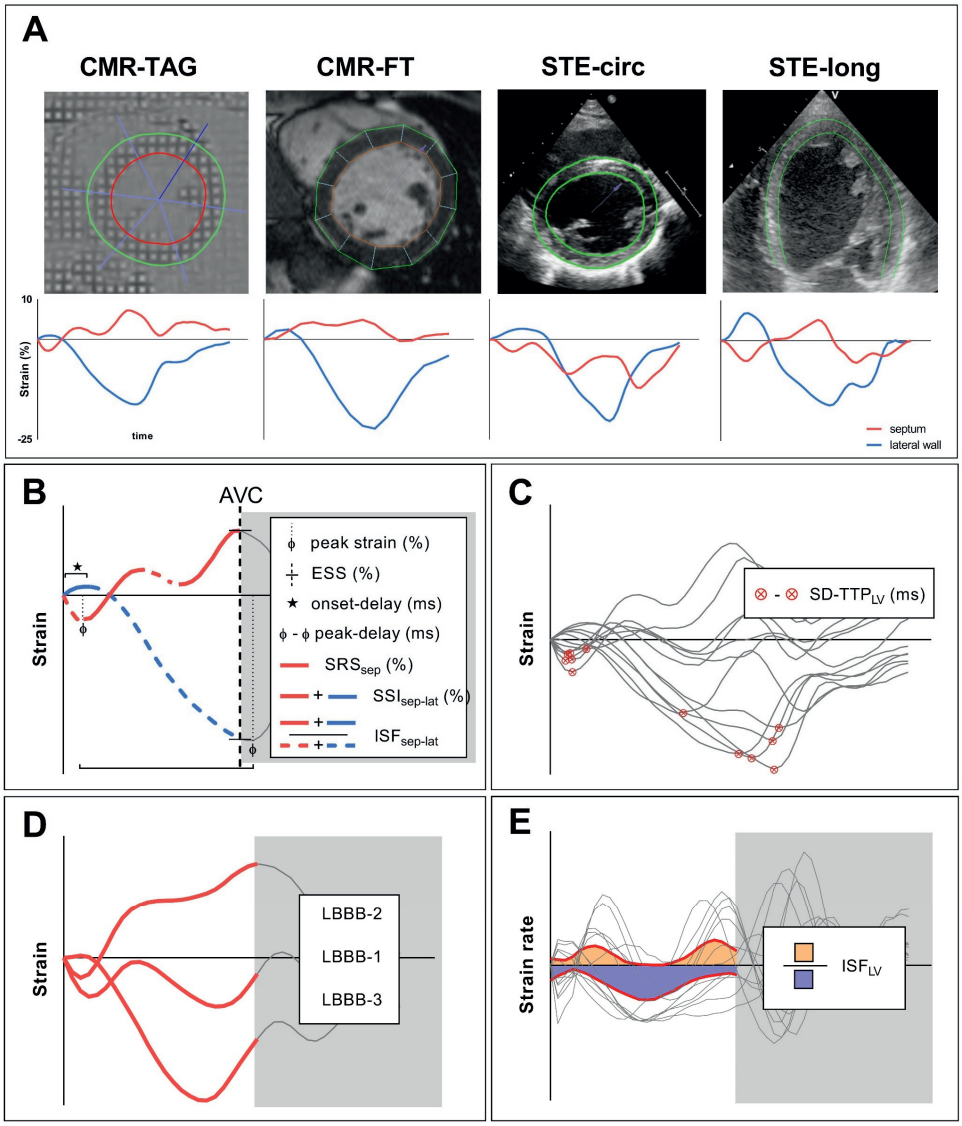


Figure 1: Imaging techniques and strain parameters. (A) Typical example of a LBBB patient with strain analysis in the circumferential (CMR-TAG, CMR-FT and STE-circ) and longitudinal (STE-long) orientation; (B) Strain parameters calculated from the septum (red) and/or lateral wall (blue) including peak negative peak strain (peak strain), end-systolic strain (ESS), septal to lateral time delay onset contraction (onset-delay) and peak contraction (peak-delay), systolic rebound stretch of the septum (SRS_{sep}), systolic stretch index ($SSI_{sep-lat}$) and internal stretch index ($ISF_{sep-lat}$); (C) the standard deviation of time to peak strain of all segments ($SD\text{-}TTP_{LV}$); (D) septal strain patterns defined as double peaked shortening (LBBB-1), predominant stretching (LBBB-2) or pseudonormal shortening (LBBB-3); (E) The internal stretch factor including all LV segments (ISF_{LV}).

Categorical variables are presented as absolute numbers and percentages. Strain parameters were compared between CRT responder groups by an independent student t-test, or a non-parametric test when appropriate. Correlations between strain parameters and volumetric CRT response were assessed using the Pearson's correlation coefficient or when normal distribution was absent, the Spearman's Rho correlation coefficient. Receiver operating characteristics (ROC) curve analysis was used to determine the predictive value of all parameters. To test the additional value of strain parameters on top of guideline criteria, multivariable linear regression analysis was performed by addition of the best performing strain parameter (based on R^2) to a model with QRS duration and QRS morphology. A p-value of <0.05 was considered statistically significant.

RESULTS

Twenty-six patients completed the study protocol including clinical follow-up of twelve months. One patient was lost to follow-up because of non-cardiac death (lung carcinoma). A detailed description of the patient characteristics is given in table 1. Mean LVESV change after twelve months was -29±27% with 17 (65%) patients becoming CRT responders.

Strain parameters and their relation to CRT response

Basic strain values measured as peak strain of the septal and lateral wall showed weak correlations with LVESV change as demonstrated in figure 2. On the other hand, ESS_{sep} showed one of the highest coefficients of determination of all parameters using CMR-TAG (R^2 0.60, p<0.001). Other imaging techniques showed good results for ESS_{sep} as well (CMR-FT R^2 0.50; STE-circ R^2 0.43; and STE-long R^2 0.43) as illustrated in figure 3. Dyssynchrony of all LV segments measured by SD-TTP_{LV} showed high correlations using CMR-TAG (R^2 0.61, p<0.001), but were disappointing for other imaging techniques (all R^2 ≤0.14).

Table 1. Patient characteristics at baseline and at twelve months follow-up

Variable	**Total group (n=26)**	**Responders (n=17)**	**Non-responders (n=9)**
Age (years)	65 ± 9	63 ± 10	68 ± 8
Gender (n, % male)	15 (58%)	9 (53%)	6 (67%)
QRS duration (ms)	182 (166 – 193)	187 (180 – 202)**	165 (143 – 176)**
QRS morphology (n, % LBBB)	21 (81%)	16 (94%)*	5 (56%)*
Etiology (n, % ICMP)	7 (27%)	1 (6%)**	6 (67%)**
NYHA class (n, %)			
Class II	17 (65%)	12 (71%)	5 (56%)
Class III	9 (35%)	5 (29%)	4 (44%)
Medication (n, %)			
Beta-blockers	22 (85%)	15 (88%)	7 (78%)
Diuretics	21 (81%)	14 (83%)	7 (78%)
ACE / ATII inhibitors	17 (65%)	11 (65%)	6 (67%)
Aldosterone antagonist	10 (38%)	8 (47%)	2 (22%)
Lab – creatinine value (unit)	76 (68 – 85)	76 (67 – 79)	80 (69 – 95)
Lab – BNP value (unit)	636 (230 – 1603)	686 (276 – 1591)	554 (214 – 1607)
CMR – LVEDV (ml)	313 ± 100	348 ± 105**	248 ± 46**
CMR – LVESV (ml)	234 ± 98	266 ± 105**	174 ± 44**
CMR – LVEF (%)	27 ± 9	25 ± 10	30 ± 6
CMR – LV mass (gr)	130 (117 – 156)	145 (124 – 173)*	115 (97 – 132)*
CMR – Scar (% LV mass)	1.8 (0.0 – 8.6)	0.0 (0.0 – 1.9)**	9.4 (5.0 – 19.5)**
CMR – Scar pattern (n, % ICMP)	8 (31%)	2 (12%)**	6 (67%)**
CMR – RVEF (%)	51 ± 12	49 ± 13	54 ± 10
Echo – Change in LVESV after twelve months (%)	-29 ± 27	-44 ± 17**	0 ± 14**

BMI, body mass index; LBBB, left bundle branch block; BNP brain natriuretic peptide; ICMP, ischemic cardiomyopathy; LVEDV, left ventricular end-diastolic volume; LVESV, left ventricular end-systolic volume; LVEF, left ventricular ejection fraction; RVEF, right ventricular ejection fraction. Statistical difference between responders and non-responders marked with $p<0.05$* and with $p<0.01$**

Other dyssynchrony measures (onset-delay; peak-delay) showed weaker coefficients of determination with LVESV change and results were subject to large variation between imaging techniques. Discoordination markers measured from the septal and lateral wall were all moderately associated with LVESV change and predictive performance was similar for different imaging techniques. Of these parameters, $ISF_{sep-lat}$ showed best results (CMR-TAG R^2 0.47; CMR-FT R^2 0.39; STE-circ R^2 0.48; and STE-long R^2 0.39, all $p<0.001$). Discoordination of all LV segments measured by ISF_{LV} yielded one of the highest coefficient of determination using CMR-TAG (R^2 0.57, $p<0.001$) while other imaging techniques showed poor results (all R^2 ≤0.32). The $CURE_{LV}$ parameter showed weak coefficients of determination with LVESV change, irrespective of imaging technique.

Visual classification of septal strain patterns

As demonstrated in figure 4, CMR-TAG and CMR-FT classified half of the patients as LBBB-2 pattern, whereas LBBB-2 pattern was found in only a quarter of the patients by means of STE techniques. In general, the LBBB-2 pattern was associated to the largest reduction in LVESV, irrespective of its technique. Patients with pattern LBBB-1 showed relatively less reverse remodeling and results differed more between techniques. The LBBB-3 pattern is in particular of interest to exclude non-responders to CRT but only CMR-TAG was accurate in doing this.

Patient characteristics and their role in CRT response

In this study, patients with ICMP showed less reduction in LVESV compared to patients with NICMP (-7±30% vs. -36±21%; p=0.010). In addition, scar size was significantly related with LVESV change (R^2 0.42; $p<0.001$). Subgroup analysis by gender revealed no significant differences in LVESV change between males and females (-24±27% vs. -35±26%; p=0.295). Patients with QRS duration ≥150ms showed a trend towards more LVESV change compared to <150ms patients (-33±24% vs. -6±33%; p=0.063). However, patients with strict LBBB morphology showed a significantly larger LVESV reduction compared to patients with intraventricular conduction delay (IVCD) morphology (-35±24% vs. -3±22%; p=0.013).

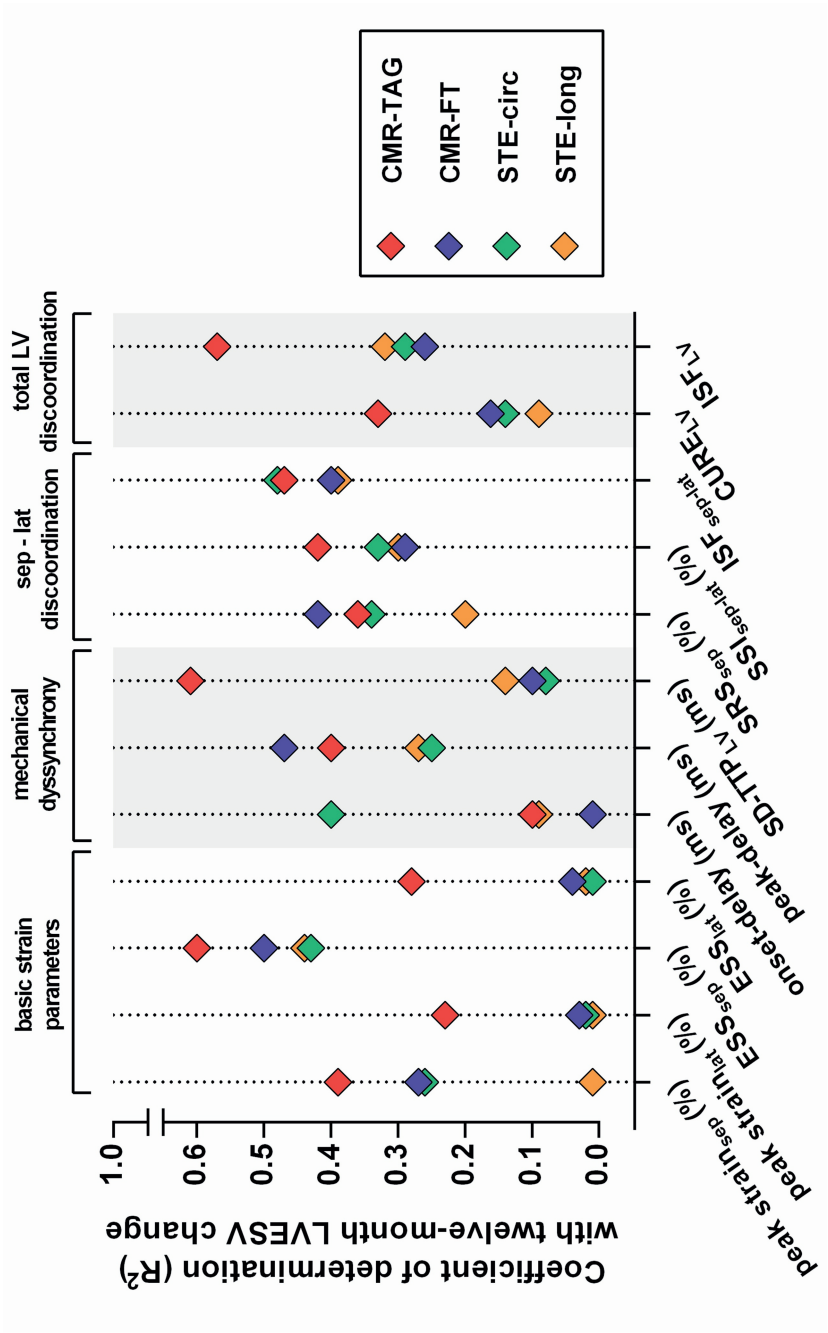


Figure 2: Coefficient of determination (R^2) of all strain parameters towards reverse remodeling after CRT. Coefficient of determination of all strain parameters towards changes in LVESV after twelve months CRT are displayed for CMR-TAG (red); CMR-FT (blue); STE-circ (green) and STE-long (orange). For other abbreviations see figure 1.

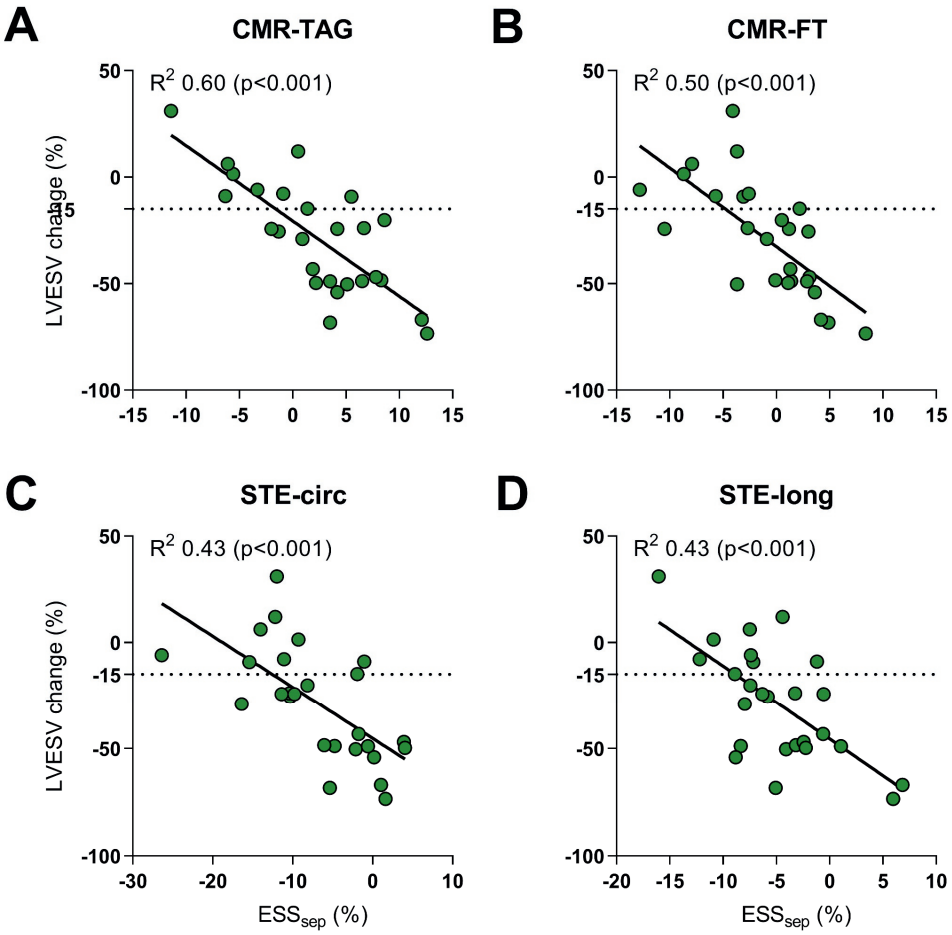


Figure 3: Correlation between end-systolic septal strain (ESS_{sep}) and LVESV change per imaging technique. The basic strain parameter end-systolic septum strain (ESS_{sep}) consistently shows a high coefficient of determination with LVESV change independent of imaging modality (A) CMR-TAG; (B) CMR-FT; (C) STE-circ and (D) STE-long.

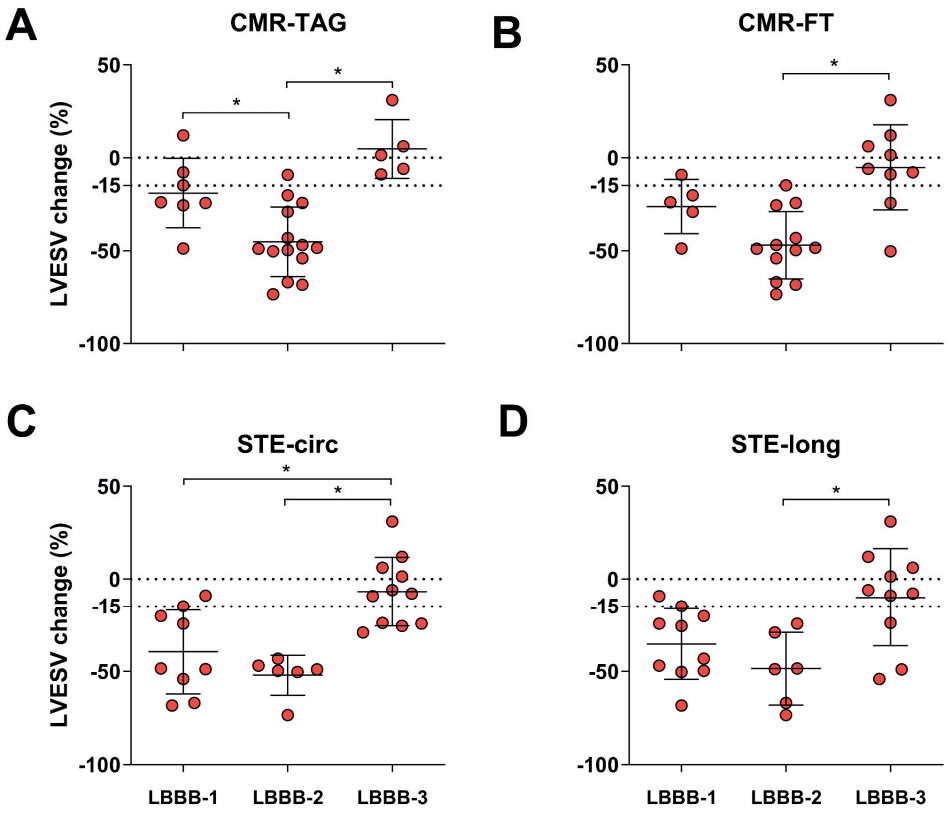


Figure 4: Classification of septal strain patterns to estimate CRT response. Septum strain patterns are classified to pre-specified categories: double peaked shortening (LBBB-1), predominant stretching (LBBB-2) or pseudonormal shortening (LBBB-3) using (A) CMR-TAG; (B) CMR-FT; (C) STE-circ and (D) STE-long. Statistical differences between LBBB categories are marked with an asterisk.

Septal strain in relation to present guideline criteria

QRS duration and QRS morphology were both significantly related with CRT response in univariable linear regression analysis. Subsequently, the best overall performing strain parameter by means of the highest R2 in relation to LVESV change, ESSsep, was implemented in a multivariable model. Multivariable linear regression analysis showed that ESSsep remained independently related to LVESV change after adjustment for QRS duration and QRS morphology as demonstrated in table 2. This finding was irrespective of the imaging technique used for ESSsep assessment (adjusted model 1-4).

DISCUSSION

This study offered the unique opportunity to compare a variety of strain parameters using multiple imaging techniques in a population that is eligible for CRT. Measures of dyssynchrony (SD-TTP_{LV}) and discoordination (ISF_{LV}) were strongly related to CRT response when using CMR-TAG. However, these parameters showed weaker correlations for CMR-FT and STE techniques. In contrast, the end-systolic septal strain parameter showed a consistent good relation to reverse remodeling after CRT, irrespective of assessment technique. This parameter demonstrated predictive value on top of current guideline criteria for each imaging technique.

Comparison of strain parameters

Two types of strain parameters that can be assessed are dyssynchrony (regional timing differences in time units) and discoordination (inefficient contraction patterns in % strain units). Both types can be calculated on a regional (i.e. septal to lateral) and segmental (i.e. 17 segments model) scale. In patients with LBBB, dyssynchrony is a direct consequence of the conduction disorder with early activation of the septum and delayed activation of the lateral wall.

Table 2. Linear regression analysis to test the additional value of end-systolic septal strain on top of guideline criteria per imaging technique

Guideline criteria + ESS_{sep} per imaging technique	**Univariable analysis**			**Adjusted model 1**		
CMR tagging	**beta**	**95% CI**	**P-value**	**beta**	**95% CI**	**P-value**
QRS duration (per ms)	-0.41	-0.74 – -0.09	0.015	-0.18	-0.42 – 0.07	0.146
QRS morphology (LBBB)	-31.99	-56.45 – -7.53	0.013	-10.63	-29.55 – 8.29	0.256
CMR-TAG ESS_{sep} (per %)	**-3.54**	**-4.77 – -2.32**	**<0.001**	**-2.95**	**-4.25 – -1.66**	**<0.001**
CMR feature tracking				**Adjusted model 2**		
QRS duration (per ms)	-0.41	-0.74 – -0.09	0.015	-0.15	-0.42 – 0.12	0.265
QRS morphology (LBBB)	-31.99	-56.45 – -7.53	0.013	-17.68	-37.52 – 2.17	0.078
CMR-FT ESS_{sep} (per %)	**-3.69**	**-5.26 – -2.13**	**<0.001**	**-2.99**	**-4.56 – -1.42**	**0.001**
STE circumferential				**Adjusted model 3**		
QRS duration (per ms)	-0.41	-0.74 – -0.09	0.015	-0.20	-0.49 – 0.09	0.172
QRS morphology (LBBB)	-31.99	-56.45 – -7.53	0.013	-13.27	-36.13 – 9.60	0.242
STE-CIRC ESS_{sep} (per %)	**-2.41**	**-3.59 – -1.23**	**<0.001**	**-1.81**	**-3.08 – -0.54**	**0.007**
STE longitudinal				**Adjusted model 4**		
QRS duration (per ms)	-0.41	-0.74 – -0.09	0.015	-0.20	-0.51 – 0.10	0.186
QRS morphology (LBBB)	-31.99	-56.45 – -7.53	0.013	-7.31	-33.20 – 18.58	0.564
STE-CIRC ESS_{sep} (per %)	**-3.43**	**-5.08 – -1.79**	**<0.001**	**-2.62**	**-4.70 – -0.54**	**0.016**

ESS_{sep}, end-systolic septal strain; LBBB, left bundle branch block

Contraction of the septum takes place under low LV pressure (i.e. low wall tension) whereas the lateral wall contracts during rising LV pressures, thus increasing regional work load.(4) Consequently, compensatory mechanisms increase contractility of the lateral wall whereas contractility of the septum is reduced. This results in the lateral wall pushing the septum back during systole (i.e. discoordination), reducing LV pump function efficiency. Our results indicate that both dyssynchrony and discoordination parameters measured on a segmental scale (i.e. SD-TTP_{LV} and ISF_{LV}) were strongly related with CRT response. From a physiological point of view, the ISF_{LV} parameter proposed by Kirn et al. is closest related to the amount of inefficient pump function that can be attributed to the LBBB conduction disorder by indexing the amount of systolic stretching (i.e. wasting myocardial work) to the amount of systolic shortening (i.e. useful myocardial work).(8) In contrast, assessing the circumferential uniformity of segmental strain values by complex Fourier analysis (i.e. CURE index) showed rather disappointing association with CRT response.(13) Possibly, the presence of stretching segments instead of non-uniformity in contraction determine benefit from CRT.

Septal strain analysis

Typical septal contraction patterns have been described to identify 'true' LBBB activation using patient data combined with computer modeling.(16,24,25) Typical LBBB strain patterns were characterized by double peaked shortening (LBBB-1) or predominant stretching (LBBB-2) of the septum.(23) Patients lacking true LBBB activation were characterized by pseudo-normal shortening of the septum (LBBB-3) and showed less reverse remodeling compared to LBBB-1 and LBBB-2 patients. Quantification of septal behavior by end-systolic septal strain (ESS_{sep}) showed a consistent high correlation with LVESV change, irrespective of imaging technique (figure 3). Of note, ESS_{sep} and the septal strain patterns are interdependent as a negative ESS_{sep} value represents LBBB-3 pattern whereas positive ESS_{sep} values represent LBBB-2 pattern. Assessment of ESS_{sep} is relatively simple as illustrated in figure 1 and requires strain analysis of the septum only. We found more positive ESS_{sep} values (i.e. net septal stretch through systole) to be associated with more extensive reverse remodeling after CRT. Preserved septal contraction by a negative ESS_{sep}, on the other hand, showed less room for improvement after CRT. Previous studies showed that electrical

resynchronization improves systolic function by recruiting myocardial work from the septum.(6,7) Therefore, systolic rebound stretch of the septum (SRS_{sep}) is used to predict CRT outcome.(7,9,26) In our study, ESS_{sep} was even closer related with LVESV changes than SRS_{sep}, possibly because ESS_{sep} is the result of both systolic shortening and stretching whereas SRS_{sep} merely measures the cumulative amount of systolic stretching. In a multivariable model, ESS_{sep} demonstrated predictive value on top of guideline criteria (i.e. QRS duration and QRS morphology) irrespective of the imaging technique used.

Comparison of strain imaging techniques

Previously, we compared strain values between imaging techniques and found that most parameters were not interchangeable for different modalities.(20) The present study demonstrates that there is only one parameter that performs equally well for all techniques, when related to CRT response. For the other strain parameters, CMR-TAG demonstrated higher correlation coefficients with LVESV change compared to other imaging techniques. Strain parameters including all LV segments (i.e. ISF_{LV} and SD-TTP_{LV}) performed best for CMR-TAG, but results were rather disappointing for CMR-FT and STE techniques. Differences were most pronounced for SD-TTP_{LV} measuring the standard deviation in segmental time to peak contraction throughout the LV. A possible explanation for this finding might be that measuring SD-TTP_{LV} requires not only high image quality to visualize all individual segments, but also sufficient temporal resolution to measure segmental timing differences. CMR-TAG combines excellent image quality with high frame rates whereas CMR-FT might be hampered by the lower temporal resolution that was used for cine imaging, and STE by the lower image quality and higher inter-study variation compared to CMR-TAG.(27) In this study, temporal resolution of the cine images for CMR-FT analysis was lower compared to the high temporal resolution of the CMR-TAG sequence (~40ms vs. ~14ms). Using higher temporal resolutions for CMR-FT might improve predictive performance of this technique, although a temporal resolution of ~40ms is typically used in standard cine-imaging protocols. CMR-FT enables myocardial strain analysis using specialized post-processing software on standard cine images.(12,28) Although this relatively new technique has not been extensively validated yet, we recently showed reasonable agreement with CMR-TAG.(20) Predictive performance of CMR-FT was highest for strain

parameters derived from the septal and lateral wall (ESS_{sep}; peak-delay; SRS_{sep}; $ISF_{sep-lat}$) whereas parameters including all LV segments (SD-TTP_{LV}; ISF_{LV}) were poorly related to CRT response. Possibly, the measurement variability of CMR-FT is too high to sample strain on a segmental scale.(29) Despite promising results of septal strain measures in the present study, data on CMR-FT in this specific patient population are scarce and further validation of this technique is needed.

In general, performance of STE was comparable to CMR-FT. STE analysis was performed in both the circumferential and longitudinal direction, each with associated strengths and weaknesses. Circumferential strain markers are considered to be more sensitive to deformation abnormalities because of the predominant circumferential fiber orientation.(30) Echocardiographic image quality, however, is often more favorable in the AP4CH view (STE-long) compared to the PSAX view (STE-circ). Taken together, overall performance of STE-circ and STE-long was very similar.

Clinical implications

Myocardial strain imaging provides new diagnostic tools that could potentially improve patient selection for CRT. At present, various strain parameters and multiple imaging techniques have been proposed to serve as clinical markers of CRT response. In a first step to evaluate the clinical implications of these markers, we performed a systematic comparison of strain parameters on a multi-modality level. We found the end-systolic septal strain parameter to be strongly related to CRT response, irrespective of modality. Although CMR-TAG demonstrates overall superior results compared to other imaging techniques, its availability is limited in clinical practice. On the other hand, standard CMR imaging is increasingly used to screen CRT candidates by measuring LV ejection fraction combined with scar visualization to target LV lead placement.(31) Additional CMR-FT strain analysis of the septum could potentially expand diagnostic yield of this comprehensive imaging technique. When CMR imaging is not accessible, STE can also be used as a good alternative to estimate CRT benefit. In general, the end-systolic septal strain parameter can be obtained by any available strain imaging technique and provides predictive value on top of current guideline criteria. The application of strain imaging has yet not been included in daily practice, but it is likely to become a useful application when evaluating heart

failure patients for CRT implantation. This may be of particular interest in CRT candidates with unfavorable patient characteristics (ICMP, IVCD morphology, shorter QRS duration), in whom benefit from CRT is doubted.

Limitations

The relatively small sample size is the main limitation of this study. Due to the limited availability of CMR-TAG sequences and post-processing software in clinical practice, only a small proportion of the original MARC population was included in the present sub-study. Despite the limited sample size, this is the first study to perform a systematic comparison between strain parameters and strain imaging techniques in relation to CRT response. Secondly, only a small proportion of the patients had ischemic CMP which limits the confounding effects of scar tissue on strain parameters. For example, a myocardial infarction located at the septum might influence septal strain assessment with less negative or even positive strain values due to akinetic tissue or passive stretching, thus resembling strain patterns seen in patients with explicit discoordination. Unfortunately, the number of patients with myocardial infarction was too low to evaluate the effects of septal scar on strain parameters. The influence of scarred segments, however, has previously been investigated for other discoordination parameters. These studies showed a limited effect of myocardial scarring on the predictive value of these parameters.(7,9,23)

CONCLUSION

In conclusion, end-systolic septal strain showed a consistent good relation to reverse remodeling after CRT, irrespective of the technique used for assessment. Measuring ESS_{sep} by any available strain imaging technique provides predictive value on top of current guideline criteria.

REFERENCES

1. Ponikowski P, Voors AA, Anker SD, Bueno H, Cleland JG, Coats AJ, Falk V, Gonzalez-Juanatey JR, Harjola VP, Jankowska EA, Jessup M, Linde C, Nihoyannopoulos P, Parissis JT, Pieske B, Riley JP, Rosano GM, Ruilope LM, Ruschitzka F, Rutten FH, van der Meer P. 2016 ESC Guidelines for the diagnosis and treatment of acute and chronic heart failure: The Task Force for the diagnosis and treatment of acute and chronic heart failure of the European Society of Cardiology (ESC)Developed with the special contribution of the Heart Failure Association (HFA) of the ESC. Eur Heart J. 2016 7/14/2016;37(27):2129-2200.
2. Daubert C, Behar N, Martins RP, Mabo P, Leclercq C. Avoiding non-responders to cardiac resynchronization therapy: a practical guide. Eur Heart J. 2016 7/1/2016.
3. Khidir MJ, Delgado V, Ajmone Marsan N, Schalij MJ, Bax JJ. QRS duration versus morphology and survival after cardiac resynchronization therapy. ESC Heart Fail. 2017 Feb;4(1):23-30.
4. Zweerink A, de Roest GJ, Wu L, Nijveldt R, de Cock CC, van Rossum AC, Allaart CP. Prediction of Acute Response to Cardiac Resynchronization Therapy by Means of the Misbalance in Regional Left Ventricular Myocardial Work. J Card Fail. 2016 Feb;22(2):133-142.
5. Prinzen FW, Vernooy K, De Boeck BW, Delhaas T. Mechano-energetics of the asynchronous and resynchronized heart. Heart Fail Rev. 2011 5/2011;16(3):215-224.
6. Russell K, Eriksen M, Aaberge L, Wilhelmsen N, Skulstad H, Gjesdal O, Edvardsen T, Smiseth OA. Assessment of wasted myocardial work: a novel method to quantify energy loss due to uncoordinated left ventricular contractions. Am J Physiol Heart Circ Physiol. 2013 Oct 01;305(7):H996-1003.
7. De Boeck BWL, Teske AJ, Meine M, Leenders GE, Cramer MJ, Prinzen FW, Doevendans PA. Septal rebound stretch reflects the functional substrate to cardiac resynchronization therapy and predicts volumetric and neurohormonal response. European Journal of Heart Failure. 2009 9/2009;11(9):863-871.
8. Kirn B, Jansen A, Bracke F, van Gelder B, Arts T, Prinzen FW. Mechanical discoordination rather than dyssynchrony predicts reverse remodeling upon cardiac resynchronization. American Journal of Physiology-Heart and Circulatory Physiology. 2008 8/2008;295(2):H640-H646.
9. Lumens J, Tayal B, Walmsley J, Delgado-Montero A, Huntjens PR, Schwartzman D, Althouse AD, Delhaas T, Prinzen FW, Gorcsan J, III. Differentiating Electromechanical From Non-Electrical Substrates of Mechanical Discoordination to Identify Responders to Cardiac Resynchronization Therapy. Circ Cardiovasc Imaging. 2015 9/2015;8(9):e003744.
10. Jackson T, Sohal M, Chen Z, Child N, Sammut E, Behar J, Claridge S, Carr-White G, Razavi R, Rinaldi CA. A U-shaped type II contraction pattern in patients with strict left bundle branch block predicts super-response to cardiac resynchronization therapy. Heart Rhythm. 2014 10/2014;11(10):1790-1797.
11. Revah G, Wu V, Huntjens PR, Piekarski E, Chyou JY, Axel L. Cardiovascular magnetic resonance features of mechanical dyssynchrony in patients with left bundle branch block. Int J Cardiovasc Imaging. 2016 6/15/2016.

12. Pedrizzetti G, Claus P, Kilner PJ, Nagel E. Principles of cardiovascular magnetic resonance feature tracking and echocardiographic speckle tracking for informed clinical use. J Cardiovasc Magn Reson. 2016 2016;18(1):51.
13. Bilchick KC, Dimaano V, Wu KC, Helm RH, Weiss RG, Lima JA, Berger RD, Tomaselli GF, Bluemke DA, Halperin HR, Abraham T, Kass DA, Lardo AC. Cardiac Magnetic Resonance Assessment of Dyssynchrony and Myocardial Scar Predicts Function Class Improvement Following Cardiac Resynchronization Therapy. JACC: Cardiovascular Imaging. 2008 9/2008;1(5):561-568.
14. Russel IK, Zwanenburg JJ, Germans T, Marcus JT, Allaart CP, de Cock CC, Gotte MJ, van Rossum AC. Mechanical dyssynchrony or myocardial shortening as MRI predictor of response to biventricular pacing? J Magn Reson Imaging. 2007 12/2007;26(6):1452-1460.
15. Andersson LG, Wu KC, Wieslander B, Loring Z, Frank TF, Maynard C, Gerstenblith G, Tomaselli GF, Weiss RG, Wagner GS, Ugander M, Strauss DG. Left ventricular mechanical dyssynchrony by cardiac magnetic resonance is greater in patients with strict vs nonstrict electrocardiogram criteria for left bundle-branch block. Am Heart J. 2013 Jun;165(6):956-963.
16. Risum N, Tayal B, Hansen TF, Bruun NE, Jensen MT, Lauridsen TK, Saba S, Kisslo J, Gorcsan J, III, Sogaard P. Identification of Typical Left Bundle Branch Block Contraction by Strain Echocardiography Is Additive to Electrocardiography in Prediction of Long-Term Outcome After Cardiac Resynchronization Therapy. J Am Coll Cardiol. 2015 8/11/2015;66(6):631-641.
17. Maass AH, Vernooy K, Wijers SC, van 't Sant J, Cramer MJ, Meine M, Allaart CP, De Lange FJ, Prinzen FW, Gerritse B, Erdtsieck E, Scheerder COS, Hill MRS, Scholten M, Kloosterman M, Ter Horst IAH, Voors AA, Vos MA, Rienstra M, Van Gelder IC. Refining success of cardiac resynchronization therapy using a simple score predicting the amount of reverse ventricular remodelling: results from the Markers and Response to CRT (MARC) study. Europace. 2018 Feb 1;20(2):e1-e10.
18. Zwanenburg JJ, Gotte MJ, Kuijer JP, Heethaar RM, van Rossum AC, Marcus JT. Timing of cardiac contraction in humans mapped by high-temporal-resolution MRI tagging: early onset and late peak of shortening in lateral wall. Am J Physiol Heart Circ Physiol. 2004 5/2004;286(5):H1872-H1880.
19. Miller CA, Borg A, Clark D, Steadman CD, McCann GP, Clarysse P, Croisille P, Schmitt M. Comparison of local sine wave modeling with harmonic phase analysis for the assessment of myocardial strain. J Magn Reson Imaging. 2013 8/2013;38(2):320-328.
20. van Everdingen WM, Zweerink A, Nijveldt R, Salden OAE, Meine M, Maass AH, Vernooy K, De Lange FJ, van Rossum AC, Croisille P, Clarysse P, Geelhoed B, Rienstra M, Van Gelder IC, Vos MA, Allaart CP, Cramer MJ. Comparison of strain imaging techniques in CRT candidates: CMR tagging, CMR feature tracking and speckle tracking echocardiography. Int J Cardiovasc Imaging. 2017 Oct 17.
21. Tanaka H, Nesser HJ, Buck T, Oyenuga O, Janosi RA, Winter S, Saba S, Gorcsan J, 3rd. Dyssynchrony by speckle-tracking echocardiography and response to cardiac resynchronization therapy: results of the Speckle Tracking and Resynchronization (STAR) study. Eur Heart J. 2010 Jul;31(14):1690-1700.

22. Pouleur AC, Knappe D, Shah AM, Uno H, Bourgoun M, Foster E, McNitt S, Hall WJ, Zareba W, Goldenberg I, Moss AJ, Pfeffer MA, Solomon SD, Investigators M-C. Relationship between improvement in left ventricular dyssynchrony and contractile function and clinical outcome with cardiac resynchronization therapy: the MADIT-CRT trial. Eur Heart J. 2011 Jul;32(14):1720-1729.
23. Leenders GE, Lumens J, Cramer MJ, De Boeck BW, Doevendans PA, Delhaas T, Prinzen FW. Septal deformation patterns delineate mechanical dyssynchrony and regional differences in contractility: analysis of patient data using a computer model. Circ Heart Fail. 2012 1/2012;5(1):87-96.
24. Risum N, Strauss D, Sogaard P, Loring Z, Hansen TF, Bruun NE, Wagner G, Kisslo J. Left bundle-branch block: the relationship between electrocardiogram electrical activation and echocardiography mechanical contraction. Am Heart J. 2013 Aug;166(2):340-348.
25. Risum N, Jons C, Olsen NT, Fritz-Hansen T, Bruun NE, Hojgaard MV, Valeur N, Kronborg MB, Kisslo J, Sogaard P. Simple regional strain pattern analysis to predict response to cardiac resynchronization therapy: rationale, initial results, and advantages. Am Heart J. 2012 Apr;163(4):697-704.
26. Leenders GE, De Boeck BW, Teske AJ, Meine M, Bogaard MD, Prinzen FW, Doevendans PA, Cramer MJ. Septal rebound stretch is a strong predictor of outcome after cardiac resynchronization therapy. J Card Fail. 2012 May;18(5):404-412.
27. Grothues F, Moon JC, Bellenger NG, Smith GS, Klein HU, Pennell DJ. Interstudy reproducibility of right ventricular volumes, function, and mass with cardiovascular magnetic resonance. Am Heart J. 2004 Feb;147(2):218-223.
28. Schuster A, Hor KN, Kowallick JT, Beerbaum P, Kutty S. Cardiovascular Magnetic Resonance Myocardial Feature Tracking: Concepts and Clinical Applications. Circ Cardiovasc Imaging. 2016 4/2016;9(4):e004077.
29. Wu L, Germans T, Guclu A, Heymans MW, Allaart CP, van Rossum AC. Feature tracking compared with tissue tagging measurements of segmental strain by cardiovascular magnetic resonance. J Cardiovasc Magn Reson. 2014 2014;16:10.
30. Helm RH, Leclercq C, Faris OP, Ozturk C, McVeigh E, Lardo AC, Kass DA. Cardiac dyssynchrony analysis using circumferential versus longitudinal strain: implications for assessing cardiac resynchronization. Circulation. 2005 5/31/2005;111(21):2760-2767.
31. Sommer A, Kronborg MB, Norgaard BL, Poulsen SH, Bouchelouche K, Bottcher M, Jensen HK, Jensen JM, Kristensen J, Gerdes C, Mortensen PT, Nielsen JC. Multimodality imaging-guided left ventricular lead placement in cardiac resynchronization therapy: a randomized controlled trial. Eur J Heart Fail. 2016 Nov;18(11):1365-1374.

SUPPLEMENTAL MATERIAL

Image acquisition: cardiac magnetic resonance

Typical image acquisition parameters for cardiac magnetic resonance (CMR) imaging were: (1) cine imaging: slice thickness 5mm, slice gap 5mm, echo time (TE) 1.6ms, repetition time (TR) 3.2ms, in-plane spatial resolution 1.5 by 2.1mm, flip angle 60 degrees. Temporal resolution was <50ms and the number of reconstructed temporal phases within the cardiac cycle was set at 20.(2) High temporal cine imaging: TE 1.7ms, TR 3.4ms. Temporal resolution was <15ms and the number of reconstructed temporal phases within the cardiac cycle was set at 55. (3) Myocardial tagging: slice thickness 6mm, TE 1.7ms, TR 3.6ms, in-plane spatial resolution 1.3 by 4.3mm, flip angle 20 degrees, tag spacing 7mm. Temporal resolution was <15ms and the number of reconstructed temporal phases within the cardiac cycle was set at 55.

Post-processing: CMR-TAG

Post-processing of CMR myocardial tagging (CMR-TAG) images was performed by a semi-automated procedure. After selecting the area of interest, endo- and epi-cardial contours were manually drawn in the end-systolic phase and automatically propagated. A template was placed dividing the left ventricle (LV) in six equally sized regions (anterior, anterolateral, inferolateral, inferior, inferoseptal, anteroseptal). The myocardium was divided in three layers (endo-, mid-, epi-wall layer). Septum strain was averaged from the anteroseptal and inferoseptal segments of the mid-wall layer in both the mid-LV and basal slice. This was repeated for the lateral wall strain averaging the anterolateral and inferolateral segments. Individual strain curves were discarded in case of low signal-to-noise ratio as judged by two independent investigators. The presence of at least two analyzable strain curve (out of four), for both the septum and the lateral wall, resulted in inclusion of the patient.

Post-processing: CMR-FT

For post-processing of CMR feature tracking (CMR-FT) images, first the endo- and epi-cardial contours were manually drawn in both end-diastolic and end-systolic frames and propagated automatically. A template was placed dividing the LV in six regions, similar to the CMR-TAG post-processing technique. Both endocardial and epicardial features were included for strain analysis. The

processing steps for quality screening and averaging segments are also similar to the CMR-TAG analysis.

Post-processing: STE

For speckle tracking echocardiography (STE) analysis, a region of interest was placed by user defined markers at the endocardial border on the apical four chamber (AP4CH) view for longitudinal strain and on the parasternal short axis (PSAX) view of the mitral valve level and papillary muscle level for circumferential strain. Endocardial features were included for strain analysis. The myocardial wall was automatically separated into six segments for all views, based on the American Heart Association 17 segment model.(1) Segments were excluded, even after repeated adjustment of the ROI, if adequate tracking was not achievable. For septal single wall analysis, an ROI was placed endocardial on AP4CH view images along the interventricular septum, from base to apex, thereby excluding the apical cap. The marker for reference length (L_0) was placed at onset of QRS-complex. Results were stored and exported for offline analysis with Matlab 2014b (Mathworks, Natick, MA, USA). Author written Matlab scripts were implemented, with input of valve closure times and semi-automatic calculation of strain parameters. The processing steps of the PSAX images (STE-circ) for quality screening and averaging segments are similar to the CMR-TAG analysis. For AP4CH images (STE-long), a minimum of two out of three segments representing the septal wall (i.e. basal, mid and apical inferoseptum) were averaged, this was repeated for the lateral wall (basal, mid, and apical lateral). Septal single wall analysis resulted in an averaged strain curve for specific septum strain measurements.

Strain parameters

Basic strain parameters were obtained for the septal and lateral wall and include the maximal negative peak strain during the entire cardiac cycle (peak strain); and the end-systolic strain value at aortic valve closure (ESS). Dyssynchrony was quantified by measuring the septum to lateral delay in onset shortening (onset-delay); the difference in time to peak contraction (peak-delay);(2) and the standard deviation of time to peak contraction on a segmental scale throughout the LV (SD-TTP_{LV}).(3) Discoordination of the septal and lateral wall was measured by systolic rebound stretch of the septum (SRS_{sep}) as the cumulative amount of

systolic stretch after initial shortening; the systolic stretch index ($SSI_{sep-lat}$) measuring systolic stretch of both the septum and the lateral wall; and the internal stretch factor ($ISF_{sep-lat}$) calculated as the fraction of the total amount of stretch in both regions divided by the total amount of shortening in both regions.(4-6) Discoordination markers derived from segmental strains of the total LV include the circumferential uniformity ratio estimate ($CURE_{LV}$) index that measures the variation in segmental strains per time point using Fourier analysis, ranging from 0 (dyssynchronous) to 1 (synchronous); and the internal stretch factor of the total LV (ISF_{LV}) by dividing the total amount of stretch by the total amount of shortening. Integrating the average positive strain rate during systole resulted in the total amount of stretch, while integrating average negative strain rate resulted in the total amount of shortening.(5,7) Septal strain patterns were classified as: double peaked systolic shortening (LBBB-1); early pre-ejection shortening followed by prominent systolic stretch (LBBB-2); and pseudonormal shortening with a late-systolic shortening peak and less pronounced end-systolic stretch (LBBB-3).(8,9)

Echocardiographic assessment of CRT outcome

LV end-diastolic volume (LVEDV), end-systolic volume (LVESV), and ejection fraction (LVEF) were measured by two experienced observers and in accordance with the guidelines of the American Society of Echocardiography and European Association of Echocardiography.(10) Echocardiographic volumes were obtained using the biplane Simpson's method. If image quality of the apical two chamber view was deemed unsuitable for reliable biplane volume assessment, solely the AP4CH view was used instead. All echocardiographic parameters were measured on three separate beats and averaged.

Results

From all segments, 94% were considered analyzable with CMR-TAG, 87% with CMR-FT, 87% with STE-circ and 95% with STE-long. Frame rate of echocardiographic images was on average 65±11Hz, which corresponds to a temporal resolution of ~15ms. Temporal resolution of CMR-TAG was ~14ms, while it was ~40ms for CMR-FT.

REFERENCES

1. Cerqueira MD, Weissman NJ, Dilsizian V, Jacobs AK, Kaul S, Laskey WK, Pennell DJ, Rumberger JA, Ryan T, Verani MS. Standardized myocardial segmentation and nomenclature for tomographic imaging of the heart. A statement for healthcare professionals from the Cardiac Imaging Committee of the Council on Clinical Cardiology of the American Heart Association. Circulation. 2002 1/29/2002;105(4):539-542.
2. Tanaka H, Nesser HJ, Buck T, Oyenuga O, Janosi RA, Winter S, Saba S, Gorcsan J, 3rd. Dyssynchrony by speckle-tracking echocardiography and response to cardiac resynchronization therapy: results of the Speckle Tracking and Resynchronization (STAR) study. Eur Heart J. 2010 Jul;31(14):1690-1700.
3. Pouleur AC, Knappe D, Shah AM, Uno H, Bourgoun M, Foster E, McNitt S, Hall WJ, Zareba W, Goldenberg I, Moss AJ, Pfeffer MA, Solomon SD, Investigators M-C. Relationship between improvement in left ventricular dyssynchrony and contractile function and clinical outcome with cardiac resynchronization therapy: the MADIT-CRT trial. Eur Heart J. 2011 Jul;32(14):1720-1729.
4. De Boeck BWL, Teske AJ, Meine M, Leenders GE, Cramer MJ, Prinzen FW, Doevendans PA. Septal rebound stretch reflects the functional substrate to cardiac resynchronization therapy and predicts volumetric and neurohormonal response. European Journal of Heart Failure. 2009 9/2009;11(9):863-871.
5. Kirn B, Jansen A, Bracke F, van Gelder B, Arts T, Prinzen FW. Mechanical discoordination rather than dyssynchrony predicts reverse remodeling upon cardiac resynchronization. American Journal of Physiology-Heart and Circulatory Physiology. 2008 8/2008;295(2):H640-H646.
6. Lumens J, Tayal B, Walmsley J, Delgado-Montero A, Huntjens PR, Schwartzman D, Althouse AD, Delhaas T, Prinzen FW, Gorcsan J, III. Differentiating Electromechanical From Non-Electrical Substrates of Mechanical Discoordination to Identify Responders to Cardiac Resynchronization Therapy. Circ Cardiovasc Imaging. 2015 9/2015;8(9):e003744.
7. Bilchick KC, Dimaano V, Wu KC, Helm RH, Weiss RG, Lima JA, Berger RD, Tomaselli GF, Bluemke DA, Halperin HR, Abraham T, Kass DA, Lardo AC. Cardiac Magnetic Resonance Assessment of Dyssynchrony and Myocardial Scar Predicts Function Class Improvement Following Cardiac Resynchronization Therapy. JACC: Cardiovascular Imaging. 2008 9/2008;1(5):561-568.
8. Leenders GE, Lumens J, Cramer MJ, De Boeck BW, Doevendans PA, Delhaas T, Prinzen FW. Septal deformation patterns delineate mechanical dyssynchrony and regional differences in contractility: analysis of patient data using a computer model. Circ Heart Fail. 2012 1/2012;5(1):87-96.
9. Marechaux S, Guiot A, Castel AL, Guyomar Y, Semichon M, Delelis F, Heuls S, Ennezat PV, Graux P, Tribouilloy C. Relationship between two-dimensional speckle-tracking septal strain and response to cardiac resynchronization therapy in patients with left ventricular dysfunction and left bundle branch block: a prospective pilot study. J Am Soc Echocardiogr. 2014 5/2014;27(5):501-511.

10. Lang RM, Badano LP, Mor-Avi V, Afilalo J, Armstrong A, Ernande L, Flachskampf FA, Foster E, Goldstein SA, Kuznetsova T, Lancellotti P, Muraru D, Picard MH, Rietzschel ER, Rudski L, Spencer KT, Tsang W, Voigt JU. Recommendations for cardiac chamber quantification by echocardiography in adults: an update from the American Society of Echocardiography and the European Association of Cardiovascular Imaging. Eur Heart J Cardiovasc Imaging. 2015 3/2015;16(3):233-270.

Table S1. Comparison of strain parameters between responders (R) and non-responders (NR)

	N = 26	CMR tagging			CMR feature tracking			STE circumferential			STE longitudinal		
		R	NR	*p*-value	R	NR	*p*-value	R	NR	*p*-value	R	NR	*p*-value
basic strain parameters	peak strain septum (%)	-3 ± 2	-6 ± 3	0.013	-4 ± 3	-7 ± 4	0.061	-9 ± 4	-13 ± 7	0.150	-8 ± 5	-8 ± 3	0.981
	peak strain lateral (%)	-14 ± 2	-12 ± 3	0.031	-13 ± 4	-12 ± 4	0.327	-15 ± 6	-17 ± 4	0.355	-8 ± 5	-11 ± 4	0.060
	ESS_{sep} (%)	+5 ± 4	-3 ± 5	0.001	+1 ± 4	-5 ± 4	0.003	-4 ± 6	-11 ± 7	0.030	-3 ± 5	-8 ± 4	0.009
	ESS_{lat} (%)	-14 ± 2	-11 ± 4	0.057	-13 ± 3	-11 ± 4	0.486	-14 ± 6	-16 ± 4	0.410	-7 ± 6	-10 ± 4	0.072
dyssynchrony parameters	onset-delay (ms)	58 (46 – 68)	44 (28 – 54)	0.059	67 (47 – 87)	44 (0 – 82)	0.381	70 (20 – 130)	44 (0 – 50)	0.012	76 (36 – 126)	44 (15 – 85)	0.118
	peak-delay (ms)	330 ± 92	140 ± 88	<0.001	226 ± 104	109 ± 47	<0.001	172 ± 119	92 ± 47	0.024	176 ± 102	90 ± 65	0.017
	$SD\text{-}TTP_{LV}$ (ms)	175 ± 31	97 ± 30	<0.001	165 ± 48	143 ± 35	0.196	155 ± 52	133 ± 54	0.329	140 ± 48	124 ± 44	0.429
sep – lat discoordination	SRS_{sep} (%)	9 ± 4	3 ± 3	<0.001	5 ± 3	2 ± 2	0.004	5 ± 4	1 ± 1	0.004	4 ± 3	2 ± 2	0.031
	$SSI_{sep\text{-}lat}$ (%)	11 ± 5	4 ± 3	<0.001	6 ± 4	3 ± 2	0.013	7 ± 5	2 ± 1	<0.001	5 ± 4	2 ± 2	0.009
	$ISF_{sep\text{-}lat}$	0.54 ± 0.21	0.21 ± 0.15	<0.001	0.36 ± 0.22	0.16 ± 0.11	0.006	0.32 ± 0.15	0.12 ± 0.08	<0.001	0.47 ± 0.23	0.16 ± 0.08	<0.001
total LV discoordination	$CURE_{LV}$	0.78 ± 0.09	0.88 ± 0.04	<0.001	0.75 ± 0.10	0.80 ± 0.06	0.134	0.77 ± 0.05	0.81 ± 0.07	0.164	0.81 ± 0.04	0.84 ± 0.06	0.197
	ISF_{LV}	0.57 ± 0.19	0.24 ± 0.10	<0.001	0.40 ± 0.18	0.25 ± 0.12	0.020	0.42 ± 0.09	0.25 ± 0.11	<0.001	0.39 ± 0.17	0.23 ± 0.11	0.009

R, responders; NR, non-responders; ESS, end-systolic strain; onset-delay, septal to lateral delay onset contraction; peak-delay, septal to lateral peak delay shortening; $SD\text{-}TTP_{LV}$, standard deviation in time to peak contraction of the total LV; SRS_{sep}, systolic rebound stretch of the septum; $SSI_{sep\text{-}lat}$, systolic stretch index; $ISF_{sep\text{-}lat}$, internal stretch factor of the septal and lateral wall; $CURE_{LV}$, circumferential uniformity ratio estimate of the total LV; ISF_{LV}, internal stretch factor of the total LV.

Table S2. Coefficient of determination (R^2) and area under the curve (AUC) of strain parameters and CRT response (echocardiographic LVESV change after twelve months)

	N = 26	CMR tagging		CMR feature tracking		STE circumferential		STE longitudinal	
		R^2	AUC	R^2	AUC	R^2	AUC	R^2	AUC
basic strain parameters	peak strain septum (%)	**0.39**; *p*<0.001	**0.85**; *p*=0.002	**0.27**; *p*=0.007	**0.73**; *p*=0.064	**0.26**; *p*=0.009	**0.70**; *p*=0.106	**0.01**; *p*=0.701	**0.50**; *p*=0.921
	peak strain lateral (%)	**0.23**; *p*=0.013	**0.77**; *p*=0.026	**0.03**; *p*=0.392	**0.61**; *p*=0.344	**0.02**; *p*=0.466	**0.62**; *p*=0.341	**0.02**; *p*=0.467	**0.73**; *p*=0.060
	ESS_{sep} (%)	**0.60**; *p*<0.001	**0.89**; *p*<0.001	**0.50**; *p*<0.001	**0.87**; *p*<0.001	**0.43**; *p*<0.001	**0.79**; *p*=0.014	**0.43**; *p*<0.001	**0.80**; *p*=0.012
	ESS_{lat} (%)	**0.28**; *p*=0.005	**0.72**; *p*=0.066	**0.04**; *p*=0.348	**0.58**; *p*=0.554	**0.01**; *p*=0.611	**0.61**; *p*=0.404	**0.02**; *p*=0.494	**0.72**; *p*=0.067
dyssynchrony parameters	onset-delay (ms)	**0.10**; *p*=0.122	**0.73**; *p*=0.064	**0.01**; *p*=0.612	**0.61**; *p*=0.376	**0.40**; *p*<0.001	**0.80**; *p*=0.010	**0.09**; *p*=0.137	**0.69**; *p*=0.116
	peak-delay (ms)	**0.40**; *p*=0.001	**0.90**; *p*<0.001	**0.47**; *p*<0.001	**0.85**; *p*=0.002	**0.25**; *p*=0.010	**0.70**; *p*=0.106	**0.27**; *p*=0.007	**0.75**; *p*=0.044
	$SD\text{-}TTP_{LV}$ (ms)	**0.61**; *p*<0.001	**0.94**; *p*<0.001	**0.10**; *p*=0.113	**0.67**; *p*=0.188	**0.08**; *p*=0.151	**0.60**; *p*=0.460	**0.14**; *p*=0.061	**0.52**; *p*=0.825
sep – lat discoordination	SRS_{sep} (%)	**0.36**; *p*<0.001	**0.88**; *p*<0.001	**0.42**; *p*<0.001	**0.82**; *p*=0.006	**0.34**; *p*=0.002	**0.79**; *p*=0.018	**0.20**; *p*=0.020	**0.73**; *p*=0.062
	$SSI_{sep\text{-}lat}$ (%)	**0.42**; *p*<0.001	**0.91**; *p*<0.001	**0.29**; *p*=0.004	**0.77**; *p*=0.031	**0.33**; *p*=0.002	**0.84**; *p*=0.006	**0.30**; *p*=0.004	**0.80**; *p*=0.010
	$ISF_{sep\text{-}lat}$	**0.47**; *p*<0.001	**0.92**; *p*<0.001	**0.39**; *p*<0.001	**0.83**; *p*=0.007	**0.48**; *p*<0.001	**0.90**; *p*=0.001	**0.39**; *p*<0.001	**0.94**; *p*<0.001
total LV discoordination	$CURE_{LV}$	**0.33**; *p*=0.002	**0.86**; *p*=0.004	**0.15**; *p*=0.047	**0.61**; *p*=0.373	**0.14**; *p*=0.063	**0.66**; *p*=0.197	**0.09**; *p*=0.139	**0.66**; *p*=0.201
	ISF_{LV}	**0.57**; *p*<0.001	**0.96**; *p*<0.001	**0.26**; *p*=0.008	**0.75**; *p*=0.039	**0.29**; *p*=0.004	**0.92**; *p*<0.001	**0.32**; *p*=0.003	**0.77**; *p*=0.024

AUC, area under the curve; R^2, coefficient of determination; for other abbreviations see table S1.

Table S3. Predictive value of strain parameters for CRT volumetric response (reduction in LVESV at twelve months ≥15%)

	N = 26	CMR tagging			CMR feature tracking			STE circumferential			STE longitudinal		
		AUC	sens/spec	cut-off value	AUC	sens/spec	cut-off value	AUC	sens/spec	cut-off value	AUC	sens/spec	cut-off value
basic strain parameters	peak strain septum (%)	0.85	71% / 89%	-3.0	0.73	65% / 89%	-4.6	0.70	82% / 56%	-12.9	0.50	18% / 10%	-2.0
	peak strain lateral (%)	0.77	82% / 67%	-12.4	0.61	71% / 56%	-10.9	0.62	71% / 67%	-16.9	0.73	59% / 89%	-8.0
	ESS_{sep} (%)	0.89	82% / 89%	+1.6	0.87	82% / 89%	-1.4	0.79	88% / 67%	-10.6	0.80	71% / 78%	-6.2
	ESS_{lat} (%)	0.72	82% / 67%	-11.8	0.58	82% / 44%	-9.6	0.61	59% / 67%	-15.1	0.72	65% / 78%	-8.2
dyssynchrony	onset-delay (ms)	0.73	82% / 56%	44	0.61	76% / 56%	38	0.80	53% / 100%	60	0.69	71% / 67%	54
	peak-delay (ms)	0.90	82% / 89%	221	0.75	59% / 100%	200	0.70	47% / 100%	165	0.75	82% / 56%	96
	SD-TTP_{LV} (ms)	0.94	88% / 89%	138	0.67	41% / 100%	180	0.60	82% / 44%	112	0.52	35% / 89%	0.15
sep – lat discoordination	SRS_{sep} (%)	0.88	88% / 78%	5.0	0.82	76% / 78%	2.8	0.79	59% / 100%	3.7	0.73	76% / 67%	1.7
	$SSI_{sep-lat}$ (%)	0.91	88% / 89%	6.0	0.77	65% / 78%	4.5	0.84	71% / 100%	4.3	0.80	77% / 78%	2.8
	$ISF_{sep-lat}$	0.92	82% / 89%	0.30	0.83	76% / 78%	0.22	0.90	94% / 78%	0.15	0.94	88% / 89%	0.22
total LV discoordination	$CURE_{LV}$	0.86	59% / 100%	0.80	0.61	24% / 100%	0.70	0.66	65% / 67%	0.79	0.66	100% / 33%	0.88
	ISF_{LV}	0.96	94% / 89%	0.34	0.75	71% / 78%	0.29	0.92	100% / 78%	0.29	0.77	53% / 100%	0.37

AUC, area under the curve; sens, sensitivity; spec, specificity; for other abbreviations see table S1.

Table S4. Septal strain patterns and volumetric CRT response (echocardiographic LVESV change after twelve months)

N = 26	CMR tagging	CMR feature tracking	STE circumferential	STE longitudinal
LBBB-1	-19 ± 19* n=7 (27%)	-26 ± 15 n=5 (19%)	-39 ± 23† n=9 (35%)	-35 ± 19 n=10 (38%)
LBBB-2	-45 ± 19*‡ n=14 (54%)	-47 ± 18‡ n=12 (46%)	-52 ± 11‡ n=6 (23%)	-49 ± 20‡ n=6 (23%)
LBBB-3	+5 ± 16‡ n=5 (19%)	-5 ± 23‡ n=9 (35%)	-7 ± 19†‡ n=11 (42%)	-10 ± 26‡ n=10 (38%)

LBBB-1, double peaked shortening and LBBB-2, predominant stretching represent abnormal septal strain patterns. The LBBB-3 pattern represents pseudonormal shortening of the septum. Statistical differences between LBBB categories per imaging modality are marked with: * pattern 1 vs. 2, † pattern 1 vs. 3, ‡ pattern 2 vs. 3.

Table S5. Predictive value of septal strain patterns for volumetric CRT response (reduction in LVESV at twelve months ≥15%)

N = 26	CMR tagging		CMR feature tracking		STE circumferential		STE longitudinal	
	R	NR	R	NR	R	NR	R	NR
LBBB-1 or LBBB-2	n=17 (65%)	n=4 (15%)	n=15 (58%)	n=2 (8%)	n=13 (50%)	n=2 (8%)	n=14 (54%)	n=2 (8%)
LBBB-3	n=0 (0%)	n=5 (19%)	n=2 (8%)	n=7 (27%)	n=4 (15%)	n=7 (27%)	n=3 (12%)	n=7 (27%)
sens/spec	**100% / 56%**		**88% / 78%**		**76% / 78%**		**82% / 78%**	

R, responders; NR, non-responders; sens, sensitivity; spec, specificity; for other abbreviations see table S4

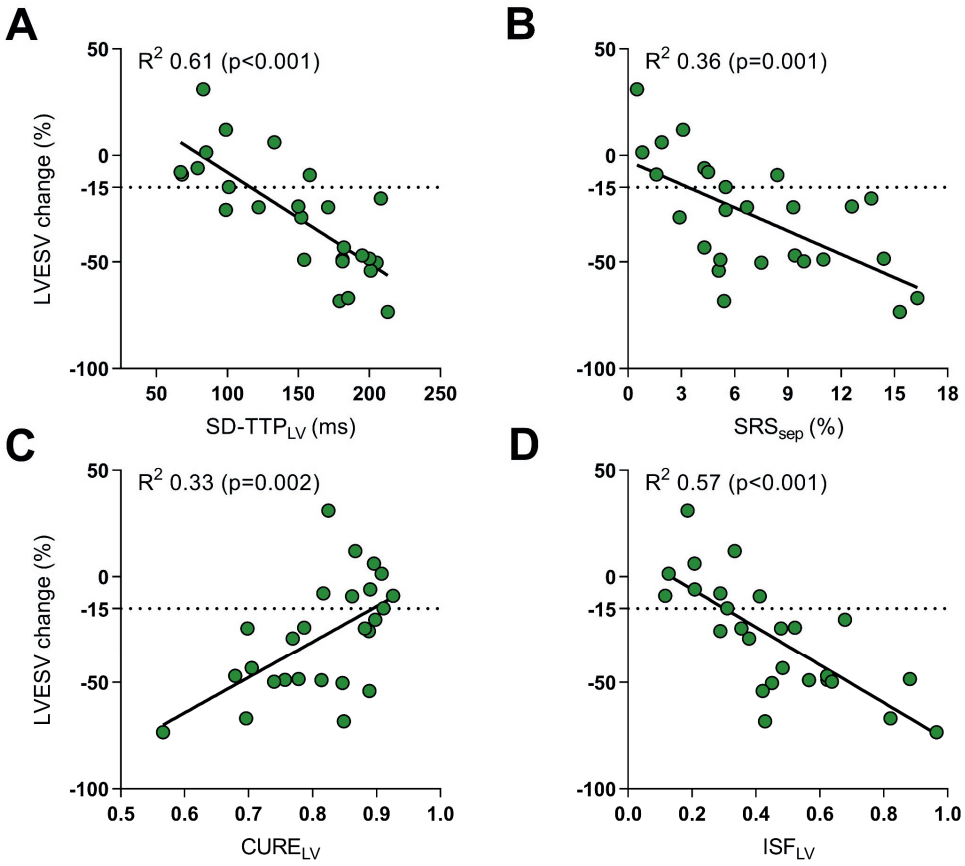


Figure S1: Correlation between conventional strain markers quantified by the CMR-TAG technique and LVESV change. Conventional strain parameters quantified by CMR-TAG technique are depicted for (A) SD-TTP_{LV} ; (B) SRS_{sep} ; (C) the CURE index and (D) ISF_{LV}. SD-TTP_{LV}, standard deviation in time to peak contraction of the total LV; SRS_{sep}, systolic rebound stretch of the septum; $CURE_{LV}$, circumferential uniformity ratio estimate of the total LV; ISF_{LV}, internal stretch factor of the total LV

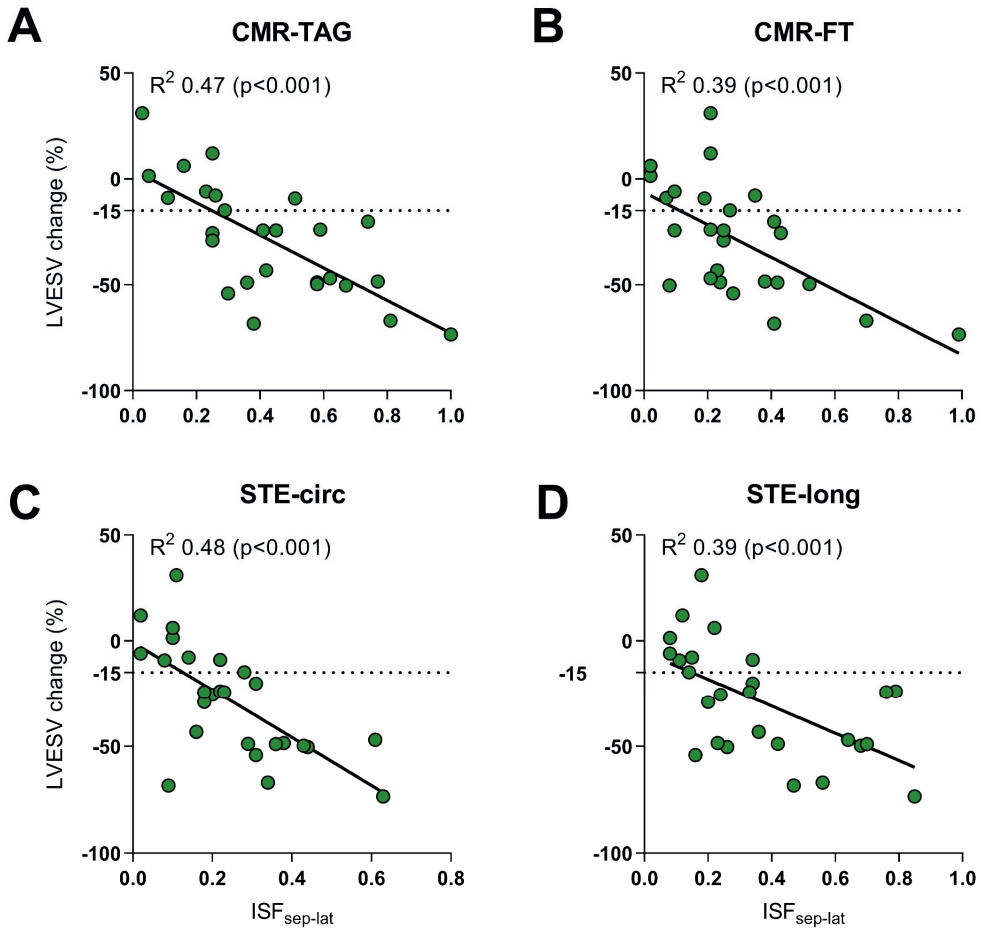


Figure S2: Correlation between the internal stretch factor of the septal and lateral wall ($ISF_{sep-lat}$) and LVESV change per imaging technique. The internal stretch factor calculated from the septal and lateral wall strain ($ISF_{sep-lat}$) correlates with CRT response for each imaging modality and is depicted for: (A) CMR-TAG; (B) CMR-FT; (C) STE-circ and (D) STE-long.

Chapter 7

Strain Analysis in CRT Candidates Using the Novel Segment Length in Cine (SLICE) Post-processing Technique on Standard CMR Cine Images

Eur Radiology 2017;27:5158-5168

Alwin Zweerink
Cornelis P. Allaart
Joost P.A. Kuijer
LiNa Wu
Aernout M. Beek
Peter M. van de Ven
Mathias Meine
Pierre Croisille
Patrick Clarysse
Albert C. van Rossum
Robin Nijveldt

ABSTRACT

Aims: Although myocardial strain analysis is a potential tool to improve patient selection for Cardiac Resynchronization Therapy (CRT), there is currently no validated clinical approach to derive segmental strains. This study evaluates the novel segment length in cine (SLICE) technique to derive segmental strains from standard Cardiovascular Magnetic Resonance (CMR) cine images in CRT candidates.

Methods: Twenty-seven patients with left bundle branch block underwent CMR examination including cine imaging and myocardial tagging (CMR-TAG). SLICE was performed by measuring segment length between anatomic landmarks throughout all phases on short-axis cines. This measure of frame-to-frame segment length change was compared to CMR-TAG circumferential strain measurements. In addition, conventional markers of CRT response were calculated.

Results: Segmental strains showed good to excellent agreement between SLICE and CMR-TAG (septum strain, ICC 0.76; lateral wall strain, ICC 0.66). Conventional markers of CRT response also showed close agreement between both methods (ICC 0.61-0.78). Reproducibility of SLICE was excellent for intra-observer testing (all ICC ≥0.76) and good for inter-observer testing (all ICC ≥0.61).

Conclusions: The novel SLICE post-processing technique on standard CMR cine images offers both accurate and robust segmental strain measures compared to the 'gold standard' CMR-TAG technique, and has the advantage of being widely available.

INTRODUCTION

Myocardial strain analysis plays a key role in the quantitative assessment of global left ventricular (LV) function in various cardiac pathologies and provides prognostic information over conventional parameters.(1) Heart failure (HF) patients with left bundle branch block (LBBB) show regional timing differences causing an imbalanced contractile function throughout the LV and, in particular, across the septal and lateral wall.(2-4) Segmental strains can be used to calculate parameters of mechanical discoordination (opposing shortening and stretching within the LV). This paradoxical wall deformation underlies an inefficient pump function and is considered to be the functional substrate amenable to resynchronization. Therefore, segmental strain measurements are increasingly recognized for their additional value in the selection of HF patients for cardiac resynchronization therapy (CRT).(4-7)

Echocardiographic techniques, such as the speckle tracking method, provide strain measures on a global and segmental scale. Although echocardiography is widely available, strain analysis is highly dependent on the image quality provided by the acoustic window and remains limited because of its reproducibility.(8,9) In the meantime, Cardiovascular Magnetic Resonance (CMR) has rapidly emerged as a robust imaging modality with high accuracy to provide detailed information on cardiac morphology, function, and tissue characterisation.(10) In particular, CMR myocardial tissue tagging (CMR-TAG) produces high quality strain measures on a global and segmental level. It is considered to be the gold standard, but is not widely available and predominantly used for scientific purposes.(11) On the other hand, CMR cine imaging is part of every standard clinical protocol and is increasingly utilized in the screening of CRT candidates to determine the LV ejection fraction. Therefore, CMR feature tracking (CMR-FT) post-processing techniques have been developed to derive strain measurements from standard cine images.(12) Although global strain measures show reasonable agreement with the CMR-TAG technique, segmental strain measures have repeatedly been proven to be insufficient.(13-17) This study evaluates the novel segment length in cine (SLICE) post-processing technique on standard CMR cine images to derive accurate segmental strain measures in CRT candidates without the use of commercial software.

METHODS

Study population

A subset of twenty-seven patients who underwent CMR examination including CMR-TAG was selected from the Markers And Response to CRT (MARC) study.(18) This multi-center, prospective, non-randomized study was designed to investigate the relation of a set of (bio) markers to predict response to CRT. Inclusion and exclusion criteria are reported in the supplemental materials. All subjects gave written informed consent and the local medical ethics committee (VU University Medical Center, Amsterdam) approved data collection and management. The investigation conforms with the principles outlined in the Declaration of Helsinki.

Image acquisition

CMR imaging was performed on a 1.5T whole body system (Magnetom Avanto, Siemens, Erlangen, Germany) with the use of a phased array cardiac receiver coil. Both CMR cine images and CMR-TAG images were obtained in the same examination. Typical image acquisition parameters are given in the supplemental materials. Standard CMR cine images were acquired using a retrospectively ECG-gated balanced steady-state free-precession (SSFP) sequence during end-expiratory breath holding. A stack of 8-12 consecutive short axis cine images was acquired covering the full LV. Subsequently, high temporal resolution cine imaging of the LV in the three-chamber view was performed to assess the opening and closure times of the mitral and aortic valve. CMR-TAG images were acquired at 3 short-axis slices (basal, mid, apical) using a complementary spatial modulation of magnetization (CSPAMM) line tagging sequence with segmented ECG-gated acquisitions and serial breath holds.(19) Myocardial scar territory was assessed by late gadolinium enhancement imaging, and infarct size was measured using the full width at half maximum method.(20)

Post-processing images using the segment length in cine (SLICE) technique

The SLICE analysis of standard cine images was performed by two post-processing steps as illustrated in figure S1 in the supplemental materials. First, the slice position with short-axis cine images, corresponding with the mid-LV slice-location of CMR-TAG images, was selected in Qmass (v7.6, Medis, Leiden,

The Netherlands). Two endocardial anatomic landmarks (trabeculae) delimiting the septum were chosen in the end-diastolic frame and checked for traceability throughout the cardiac cycle (i.e. limited through-plane motion). Marks were placed perpendicular to the myocardium throughout all phases. This procedure was repeated for the lateral wall segment. Subsequently, marked cine images were exported to ImageJ (21) for the second processing step. Segment length of the septum was manually measured between both marks, over the midline of the myocardium in each phase, and expressed as a percentage of the end-diastolic segment length (figure 1A). This procedure was repeated for the lateral wall segment. This measure of frame-to-frame segment length change was compared to CMR-TAG circumferential strain measurements in a similar slice position, as described below.

Post-processing myocardial tissue tagging (CMR-TAG)

The CMR-TAG analysis was performed by dedicated software using the SinMod technique (inTag, CREATIS, Lyon, France).(22) The software runs as a plug-in for OsiriX (v6.5, Pixmeo, Switzerland). The semi-automated analysis is described in the supplemental materials.

Measures of basic strains, mechanical dyssynchrony and discoordination

Four subsets of strain parameters were evaluated including (i) basic strains, (ii) mechanical dyssynchrony, (iii) discoordination, and (iv) pre-specified septal strain patterns. (i) Systolic strain was calculated as the percentage change in segment length at end-systole in comparison to end-diastole. (ii) Time based dyssynchrony parameters were defined by the delay in onset contraction between the septal and lateral wall (onset-delay) and the time difference between peak shortening (peak-delay).(5) (iii) Strain based discoordination markers were assessed by the following commonly used markers: systolic rebound stretch of the septum (SRS) was defined as the cumulative amount of systolic stretch after initial shortening;(5) SRS was combined with stretch of the lateral wall to calculate the systolic stretch index (SSI);(23) the internal stretch factor (ISF) was calculated by dividing the total amount of systolic stretch (SSI) by the total amount of systolic shortening in both regions.(4) Furthermore, septal flash (SF) was measured as the amount of shortening of the septum before stretching during the isovolumetric contraction phase.(24)

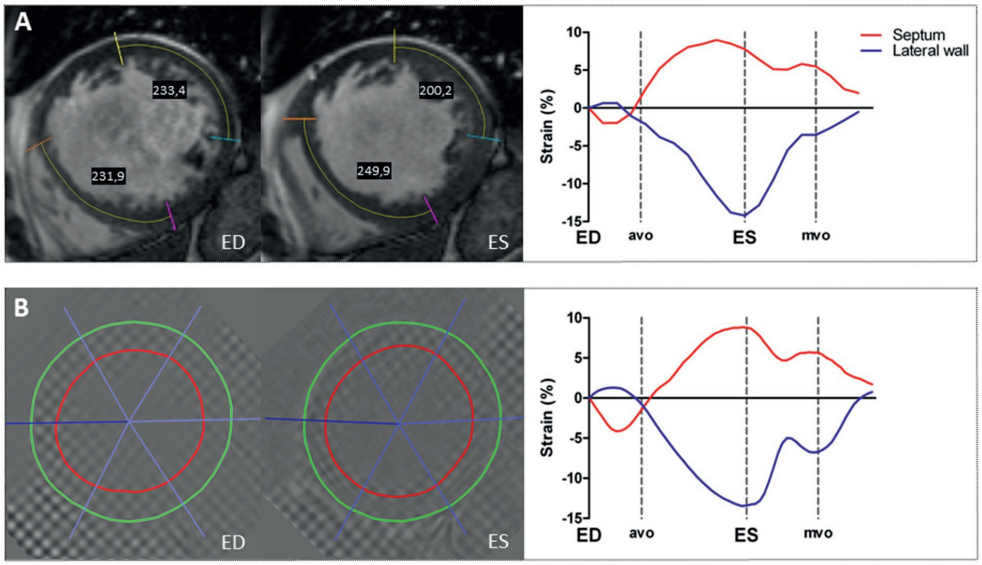


Figure 1: Segmental strain analysis by the SLICE method and the 'gold standard' CMR-TAG technique. A typical example of a LBBB patient with strain analysis using the SLICE technique on short axis cine images (A) and using the 'gold standard' CMR-TAG technique (B). On the cine images, the lateral wall segment shortens from 233.4 to 200.2 pixels corresponding with the -14.2% systolic strain, whereas the septum lengthens from 231.9 to 249.9 pixels corresponding with the +7.7% systolic strain. These (end-systolic, ES) strain values are displayed in the right diagram (A). Automated strain analysis of the tagged images shows similar results in this patient (B). ED, end-diastole; avo, aortic valve opening; ES, end-systole by aortic valve closure; mvo, mitral valve opening.

(iv) Septal strain patterns were classified as: double peaked systolic shortening (LBBB-1); early pre-ejection shortening followed by prominent systolic stretch (LBBB-2); and pseudonormal shortening with a late-systolic shortening peak and less pronounced end-systolic stretch (LBBB-3).(25) Figure 2 illustrates the assessment of dyssynchrony and discoordination parameters and figure 3 shows the pre-specified septal strain patterns.

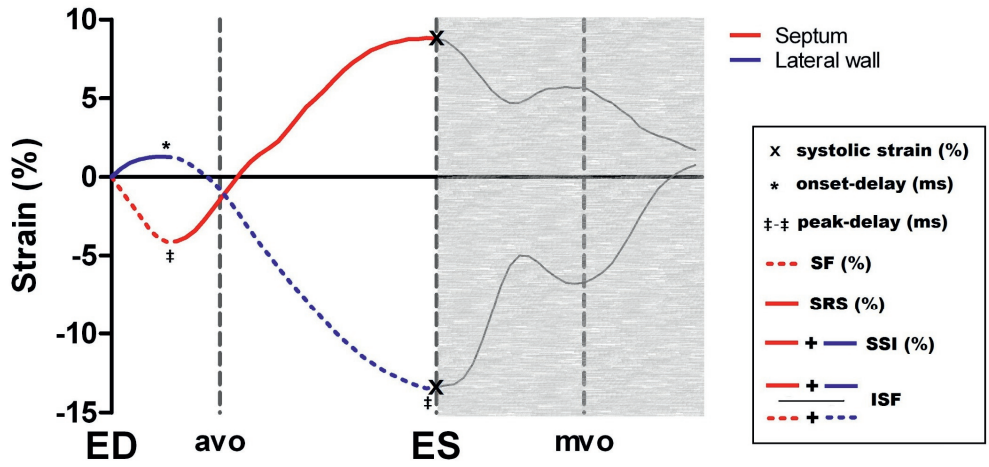


Figure 2: Measures of mechanical dyssynchrony and discoordination. This diagram displays time-based parameters of mechanical dyssynchrony, including septum to lateral delay in onset contraction (onset-delay) and difference in time to peak strain between the septum and lateral wall (peak-delay). Strain based parameters of discoordination are septal flash (SF), systolic rebound stretch of the septum (SRS), systolic stretch index (SSI) and internal stretch index (ISF).

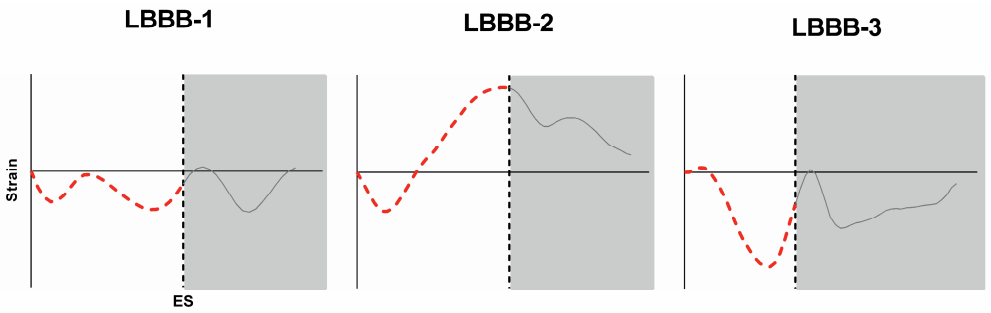


Figure 3: Pre-specified septum strain patterns. Septum strain patterns are classified as double peaked shortening (LBBB-1); predominant stretching (LBBB-2) or pseudonormal shortening (LBBB-3).

Statistics

The commercially available Statistical Package for Social Sciences software (IBM SPSS Statistics for Windows, Version 20.0. Armonk, NY, USA) was used for statistical analysis. Continuous variables were expressed as mean±standard deviation. Non-parametric data were expressed as median (25-75% interquartile range). Categorical variables were presented as absolute numbers and percentages. Agreement between strain values measured by the SLICE and CMR-TAG method was assessed using a two-way mixed-effect intra-class correlation coefficient for absolute agreement (ICC) and Bland-Altman analysis. Intra- and inter-observer variabilities were expressed using two-way random ICCs. First, the primary executive investigator independently analysed all images. Secondly, 15 randomly selected patients were re-analysed by the same investigator to assess intra-observer agreement. Lastly, a second reader analysed the same subset of patients for inter-observer agreement. Analysis per reader was strictly separated. Agreement was considered excellent (ICC ≥0.75), good (ICC 0.6-0.74), moderate (ICC 0.4-0.59) or poor (ICC <0.40).(26) Agreement of septal strain patterns assessed by SLICE and CMR-TAG was tested by Cohen's Kappa coefficient, using the following scale: excellent (k ≥0.81), good (k 0.61-0.8), moderate (k 0.41-0.60) or poor (k <0.40).(27) A Student t-test (independent or paired) or non-parametric test was used to compare groups when appropriate. Correlations were assessed using Pearson's correlation coefficient or, when normal distribution was absent, Spearman's Rho correlation coefficient. A p-value of <0.05 was considered statistically significant.

RESULTS

Twenty-seven CRT candidates (age 65±10 y, 16 men) were included in this study. Baseline patient characteristics are listed in table 1. From a total of 54 CMR-TAG septum segments, 48 (89%) were considered analysable. For the lateral wall, this was 49 (91%) of the 54 segments, resulting in a total of 97 (90%) out of the 108 CMR-TAG segments. For the SLICE analysis method, all 27 (100%) septum and all 27 (100%) lateral wall segments were analysable.

Segmental strain measures by SLICE and CMR-TAG

Measures of segmental strain, dyssynchrony and discoordination analysed by the SLICE and CMR-TAG techniques are given in table 2.

Table 1 Patient characteristics

Parameter	N = 27
Clinical	
Age (years)	65 ± 10
Sex (male/female)	16 / 11
Aetiology (ICMP/NICMP)	7 / 20
QRS duration (ms)	183 (167-194)
CMR	
Indexed EDV (m/m²)	145 (135-183)
Indexed ESV (ml/m²)	100 (90-151)
Indexed LV mass (gr/m²)	68 (59-85)
EF (%)	27 ± 9
CO (L/min)	5.6 ± 1.6
Scar mass ICMP (% LV mass), N = 7	15 (5-20)

CMR, cardiovascular magnetic resonance, ICMP, ischemic cardiomyopathy; NICMP, non-ischemic cardiomyopathy; EDV, end-diastolic volume; ESV, end-systolic volume; EF, ejection fraction; CO, cardiac output.

Comparing segmental strains within the same patient using the 'reference' CMR-TAG technique showed significantly more negative systolic values in the lateral wall compared to the septum (-12.5±3.5% vs. +3.5±6.4%; p<0.001). The lateral wall generally followed a normal contraction pattern with relative small variation in systolic strain (range -16.2% to -2.0%) while the septum often demonstrated an opposite strain pattern with large variation in systolic strain among patients (range -8.4% to +14.3%). Using the SLICE technique, segmental systolic strain was also found to be significantly more negative in the lateral wall compared to the septum (-13.9±4.0% vs. +1.0±6.4%; p<0.001). Variation in systolic strain was comparably less in the lateral wall (range -21.0% to -7.5%) than in the septum (-12.5% to +9.5%). Comparing absolute strain values between the SLICE and the CMR-TAG technique, more negative systolic strain values were found both in the lateral wall and the septum using the former analysis (-13.9±4.0% vs. -12.5±3.5%; p=0.018 and +1.0±6.4% vs. +3.5±6.4%; p=0.003 respectively). For most strain based discoordination parameters, the SLICE method tended to produce slightly lower values compared to the CMR-TAG method (table 2 and 3).

Table 2 Basic strain parameters, dyssynchrony and discoordination by SLICE and CMR-TAG

	Parameter N = 27	SLICE	CMR-TAG	mean difference	R^2
basic strain parameters	systolic strain septum (%)	+1.0 ± 6.4	+3.5 ± 6.4	-2.5 ± 3.9	0.66
	systolic strain rate septum (%/s)	+2.3 ± 18.1	+8.9 ± 17.9	-6.6 ± 10.1	0.68
	diastolic strain rate septum (%/s)	+1.3 ± 14.6	-2.4 ± 12.2	+3.7 ± 10.8	0.48
	systolic strain lateral wall (%)	-13.9 ± 4.0	-12.5 ± 3.5	-1.4 ± 2.9	0.50
	systolic strain rate lateral wall (%/s)	-36.4 ± 10.9	-32.8 ± 9.4	-3.6 ± 7.7	0.53
	diastolic strain rate lateral wall (%/s)	-32.9 ± 15.4	-27.9 ± 12.2	-5.0 ± 8.4	0.70
dyssynchrony	onset-delay (ms)	75 ± 34	58 ± 5	+17 ± 29	0.29
	peak-delay (ms)	241 ± 130	239 ± 114	+2 ± 121	0.27
discoordination	SF (%)	1.9 ± 2.1	1.9 ± 1.8	0.0 ± 1.5	0.51
	SRS (%)	6.3 ± 3.9	8.5 ± 5.2	-2.3 ± 3.0	0.66
	SSI (%)	7.9 ± 4.7	9.9 ± 6.0	-1.9 ± 3.2	0.73
	ISF	0.38 ± .23	0.51 ± .28	-0.13 ± 0.20	0.48

SLICE, segment length in cine; CMR-TAG, myocardial tagging; onset-delay, septum to lateral delay onset contraction; peak-delay, time difference in peak shortening between septum and lateral wall; SF, septal flash; SRS, systolic rebound stretch of the septum; SSI, systolic stretch index; ISF, internal stretch factor.

Table 3 Detection of differences in strain parameters between ICMP and NICMP patients

	Parameter N = 27	SLICE			CMR-TAG		
		ICMP	NICMP	p-value	ICMP	NICMP	p-value
basic strain parameters	systolic strain septum (%)	-7.4	+4.0	<0.001	-4.1	+6.2	<0.001
	systolic strain rate septum (%/s)	-21.3	+10.6	<0.001	-12.4	+16.4	<0.001
	diastolic strain rate septum (%/s)	+18.3	-4.6	<0.001	+12.2	-7.4	<0.001
	systolic strain lateral wall (%)	-9.7	-15.3	<0.001	-8.9	-13.7	0.030
	systolic strain rate lateral wall (%/s)	-26.8	-39.7	0.005	-23.5	-36.0	0.001
	diastolic strain rate lateral wall (%/s)	+16.3	+38.8	<0.001	+15.2	+32.4	<0.001
dyssynchrony	onset-delay (ms)	81	73	0.713	41	63	0.166
	peak-delay (ms)	108	287	0.001	135	275	<0.001
discoordination	SF (%)	0.9	2.3	0.147	0.8	2.3	0.050
	SRS (%)	2.4	7.6	0.001	4.5	9.9	0.014
	SSI (%)	4.4	9.2	0.017	5.1	11.5	0.012
	ISF	0.18	0.46	0.004	0.26	0.60	0.002

SLICE, segment length in cine; CMR-TAG, myocardial tagging; ICMP, ischemic cardiomyopathy; NICMP, non-ischemic cardiomyopathy; onset-delay, septum to lateral delay onset contraction; peak-delay, time difference in peak shortening between septum and lateral wall; SF, septal flash; SRS, systolic rebound stretch of the septum; SSI, systolic stretch index; ISF, internal stretch factor.

Agreement SLICE and CMR-TAG

Systolic strain values of the septum and the lateral wall showed close agreement between the SLICE and CMR-TAG technique, as illustrated in figure 4. Bland-Altman analysis affirms agreement between both methods, with slightly more negative strain values for the SLICE analysis compared to the CMR-TAG analysis (mean difference: -1.95±6.8%). Measures of absolute agreement for segmental strains, strain rates, and indices of dyssynchrony and discoordination are summarized in table 4. Overall, discoordination parameters demonstrated good agreement between both methods, whereas measures of mechanical dyssynchrony showed moderate agreement. Classification of septal strain patterns showed good agreement between both modalities as presented in table 5.

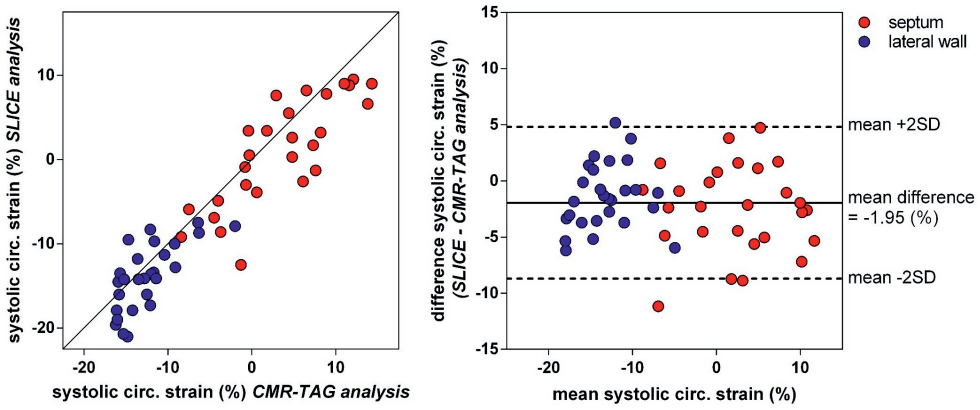


Figure 4: Agreement of segmental strains between the SLICE and the CMR-TAG technique. The left panel shows the correlation between systolic strains measured by CMR-TAG and SLICE. Corresponding Bland-Altman analysis (right panel) shows close agreement between the CMR-TAG and SLICE technique with the SLICE analysis resulting in slightly more negative strain values compared to the CMR-TAG analysis.

Table 4 Intraclass correlation coefficient for absolute agreement (ICC) and 95% CI

		SLICE – CMR-TAG N = 27	SLICE intra-observer N = 15	SLICE inter-observer N = 15
basic strain parameters	systolic strain septum (%)	**ICC 0.76** (0.43, 0.90)	**ICC 0.94** (0.82, 0.98)	**ICC 0.86** (0.63, 0.95)
	systolic strain rate septum (%/s)	**ICC 0.78** (0.47, 0.91)	**ICC 0.94** (0.82, 0.98)	**ICC 0.86** (0.63, 0.95)
	diastolic strain rate septum (%/s)	**ICC 0.66** (0.39, 0.83)	**ICC 0.93** (0.79, 0.98)	**ICC 0.87** (0.67, 0.96)
	systolic strain lateral wall (%)	**ICC 0.66** (0.35, 0.83)	**ICC 0.77** (0.36, 0.92)	**ICC 0.67** (-0.05, 0.90)
	systolic strain rate lateral wall (%/s)	**ICC 0.68** (0.39, 0.85)	**ICC 0.76** (0.35, 0.92)	**ICC 0.61** (-0.05, 0.87)
	diastolic strain rate lateral wall (%/s)	**ICC 0.77** (0.47, 0.90)	**ICC 0.91** (0.71, 0.97)	**ICC 0.74** (0.06, 0.92)
dyssynchrony	onset-delay (ms)	**ICC 0.45** (0.09, 0.71)	**ICC -0.21** (-0.54, 0.27)	**ICC 0.20** (-0.36, 0.64)
	peak-delay (ms)	**ICC 0.52** (0.17, 0.57	**ICC 0.74** (0.39, 0.91)	**ICC 0.37** (-0.15, 0.73)
discoordination	SF (%)	**ICC 0.71** (0.46, 0.86)	**ICC 0.72** (0.34, 0.90)	**ICC 0.36** (-0.18, 0.73)
	SRS (%)	**ICC 0.70** (0.27, 0.87)	**ICC 0.83** (0.57, 0.94)	**ICC 0.73** (0.37, 0.90)
	SSI (%)	**ICC 0.78** (0.49, 0.90)	**ICC 0.81** (0.49, 0.93)	**ICC 0.72** (0.35, 0.89)
	ISF	**ICC 0.61** (0.22, 0.81)	**ICC 0.91** (0.74, 0.97)	**ICC 0.61** (0.16, 0.85)

SLICE, segment length in cine; CMR-TAG, myocardial tagging; onset-delay, septum to lateral delay onset contraction; peak-delay, time difference peak shortening between septum and lateral wall; SF, septal flash; SRS, systolic rebound stretch of the septum; ISF, internal stretch factor.

Table 5 Cross table with LBBB patterns between SLICE and CMR-TAG, SLICE intra-observer and SLICE inter-observer

		CMR-TAG N = 27			**SLICE intra-observer N = 15**			**SLICE inter-observer N = 15**		
		LBBB-1 n (%)	LBBB-2 n (%)	LBBB-3 n (%)	LBBB-1 n (%)	LBBB-2 n (%)	LBBB-3 n (%)	LBBB-1 n (%)	LBBB-2 n (%)	LBBB-3 n (%)
SLICE	LBBB-1 n (%)	**5 (19)**	2 (7)	0 (0)	**1 (7)**	1 (7)	1 (7)	**2 (13)**	0 (0)	1 (7)
	LBBB-2 n (%)	2 (7)	**11 (41)**	0 (0)	1 (7)	**8 (53)**	0 (0)	1 (7)	**8 (53)**	0 (0)
	LBBB-3 n (%)	1 (4)	0 (0)	**6 (22)**	0 (0)	0 (0)	**3 (20)**	0 (0)	0 (0)	**3 (20)**
		Total agreement: **81%** Kappa value: **0.71 (p<0.001)**			Total agreement: **80%** Kappa value: **0.64 (p=0.001)**			Total agreement: **87%** Kappa value: **0.77 (p<0.001)**		

SLICE, segment length in cine; CMR-TAG, myocardial tagging; LBBB-1, left bundle branch block pattern 1; LBBB-2, left bundle branch block pattern 2; LBBB-3, left bundle branch block pattern 3

Reproducibility of SLICE

For intra-observer variability assessment, SLICE analysis was repeated by the primary investigator in a subset of 15 patients, and showed excellent agreement between segmental systolic strains as displayed in table 4. Intra-observer variability for all other strain based discoordination parameters also proved to be excellent, with the exception of SF (good agreement). Intra-observer agreement for indices of mechanical dyssynchrony was good for peak-delay, but poor for onset-delay. Intra-observer agreement for the classification of septum strain patterns was good. Additionally, a second observer independently analysed the same subset of patients to determine the inter-observer variability, which was excellent for segmental systolic strains in the septum and good for the lateral wall. Inter-observer variability for parameters of discoordination and mechanical dyssynchrony were found to be good for all discoordination parameters, with the exception of SF (poor agreement), and poor for parameters of mechanical dyssynchrony. Inter-observer agreement was good for the classification of septal strain patterns.

Detection of mechanical discoordination

Mechanical discoordination was assessed by calculating the commonly used parameters SRS, SSI and ISF (5,6,23). Figure 5 illustrates these parameters assessed by the SLICE method and the CMR-TAG method to be strongly correlated. Using the 'reference' CMR-TAG technique, significant differences in discoordination values were detected between ischemic cardiomyopathy (ICMP) and non-ischemic (NICMP) patients with the ICMP group showing lower rates compared to NICMP patients (SRS 4.5±4.3% vs. 9.9±4.8%; p=0.014; SSI 5.1±4.4% vs. 11.5±5.7%; p=0.012; ISF 0.26±0.14 vs. 0.60±0.26; p=0.002). Using the SLICE technique similar differences were detected between the ICMP- and NICMP-group (SRS 2.4±2.7% vs. 7.6±3.3%; p=0.001; SSI 4.4±5.0% vs. 9.2±4.0%; p=0.017; ISF 0.18±0.15 vs. 0.46±0.21; p=0.004), see table 3.

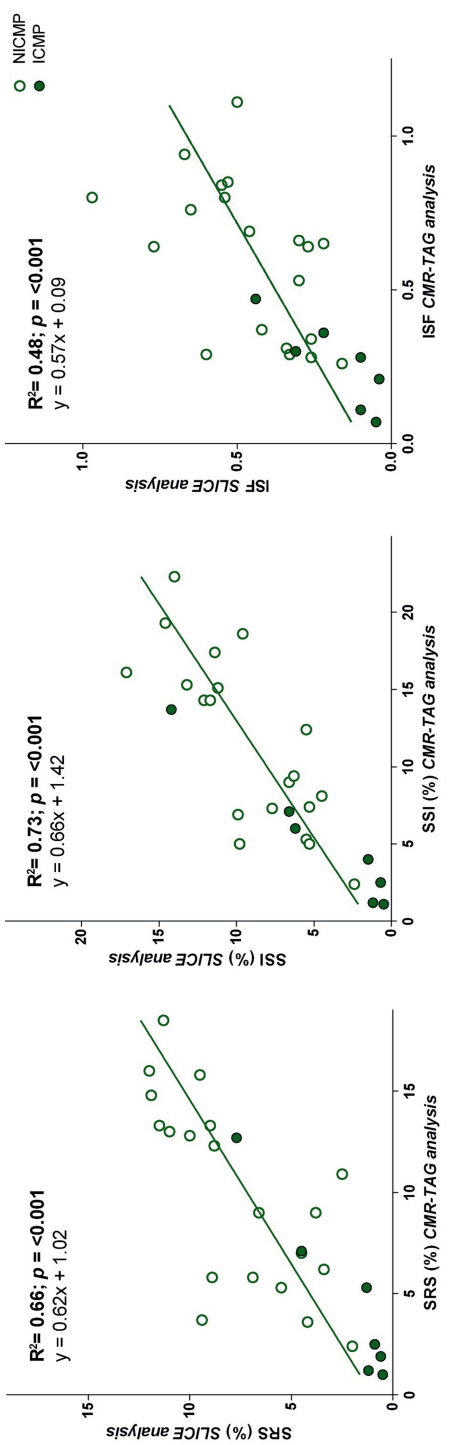


Figure 5: Agreement predictors of CRT response between the SLICE and CMR-TAG technique. There is a strong correlation between SLICE and CMR-TAG derived strain measures with respect to the commonly used predictors of CRT response being SRS (left panel), SSI (middle panel) and ISF (right panel).

DISCUSSION

This study demonstrates that the SLICE post-processing technique on standard CMR cine images offers both accurate and robust circumferential strain measures compared to the gold standard CMR-TAG technique in CRT candidates. Strain measures on a segmental scale, particularly of interest in this patient group to predict CRT response, show close agreement with the CMR-TAG technique, whereas recently published data on CMR-FT software showed disappointing results.(13-17)

Chronic HF patients with LBBB, eligible for CRT, show large diversity in the manifestation of mechanical timing differences (dyssynchrony) and deformation abnormalities (discoordination) throughout the LV. Traditionally, echocardiographic modalities offer high temporal resolution imaging which enables the assessment of regional timing differences throughout the LV. However, echocardiographic dyssynchrony parameters showed disappointing results in the PROSPECT study.(8) More recent, single center studies showed mechanical discoordination rather than mechanical dyssynchrony to be predictive for CRT response.(4-7) In this study, quantification of mechanical discoordination showed wide variation among CRT candidates, ranging from a normally coordinated to a severely discoordinated LV contraction pattern, with predominant stretching of the septum during systole (LBBB-2 pattern). Because of this wide inter-person variation in segmental strains and discoordination rates, segmental strain analysis holds the potential to discriminate between CRT responders and non-responders at baseline. Using SLICE, the presence of a paradoxical septum movement was distinctly noticeable by qualitative assessment of the SLICE strain-curve (figure 1A). Classification of septum strains to pre-specified strain patterns (figure 3) showed good agreement between the SLICE and CMR-TAG method. Classification of a pseudonormal (LBBB-3) septum strain pattern is of clinical relevance as this pattern is associated with smaller benefit of CRT compared to other septum strain patterns.(25) Quantification of strain patterns by measuring regional systolic strains, the cumulative amount of SRS, SSI and the discoordination rate ISF showed good to excellent agreement with the CMR-TAG technique (figure 5). These are conventional markers of mechanical discoordination that have been shown to be accurate in the prediction of CRT response in multiple single center studies.(4-6,23) In addition,

sensitivity of the SLICE technique proved to be high enough to detect the differences in discoordination values that were found between IMCP- and NICMP-patients. Patients with an ICMP have significantly lower discoordination values compared to NICMP patients, which might explain the lack of CRT response in this subgroup of patients. In general, the SLICE technique tends to produce slightly lower discoordination values compared to the CMR-TAG standard. This might be due to the lower temporal resolution that was used for cine imaging compared to CMR-TAG (~50ms vs. ~15ms) being less sensitive for peak strain values.(28) It is possible that this shortcoming in temporal resolution had a larger effect on the assessment of time-based dyssynchrony parameters, which could explain the lack of agreement and reproducibility that was found for these parameters. However, dyssynchrony parameters have limited predictive value for the selection of CRT patients.(8) Therefore, future studies should focus on the classification of septal strain patterns and discoordination markers, which can be accurately derived by the SLICE post-processing technique. Also, accelerated CMR imaging techniques such as parallel imaging can overcome this problem by improving the spatiotemporal resolution of the cine image acquisition.(29) However, since the SLICE technique is intended as a post-processing technique on standard cine images, a temporal resolution of ~50ms was used for the acquisition of cine images as this is typical in most standard clinical protocols.

Conceptual differences between the SLICE and CMR-TAG techniques should be considered. CMR-TAG sequences cover the LV with magnetization saturated bands in a grid format at end-diastole.(30) Post-processing of these 'tagged' images by tracing the displacement of the taglines throughout the cardiac cycle produces high quality measures of intramural shortening. On the other hand, SLICE is performed by measuring total segment length between two anatomic landmarks throughout all phases on standard cine images. This method produces a measure of relative frame-to-frame segment length change that, in essence, approximates the net result of all intramural strains combined throughout the segment. A disadvantage of the SLICE method is that it derives strain measures from the apparent in-plane motion of the anatomic landmarks. However, this apparent in-plane movements may also be caused by through-plane displacements of oblique or tapering structures that form the anatomic

landmarks. For this reason we could only analyse the mid-LV slice, since this plane is relatively motion independent. CMR-FT software neglects these pitfalls and the user is not able to track and trace the analysis steps. This might be the reason for the previous failure of segmental strain analysis by the CMR-FT software. Another consequential disadvantage is the inability to determine LV torsion, as this analysis requires both basal and apical rotation measurements.

To our knowledge, this is the first study to demonstrate a post-processing technique on standard CMR cine images that offers both accurate and robust circumferential strain measures on a segmental scale in CRT candidates. Both the visual classification of septal strain patterns and the quantification of conventional discoordination parameters being SRS, SSI and ISF showed close agreement with the 'gold standard' CMR-TAG technique, bringing the use of accurate predictors of CRT response a step closer to clinical practice.

Some limitations need to be addressed. Firstly, the present study was specified to HF patients with LBBB only. However, this might also be considered a strength of this study since segmental strains are particularly of interest in this specific population. Secondly, some geographic selection bias may have occurred as only study participants that were included close to our center were invited to participate in the present CMR sub study. Furthermore, the processing time for the CMR-TAG analysis was less than 20 minutes compared to a maximum of 60 minutes for the SLICE method. Although the SLICE technique was more time consuming in the present study, previously used CMR-TAG post-processing software techniques also proved to be time consuming and less user-friendly compared to the new SinMod technique by inTag.

For future studies, the SLICE processing time can be substantially reduced (halved) by limiting the analysis to the systolic phase, since diastolic strains are not incorporated in discoordination markers (figure 2). In fact, segmental systolic strains can already be calculated after analysing 2 frames providing both end-diastolic and end-systolic segment length (figure 1A). The number of frames that is required per strain parameter is displayed in figure S2 in the supplemental materials. Further reduction of processing time, as well as improvement of reproducibility and clinical applicability, can be achieved by automated

assessment. Additionally, implementing radial taglines to standard cine imaging will facilitate the detection of the landmarks thus further enhancing strain analysis. Ultimately, SLICE might serve as a new principle for integration in CMR-FT algorithms.

CONCLUSION

In conclusion, the novel SLICE post-processing technique requires standard cine images only and provides both accurate and robust myocardial strain measures on a segmental scale in HF patients with LBBB. Future studies will focus on the prognostic value of these strain measures in CRT candidates.

REFERENCES

1. Kalam K, Otahal P, Marwick TH (2014) Prognostic implications of global LV dysfunction: a systematic review and meta-analysis of global longitudinal strain and ejection fraction. Heart 100:1673-1680
2. Gjesdal O, Remme EW, Opdahl A et al (2011) Mechanisms of Abnormal Systolic Motion of the Interventricular Septum During Left Bundle-Branch Block. Circulation-Cardiovascular Imaging 4:264-U109
3. Leenders GE, Lumens J, Cramer MJ et al (2012) Septal Deformation Patterns Delineate Mechanical Dyssynchrony and Regional Differences in Contractility Analysis of Patient Data Using a Computer Model. Circulation-Heart Failure 5:87-U190
4. Prinzen FW, Vernooy K, De Boeck BW, Delhaas T (2011) Mechano-energetics of the asynchronous and resynchronized heart. Heart Fail Rev 16:215-224
5. De Boeck BWL, Teske AJ, Meine M et al (2009) Septal rebound stretch reflects the functional substrate to cardiac resynchronization therapy and predicts volumetric and neurohormonal response. European Journal of Heart Failure 11:863-871
6. Kirn B, Jansen A, Bracke F, van Gelder B, Arts T, Prinzen FW (2008) Mechanical discoordination rather than dyssynchrony predicts reverse remodeling upon cardiac resynchronization. American Journal of Physiology-Heart and Circulatory Physiology 295:H640-H646
7. Risum N, Tayal B, Hansen TF et al (2015) Identification of Typical Left Bundle Branch Block Contraction by Strain Echocardiography Is Additive to Electrocardiography in Prediction of Long-Term Outcome After Cardiac Resynchronization Therapy. J Am Coll Cardiol 66:631-641
8. Chung ES, Leon AR, Tavazzi L et al (2008) Results of the Predictors of Response to CRT (PROSPECT) trial. Circulation 117:2608-2616
9. Kapetanakis S, Kearney MT, Siva A, Gall N, Cooklin M, Monaghan MJ (2005) Real-Time Three-Dimensional Echocardiography: A Novel Technique to Quantify Global Left Ventricular Mechanical Dyssynchrony. Circulation 112:992-1000
10. Raman SV, Simonetti OP (2009) The CMR examination in heart failure. Heart Fail Clin 5:283-300, v
11. Oyenuga OA, Onishi T, Gorcsan J, III (2011) A practical approach to imaging dyssynchrony for cardiac resynchronization therapy. Heart Fail Rev 16:397-410
12. Claus P, Omar AM, Pedrizzetti G, Sengupta PP, Nagel E (2015) Tissue Tracking Technology for Assessing Cardiac Mechanics: Principles, Normal Values, and Clinical Applications. JACC Cardiovasc Imaging 8:1444-1460
13. Augustine D, Lewandowski AJ, Lazdam M et al (2013) Global and regional left ventricular myocardial deformation measures by magnetic resonance feature tracking in healthy volunteers: comparison with tagging and relevance of gender. J Cardiovasc Magn Reson 15:8
14. Harrild DM, Han Y, Geva T, Zhou J, Marcus E, Powell AJ (2012) Comparison of cardiac MRI tissue tracking and myocardial tagging for assessment of regional ventricular strain. Int J Cardiovasc Imaging 28:2009-2018
15. Morton G, Schuster A, Jogiya R, Kutty S, Beerbaum P, Nagel E (2012) Inter-study reproducibility of cardiovascular magnetic resonance myocardial feature tracking. J Cardiovasc Magn Reson 14:43

16. Singh A, Steadman CD, Khan JN et al (2015) Intertechnique agreement and interstudy reproducibility of strain and diastolic strain rate at 1.5 and 3 Tesla: a comparison of feature-tracking and tagging in patients with aortic stenosis. J Magn Reson Imaging 41:1129-1137
17. Wu L, Germans T, Guclu A, Heymans MW, Allaart CP, van Rossum AC (2014) Feature tracking compared with tissue tagging measurements of segmental strain by cardiovascular magnetic resonance. J Cardiovasc Magn Reson 16:10
18. ClinicalTrials.gov Identifier: NCT01519908,
19. Zwanenburg JJ, Gotte MJ, Kuijer JP, Heethaar RM, van Rossum AC, Marcus JT (2004) Timing of cardiac contraction in humans mapped by high-temporal-resolution MRI tagging: early onset and late peak of shortening in lateral wall. Am J Physiol Heart Circ Physiol 286:H1872-H1880
20. Flett AS, Hasleton J, Cook C et al (2011) Evaluation of techniques for the quantification of myocardial scar of differing etiology using cardiac magnetic resonance. JACC Cardiovasc Imaging 4:150-156
21. Schneider CA, Rasband WS, Eliceiri KW (2012) NIH Image to ImageJ: 25 years of image analysis. Nat Methods 9:671-675
22. Miller CA, Borg A, Clark D et al (2013) Comparison of local sine wave modeling with harmonic phase analysis for the assessment of myocardial strain. J Magn Reson Imaging 38:320-328
23. Lumens J, Tayal B, Walmsley J et al (2015) Differentiating Electromechanical From Non-Electrical Substrates of Mechanical Discoordination to Identify Responders to Cardiac Resynchronization Therapy. Circ Cardiovasc Imaging 8:e003744
24. Marwick TH (2014) Selection for cardiac resynchronization therapy: all in a flash? JACC Cardiovasc Imaging 7:980-982
25. Leenders GE, Lumens J, Cramer MJ et al (2012) Septal deformation patterns delineate mechanical dyssynchrony and regional differences in contractility: analysis of patient data using a computer model. Circ Heart Fail 5:87-96
26. Castillo E, Osman NF, Rosen BD et al (2005) Quantitative assessment of regional myocardial function with MR-tagging in a multi-center study: interobserver and intraobserver agreement of fast strain analysis with Harmonic Phase (HARP) MRI. J Cardiovasc Magn Reson 7:783-791
27. Landis JR, Koch GG (1977) The measurement of observer agreement for categorical data. Biometrics 33:159-174
28. Lorsakul A, Gamarnik V, Duan Q et al (2012) Impact of temporal resolution on LV myocardial regional strain assessment with real-time 3D ultrasound. Conf Proc IEEE Eng Med Biol Soc 2012:4075-4078
29. Kozerke S, Plein S (2008) Accelerated CMR using zonal, parallel and prior knowledge driven imaging methods. J Cardiovasc Magn Reson 10:29
30. Zerhouni EA, Parish DM, Rogers WJ, Yang A, Shapiro EP (1988) Human heart: tagging with MR imaging--a method for noninvasive assessment of myocardial motion. Radiology 169:59-63

SUPPLEMENTAL MATERIAL

Study population

Inclusion criteria for the original MARC study were sinus rhythm, moderate to severe heart failure (New York Heart Association class II and III), intrinsic QRS-width ≥130ms with LBBB or ≥150ms without LBBB for patients with NYHA class II, intrinsic QRS-width ≥120ms with LBBB or ≥150ms without LBBB for patients with NYHA class III and at least 3 months stable optimal tolerated medical therapy. Patients with myocardial infarction within 40 days prior to study inclusion, coronary artery bypass graft or valve surgery within 90 days prior to study inclusion, previous pacemaker implantation or the presence of severe aortic stenosis were excluded.

Image acquisition

Typical image acquisition parameters: (1) cine imaging: slice thickness 5mm, slice gap 5mm, echo time (TE) 1.6ms, repetition time (TR) 3.2ms, temporal resolution <50ms, in-plane spatial resolution 1.5 by 2.1mm, flip angle 60 degrees. The number of reconstructed temporal phases within the cardiac cycle was set at 20; (2) high temporal cine imaging: TE 1.7ms, TR 3.4ms, temporal resolution ~15ms; (3) myocardial tagging: slice thickness 6mm, TE 1.7ms, TR 3.6ms, temporal resolution <15ms, in-plane spatial resolution 1.3 by 4.3mm, flip angle 20 degrees, tag spacing 7mm. The number of reconstructed temporal phases within the cardiac cycle was set at 55.

Post-processing myocardial tissue tagging (CMR-TAG)

After selecting the area of interest, endo- and epi-cardial contours were manually drawn in the end-systolic phase and automatically propagated (figure 1B). A template was placed dividing the LV in 6 equally sized regions (anterior, anterolateral, inferolateral, inferior, inferoseptal, anteroseptal). The myocardium was divided in 3 layers (endo-, mid-, epi-wall layer). Septum strain was calculated as the averaged strain from both the anteroseptal and inferoseptal segments of the mid-wall layer. Lateral wall strain was calculated as the averaged strain from both the anterolateral and inferolateral segments of the mid-wall layer. Individual strain curves were discarded in case of low signal-to-noise ratio as judged by two independent investigators. The presence of at least one analysable strain curve out of the two curves per segment resulted in inclusion of the patient for SLICE analysis.

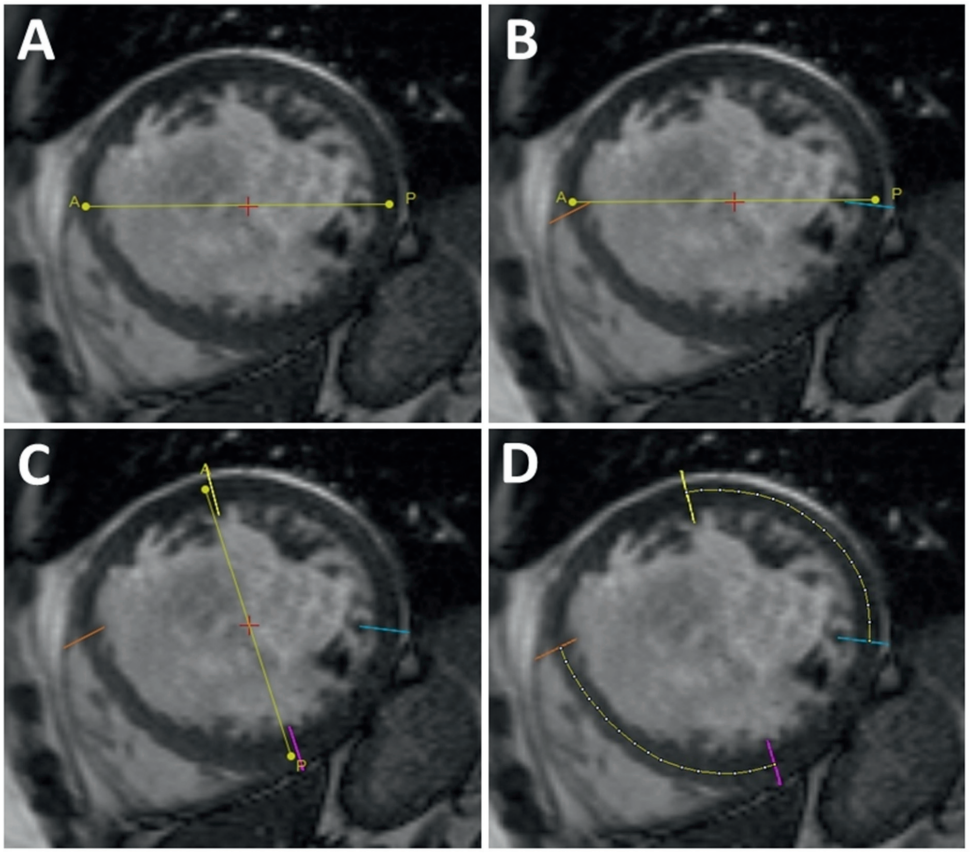


Figure S1: Determination of the anatomical landmarks in the end-diastolic frame. Step-by-step illustration to define anatomical landmarks in the end-diastolic mid-LV short-axis cine. First, a straight line was drawn from the anterior RV insertion point (marked as A) through the LV center point to locate the posterolateral region (marked as P) as shown in diagram (A). Subsequently, marks were placed perpendicular to the myocardium at the nearest trabecula that were traceable throughout the cardiac cycle, diagram (B). This procedure was repeated for the posterior RV insertion point (marked as P) and the anterolateral region (marked as A), diagram (C). Segment length was measured in ImageJ between both marks using a segmented line, diagram (D).

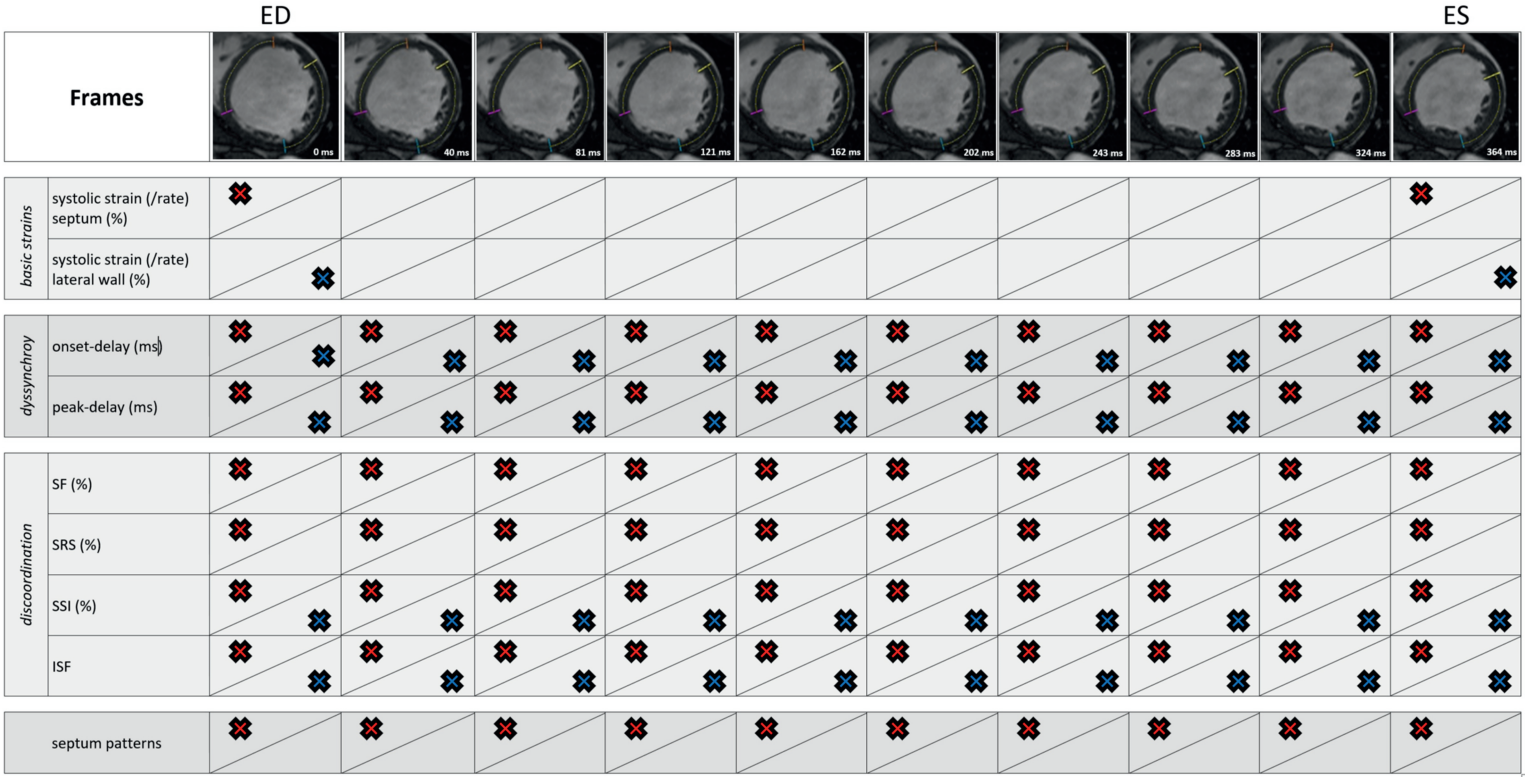


Figure S2: Number of frames analysed per strain parameter. Assessing basic strains (systolic strain, systolic strain rate and diastolic strain rate) requires only SLICE analysis of the end-diastolic (ED) and end-systolic (ES) frame. Obtaining dyssynchrony markers (onset-delay and peak-delay) requires SLICE processing of the septum and lateral wall in systolic frames. Discoordination markers can be calculated after analyzing septum SLICE in systolic frames (SF and SRS) or both the septum and lateral wall (SSI and ISF). Classification of septum strain patterns requires SLICE analysis of the septum in systolic frames. Red cross indicates septum SLICE analysis, blue cross indicates lateral wall SLICE analysis.

Chapter 8

Strain Segment Length in Cine (SLICE) Strain Analysis: a Practical Approach to Estimate Potential Benefit from Cardiac Resynchronization Therapy

Submitted

Alwin Zweerink
Robin Nijveldt
Natalia J. Braams
Alexander H. Maass
Kevin Vernooy
Frederik J. de Lange
Mathias Meine
Bastiaan Geelhoed
Michiel Rienstra
Isabelle C. van Gelder
Marc A. Vos
Albert C. van Rossum
Cornelis P. Allaart

ABSTRACT

Aims: Segment length in cine (SLICE) strain analysis on standard CMR cine images was recently validated against gold standard myocardial tagging. The present study aims to explore predictive value of SLICE for cardiac resynchronization therapy (CRT) response.

Methods and results: Fifty-seven patients with heart failure and left bundle branch block were prospectively enrolled in this multi-center study and underwent CMR examination before CRT implantation. Circumferential strains of the septal and lateral wall were measured by SLICE on short-axis cine images. In addition, timing and strain pattern parameters were assessed. After twelve months, CRT response was quantified by the echocardiographic change in LV end-systolic volume (LVESV). Mean LVESV change after twelve months was -32±27%. In contrast to timing parameters, strain pattern parameters being systolic rebound stretch of the septum (SRS_{sep}), systolic stretch index ($SSI_{sep\text{-}lat}$), and internal stretch factor ($ISF_{sep\text{-}lat}$) all correlated significantly with LVESV change (R -0.56; R -0.53; and R -0.58, respectively). Of all strain parameters, end-systolic septal strain (ESS_{sep}) showed strongest correlation with LVESV change (R -0.63). Multivariable analysis showed ESS_{sep} to be independently related to LVESV change together with age and QRS_{AREA}.

Conclusion: The practicable SLICE strain technique helps the clinician to estimate potential benefit from CRT by analyzing standard CMR cine images without the need for commercial software. Of all strain parameters, end-systolic septal strain (ESS_{sep}) demonstrated the strongest correlation with reverse remodeling after CRT. This parameter can be measured in around twelve minutes, and is additive to clinical (age) and electrical (QRS_{AREA}) parameters in estimating potential benefit from CRT.

INTRODUCTION

Cardiac Resynchronization Therapy (CRT) is an established therapy for patients with chronic heart failure, reduced left ventricular (LV) ejection fraction and left bundle branch block (LBBB). Patient selection is primarily guided by the electrocardiogram (ECG), but this results in approximately one-third of patients not benefitting from the therapy.(1-2) Additional criteria are therefore needed to improve patient selection for CRT. Myocardial strain imaging provides mechanical information on LV regional timing differences (also known as dyssynchrony) and inefficient contraction patterns (also known as discoordination). Strain parameters have been linked to CRT outcome in prior studies.(3-6) At present, multiple strain imaging tools are commercially available for both cardiovascular magnetic resonance imaging (CMR) and echocardiographic modalities.(7-8) CMR strain analysis requires additional tagging sequences (CMR-TAG), or can be performed on standard cine images using specialized feature tracking (CMR-FT) software. In addition, we recently validated the novel segment length in cine (SLICE) technique. The purpose of SLICE is to provide the clinician a simple and transparent method to estimate benefit from CRT. More specifically, SLICE consists of a series of manual frame-to-frame segment length measurements between anatomic landmarks on standard short-axis CMR cines.(9) This technique showed excellent intra-observer and good inter-observer reproducibility for measuring circumferential strains. Moreover, SLICE showed good agreement with gold standard CMR-TAG and holds the advantage of being widely available as it requires no additional image acquisition sequences (i.e. tagging), or commercial post-processing software (i.e. feature tracking). The aim of the present study was to evaluate SLICE as a practicable strain technique to estimate potential benefit from CRT using standard CMR cine images.

METHODS

Study population

This study was part of the Markers And Response to CRT (MARC) study, a non-randomized, multi-center study that investigated the role of various clinical-, ECG-, echocardiographic-, and biomarker parameters to predict LV reverse remodeling after CRT.(10) The MARC study prospectively enrolled two-hundred-forty patients planned for CRT implantation in six medical centers in the Netherlands. Previously, we validated SLICE against CMR-TAG in twenty-seven patients who underwent CMR examination with additional CMR-TAG imaging.(9) In the present study, fifty-seven patients were included who underwent standard CMR examination in three participating hospitals (Amsterdam University Medical Centers, location VU medical center; Maastricht University Medical Centre; University Medical Centre Groningen). All subjects gave written informed consent and the local medical ethics committee (Amsterdam University Medical Centers, location VU medical center) approved data collection and management. The investigation conforms with the principles outlined in the Declaration of Helsinki.

Definition of CRT response

Echocardiographic assessment of LV volumes was performed before, and twelve months after CRT implantation. LV end-systolic volume (LVESV) was measured using the biplane Simpson's method by two experienced observers. Patients with ≥15% reduction in LVESV were classified as CRT responders.

Image acquisition

Patients underwent CMR examination using a 1.5 Tesla magnetic resonance scanner (Magnetom Avanto or Aera, Siemens, Erlangen, Germany; or Philips Intera CV, Philips Healthcare, Best, The Netherlands). Standard CMR cine images were acquired using a retrospectively ECG-gated balanced steady-state free-precession (SSFP) sequence with standard short-axis and long-axis orientations to measure LV volumes and calculate LV ejection fraction. Typically, temporal resolution was <50ms and the number of reconstructed temporal phases within the cardiac cycle was set between 20 and 30. Typical image acquisition parameters were: slice thickness/slice gap: 5/5 mm, 8/0mm or 6/4mm; echo time (TE)/repetition time (TR): 1.6ms/3.2ms; in-plane spatial

resolution: 1.5 by 2.1mm; flip angle: 45 to 75 degrees. Cine imaging of the LV in the three-chamber view was performed to assess aortic valve closure (AVC). Myocardial scar territory was assessed by late gadolinium enhancement (LGE) imaging, and infarct size was measured using the full width at half maximum method.(11) All CMR data were analyzed using dedicated offline software (QMassMR version 7.6, Medis, Leiden, The Netherlands).

SLICE strain analysis

A detailed description of the SLICE analysis post-processing steps has been published previously.(9) In brief, the mid-LV slice position with short-axis cine images was selected (QMassMR version 7.6, Medis, Leiden, The Netherlands). Two endocardial anatomic landmarks (trabeculae) delimiting the septal segment were chosen in the end-diastolic (ED) frame. Marks were placed perpendicular to the myocardium following the anatomic landmarks throughout all phases. This was repeated for the lateral wall segment. Subsequently, marked cine images were exported to ImageJ to measure segment length measurements between the marks over the myocardium midline in each phase using the segmented line tool, see figure 1A. Segments lengths were expressed as a percentage of the ED segment length, and the frame-to-frame segment length change was plotted as a strain curve, see figure 1B.

Strain parameters

Four subsets of strain parameters were evaluated. First, basic strain values were quantified by the septal and lateral peak negative strain (peak strain); and end-systolic strain (ESS) at the time of AVC. Secondly, timing differences were measured by the septal-to-lateral delay in onset of shortening (onset-delay); and the septal-to-lateral time difference in peak contraction (peak-delay); Thirdly, strain pattern parameters included systolic rebound stretch of the septum (SRS_{sep}); the systolic stretch index ($SSI_{sep\text{-}lat}$); and the internal stretch index ($ISF_{sep\text{-}lat}$). Lastly, septal strain patterns were visually classified to the following pre-specified patterns: double peaked systolic shortening (LBBB-1); early pre-ejection shortening followed by prominent systolic stretch (LBBB-2); and pseudonormal shortening with a late-systolic shortening peak and less pronounced end-systolic stretch (LBBB-3).

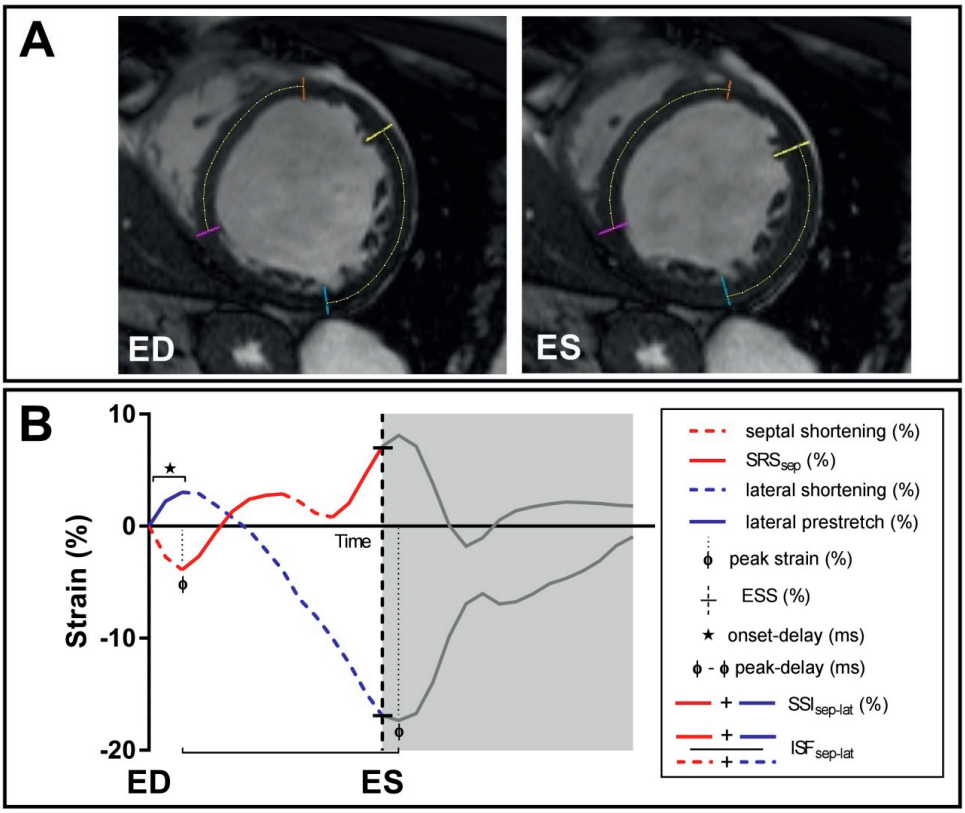


Figure 1: SLICE analysis and measurement of strain parameters. (A) Typical example of a LBBB patient with SLICE analysis of the septal and lateral wall in the end-diastolic (ED) and end-systolic (ES) frame. (B) Strain curves of the septal (red) and lateral (blue) wall with measurement of basic strain values as the maximal negative strain value (peak strain) and end-systolic strain value (ESS) at aortic valve closure; timing differences measured as the septal to lateral delay in onset contraction (onset-delay) and peak negative strain delay (peak-delay); and inefficient strain patterns measured as systolic rebound stretch of the septum (SRS_{sep}), systolic stretch index ($SSI_{sep-lat}$) and internal stretch index ($ISF_{sep-lat}$).

Electrocardiographic and echocardiographic parameters

A detailed description of the ECG- and echocardiographic analysis has been published previously.(10) In brief, a baseline 12-lead ECG was recorded for QRS duration measurements and QRS morphology assessment. Subsequently, a 3D vector loop was constructed from the 12-lead ECG to calculate the QRS_{AREA}. The presence of apical rocking was assessed during baseline echocardiography, and defined as a short systolic septal-to-lateral rocking motion of the apex.(12) In addition, the interventricular mechanical delay (IVMD) was measured as the timing difference between left and right ventricular pre-ejection intervals. Subsequently, the CRT-Age-Vectorcardiographic QRS_{AREA} -IVMD-Apical Rocking (CAVIAR) score was calculated as previously described in the MARC main study.(10)

Statistical analysis

Statistical analysis was performed in the study core lab (University Medical Center Groningen, Groningen, The Netherlands) using the R software (R Foundation for Statistical Computing, Vienna, Austria). Continuous variables are expressed as mean ± standard deviation or in absence of a normal distribution as median and interquartile range. Categorical variables are presented as numbers and percentages. Strain parameters were compared between CRT responder and non-responder groups by an independent student t-test, or a non-parametric test when appropriate. Correlations between strain parameters and echocardiographic CRT response were assessed using the Pearson's correlation coefficient or when normal distribution was absent, the Spearman's Rho correlation coefficient. Receiver operating characteristics (ROC) curve analysis was used to find optimal cut-off values and determine predictive value of strain parameters. Univariable linear regression analysis was performed to assess the association of other (clinical, CMR and CAVIAR) baseline parameters with echocardiographic CRT response. To test the additional value of SLICE strain analysis on top of conventional determinants of CRT response, multivariable linear regression analysis was performed by entering the best performing strain parameter (based on R) to a model with standard CMR parameters (model 1), clinical parameters (model 2) and the CAVIAR score parameters (model 3). A p-value of <0.05 was considered statistically significant.

RESULTS

After screening sixty-three patients, three patients were excluded from the analysis due to incomplete- or insufficient quality of the CMR scan. Of the remaining sixty patients, fifty-seven patients completed the one-year follow up. One patient was lost to follow-up because of non-cardiac death (lung carcinoma), one withdrew informed consent, and one lacked sufficient image-quality during echocardiographic examination. Patient characteristics of the remaining fifty-seven patents are presented in table 1. Mean LVESV change after one year was -32±27% with 14 (25%) patients showing <15% reduction in LVESV (CRT non-responders).

Strain parameters and CRT response

Strain values for the total patient group, and both responder and non-responder subgroups are presented in table S1 of the appendix. Basic strain values measured as peak strain in the septal and lateral wall region showed weak correlations with LVESV change as demonstrated in table 2. In contrast, the basic strain parameter end-systolic septal strain (ESS_{sep}) showed the highest correlation coefficient of all parameters (R -0.63, p<0.001) with good predictive value for CRT response (AUC 0.81, p<0.001) as illustrated in figure 2. Timing parameters onset-delay and peak-delay were unrelated to LVESV change and yielded no predictive value for CRT response. On the other hand, strain pattern parameters all correlated with LVESV change (SRS_{sep} R -0.56; $SSI_{sep-lat}$ R -0.53; $ISF_{sep-lat}$; R -0.58, all p<0.001) and yielded good predictive value for CRT response (SRS_{sep} AUC 0.80; $SSI_{sep-lat}$ AUC 0.82; $ISF_{sep-lat}$ AUC 0.82, all p<0.001). As demonstrated in figure 3, septal strain curves were visually classified as LBBB-1 pattern in 25%, LBBB-2 in 44%, and LBBB-3 in 32% of the patients. Patients with pattern LBBB-1 or LBBB-2 demonstrated significantly more reverse remodeling compared to pattern LBBB-3. In addition, the response rate in the LBBB-1 and LBBB-2 was a two-fold higher than the response rate in the LBBB-3 group (88% / 93% versus 44%), see table S2 of the appendix.

Table 1. Patient characteristics at baseline and twelve months follow-up

Variable	Total group (n=57)	Responders (n=43)	Non-responders (n=14)	p-value
Age (years)	65 ± 10	63 ± 10	71 ± 9	0.013
Gender (n, % male)	30 (53%)	20 (47%)	10 (71%)	0.132
Etiology (n, % ICMP)	13 (23%)	5 (12%)	8 (57%)	0.001
NYHA class (n, %)				
Class II	39 (68%)	30 (70%)	9 (64%)	
Class III	18 (32%)	13 (30%)	5 (36%)	0.741
Medication (n, %)				
Beta-blockers	50 (88%)	39 (91%)	11 (79%)	0.346
Diuretics	45 (79%)	35 (81%)	10 (71%)	0.463
ACE / ATII inhibitors	39 (68%)	29 (67%)	10 (71%)	1.000
Aldosteron antagonist	23 (40%)	19 (44%)	4 (29%)	0.361
Lab – creatinine value (unit)	80 (70 – 97)	78 (68 – 92)	90 (72 – 104)	0.232
Lab – BNP value (unit)	826 (379 – 1790)	846 (380 – 1778)	621 (363 – 2123)	0.934
ECG – QRS width (ms)	176 (165 – 188)	180 (168 – 194)	169 (152 – 176)	0.011
ECG – QRS morph (n, % LBBB)	45 (79%)	38 (88%)	7 (50%)	0.005
ECG – QRS area (μVs)	138 (118 – 159)	143 (126 – 168)	115 (78 – 126)	0.002
Echo – IVMD (ms)	50 ± 29	58 ± 25	24 ± 24	<0.001
Echo – apical rocking (n, %)	39 (68%)	34 (79%)	5 (36%)	0.006
CAVIAR score (points)	3 ± 3	4 ± 2	0 ± 2	<0.001
CMR – LVEDV (ml)	283 (227 - 338)	297 (231 – 380)	256 (220 – 297)	0.181
CMR – LVESV (ml)	208 (149 – 264)	232 (150 – 291)	184 (144 – 220)	0.142
CMR – LVEF (%)	28 ± 10	27 ± 10	30 ± 6	0.092
CMR – LV mass (gr)	131 (113 – 158)	133 (118 – 168)	129 (104 – 141)	0.248
CMR – Scar size (% LV mass)	1.3 (0.0 – 5.7)	0.0 (0.0 – 2.7)	5.7 (0.0 – 15.1)	0.028
CMR – RVEF (%)	50 ± 12	48 ± 13	53 ± 9	0.163
Echo – Change in LVESV after twelve months (%)	-32 ± 27	-44 ± 18	4 ± 15	<0.001

CAVIAR score, CRT-Age-Vectorcardiographic QRSAREA -IVMD-Apical Rocking score; ICMP, ischemic cardiomyopathy; 6MWT, six minute walk test; BNP brain natriuretic peptide; LBBB, left bundle branch block; IVMD, interventricular mechanical delay; LVEDV, left ventricular end-diastolic volume; LVESV, left ventricular end-systolic volume; LVEF, left ventricular ejection fraction; RVEF, right ventricular ejection fraction.

Table 2. Correlation coefficient (R) and area under the curve (AUC) of SLICE-derived strain parameters and CRT response (LVESV change after twelve months)

	Variable	R	p-value	AUC	p-value	cut-off value	sens/spec
basic strain parameters	Peak $strain_{sep}$ (%)	**-0.37**	0.004	0.73	0.004	-3.5%	44% / 100%
	Peak $strain_{lat}$ (%)	**0.33**	0.012	0.70	0.007	-12.5%	67% / 71%
	ESS_{sep} (%)	**-0.63**	<0.001	0.81	<0.001	0.3%	67% / 85%
	ESS_{lat} (%)	**0.44**	<0.001	0.73	0.006	-9.6%	70% / 64%
timing parameters	onset-delay (ms)	**0.06**	0.669	0.52	0.376	45ms	81% / 43%
	peak-delay (ms)	**-0.22**	0.098	0.51	0.438	264ms	53% / 71%
strain pattern parameters	SRS_{sep} (%)	**-0.56**	<0.001	0.80	<0.001	4.5%	81% / 79%
	$SSI_{sep-lat}$ (%)	**-0.53**	<0.001	0.82	<0.001	5.9%	79% / 71%
	$ISF_{sep-lat}$	**-0.58**	<0.001	0.82	<0.001	0.30	79% / 79%

R, correlation coefficient with LVESV change after twelve months; AUC, area under the curve; sens/spec, sensitivity/specificity; Peak strain, septal / lateral peak negative strain; ESS, septal / lateral end-systolic strain; onset-delay, septal to lateral delay in onset contraction; peak-delay, septal to lateral time difference in peak shortening; SRS_{sep}, systolic rebound stretch of the septum; $SSI_{sep-lat}$, systolic stretch index; $ISF_{sep-lat}$, internal stretch factor.

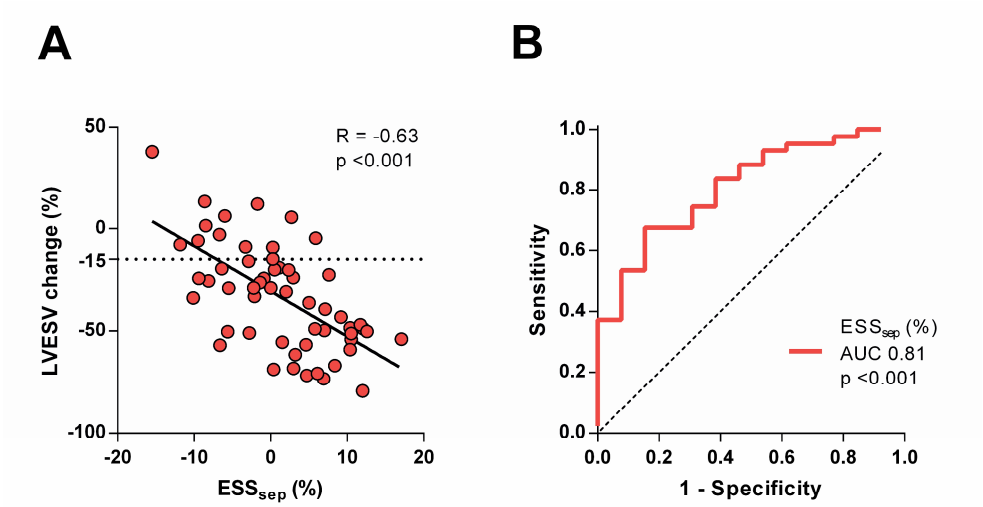


Figure 2: End-systolic septal strain and reverse remodeling after CRT. (A) The end-systolic septal strain (ESS_{sep}) parameter at baseline is strongly related with LVESV change after CRT implantation. (B) ESS_{sep} shows good predictive value for CRT response (≥ 15% LVESV reduction) as demonstrated by receiver operating characteristic (ROC) curve analysis.

Clinical parameters and CRT response

Standard CMR parameters that correlated with reverse remodeling after CRT in univariable linear regression analysis included LVEDV, LVESV, LVEF and scar size whereas LV mass and RVEF were unrelated, as demonstrated in table 3. Addition of the best performing strain parameter, ESS_{sep}, to standard CMR parameters in a multivariable model (model 1) showed ESS_{sep} to be independently related to LVESV change whereas other CMR parameters were not, although there was a trend towards significance for scar size (p=0.057). Clinical parameters that were associated with CRT response included age, gender, etiology, QRS duration and QRS morphology whereas NYHA class and renal function were unrelated. In a multivariable model with clinical determinants (model 2), ESS_{sep} showed to be independently related to LVESV change together with age. The CAVIAR score parameters age, QRS_{AREA}, IVMD, and apical rocking, were all significantly associated with CRT response. Addition of ESS_{sep} to CAVIAR (model 3), showed ESS_{sep} to be independently related to LVESV change together with age and QRS_{AREA}.

Table 3. Linear regression analysis

	Univariable analysis			Model 1		
CMR parameters / ESS_{sep}	**beta**	**95% CI**	**p-value**	**beta**	**95% CI**	**p-value**
CMR – LVEDV (per ml)	-0.08	-0.15 – -0.01	0.028	0.38	-0.14 – 0.90	0.154
CMR – LVESV (per ml)	-0.09	-0.17 – -0.02	0.012	-0.50	-1.16 – 0.17	0.146
CMR – LVEF (per %)	0.79	0.08 – 1.51	0.029	-0.94	-2.96 – 1.08	0.362
CMR – LV mass (per gr)	-0.13	-0.28 – 0.02	0.095	-	-	-
CMR – Scar size (per % LV mass)	2.22	1.21 – 3.23	<0.001	1.11	-0.03 – 2.24	0.057
CMR – RVEF (per %)	0.24	-0.35 – 0.84	0.424	-	-	-
CMR – ESS_{sep} (per %)	**-2.20**	**-2.94 – -1.47**	**<0.001**	**-1.26**	**-2.20 – -0.31**	**0.009**
Clinical parameters / ESS_{sep}				**Model 2**		
Age (per year)	**1.06**	**0.43 – 1.70**	**0.001**	**0.68**	**0.17 – 1.20**	**0.009**
Gender (male)	17.3	3.94 – 30.67	0.011	-1.24	-12.63 – 10.16	0.831
Etiology (ICMP)	30.89	16.19 – 45.58	<0.001	12.2	-1.68 – 26.08	0.085
NYHA class (per class)	10.68	-4.22 – 25.59	0.160	-	-	-
Lab – creatinine (per unit)	0.14	-0.08 – 0.35	0.208	-	-	-
ECG – QRS width (per ms)	-0.29	-0.55 – -0.02	0.033	-0.08	-0.30 – 0.14	0.481
ECG – QRS morph (LBBB)	-29.12	-44.62 – -13.63	<0.001	-9.58	-23.80 – 4.63	0.186
CMR – ESS_{sep} (per %)	**-2.20**	**-2.94 – -1.47**	**<0.001**	**-1.32**	**-2.18 – -0.47**	**0.002**
CAVIAR score / ESS_{sep}				**Model 3**		
Age (per year)	**1.06**	**0.43 – 1.70**	**0.001**	**0.63**	**0.14 – 1.13**	**0.013**
ECG – QRS area (per µVs)	**-0.32**	**-0.45 – -0.19**	**<0.001**	**-0.18**	**-0.30 – -0.05**	**0.005**
Echo – IVMD (per ms)	-0.52	-0.73 – -0.31	<0.001	-0.12	-0.35 – 0.10	0.288
Echo – apical rocking	-26.08	-39.59 – -12.56	<0.001	-2.66	-15.56 – 10.25	0.687
CMR – ESS_{sep} (per %)	**-2.20**	**-2.94 – -1.47**	**<0.001**	**-1.51**	**-2.35 – -0.67**	**<0.001**

LVEDV, left ventricular end-diastolic volume; LVESV, left ventricular end-systolic volume; LVEF, left ventricular ejection fraction; RVEF, right ventricular ejection fraction; ESS_{sep}, end-systolic septal strain; ICMP, ischemic cardiomyopathy; CAVIAR score, CRT-Age-Vectorcardiographic QRS_{AREA} -IVMD-Apical Rocking score; IVMD, interventricular mechanical delay.

DISCUSSION

This study is the first to demonstrate predictive value of the novel SLICE strain technique for functional LV recovery after CRT implantation. Various SLICE strain parameters showed to be closely related with CRT response after one year. When comparing different types of strain parameters, strain pattern- rather than timing variables correlated with CRT response. Of all strain parameters, end-systolic septal strain demonstrated the strongest correlation with LV reverse remodeling after one year. Moreover, multivariable regression analysis showed end-systolic septal strain to be additive to clinical (age) and electrical (QRS_{AREA}) parameters in estimating potential benefit from CRT.

Comparison of strain parameters

In patients with LBBB, slow cell-to-cell LV conduction results in a time-difference of electrical activation between the septal and lateral wall. Although SLICE analysis revealed mechanical contraction always to be delayed in the lateral wall relative to the septal wall, absolute time delays between the septal and lateral wall (onset-delay and peak-delay) were unrelated to the amount of echocardiographic response after CRT. These findings are in agreement with those of the predictors of response to cardiac resynchronization therapy (PROSPECT) trial, showing disappointing results of timing (i.e. dyssynchrony) parameters.(13) More recent studies suggest strain pattern- (i.e. discoordination) rather than timing parameters to be related to CRT response.(3,4,6) In contrast to timing parameters, strain pattern parameters incorporate regional function as well by measuring myocardial contraction and stretching in percentage strain units. More specifically, they measure the percentage stretching of the septum during systole (SRS_{sep}), or the percentage stretching of both the septal and lateral wall ($SSI_{sep\text{-}lat}$), or index the total amount of stretching relative to the total amount of shortening in both regions ($ISF_{sep\text{-}lat}$). Our results are in line with previous findings, (3,4,6) as each strain pattern parameter correlated with reverse remodeling after CRT and accurately predicted response to CRT (table 2).

Septal strain analysis

During LBBB, systolic stretching is most profound in early-activated (i.e. septal) segments whereas contractile function is increased in late-activated (i.e. lateral wall) regions, resulting in an imbalanced septal-to-lateral work load ratio.(14-16) CRT subsequently recruits myocardial work from the septum, leading to a homogenized work distribution and improving cardiac pump efficiency.(15-18) In the present study, we found end-systolic septal strain (ESS_{sep}) to be strongest related with reverse remodeling after CRT (R -0.63), illustrated in figure 2. This basic strain parameter reflects net septum length change throughout systole. Previously, we performed a systematic comparison of strain parameters using multiple strain imaging techniques (CMR-TAG; CMR-FT; STE) and found ESS_{sep} to be the best performing strain parameter in the prediction of CRT outcome irrespective of imaging technique.(19) The present study adds to the accumulating evidence that discoordination of the septum (measured by ESS_{sep}) forms the mechanical substrate for functional LV improvement during electrical resynchronization. Septal strain varied widely between patients with ESS_{sep} ranging between -15.5% (shortening) and 17.1% (stretching). These large differences in strain can be easily detected by SLICE and require septal analysis in only two (end-diastolic and end-systolic) frames (figure 1A). Time duration of the specific SLICE-ESS_{sep} measurement was only 12±2 minutes. Previously, our validation study showed high agreement of SLICE-ESS_{sep} with gold standard CMR tagging (ICC 0.76) with excellent intra-observer reproducibility (ICC 0.94) and good inter-observer reproducibility (ICC: 0.86).(9) Accuracy and reproducibility of SLICE-ESS_{sep} was higher compared to other strain parameters, presumably because of the wide spread in strain values ranging from strongly negative to strongly positive numbers. ROC curve analysis in the present study revealed an optimal cut-off value to predict CRT response around zero (0.3) percent. Patients with septal stretching rather than shortening during systole (positive numbers indicate stretching) are highly inefficient at baseline and leave more room for improvement in contractile function after CRT. These patients showed a three-fold larger reduction in LVESV compared to patients with preserved septal contraction. Alternatively, septal behavior can be evaluated in a subjective manner by the visual classification of septal strain curves to a pre-described pattern. Patients with a typical LBBB (i.e. LBBB-1 or LBBB-2) pattern demonstrated larger reductions in LVESV compared to patients with a pseudo-

normal (i.e. LBBB-3) which is in line with previous studies.(5,8,20) However, calculation of quantitative strain parameters may be preferable as they are less dependent on the observer's interpretation compared to the subjective classification of septal strain patterns.

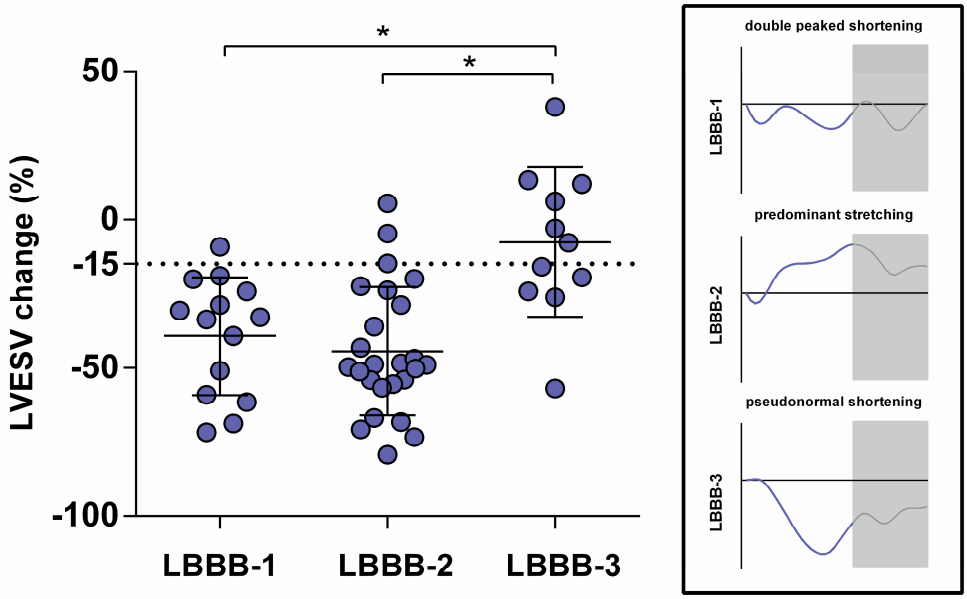


Figure 3: Visual classification of septal strain patterns to estimate CRT response. Septal strain patterns are classified to pre-specified categories: double peaked shortening (LBBB-1), predominant stretching (LBBB-2) or pseudonormal shortening (LBBB-3). Statistical differences between LBBB categories are marked with an asterisk.

The role of SLICE strain analysis in clinical practice

Firstly, the role of SLICE was investigated with respect to other CMR parameters to determine its value on top of standard information provided by CMR examination (table 3). Addition of ESS_{sep} to a model with other CMR predictors (LV dimensions, function, and scar size) showed ESS_{sep} to be the only parameter independently related to LVESV change, although there was a trend towards significance for scar size (p=0.057). In clinical practice, the role of CMR is of interest as it offers accurate LVEF measurement combined with LGE imaging to guide LV lead placement in CRT candidates.(21-25) Our results indicate that additional SLICE analysis of the septum could potentially improve diagnostic yield of CMR in CRT candidates. Clinical predictors of CRT response included age, gender, etiology, QRS width and QRS morphology (see figure 4), all considered

to be traditional determinants of CRT response.(1,26) In multivariable analysis, ESS_{sep} showed predictive value on top of clinical parameters. The additional value of SLICE may be of particular interest in CRT candidates with unfavorable patient characteristics (non-strict LBBB morphology, shorter QRSd), in whom benefit from CRT is doubted. This is demonstrated by two examples in figure 5. Lastly, the value of SLICE was evaluated with respect to a specially designed prediction model in the MARC main study. The CAVIAR response score incorporates age, QRS_{AREA} derived by vector-loop ECG analysis and two echocardiographic parameters being inter-ventricular mechanical delay (IVMD) and detection of apical rocking.(10) Addition of ESS_{sep} to CAVIAR in multivariable analysis showed ESS_{sep} to be an independent predictor of response together with age and QRS_{AREA}, whereas echocardiographic parameters (IVMD; apical rocking) were expelled from the model. These findings indicate that response to CRT is multifactorial,(2) and that combining clinical information (age) together with electrocardiographic (QRS_{AREA}) and mechanical information (SLICE-ESS_{sep}) could potentially improve patient selection for CRT. As QRS_{AREA} can be measured from a standard 12-lead ECG and SLICE-ESS_{sep} from standard CMR cine images, the work-up of CRT candidates is feasible in clinical practice.

Limitations

Some limitations need to be addressed. First, this sub-study of the MARC involves a subset of patients who underwent additional CMR examination in three of the participating hospitals. Although patient characteristics were comparable with the overall MARC population, this may have introduced some selection bias. Secondly, CMR feature tracking (CMR-FT) post-processing software is now commercially available and offers automated strain analysis on standard CMR cine images. Nevertheless, CMR-FT has several downsides as it requires the purchase of commercial software and the user is not able to track and trace the analysis steps. SLICE, on the other hand, can be performed without the use of specialized software tools. Thirdly, strain parameters that require SLICE analysis of the entire strain curve may take a long processing time (up to 60 minutes). Measuring the specific ESS_{sep} parameter, however, requires only two SLICE measurements and can be performed in around twelve minutes. Lastly, the SLICE analysis could be standardized by implementing radial taglines to standard cine imaging (figure S1, appendix).

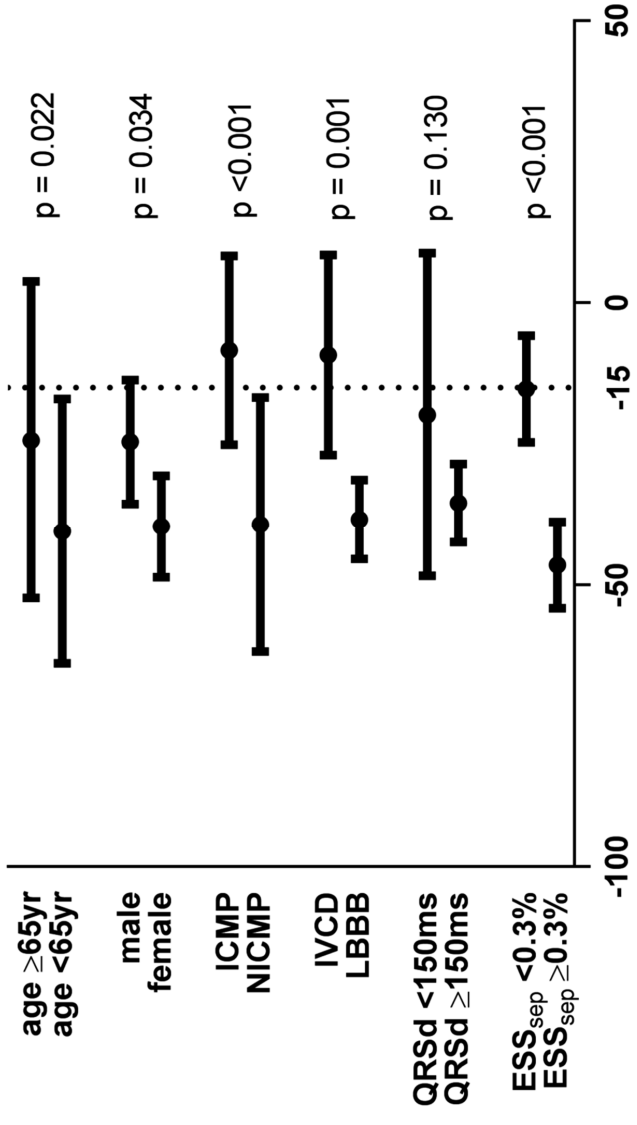


Figure 4: Clinical factors and ESS_{sep} influencing the likelihood of response to CRT. The magnitude of benefit from CRT is demonstrated for different subgroups divided by age; gender; etiology; QRS morphology; QRSd; and ESS_{sep}. Compared to clinical factors, SLICE- ESS_{sep} demonstrates relatively large discriminative power.

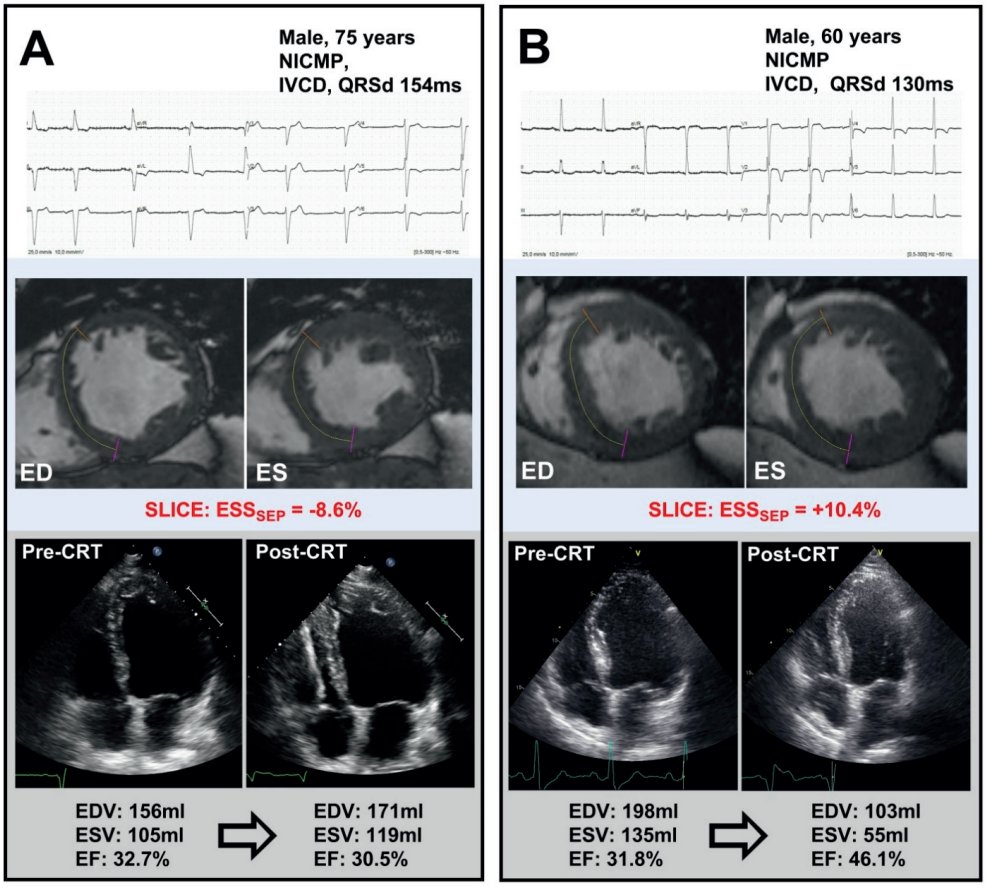


Figure 5: Two typical examples demonstrating the additional value of SLICE strain analysis in clinical practice. (A) Typical example of a grey-zone CRT candidate with mixed favorable (NICMP; QRSd ≥150ms), and unfavorable (male; age ≥65 years; IVCD) characteristics. SLICE analysis reveals a strongly negative ESS_{sep} and the patient shows no LV pump function improvement after CRT implantation. (B) Another patient with mixed favorable (NICMP; age <65 years), and unfavorable (male; IVCD; QRSd <150ms) characteristics. This patient, however, demonstrates a strongly positive ESS_{sep} and became a CRT super-responder.

CONCLUSION

The practicable SLICE strain technique helps the clinician to estimate potential benefit from CRT by analyzing standard CMR cine images without the need for commercial software. Of all strain parameters, end-systolic septal strain (ESS_{sep}) demonstrated the strongest correlation with reverse remodeling after CRT. This parameter can be measured in around twelve minutes, and is additive to clinical (age) and electrical (QRS_{AREA}) parameters in estimating potential benefit from CRT.

REFERENCES

1. Brignole M, Auricchio A, Baron-Esquivias G, Bordachar P, Boriani G, Breithardt OA, Cleland J, Deharo JC, Delgado V, Elliott PM, Gorenek B, Israel CW, Leclercq C, Linde C, Mont L, Padeletti L, Sutton R and Vardas PE. 2013 ESC guidelines on cardiac pacing and cardiac resynchronization therapy: the task force on cardiac pacing and resynchronization therapy of the European Society of Cardiology (ESC). Developed in collaboration with the European Heart Rhythm Association (EHRA). Europace. 2013;15:1070-1118.
2. Daubert C, Behar N, Martins RP, Mabo P and Leclercq C. Avoiding non-responders to cardiac resynchronization therapy: a practical guide. Eur Heart J. 2017;14;38(19):1463-1472.
3. De Boeck BWL, Teske AJ, Meine M, Leenders GE, Cramer MJ, Prinzen FW and Doevendans PA. Septal rebound stretch reflects the functional substrate to cardiac resynchronization therapy and predicts volumetric and neurohormonal response. European Journal of Heart Failure. 2009;11:863-871.
4. Kirn B, Jansen A, Bracke F, van Gelder B, Arts T and Prinzen FW. Mechanical discoordination rather than dyssynchrony predicts reverse remodeling upon cardiac resynchronization. American Journal of Physiology-Heart and Circulatory Physiology. 2008;295:H640-H646.
5. Leenders GE, Lumens J, Cramer MJ, De Boeck BW, Doevendans PA, Delhaas T and Prinzen FW. Septal deformation patterns delineate mechanical dyssynchrony and regional differences in contractility: analysis of patient data using a computer model. Circ Heart Fail. 2012;5:87-96.
6. Lumens J, Tayal B, Walmsley J, Delgado-Montero A, Huntjens PR, Schwartzman D, Althouse AD, Delhaas T, Prinzen FW and Gorcsan J, III. Differentiating Electromechanical From Non-Electrical Substrates of Mechanical Discoordination to Identify Responders to Cardiac Resynchronization Therapy. Circ Cardiovasc Imaging. 2015;8:e003744.
7. van Everdingen WM, Zweerink A, Nijveldt R, Salden OAE, Meine M, Maass AH, Vernooy K, De Lange FJ, van Rossum AC, Croisille P, Clarysse P, Geelhoed B, Rienstra M, Van Gelder IC, Vos MA, Allaart CP and Cramer MJ. Comparison of strain imaging techniques in CRT candidates: CMR tagging, CMR feature tracking and speckle tracking echocardiography. Int J Cardiovasc Imaging. 2018;34:443-456.
8. Risum N, Tayal B, Hansen TF, Bruun NE, Jensen MT, Lauridsen TK, Saba S, Kisslo J, Gorcsan J, III and Sogaard P. Identification of Typical Left Bundle Branch Block Contraction by Strain Echocardiography Is Additive to Electrocardiography in Prediction of Long-Term Outcome After Cardiac Resynchronization Therapy. J Am Coll Cardiol. 2015;66:631-641.
9. Zweerink A, Allaart CP, Kuijer JPA, Wu L, Beek AM, van de Ven PM, Meine M, Croisille P, Clarysse P, van Rossum AC and Nijveldt R. Strain analysis in CRT candidates using the novel segment length in cine (SLICE) post-processing technique on standard CMR cine images. Eur Radiol. 2017;27:5158-5168.

10. Maass AH, Vernooy K, Wijers SC, van 't Sant J, Cramer MJ, Meine M, Allaart CP, De Lange FJ, Prinzen FW, Gerritse B, Erdtsieck E, Scheerder COS, Hill MRS, Scholten M, Kloosterman M, Ter Horst IAH, Voors AA, Vos MA, Rienstra M and Van Gelder IC. Refining success of cardiac resynchronization therapy using a simple score predicting the amount of reverse ventricular remodelling: results from the Markers and Response to CRT (MARC) study. Europace. 2018;20:e1-e10.
11. Flett AS, Hasleton J, Cook C, Hausenloy D, Quarta G, Ariti C, Muthurangu V and Moon JC. Evaluation of techniques for the quantification of myocardial scar of differing etiology using cardiac magnetic resonance. JACC Cardiovasc Imaging. 2011;4:150-156.
12. Szulik M, Tillekaerts M, Vangeel V, Ganame J, Willems R, Lenarczyk R, Rademakers F, Kalarus Z, Kukulski T and Voigt JU. Assessment of apical rocking: a new, integrative approach for selection of candidates for cardiac resynchronization therapy. Eur J Echocardiogr. 2010;11:863-9.
13. Chung ES, Leon AR, Tavazzi L, Sun JP, Nihoyannopoulos P, Merlino J, Abraham WT, Ghio S, Leclercq C, Bax JJ, Yu CM, Gorcsan J, III, St John SM, De SJ and Murillo J. Results of the Predictors of Response to CRT (PROSPECT) trial. Circulation. 2008;117:2608-2616.
14. Zweerink A, de Roest GJ, Wu L, Nijveldt R, de Cock CC, van Rossum AC and Allaart CP. Prediction of Acute Response to Cardiac Resynchronization Therapy by Means of the Misbalance in Regional Left Ventricular Myocardial Work. J Card Fail. 2016;22:133-42.
15. Prinzen FW, Vernooy K, De Boeck BW and Delhaas T. Mechano-energetics of the asynchronous and resynchronized heart. Heart Fail Rev. 2011;16:215-224.
16. Russell K, Eriksen M, Aaberge L, Wilhelmsen N, Skulstad H, Gjesdal O, Edvardsen T and Smiseth OA. Assessment of wasted myocardial work: a novel method to quantify energy loss due to uncoordinated left ventricular contractions. Am J Physiol Heart Circ Physiol. 2013;305:H996-1003.
17. Cvijic M, Duchenne J, Unlu S, Michalski B, Aarones M, Winter S, Aakhus S, Fehske W, Stankovic I and Voigt JU. Timing of myocardial shortening determines left ventricular regional myocardial work and regional remodelling in hearts with conduction delays. Eur Heart J Cardiovasc Imaging. 2018;19:941-949.
18. Vernooy K, Cornelussen RN, Verbeek XA, Vanagt WY, van Hunnik A, Kuiper M, Arts T, Crijns HJ and Prinzen FW. Cardiac resynchronization therapy cures dyssynchronopathy in canine left bundle-branch block hearts. Eur Heart J. 2007;28:2148-55.
19. Zweerink A, van Everdingen WM, Nijveldt R, Salden OAE, Meine M, Maass AH, Vernooy K, de Lange FJ, Vos MA, Croisille P, Clarysse P, Geelhoed B, Rienstra M, van Gelder IC, van Rossum AC, Cramer MJ and Allaart CP. Strain imaging to predict response to cardiac resynchronization therapy: a systematic comparison of strain parameters using multiple imaging techniques. ESC Heart Fail. 2018.
20. Jackson T, Sohal M, Chen Z, Child N, Sammut E, Behar J, Claridge S, Carr-White G, Razavi R and Rinaldi CA. A U-shaped type II contraction pattern in patients with strict left bundle branch block predicts super-response to cardiac resynchronization therapy. Heart Rhythm. 2014;11:1790-1797.
21. Bertini M, Mele D, Malagu M, Fiorencis A, Toselli T, Casadei F, Cannizzaro T, Fragale C, Fucili A, Campagnolo E, Benea G and Ferrari R. Cardiac resynchronization therapy guided by multimodality cardiac imaging. Eur J Heart Fail. 2016;18:1375-1382.

22. Sommer A, Kronborg MB, Norgaard BL, Poulsen SH, Bouchelouche K, Bottcher M, Jensen HK, Jensen JM, Kristensen J, Gerdes C, Mortensen PT and Nielsen JC. Multimodality imaging-guided left ventricular lead placement in cardiac resynchronization therapy: a randomized controlled trial. Eur J Heart Fail. 2016;18:1365-1374.
23. Bilchick KC, Dimaano V, Wu KC, Helm RH, Weiss RG, Lima JA, Berger RD, Tomaselli GF, Bluemke DA, Halperin HR, Abraham T, Kass DA and Lardo AC. Cardiac Magnetic Resonance Assessment of Dyssynchrony and Myocardial Scar Predicts Function Class Improvement Following Cardiac Resynchronization Therapy. JACC: Cardiovascular Imaging. 2008;1:561-568.
24. Leyva F. The Role of Cardiovascular Magnetic Resonance in Cardiac Resynchronization Therapy. Heart Fail Clin. 2017;13:63-77.
25. Romano S, Judd RM, Kim RJ, Kim HW, Klem I, Heitner JF, Shah DJ, Jue J, White BE, Indorkar R, Shenoy C and Farzaneh-Far A. Feature-Tracking Global Longitudinal Strain Predicts Death in a Multicenter Population of Patients With Ischemic and Nonischemic Dilated Cardiomyopathy Incremental to Ejection Fraction and Late Gadolinium Enhancement. JACC Cardiovasc Imaging. 2018;11:1419-1429.
26. Hsu JC, Solomon SD, Bourgoun M, McNitt S, Goldenberg I, Klein H, Moss AJ, Foster E and Committee M-CE. Predictors of super-response to cardiac resynchronization therapy and associated improvement in clinical outcome: the MADIT-CRT (multicenter automatic defibrillator implantation trial with cardiac resynchronization therapy) study. J Am Coll Cardiol. 2012;59:2366-73.

SUPPLEMENTAL MATERIAL

Table S1. Comparison of SLICE-derived strain parameters between CRT responders and non-responders

	Variable	Total group (n=57)	Responders (n=43)	Non-responders (n=14)	p-value
basic strain parameters	Peak $strain_{sep}$ (%)	-5.4 (-8.6 – -2.9)	-4.7 (-7.9 – -2.5)	-7.8 (-12.8 – -5.0)	0.011
	Peak $strain_{lat}$ (%)	-13.6 ± 4.8	-14.5 ± 4.6	-10.8 ± 4.4	0.013
	ESS_{sep} (%)	1.3 ± 7.3	3.1 ± 6.7	-4.8 ± 6.1	<0.001
	ESS_{lat} (%)	-11.8 ± 5.5	-13.0 ± 5.1	-8.4 ± 5.5	0.012
timing parameters	onset-delay (ms)	73 ± 42	74 ± 38	70 ± 53	0.794
	peak-delay (ms)	249 (127 – 348)	268 (124 – 351)	201 (139 – 285)	0.889
strain pattern parameters	SRS_{sep} (%)	7.0 (2.5 – 12.1)	7.5 (5.2 – 13.0)	2.0 (1.3 – 4.0)	<0.001
	$SSI_{sep-lat}$ (%)	8.6 (5.1 – 14.8)	12.1 (6.8 – 15.2)	3.2 (2.0 – 7.5)	<0.001
	$ISF_{sep-lat}$	0.48 ± 0.29	0.56 ± 0.27	0.25 ± 0.19	<0.001
visual classification	septal pattern: LBBB1 LBBB2 LBBB3	 14 (25%) 25 (44%) 18 (32%)	 13 (30%) 22 (51%) 8 (19%)	 1 (7%) 3 (21%) 10 (71%)	 0.001

Peak strain, septal / lateral peak negative strain; ESS, septal / lateral end-systolic strain; onset-delay, septal to lateral delay in onset contraction; peak-delay, septal to lateral time difference in peak shortening; SRS_{sep}, systolic rebound stretch of the septum; $SSI_{sep-lat}$, systolic stretch index; $ISF_{sep-lat}$, internal stretch factor; LBBB-1, double peaked shortening; LBBB-2, initial shortening followed by predominant stretching; LBBB-3, pseudonormal shortening.

Table S2. Septal strain patterns and volumetric response (LVESV change after 12 months)

N = 57	LVESV change (%)	Response rate (n, %)
LBBB-1	-39 ± 20* n=14	13 (93%)
LBBB-2	-44 ± 22† n=25	22 (88%)
LBBB-3	-10 ± 25*† n=18	8 (44%)

LBBB-1, double peaked shortening and LBBB-2, predominant stretching represent abnormal septal strain patterns. The LBBB-3 pattern represents pseudonormal shortening of the septum. Statistical differences between LBBB categories per imaging modality are marked with: * pattern 1 vs. 3, † pattern 2 vs. 3.

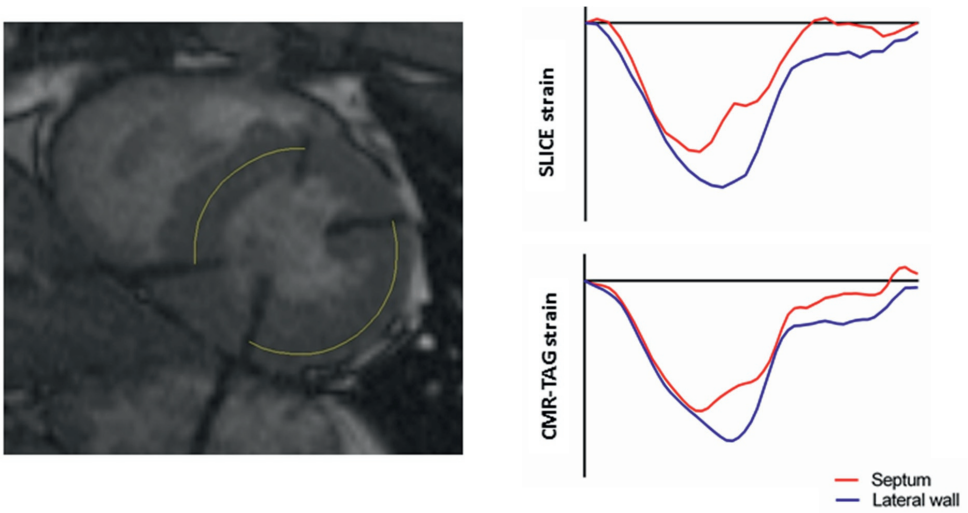


Figure S1: Modification of the SLICE technique by implementing radial taglines. Two radially oriented taglines are placed at end-diastole to form the reference points for each segment throughout the cardiac cycle. In future studies, contour tracing of these cine images could enable LV function assessment combined with fully automated SLICE strain analysis

Chapter 9

Septal Mechanics by Segment Length in Cine (SLICE) Strain Analysis Predicts Clinical Outcome After Cardiac Resynchronization Therapy

Submitted

Alwin Zweerink
Daniel J. Friedman
Igor Klem
Peter M. van de Ven
Caitlin Vink
P. Stefan Biesbroek
Steen M. Hansen
Raymond J. Kim
Albert C. van Rossum
Brett D. Atwater
Cornelis P. Allaart
Robin Nijveldt

ABSTRACT

Background**:** Previously we demonstrated that the novel segment length in cine (SLICE) strain technique on standard cardiac magnetic resonance (CMR) cine images provides accurate strain measurements, with end-systolic septal strain (ESS_{sep}) as robust predictor of cardiac resynchronization therapy (CRT) response on echocardiography.

Objectives**:** To evaluate the value of SLICE-ESS_{sep} for prediction of clinical outcome after CRT.

Methods**:** Two-hundred-eighteen patients (NYHA classes II to IV; left ventricular (LV) ejection fraction ≤35%; QRS duration ≥120ms) who underwent CMR imaging including late gadolinium enhancement (LGE) prior to CRT implantation were enrolled in this two-center study. SLICE-ESS_{sep} was manually measured on standard CMR cine imaging. The primary endpoint was a combined endpoint of death, LV assist device or heart transplantation. Secondary endpoints were appropriate implantable cardioverter defibrillator (ICD) therapy and heart failure (HF) hospitalization.

Results**:** Two-thirds of patients (65%) had a positive ESS_{sep} ≥0.9% (i.e. systolic stretching of the septum). During a median follow-up of 3.8 years, 66 (30%) patients reached the primary endpoint. Patients with positive ESS_{sep} were less likely to reach the primary endpoint (HR 0.36; $p<0.001$) and HF hospitalization (HR 0.41; $p=0.019$) compared to ESS_{sep} negative patients, although rates of ICD therapy were comparable (HR 0.66; $p=0.272$). In a multivariable model, age, renal function, LV end-diastolic volume, ESS_{sep} and septal scar provided incremental prognostic information on current guideline criteria.

Conclusions**:** SLICE strain analysis on the standard CMR cine images provides important prognostic information in CRT candidates. Systolic stretching of the septum (i.e. positive ESS_{sep}) was independently related with lower risk of death and HF events after CRT.

INTRODUCTION

Myocardial strain imaging provides information on cardiac mechanics and can reveal regional deformation abnormalities during left bundle branch block (LBBB). In true LBBB, a typical pattern is observed where the late-activated lateral wall pushes the septum back during systole (discoordination), resulting in reduced left ventricular (LV) pumping efficiency.(1) Cardiac resynchronization therapy (CRT) aims to restore LV pump function by re-coordinating contraction of LV regions. Approximately one-third of the patients meeting ACCF/AHA/HRS class I or IIa guidelines for CRT implantation obtain no benefit or demonstrate worsening heart failure (non-responder).(2,3) Myocardial strain imaging could potentially improve patient selection for CRT through improved identification of dyssynchronous mechanical substrate. Multiple imaging techniques are presently available for measuring strain including cardiac magnetic resonance (CMR) tagging, CMR feature tracking and speckle tracking echocardiography, however these require additional image acquisition and/or specialized post-processing software tools. The novel segment length in cine (SLICE) post-processing technique can be performed on the standard CMR cine images without the need for specialized software tools and has been validated compared to myocardial tagging.(4) Furthermore, SLICE showed excellent intra-observer reproducibility and good inter-observer reproducibility for measuring regional strains. Prior work demonstrated that the end-systolic septal strain (ESS_{sep}) SLICE parameter demonstrates a strong relationship with the likelihood of reverse remodeling after CRT. The present study aims to evaluate predictive value of SLICE-ESS_{sep} for clinical outcome after CRT implantation in a large patient cohort.

METHODS

Study population

Patients who underwent CMR examination within twelve months prior to CRT implantation between 2005 and 2017 were retrospectively included in this two-center study (Amsterdam University Medical Center, location Vrije Universiteit Amsterdam, the Netherlands; Duke University Medical Center, Durham, North Carolina, USA). Inclusion criteria were NYHA class II-IV heart failure symptoms, LV ejection fraction (LVEF) ≤35% measured by CMR, QRS duration (QRSd)

≥120ms (strict LBBB or non-strict LBBB defined as intraventricular conduction delay (IVCD)) and available CMR late gadolinium enhancement (LGE) images. The presence of strict LBBB morphology was assessed by the Strauss criteria.(5) Included patients who did not meet Strauss criteria were classified as IVCD. Exclusion criteria were age under 18 years, right bundle branch block and upgrade procedures from other implanted non-CRT devices. Clinical data were collected from medical records. The primary endpoint was a combined endpoint of all-cause mortality, left ventricular assist device (LVAD) or heart transplantation (HTx). All-cause mortality data were retrieved from the municipal civil registry or the Social Security Death Index. All patients were included for the primary endpoint analysis. Secondary endpoints included (i) appropriate implantable cardioverter defibrillator (ICD) therapy and (ii) heart failure hospitalization. Appropriate ICD therapy was defined as anti-tachycardia pacing (ATP) or defibrillation shock to terminate ventricular arrhythmias. All patients implanted with a CRT device equipped with ICD function (CRT-D) who routinely underwent device interrogation with regular intervals of six months were included for this specific endpoint. Heart failure hospitalization was defined as unplanned admission to the hospital for worsening heart failure. All patients who received outpatient follow-up with regular intervals of six months were included for this specific endpoint. The local medical ethics committee of the Amsterdam University Medical Center, location Vrije Universiteit Amsterdam and Duke University Medical Center approved the study protocol. The investigation conforms to the principles outlined in the Declaration of Helsinki.

Image acquisition: CMR imaging

Patients underwent CMR examination at Amsterdam University Medical Center, location Vrije Universiteit (Amsterdam, the Netherlands) or at Duke Cardiovascular Magnetic Resonance Center (Durham, North Carolina, USA), on a clinical 1.5 Tesla MR scanner (Magnetom Sonata/Avanto, Siemens, Erlangen, Germany) with dedicated phased array cardiac receiver coil. Standard CMR cine images were acquired using a retrospectively ECG-gated balanced steady-state free-precession (SSFP) sequence during end-expiratory breath holding. A stack of 8-12 consecutive short-axis cine images was acquired covering the full LV. Typical imaging parameters were: slice thickness 5mm, slice gap 5mm, voxel size

1.3*1.6mm and temporal resolution <50ms. Subsequently, LV volumes and function were quantified as LV end-diastolic volume (LVEDV), LV end-systolic volume (LVESV) and LVEF derived from the short-axis images using commercially available software on locally available workstations. Myocardial scar territory was assessed by LGE imaging, and infarct size was measured using the full width at half maximum method using dedicated offline software (QMassMR version 7.6, Medis, Leiden, The Netherlands).(6) Septal scar localization and transmurality was measured as the maximal percentage hyperenhancement of the LV wall thickness in the basal- and mid-LV level of the anteroseptal and inferoseptal segments. Posterolateral scar was similarly measured at the basal- and mid-LV level of the posterolateral segments. Patients were classified as having ischemic cardiomyopathy (ICM) in case of a history of myocardial infarction, percutaneous coronary intervention (PCI), or coronary artery bypass grafting (CABG) accompanied by associated findings on LGE-CMR.

Post-processing: SLICE analysis

A detailed description of the SLICE post-processing steps has been published previously.(4) In brief, the mid-LV slice position with short-axis cine images was selected (QMassMR version 7.6, Medis, Leiden, The Netherlands), and two endocardial anatomic landmarks (trabeculae) near the right ventricular insertion points delimiting the septum were chosen in the end-diastolic (ED) and end-systolic (ES) frames. Marks were placed perpendicular to the myocardium in each frame. Typically, ED involved the first image after R-wave triggering and ES was assessed in the three-chamber view by aortic valve closure. Subsequently, marked cine images were exported to ImageJ to measure segment length between the marks over the myocardium midline in each phase. ESS_{sep} was then calculated in % units by: [(ES septum length – ED septum length) / ED septum length] * 100 where negative numbers indicate shortening and positive numbers indicate stretching. A typical example of SLICE analysis in a patient with LBBB is illustrated in figure 1.

ESS_{sep} = (ES septum length – ED septum length) / ED septum length * 100

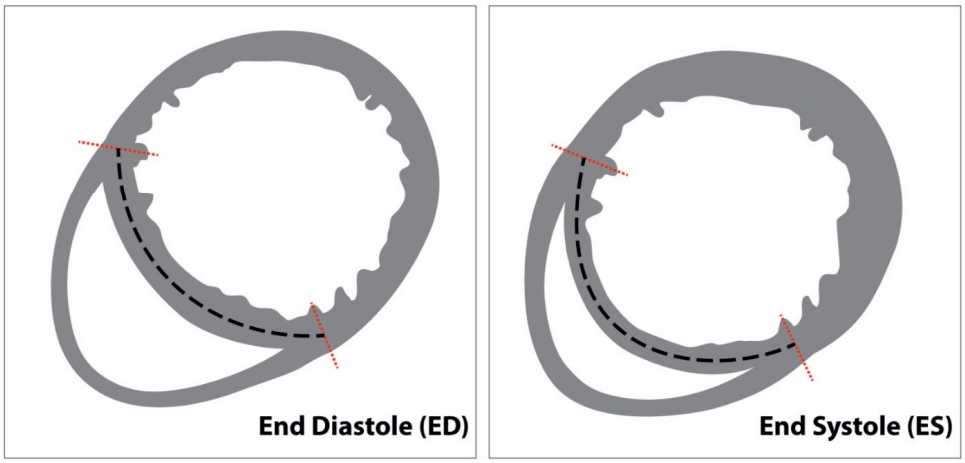


Figure 1: SLICE analysis technique. Typical example of SLICE analysis in a patient with LBBB. First, endocardial anatomic landmarks near the right ventricular insertion points delimiting the septum are identified (red dotted lines). Secondly, segment length of the septum is measured between the marks over the myocardium midline (black dotted lines). End-diastolic segment length was 412 pixels and end-systolic segment length was 474 pixels. Subsequently, end-systolic septum strain (ESS_{sep}) was calculated by: [(474 – 412) / 412] * 100 = 15% indicating systolic stretching of the septum (i.e. ESS_{sep} positive patient).

Statistics

The commercially available Statistical Package for Social Sciences software (IBM SPSS Statistics for Windows, Version 20.0. Armonk, NY, USA) was used for statistical analyses. Continuous variables are expressed as mean ± standard deviation (SD) in case normally distributed or median and interquartile range otherwise. Categorical variables are presented as frequencies and percentages. The independent-samples t-test and a Mann-Whitney test were used to compare means and distributions of continuous variables between groups. Pearson's and Spearman correlations were calculated as a measure of association depending on whether distribution was normal or not. Time to occurrence of the combined endpoint was compared between groups using Kaplan-Meier analysis and a log-rank test. The association between baseline parameters and time to the combined endpoint was tested using univariable Cox regression analysis with hazard ratios (HR) as effect-size. Parameters that showed a statistically significant effect on survival in univariable analysis were

included in a multivariable analysis using a backward elimination procedure. To test the additional value of SLICE on top of standard CMR parameters, multivariable analysis was performed where SLICE was added to a model with the other CMR parameters. To test the additional value of SLICE on top of clinical parameters, multivariable analysis was performed where SLICE and other independent CMR predictors were added to a model with the clinical parameters. A P-value of <0.05 was considered statistically significant.

RESULTS

Two-hundred-eighteen patients (35% female, median age 67 years) were included. After screening a total of 372 patients who underwent a pre-implantation CMR examination, 32 patients were excluded from the present analysis based on absence of LGE imaging, 26 patients based on a LVEF >35%, 41 patients because of RBBB, 42 patients with QRSd <120ms, 9 patients who were asymptomatic (NYHA class 1), and 4 patients because of missing data. A detailed description of the patient characteristics is given in table 1. Median time between CMR examination and CRT implantation was 40 (5 – 112) days.

Predictive value of ESS_{sep} for the primary endpoint

SLICE-derived ESS_{sep} showed large variability between patients ranging between -14.9% and 19.7% (negative numbers indicate shortening and positive numbers indicate stretching). Over a median follow-up time of 3.8 (1.7 – 5.9) years, 66 (30%) patients reached the combined endpoint of all-cause mortality, LVAD or HTx. Univariable Cox regression analysis showed that ESS_{sep} was significantly associated with the primary endpoint (HR 0.89 per %; 95%CI: 0.84 – 0.93; p<0.001). ROC curve analysis revealed an optimal cut-off value of 0.9% for predicting survival free of LVAD or HTx. Two-third of patients (65%) demonstrated ESS_{sep} ≥0.9% (ESS_{sep} positive) and the remaining patients ESS_{sep} <0.9% (ESS_{sep} negative). Comparing patient characteristics between ESS_{sep} positive and negative patients, ESS_{sep} positive patients were younger, more often female, less often had atrial fibrillation or ischemic etiology, more frequently used aldosterone antagonists, had wider QRS duration and more often strict LBBB ECG morphology, and demonstrated lower LVEF and less scar burden by CMR imaging (table 1).

Table 1. Patient characteristics

Variables	Total group (n=218)	ESS_{sep} negative (n=77)	ESS_{sep} positive (n=141)	p-value
Age (years)	67 (59 – 74)	70 (60 – 77)	65 (56 – 72)	0.001
Sex (n, % female)	77 (35%)	20 (26%)	57 (40%)	0.033
NYHA class (n, %)				
Class II	65 (30%)	29 (38%)	36 (26%)	
Class III	149 (68%)	47 (61%)	102 (72%)	
Class IV	4 (2%)	1 (1%)	3 (2%)	0.167
Device				
ICD function (CRT-D) (n, %)	210 (96%)	72 (94%)	138 (98%)	0.101
Quadripolar LV lead (n, %)	45 (21%)	17 (22%)	28 (20%)	0.699
Medical history (n, %)				
Atrial fibrillation	42 (19%)	22 (29%)	20 (14%)	0.010
Diabetes Mellitus	49 (23%)	22 (29%)	27 (19%)	0.111
Ischemic etiology	69 (32%)	36 (47%)	33 (23%)	0.001
Medication (n, %)				
Beta-blockers	181 (83%)	60 (78%)	121 (86%)	0.138
Diuretics	165 (76%)	59 (77%)	106 (75%)	0.812
ACE / ATII inhibitors	191 (88%)	66 (86%)	125 (89%)	0.529
Aldosterone antagonist	87 (40%)	22 (29%)	65 (46%)	0.041
ECG				
QRS duration ≥150ms (n, %)	132 (61%)	29 (38%)	103 (73%)	<0.001
Strict LBBB (Strauss) (n, %)	145 (66%)	35 (46%)	110 (78%)	<0.001
Laboratory results				
creatinine (µmol/L)	97 (77 – 118)	97 (80 – 132)	92 (77 – 115)	0.163
CMR				
LVEDV (ml)	299 ± 94	292 ± 111	303 ± 83	0.389
LVESV (ml)	234 ± 88	227 ± 104	238 ± 77	0.360
LVEF (%)	23 ± 7	24 ± 7	22 ± 6	0.008
Scar size (% LV mass)	1.88 (0.00 – 7.93)	5.82 (1.00 – 11.69)	0.00 (0.00 – 5.17)	<0.001
Septal scar (n, %)				
No scar	127 (58%)	33 (43%)	94 (67%)	
<25% TM	64 (29%)	33 (43%)	31 (22%)	
25-50% TM	18 (8%)	9 (12%)	9 (6%)	
>50% TM	9 (4%)	2 (3%)	7 (5%)	0.002
Posterolateral scar (n, %)				
No scar	171 (78%)	49 (64%)	122 (87%)	
<25% TM	34 (16%)	18 (23%)	16 (11%)	
25-50% TM	8 (4%)	6 (8%)	2 (1%)	
>50% TM	5 (2%)	4 (5%)	1 (1%)	<0.001
SLICE ESS_{sep} (%)	2.75 ± 5.45	-2.65 ± 3.19	5.70 ± 3.97	<0.001

NYHA, New York Heart Association dyspnea class; CRT-D, cardiac resynchronization therapy with defibrillator function; LBBB, left bundle branch block; LVEDV, left ventricular end-diastolic volume; LVESV, left ventricular end-systolic volume; LVEF, left ventricular ejection fraction; TM, transmurality

Patients with a positive ESS_{sep} demonstrated a lower likelihood of death, LVAD, or HTx after CRT implantation compared to ESS_{sep} negative patients (HR 0.36; 95%CI: 0.22 – 0.59; p<0.001), illustrated in figure 2.

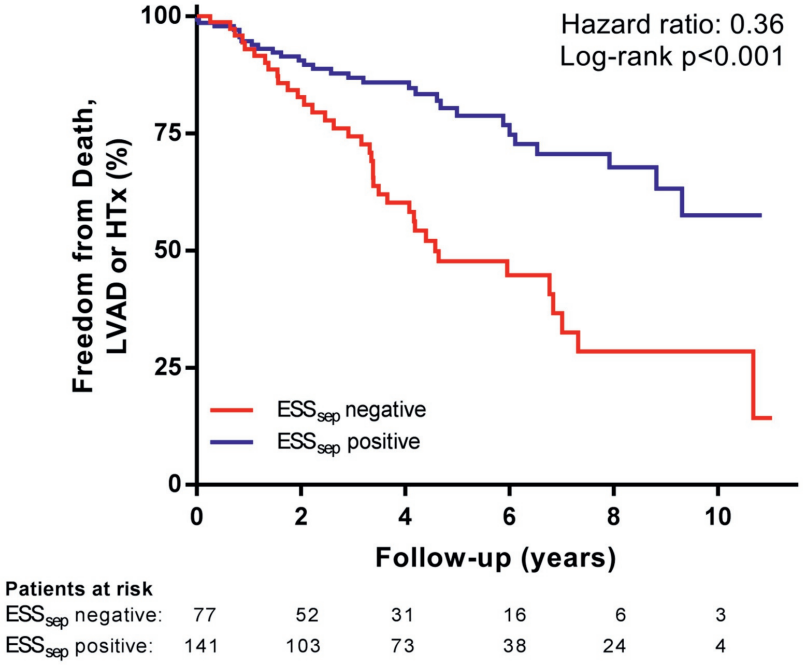


Figure 2: Kaplan-Meier curves demonstrating freedom from death, LVAD or HTx. Occurrence of the primary endpoint differed significantly between ESS_{sep} positive patients and ESS_{sep} negative patients (HR 0.36; p<0.001). Median event-free survival time was 9.3 years for SLICE-ESS_{sep} positive patients and 4.6 years for SLICE-ESS_{sep} negative patients.

Predictive value of ESSsep for the secondary endpoints

For the secondary endpoint of heart failure hospitalization, a total of 138 patients who received outpatient follow-up with regular intervals of six months were included. Over a median follow-up time of 3.2 (1.1 – 4.9) years, 28 (20%) patients were admitted to the hospital. Patients with a positive ESS_{sep} showed a longer time to HF hospitalization after CRT implantation compared to ESS_{sep} negative patients (HR 0.41; 95%CI: 0.20 – 0.87; p=0.019), illustrated in figure 3A. For the secondary endpoint of appropriate ICD therapy, a total of 177 patients implanted with a CRT-D device who routinely underwent device interrogation with regular intervals of six months were included. Over a median follow-up time

of 3.1 (1.0 – 5.4) years, 30 (17%) patients received appropriate device therapy. Freedom from ICD therapy, however, did not differ between groups (HR 0.66; 95%CI: 0.31 – 1.39; p=0.272) as illustrated in figure 3B.

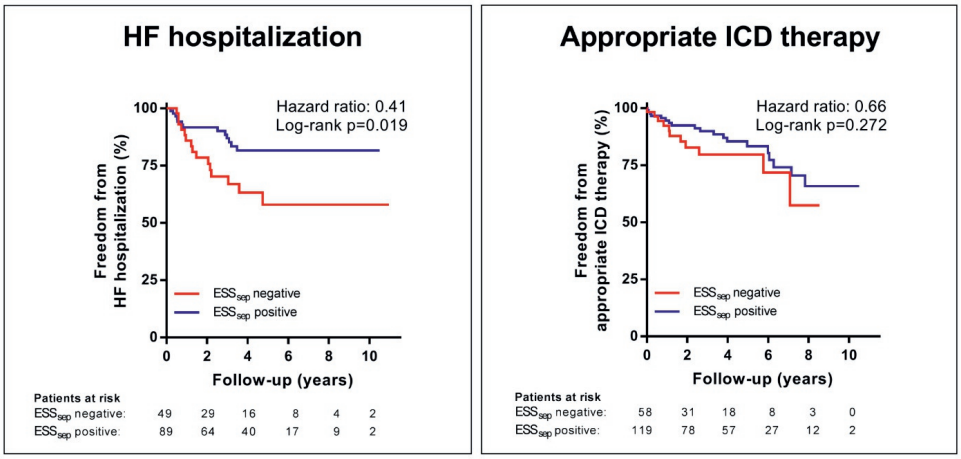


Figure 3: Kaplan-Meier curves demonstrating freedom from HF hospitalization and appropriate ICD therapy. Patients with a positive ESS_{sep} experienced lower rates of HF hospitalization (left diagram) but similar rates of appropriate ICD therapy (right diagram) compared to patients with a negative ESS_{sep}.

Effect of scar on ESSsep and CRT outcome

Myocardial scarring (both ICM and NICM) was present in 129 (59%) of the patients with a median scar size of 6.9% of LV mass. ESS_{sep} was highest in patients without scar (ESS_{sep}: 4.7±5.3%) and progressively decreased from patients with scar burden below the median (ESS_{sep}: 2.5±5.2%) to patients with highest scar burden (ESS_{sep}: 0.2 ± 4.9%), figure 4A. Concurrently, global scar size was associated with higher likelihood of death, LVAD, or HTx after CRT implantation (HR 1.78; 95%CI: 1.33 – 2.39; p<0.001).

Myocardial scarring of the septum was present in 91 (42%) patients. ESS_{sep} was highest in patients without septal scar (ESS_{sep}: 4.0±5.6%) and showed lower values in patients with <25% transmurality (ESS_{sep}: 0.6±5.3%). Interestingly, ESS_{sep} paradoxically increased with higher scar transmurality from 25-50% transmurality (ESS_{sep}: 1.2±2.9%) to >50% transmurality (ESS_{sep}: 3.2±3.0%)(figure 4B). Septal scar was associated with higher probability of death, LVAD, or HTx after CRT implantation (HR 1.51; 95%CI: 1.18 – 1.93; p=0.001).

Posterolateral scar was present in 47 (22%) patients. ESS_{sep} was highest in patients without posterolateral scar (3.6%) and progressively decreased from patients with <25% transmurality (0.2%) to 25-50% transmurality (-1.5%) and >50% transmurality (-2.6%). Posterolateral scar was associated with higher likelihood of the primary endpoint (HR 1.40; 95%CI: 1.05 – 1.85; p=0.022).

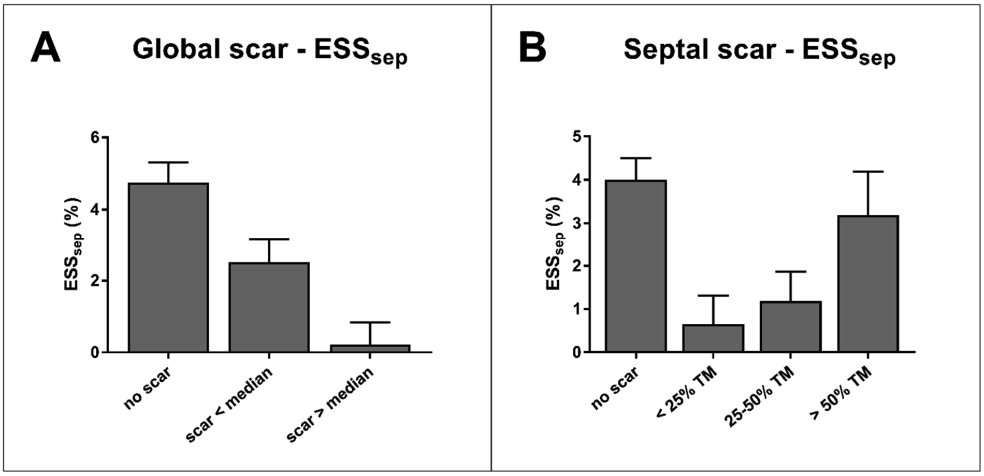


Figure 4: The effect of global scar size and septal scar on ESS_{sep}. Bar graph with error bars illustrating that ESS_{sep} progressively reduces with increasing global scar size (A). ESS_{sep} was also reduced by 0-25% septal scar transmurality, but paradoxically increased with higher scar burden (B).

Univariable and multivariable modeling

Univariable and multivariable Cox regression analysis for the primary endpoint is illustrated in figure 5. Significant CMR predictors in univariable Cox regression included ESS_{sep}, LVEDV, LVESV, scar size, septal scar and posterolateral scar. Addition of ESS_{sep} to a multivariable model with other CMR predictors showed that ESS_{sep} was independently related to the primary endpoint together with LVEDV and septal scar. Significant clinical parameters in univariable Cox regression were age, sex, atrial fibrillation, heart failure etiology, renal function, QRSd ≥150ms and QRS morphology. Addition of ESS_{sep} together with LVEDV and septal scar to a multivariable model with clinical predictors showed that ESS_{sep} was independently related to the primary endpoint together with age, renal function, LVEDV and septal scar.

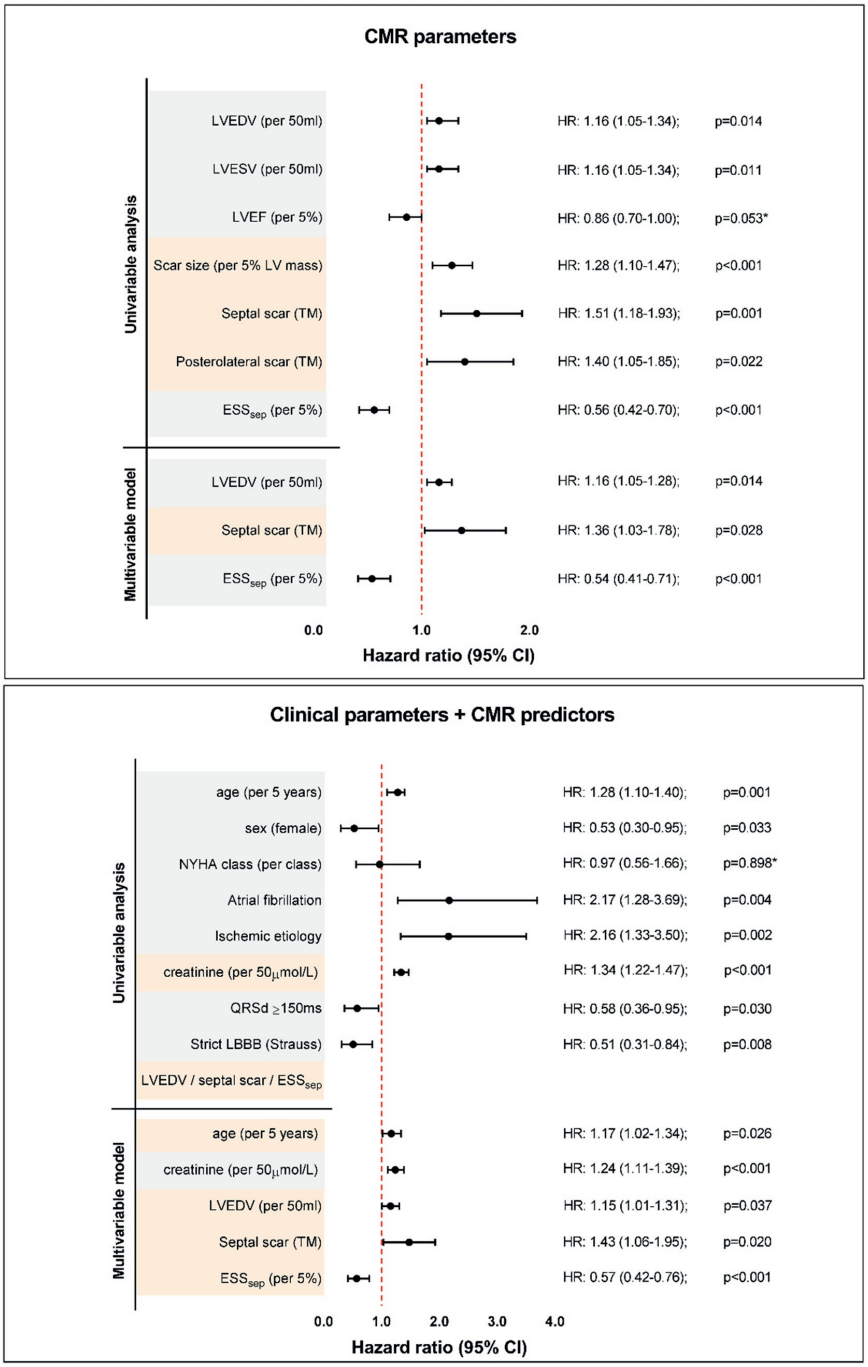


Figure 5: Univariable and multivariable risk analysis for the primary endpoint. Independent CMR predictors being LVEDV, septal scar, ESS_{sep} (top diagram) are added to a multivariable model with clinical parameters (bottom diagram). An asterisk indicates that the parameter is not included in multivariable analysis (i.e. non-significant). For abbreviations see table 1.

DISCUSSION

Previously we demonstrated that the novel SLICE strain technique on standard CMR cine images provides accurate strain measurements, with end-systolic septal strain (ESS_{sep}) as robust predictor of CRT response on echocardiography. The present study investigates the value of SLICE-ESS_{sep} for prediction of clinical outcome after CRT implantation in a large patient cohort. The main findings of this study were that a positive ESS_{sep} (i.e. systolic stretching of the septum) at baseline was associated with two- to three-fold lower rate of all-cause mortality and HF events after CRT implantation. Global myocardial scar size influenced ESS_{sep} by lowering strain values, corresponding with relatively poor outcome. Progressive regional scarring of the septum, however, paradoxically increased ESS_{sep} despite having a poor prognosis. In a multivariable model with CMR parameters, LVEDV, ESS_{sep} and septal scar were independent predictors of the primary endpoint, indicating that SLICE should be combined with LGE to exclude septal scarring as the cause of septal stretching. Moreover, a multivariable model with age, renal function, LVEDV, septal scar and ESS_{sep} provided incremental prognostic information on current guideline criteria.

Cardiac mechanics: the role of the septum

In LBBB, early-activated regions in the septum start contracting first while the lateral wall pre-stretches. After the delayed activation of the lateral wall, reinforced contraction leads to passive stretching of the septum during ejection. This paradoxical septal movement (i.e. discoordination) wastes myocardial work and reduces LV pump function efficiency, further reducing LV function and leading to symptomatic HF and premature death.(7,8) Electrical resynchronization recruits myocardial work from the septum by converting systolic stretching to systolic shortening, leading to a homogenized work distribution and improved cardiac pump efficiency.(1,9,10) Systolic stretching of the septum at baseline therefore reflects the potential for recovery of function with CRT. In line with this concept, strain parameters of the septum (such as systolic rebound stretch) have been linked to CRT outcome in prior studies by various groups.(9,11-15) Our work adds to the accumulating evidence that septal mechanics play a crucial role in assessing the detrimental effects of LBBB on LV function and therefore predict benefit from CRT. Previously we compared multiple SLICE-derived strain parameters and found that ESS_{sep} most strongly

predicted improvement in LV size and function after CRT implant. Furthermore, ESS_{sep} outperforms currently clinical available parameters, and showed consistent results using different strain imaging techniques (CMR tagging, feature tracking and speckle tracking echocardiography).(16) The present study extends the potential role of SLICE- ESS_{sep} in predicting clinical endpoints in a large population of CRT candidates who underwent CMR imaging prior to implant.

SLICE-ESS_{sep} predicts clinical outcome after CRT

All CRT candidates in the present study had delayed electrical activation with QRSd ≥120ms. Septal discoordination, however, varied widely between patients with SLICE-ESS_{sep} ranging between -14.9% (shortening) and 19.7% (stretching) indicating a fair amount of variation in expression of mechanical discoordination. ROC-curve analysis revealed an optimal cut-off value of 0.9% for prediction of the primary endpoint of death, transplant or LVAD implantation which is in line with the cut-off of 0.3% that we found previously to predict echocardiographic CRT response. Strain values around zero percent indicate the tipping point where the septum makes no contribution to LV ejection or stroke volume and starts wasting myocardial work. Comparing patients with inefficient septal mechanics (ESS_{sep} ≥0.9%) with patients with preserved septal function (ESS_{sep} <0.9%), the former leave more room for improvement and demonstrated superior outcome after CRT (figure 2), presumably by a mechanism of reversal of heart failure progression whereas no difference could be observed in the incidence of ventricular arrhythmias (figure 3).

The influence of scar tissue on ESS_{sep}

Myocardial scarring is associated with worse outcomes after CRT in both NICM and ICM patients.(17,18) We showed that global myocardial scar size reduced ESS_{sep} and was associated with poorer outcome (figure 4). Computer simulations by Leenders and Lumens have demonstrated that septal deformation in LBBB depends on both LV activation delay and LV contractility.(12) Reducing global LV contractility (by scarred segments) results in less septal discoordination with little systolic rebound stretch, and consequently, smaller benefit from CRT. Septal discoordination therefore provides integrated information on both intraventricular dyssnchrony and global LV scar size, two important

determinants of CRT response. Progressive regional scarring of the septum, however, paradoxically influenced ESS_{sep} with increased strain values (figure 4). A transmural myocardial infarction located at the septum may therefore influence septal strain assessment with positive strain values due to passive stretching (also seen in dyskinetic aneurysm), thus resembling strain patterns seen in patients with explicit discoordination. Although this increase in ESS_{sep} is expected to result in improved CRT benefit, septal scar is actually associated with poor CRT outcome.(19,20) In a multivariable model with CMR parameters (figure 5, top), ESS_{sep} remained a significant predictor of the primary endpoint together with LVEDV and septal scar (but not global scar size), indicating that additional LGE imaging should be performed to exclude transmural septal scarring as the cause of septal stretching since these patients have worse outcome after CRT.

Clinical decision making

Clinical factors that lead present patient selection for CRT are mainly derived from the ECG. Guideline criteria being QRS duration (≥150ms vs. 120-150ms) and QRS morphology (LBBB vs. IVCD) were found useful as they were both significant predictors of the primary endpoint in this study (HR 0.58 and 0.51, respectively).(3). Other clinical factors associated with time to the primary endpoint included age, gender, atrial fibrillation, heart failure etiology and renal function, which is in line with previous reports.(21,22) Since ESS_{sep} positive patients demonstrated an overall favorable clinical profile (younger, more often female, wider QRS duration with strict LBBB morphology), multivariable analysis was performed to demonstrate an independent effect (figure 5, bottom). In a model with significant clinical predictors (age, sex, atrial fibrillation, HF etiology, renal function, QRS duration and morphology), electrocardiographic parameters were removed from the model whereas ESS_{sep} remained statistically significant together with age, renal function, LVEDV and septal scar. These findings indicate that SLICE strain analysis provides predictive value over present guideline criteria. Perhaps, ESS_{sep} acts as the final common pathway of different electrical, mechanical and biological factors where mechanical discoordination is the underlying pathophysiological mechanism of the heart failure syndrome that can be corrected by CRT. In clinical practice, CMR imaging is increasingly used to screen candidates by measuring LVEF combined with LGE imaging to guide LV lead placement.(23,24) Additional SLICE analysis of the septum could potentially

improve diagnostic yield of CMR and guide future patient selection for CRT. Assessment of SLICE-ESS_{sep} requires two simple measurements at end-diastole and end-systole (figure 1), and can be performed in less than ten minutes without the need for commercial software tools.

Limitations

The major limitation of the study is the observational study design which does not allow any conclusions on causal relationships, only associations. Despite the large sample size and the use of clinical endpoints, the results should therefore be interpreted with care. In addition, there was no control group without CRT. Although SLICE negative patients showed relatively poor survival after CRT implantation, benefit from the therapy cannot be excluded since patients may have had even worse outcome without CRT.

CONCLUSION

Patients with systolic stretching of the septum (i.e. positive SLICE-ESS_{sep}) on CMR showed a markedly improved outcome after CRT implantation compared to patients lacking mechanical substrate for effective resynchronization. Moreover, SLICE-ESS_{sep} was additive to current CRT selection criteria in a prediction model together with age, renal function, LV volume and septal scar.

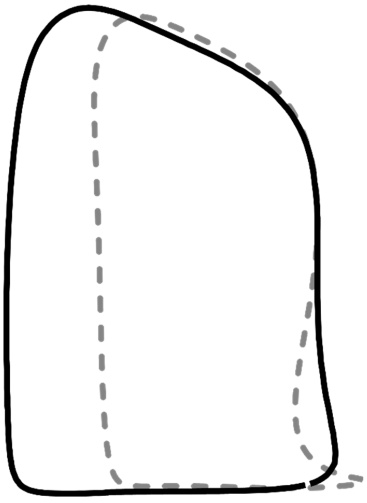
REFERENCES

1. Prinzen FW, Vernooy K, De Boeck BW, Delhaas T. Mechano-energetics of the asynchronous and resynchronized heart. Heart Fail Rev 2011;16:215-224.
2. Daubert C, Behar N, Martins RP, Mabo P, Leclercq C. Avoiding non-responders to cardiac resynchronization therapy: a practical guide. Eur Heart J 2017;14;38(19):1463-1472.
3. Yancy CW, Jessup M, Bozkurt B et al. 2013 ACCF/AHA guideline for the management of heart failure: a report of the American College of Cardiology Foundation/American Heart Association Task Force on Practice Guidelines. J Am Coll Cardiol 2013;62:e147-239.
4. Zweerink A, Allaart CP, Kuijer JPA et al. Strain analysis in CRT candidates using the novel segment length in cine (SLICE) post-processing technique on standard CMR cine images. Eur Radiol 2017;27:5158-5168.
5. Strauss DG, Selvester RH, Wagner GS. Defining left bundle branch block in the era of cardiac resynchronization therapy. Am J Cardiol 2011;107:927-34.
6. Flett AS, Hasleton J, Cook C et al. Evaluation of techniques for the quantification of myocardial scar of differing etiology using cardiac magnetic resonance. JACC Cardiovasc Imaging 2011;4:150-156.
7. Hawkins NM, Wang D, McMurray JJ et al. Prevalence and prognostic impact of bundle branch block in patients with heart failure: evidence from the CHARM programme. Eur J Heart Fail 2007;9:510-7.
8. Zweerink A, de Roest GJ, Wu L et al. Prediction of Acute Response to Cardiac Resynchronization Therapy by Means of the Misbalance in Regional Left Ventricular Myocardial Work. J Card Fail 2016;22:133-42.
9. De Boeck BWL, Teske AJ, Meine M et al. Septal rebound stretch reflects the functional substrate to cardiac resynchronization therapy and predicts volumetric and neurohormonal response. European Journal of Heart Failure 2009;11:863-871.
10. Russell K, Eriksen M, Aaberge L et al. Assessment of wasted myocardial work: a novel method to quantify energy loss due to uncoordinated left ventricular contractions. Am J Physiol Heart Circ Physiol 2013;305:H996-1003.
11. Kirn B, Jansen A, Bracke F, van Gelder B, Arts T, Prinzen FW. Mechanical discoordination rather than dyssynchrony predicts reverse remodeling upon cardiac resynchronization. American Journal of Physiology-Heart and Circulatory Physiology 2008;295:H640-H646.
12. Leenders GE, Lumens J, Cramer MJ et al. Septal deformation patterns delineate mechanical dyssynchrony and regional differences in contractility: analysis of patient data using a computer model. Circ Heart Fail 2012;5:87-96.
13. Risum N, Tayal B, Hansen TF et al. Identification of Typical Left Bundle Branch Block Contraction by Strain Echocardiography Is Additive to Electrocardiography in Prediction of Long-Term Outcome After Cardiac Resynchronization Therapy. J Am Coll Cardiol 2015;66:631-641.
14. Gorcsan J, 3rd, Anderson CP, Tayal B et al. Systolic Stretch Characterizes the Electromechanical Substrate Responsive to Cardiac Resynchronization Therapy. JACC Cardiovasc Imaging 2018.
15. Leenders GE, De Boeck BW, Teske AJ et al. Septal rebound stretch is a strong predictor of outcome after cardiac resynchronization therapy. J Card Fail 2012;18:404-12.

16. Zweerink A, van Everdingen WM, Nijveldt R et al. Strain imaging to predict response to cardiac resynchronization therapy: a systematic comparison of strain parameters using multiple imaging techniques. ESC Heart Fail 2018.
17. Leyva F, Foley PW, Chalil S et al. Cardiac resynchronization therapy guided by late gadolinium-enhancement cardiovascular magnetic resonance. J Cardiovasc Magn Reson 2011;13:29.
18. Adelstein EC, Althouse AD, Schwarzman D, Jain SK, Soman P, Saba S. Scar burden, not intraventricular conduction delay pattern, is associated with outcomes in ischemic cardiomyopathy patients receiving cardiac resynchronization therapy. Heart Rhythm 2018.
19. White JA, Yee R, Yuan X et al. Delayed enhancement magnetic resonance imaging predicts response to cardiac resynchronization therapy in patients with intraventricular dyssynchrony. J Am Coll Cardiol 2006;48:1953-60.
20. Duckett SG, Ginks M, Shetty A et al. Adverse response to cardiac resynchronisation therapy in patients with septal scar on cardiac MRI preventing a septal right ventricular lead position. J Interv Card Electrophysiol 2012;33:151-60.
21. Khatib M, Tolosana JM, Trucco E et al. EAARN score, a predictive score for mortality in patients receiving cardiac resynchronization therapy based on pre-implantation risk factors. Eur J Heart Fail 2014;16:802-9.
22. Gasparini M, Klersy C, Leclercq C et al. Validation of a simple risk stratification tool for patients implanted with Cardiac Resynchronization Therapy: the VALID-CRT risk score. Eur J Heart Fail 2015;17:717-24.
23. Romano S, Judd RM, Kim RJ et al. Feature-Tracking Global Longitudinal Strain Predicts Death in a Multicenter Population of Patients With Ischemic and Nonischemic Dilated Cardiomyopathy Incremental to Ejection Fraction and Late Gadolinium Enhancement. JACC Cardiovasc Imaging 2018;11:1419-1429.
24. Bilchick KC, Dimaano V, Wu KC et al. Cardiac Magnetic Resonance Assessment of Dyssynchrony and Myocardial Scar Predicts Function Class Improvement Following Cardiac Resynchronization Therapy. JACC: Cardiovascular Imaging 2008;1:561-568.

PART II

DEVICE OPTIMIZATION



Chapter 10

Can We Use the Intrinsic Left Ventricular Delay (QLV) to Optimize the Pacing Configuration for Cardiac Resynchronization Therapy with a Quadripolar Left Ventricular Lead?

Circ Arrhythmia Electrophysiology 2018;11:e005912

Alwin Zweerink*
Wouter M. van Everdingen*
Maarten J. Cramer
Pieter A. Doevendans
Uyên Châu Nguyên
Albert C. van Rossum
Frits W. Prinzen
Kevin Vernooy
Cornelis P. Allaart
Mathias Meine

* Both authors contributed equally to this work

ABSTRACT

Background: Previous studies indicated the importance of the intrinsic left ventricular (LV) electrical delay ("QLV") for optimal benefit to cardiac resynchronization therapy (CRT). We investigated the use of QLV for achieving optimal acute hemodynamic response to CRT with a quadripolar LV lead.

Methods and results: Forty-eight heart failure patients with a left bundle branch block were prospectively enrolled (31 male, age: 66±10 years, LV ejection fraction: 28±8%, QRS duration: 176±14ms). Immediately after CRT implantation, invasive LV pressure-volume loops were recorded during biventricular pacing with each separate electrode at four atrioventricular delays. Acute CRT response, measured as change in stroke work (Δ%SW) compared to intrinsic conduction, was related to intrinsic interval between Q on the electrocardiogram and LV sensing delay (QLV), normalized for QRS duration (QLV/QRSd), and electrode position. QLV/QRSd was 84±9% and variation between the four electrodes 9±5%. Δ%SW was 89±64% and varied by 39±36% between the electrodes. In univariate analysis, an anterolateral or lateral electrode position and a high QLV/QRSd had a significant association with a large Δ%SW (all $p<0.01$). In a combined model, only QLV/QRSd remained significantly associated with Δ%SW ($p<0.05$). However, a direct relation between QLV/QRSd and Δ%SW was only seen in 24 patients, while 24 patients showed an inverse relation.

Conclusions: The large variation in acute hemodynamic response indicates that the choice of the stimulated electrode on a quadripolar lead is important. Although QLV/QRSd was associated with acute hemodynamic response at group level, it cannot be used to select the optimal electrode in the individual patient.

INTRODUCTION

Cardiac resynchronization therapy (CRT) is a proven therapy for patients with heart failure and left ventricular (LV) conduction disorder, according to most recent international guidelines.(1) CRT improves prognosis, reduces mortality and morbidity, and induces reverse remodeling through electromechanical resynchronization.(2,3) Unfortunately, a substantial number of eligible patients (i.e. around 30-40%) show no significant response to CRT.(4) An important cause of poor CRT response is a suboptimal placed LV lead.(5) A suboptimal placed LV lead may hamper successful resynchronization, as the distally wedged pacing electrodes may be close to an infarcted region or remote from the electromechanical 'hotspot'.(6) In order to reach this 'hotspot', quadripolar LV leads may be of beneficial use.(7) As the tip of a quadripolar lead is often wedged in a tributary of the coronary sinus, its electrodes will span a range from apical to basal regions of the LV wall.(8) Despite several studies on quadripolar leads,(9,10)the exact benefit of the additional pacing sites on LV function remains relatively unknown.(8) Most studies only compared the benefit of the proximal electrodes to the distal electrode.(9,10) These studies were small, used non-invasive techniques to measure acute hemodynamic response with low signal to noise ratios, or a fixed atrioventricular (AV) delay.(8) Moreover, non-invasive methods to select the optimal electrode of a quadripolar LV lead are lacking. Potential optimization methods are parameters of electrical delay derived from the ECG and/or intracardiac electrogram. The QLV interval is one of these electrical delays, defined by the delay between 'Q' on the surface ECG and local LV depolarization on the intracardiac electrogram at a given LV pacing site (figure 1).(11) The QLV may be normalized using the intrinsic QRS duration (QLV/QRSd).(12) A few studies reported that an apical and/or anterior LV lead position may be suboptimal for CRT response, while electrodes placed basal or mid-ventricular in a lateral position yield more favorable response.(13,14) However, these studies compared bipolar LV leads in different patients, without taking interpatient variability in consideration.

The hypothesis of this study is that biventricular pacing at a site with largest QLV/QRSd ratio provides the largest acute hemodynamic response. Therefore, the aim of the study was to associate the acute hemodynamic response of each electrode of the quadripolar LV lead was measured by invasive pressure-volume loops (PV-loops) with electrical and anatomical parameters.

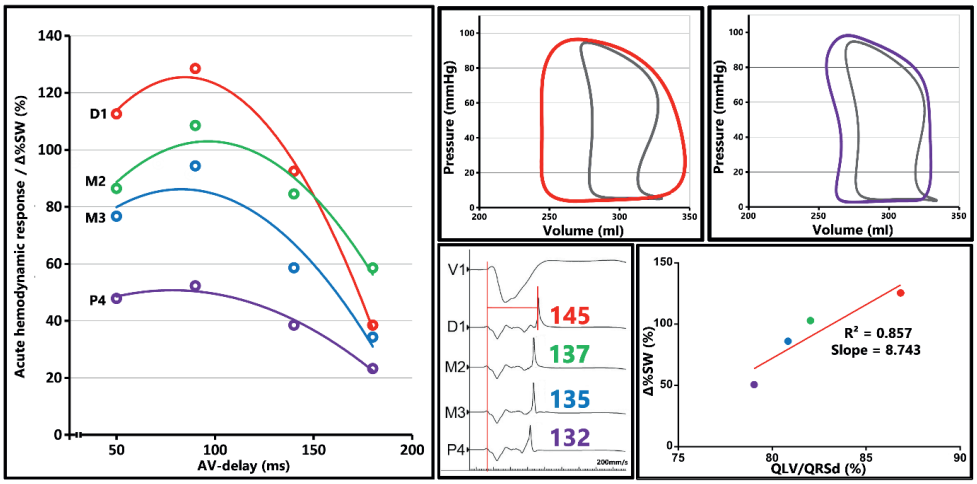


Figure 1: Method to determine the optimal pacing site of CRT with a quadripolar LV lead. The acute hemodynamic response is determined by calculating the increase in stroke work (Δ%SW) of pressure-volume (PV) loops of four atrioventricular (AV) delays and four electrodes compared to loops during right atrial pacing with intrinsic conduction (grey PV-loops). PV-loops of D1 (red) and M2 (green) are displayed in the upper right corner. For each tested AV-delay and electrode, Δ%SW is plotted in the left panel. Delays are determined between Q on the surface ECG (V1) and local LV depolarization at the electrodes of the quadripolar lead (QLV) (middle lower panel). The QLV/QRSd ratio is plotted against Δ%SW of each electrode at the optimal AV-delay, and a trendline is fitted. Electrode colors: D1: red, M2: green, M3: blue, P4: purple.

METHODS

Patient cohort

The observational OPTICARE-QLV study, was performed between 2014 and 2017 in three university medical center (University Medical Center Utrecht, Utrecht; VU University Medical Center, Amsterdam; and Maastricht University Medical Center, Maastricht; all in the Netherlands). A total of 51 consecutive patients planned for CRT implantation were included, with moderate to severe heart failure (i.e. NYHA class II or III), LV ejection fraction ≤35%, optimal pharmacological therapy, sinus rhythm, and a left bundle branch block (LBBB) according to Strauss criteria.(15) Exclusion criteria were severe aortic valve stenosis, mechanical aortic valve replacement, and the presence of LV thrombus. All subjects gave written informed consent. The study was performed according to the Declaration of Helsinki and in agreement with the local medical ethics committees. As the data of this study is also used for future publications, the

data, analytic methods, and study materials will not be made available to other researchers for purposes of reproducing the results or replicating the procedure.

CRT implantation

All patients underwent electrocardiographic (ECG), echocardiographic examination and cardiac magnetic resonance imaging (CMR) prior to device implantation. CMR (or echocardiography) derived LV volumes were used to calibrate the conductance catheter-derived baseline volumes. CRT implantation was performed under local anesthesia. RV and right atrial (RA) leads were placed transvenously at conventional positions. The quadripolar LV lead (Quartet 1458Q, St. Jude Medical, Saint Paul, Minnesota, United States) was placed in one of the coronary veins overlying the LV free wall. A site in the lateral, antero- or posterolateral position was preferred. After electrophysiological measurements, the three leads were connected to a St. Jude Medical CRT-device.

Electrophysiological measurements

Electrophysiological (EP) measurements were performed using an on-site dedicated EP system. EP system settings of the three participating centers were matched to study protocols. The EP system was used to record simultaneous registrations of the twelve-lead surface ECG and the three implanted leads. Delays of specific pacing modalities were recorded and delays between pacing artefacts and local depolarization at the leads were measured. For each electrode (i.e. D1, M2, M3, and P4), QLV was defined as the intrinsic conduction time from first Q on the surface ECG to local LV depolarization at the electrode of the quadripolar LV lead (QLV) (figure 1). The ratio between QLV and the intrinsic QRS duration was also calculated for each electrode (QLV/QRSd). We used QLV/QRSd to uniform results on conduction delay between patients. Next, RA pacing to RV sensing interval (RAp-RVs) was measured and used to calculate the patient specific AV delays. The delay between RV pacing to LV sensing interval (RVp-LVs) was measured as a parameter of paced interventricular conduction delay.

Hemodynamic measurements

Directly after device implantation, a dedicated PV-loop conductance catheter (CD Leycom, Zoetermeer, The Netherlands) was inserted via the femoral artery and placed in the LV cavity. PV-loops were recorded for biventricular pacing with each individual electrode of the quadripolar lead, in-between baseline recordings during intrinsic conduction. The LV electrode was used as a cathode with the RV-coil as anode, resulting in four different pacing vectors. Only configurations without phrenic nerve stimulation close to the myocardial pacing threshold were used. For each electrode, four AV-delays were determined to approximate 20%, 40%, 60% and 80% of the patient's intrinsic AV conduction time (RAp-RVs interval). The interventricular delay was programmed to 40ms LV first, as LV pacing 40ms before RV pacing is favorable in 80% of CRT patients.(16) The order in which the electrodes were tested was varied between patients. To keep heartrate constant, PV-loops were recorded during atrial pacing, with a frequency of 5-10 bpm above intrinsic rhythm. Recordings lasted 60 beats per pacing configuration, after excluding all inappropriate beats (i.e. extra systoles with one preceding and two subsequent beats). PV-loops during intrinsic conduction (i.e. RA pacing) were recorded for 30 beats at the same heart rate. The area of the PV-loop was used to calculate stroke work (SW). To account for baseline drift,(17) the effect of biventricular pacing was quantified as change in SW, calculated as a %-change (Δ%SW) compared to the mean of the two adjoining baseline measurements. For each electrode, a parabolic curve was fitted to change in Δ%SW obtained from the four AV delays (figure 1). The highest value of each parabolic curve was noted as the optimal change in Δ%SW and corresponding AV-delay for the specific electrode.

Lead position

After lead placement, fluoroscopy images were made in the left anterior oblique (LAO) 40° and in the in the right anterior oblique (RAO) 30° view to determine the specific position of each quadripolar LV lead electrode in the longitudinal direction (figure 2). On the RAO 30° view the distance between base of the LV and each electrode was divided by the distance between base and apex, in order to obtain the RAO-ratio (figure 2). The RAO-ratio was divided in three even groups, resulting in basal, mid, and apical positioned electrodes. For the LAO 40° view, the ventricle was divided in five equally sized regions overlying the LV free

wall in the circumferential direction (i.e. anterior, anterolateral, lateral, posterolateral, and posterior).(7)

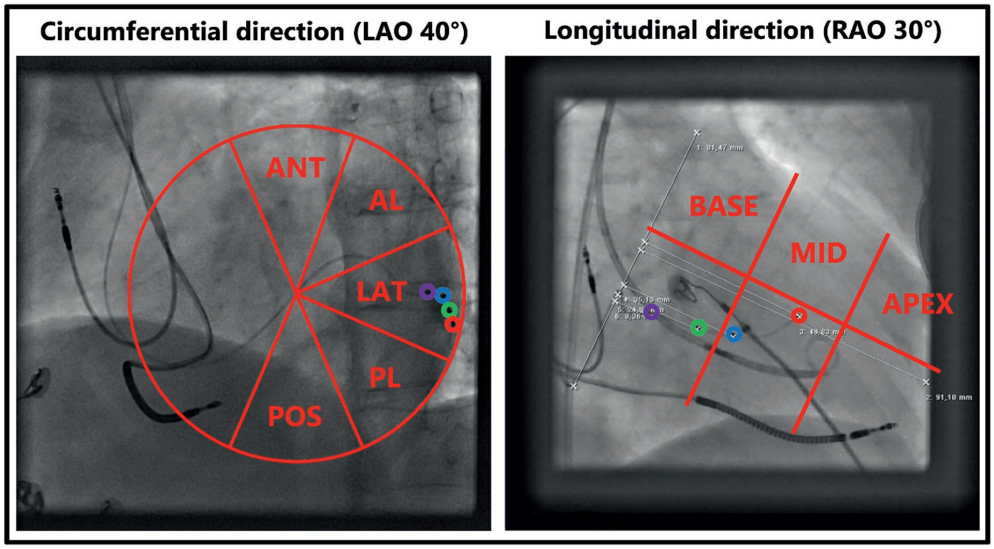


Figure 2: Anatomical position of the quadripolar LV lead electrodes. The quadripolar left ventricular (LV) lead and electrode position are determined using fluoroscopy in two views. In the circumferential direction, the left anterior oblique (LAO) 40° view was used to divide the LV in an anterior (ANT), anterolateral (AL), lateral (LAT), posterolateral (PL), and posterior segment (POS). In the longitudinal direction, the LV is divided in three evenly spaced segments based on the right anterior oblique (RAO) 30° view: base, mid and apex. The most distal electrode (D1) is red, the first mid electrode (M2) green, the second mid electrode (M3) blue and the proximal electrode (P4) purple.

Statistical analysis

Statistical analysis was performed using SPSS statistics version 23 (IBM, Armonk, New York, USA). Data is presented as mean ± standard deviation or median and interquartile range, based on normality of data. Of certain parameters, the variation between electrodes was calculated for each individual patient by subtracting the lowest value from the highest value. The average variation and standard deviation of the entire cohort were calculated with these values. To account for repeated measurements, differences in observed parameters between electrodes were compared in generalized estimated equation (GEE), with pairwise comparison. GEE's were also used to assess the value of expected predictors (i.e. electrode position in longitudinal and circumferential direction,

RVp-LVs, QLV and QLV/QRSd ratio) of change in Δ%SW on a group level. All parameters were tested separately, while both parameters on anatomical position were combined, after which each parameter with $p<0.10$ was incorporated in a combined model. In case of significance of QLV and QLV/QRSd, a single parameter was chosen based on the highest beta coefficient and p-value. The relation between hemodynamic response (Δ%SW) and QLV/QRSd of all four electrodes was calculated for each patient. A line was fitted to the four data points, of which the coefficient of determination and slope were noted (figure 1). Patients were divided in two groups based on the slope: patients with a positive slope and a negative slope. The average slope of all patients reflects the relation between QLV/QRSd and change in Δ%SW. The two groups were compared on baseline parameters using an independent T-test or Mann Whitney U test. A Chi-square test was used for categorical variables. A p-value below 0.05 was considered significant for the GEE in table 3. Due to the large number of comparisons, a p-value below 0.01 was considered significant for all remaining tests.

RESULTS

Fifty-one patients were included prospectively in the study, of which three were excluded from the analysis due to unreliable baseline PV-loops. Twenty-six patients were included in the University Medical Center Utrecht, sixteen in the VU University Medical Center and six in het Maastricht University Medical Center. Unacceptably high pacing thresholds precluded using electrode M2 in three patients, and electrode P4 in three other patients. Values in the remaining 48 patients and 186 electrodes were as follows: QLV: 140.2±19.7ms, QLV/QRSd: 79.9±9.2%, RVp-LVs: 146.4±23.0ms (table 1).

Table 1. Baseline characteristics

Parameter	Total cohort (n=48)	Direct relation QLV/QRSd-%SW (n=24)	Inverse relation QLV/QRSd-%SW (n=24)	p-value
Age (years)	65.9 ± 9.5	66.2 ± 10.2	65.7 ± 8.8	0.845
Sex (n, % of male)	31 (65%)	17 (71%)	14 (58%)	0.547
Type of cardiomyopathy (n, % of ICM)	13 (27%)	7 (29%)	10 (42%)	0.547
NYHA-class (n, %)				
II	33 (69%)	16 (67%)	17 (71%)	
III	15 (31%)	8 (33%)	7 (29%)	1.000
PR duration (ms)	182.8 ± 31.3	186.6 ± 33.7	179 ± 28.8	0.403
QRS duration (ms)	175.6 ± 13.6	174.2 ± 12.6	176.9 ± 14.6	0.504
Mean QLV (ms)	140.2 ± 19.7	134.2 ± 21.8	146.3 ± 15.5	0.032
Mean QLV/QRSd (%)	79.9 ± 9.2	77.1 ± 11.5	82.7 ± 4.9	0.034
QLV/QRSd variation (%)	8.8 ± 4.7	8.0 ± 3.8	9.6 ± 5.5	0.227
Mean RVp-LVs (ms)	146.4 ± 23.0	145.2 ± 28.2	147.6 ± 17.2	0.726
LV EDV (ml)	210.8 ± 66.0	233.6 ± 69.9	188.1 ± 54.1	0.015
LV ESV (ml)	154.3 ± 61.4	174.9 ± 66.6	133.7 ± 48.9	0.018
LV EF (%)	28.5 ± 8.4	26.3 ± 6.7	30.4 ± 8.8	0.067
LV EDD (mm)	61.6 ± 7.5	63.0 ± 8.7	60.2 ± 6.1	0.206
Creatinine	90.1 ± 22.7	92.8 ± 24.1	86.3 ± 21.6	0.336
Log BNP	1.89 ± 0.54	2.03 ± 0.59	1.76 ± 0.48	0.125
Medication (n, %)				
ACE-inhibitor or ATII-antagonist	47 (98%)	24 (100%)	23 (96%)	1.000
Beta-blocker	42 (88%)	22 (92%)	20 (83%)	0.724
Diuretic	32 (67%)	16 (67%)	16 (67%)	1.000
Aldosterone-antagonist	29 (60%)	11 (46%)	18 (75%)	0.075
Anticoagulant	30 (63%)	12 (50%)	18 (75%)	0.135
Comorbidities (n, %)				
Hypertension	17 (71%)	5 (21%)	12 (50%)	0.069
Renal failure	4 (17%)	1 (4%)	3 (13%)	0.609
Circumferential electrode position (n, %)				
Anterior	0	0	0	
Anterolateral	31 (17%)	18 (20%)	13 (14%)	
Lateral	108 (58%)	44 (45%)	64 (68%)	
Posterolateral	44 (24%)	27 (29%)	17 (18%)	0.021
Posterior	3 (2%)	3 (3%)	0	
Longitudinal electrode position (n, %)				
Basal	60 (32%)	28 (30%)	32 (34%)	
Mid	101 (54%)	46 (50%)	55 (59%)	0.053
Apical	25 (13%)	18 (20%)	7 (7%)	

Direct relation: patients with a direct relation between QLV/QRSd and change in stroke work (Δ%SW). Inverted relation: patients with an inverse relation between QLV/QRSd and Δ%SW. ACE: angiotensin converter enzyme, ATII: angiotensin receptor II, EDD: end-diastolic diameter, EDV: end-diastolic volume, ESV: end-systolic volume, ICM: ischemic cardiomyopathy, LV: left ventricular, LVEF: left ventricular ejection fraction, MI: myocardial infarction, n: number, NYHA-class: New York Heart Association functional class, QLV: Q to LV sensing delay, QLV/QRSd: ratio of QLV and QRS duration ratio.

In the longitudinal direction, distal electrodes (i.e. D1 and M2) were more often positioned apical, while the position of proximal electrodes (i.e. M3 and P4) was more often basal (table 2). In the LAO view, there were no significant differences in positioning of the electrodes. Overall, most electrodes were positioned in a lateral segment (n=108; 58%). There was no apparent resemblance between the bullseye of QLV/QRSd and acute hemodynamic response (figure 3).

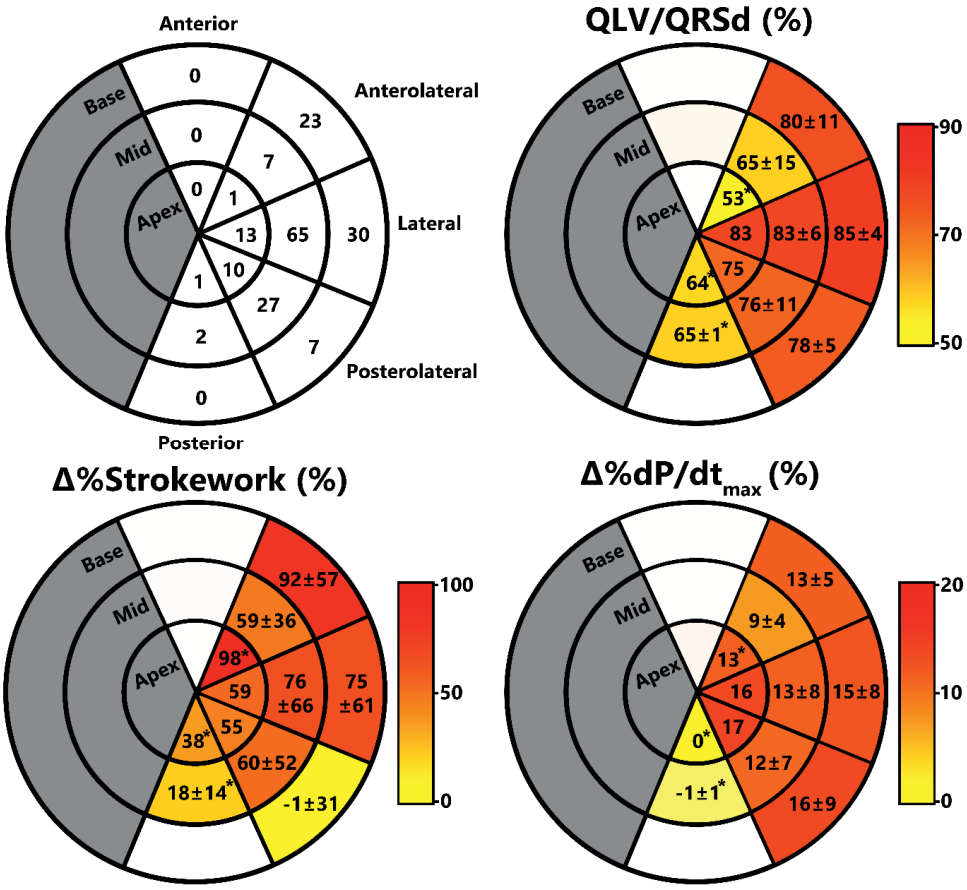


Figure 3: Anatomical representation of electrode position, electrical delay and hemodynamic response. The bullseye in the upper left corner displays the anatomical position of the 192 electrodes divided in 15 segments. The average and standard deviation of the QLV/QRSd of each segment are displayed in the upper right corner. Average acute hemodynamic response in percentage increase in stroke work and dP/dt_{max} of each segment are displayed in the lower two bullseyes. The one basal anterior electrode had no capture and therefore no hemodynamic values. *: values represent only 1 or 2 electrodes.

Large differences in QLV/QRSd were primarily seen in the anterolateral positioned electrodes, with higher values in the basal segment compared to the apical segment. Δ%SW showed lower values in posterolateral and posterior positioned electrodes, while Δ%dP/dt_{max} was lowest in the posterior positioned electrodes. On average, QLV/QRSd of the distal electrode (D1) was significantly lower compared to the other three electrodes, although the variation between the electrodes was only 8.8±4.7% (table 2).

Table 2. Electrode characteristics

Parameters (n=48)	**D1 (n=48)**	**M2 (n=45)**	**M3 (n=48)**	**P4 (n=45)**	**p-value**
Longitudinal position (n, %)					
Basal	0 (0%)	5 (10%)	22 (46%)	33 (73%)	
Mid	34 (71%)	34 (71%)	34 (48%)	10 (21%)	
Apical	14 (29%)	6 (13%)	3 (6%)	2 (4%)	**<0.001**
Circumferential position (n, %)					
Anterior	0	0	0	0	
Anterolateral	4 (8%)	7 (16%)	8 (17%)	12 (25%)	
Lateral	27 (56%)	30 (67%)	28 (58%)	23 (51%)	
Posterolateral	17 (35%)	7 (16%)	11 (23%)	9 (20%)	
Posterior	0	1 (2%)	1 (2%)	1 (2%)	0.270
Pacing threshold (V)	0.7 (0.3-1.8)	0.7 (0.4-2.2)	0.6 (0.4-1.8)	1.8 (0.5-5.2)*	**<0.001**
PNS threshold (V)	10.0 (2.0-10.0)†	10.0 (1.5-10.0)	10.0 (2.9-10)	10.0 (7.0 – 10.0)†	**0.002**
QLV (ms)	135.5 ± 19.2*	142.1 ± 20.2	141.9 ± 21.1	144.3 ± 20.0	**<0.001**
QLV/QRSd (%)	77.1 ± 8.7*	80.6 ± 9.7	80.8 ± 10.0	82.1 ± 9.8	**<0.001**
RVp-LVs (ms)	131.8 ± 23.7*	144.9 ± 23.9*	151.3 ± 23.8*	158.1 ± 24.5*	**<0.001**
Δ%SW (%)	67.4 ± 55.0	74.4 ± 55.4	70.9 ± 64.4	63.1 ± 63.2	0.011
Δ%dP/dt_{max} (%)	13.5 ± 8.8	13.5 ± 9.5	12.7 ± 9.3	13.3 ± 10.6	0.255

Mean and standard deviation with ± symbol, median and interquartile range between brackets. Phrenic nerve stimulation (PNS) thresholds were measured to a maximum of 10V. RVp-LVs: right ventricular pacing and left ventricular sensing interval. For other abbreviations, see table 1. *: p<0.001 compared to all other electrodes. †: p<0.01 between indicated electrodes.

RVp-LVs delay showed larger and significant differences between all electrodes (RVp-LVs variation: 27.8±13.2ms), with lowest values for the distal electrode, increasing towards the proximal electrode. The pacing threshold of electrode P4 was often higher, while phrenic nerve stimulation occurred less using this electrode. Despite these differences in electrical properties of the electrodes, no electrode consistently provided the largest increase in Δ%SW (D1 in 17 (35%), M2 in 10 (21%), M3 in 6 (13%) and P4 in 15 (31%) patients). The mean acute hemodynamic response of biventricular pacing was 68.9±59.3 for Δ%SW and 13.3±9.5 for Δ%dP/dt$_{max}$. The variation in Δ%SW had a large distribution between patients (figure 4), mean variation Δ%SW between the electrodes of a quadripolar lead was 38.8±36.4%, while Δ%dP/dt$_{max}$ had a variation of 4.9±2.9% (supplementary figure 1).

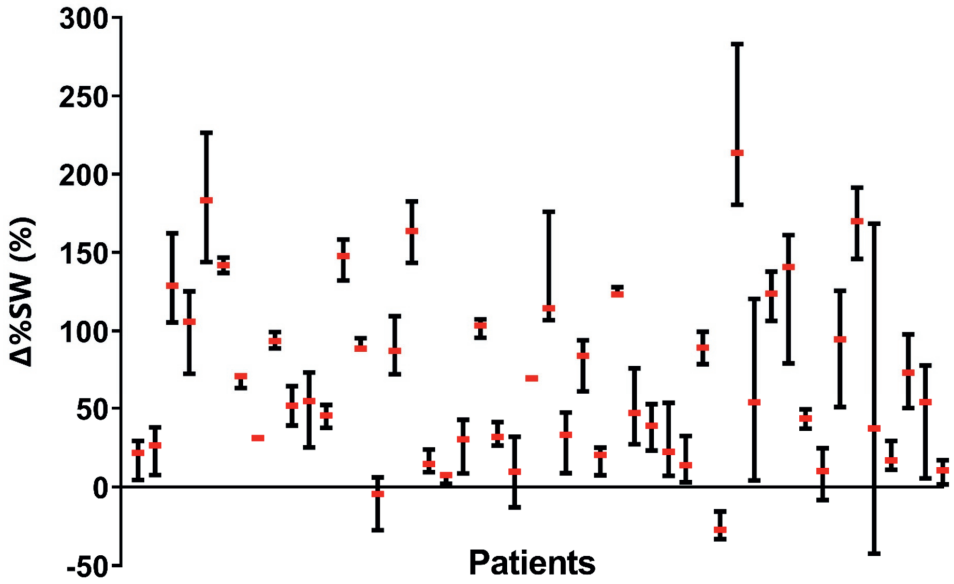


Figure 4: Change in stroke work per patient. Smallest, largest and median %-change in stroke work (Δ%SW) per patient. The red dashes depict the median, upper and lower bars the smallest and largest value obtained with one of the four electrodes of the quadripolar LV lead. Patients are ranked in the same order as figure 5; on the slope and direction of the R^2.

Results at group level

Biventricular pacing with the electrode of maximal QLV or QLV/QRSd tended to result towards a smaller increase of Δ%SW compared to selecting the electrode with highest achievable Δ%SW (67.8±51.2 vs. 88.7±63.8 %SW, p=0.05). The difference between biventricular pacing with the electrode with highest RVp-LVs, was significant compared to the highest achievable Δ%SW (67.8±51.2 vs. 88.7±63.8 %SW, p<0.001). A significant association between %SW and QLV/QRSd was observed at group level (table 3). This analysis showed that with each percent increase in QLV/QRSd, Δ%SW increased with 0.9% in a single variable model and 0.8% in a combined model. A combined GEE model of anatomical position also showed a significant association between electrode position in the circumferential direction and Δ%SW change. Electrodes in the anterolateral or lateral position were associated with ~10% higher Δ%SW values compared to posterior and posterolateral positioned electrodes (p<0.05 for both comparisons). There was no association between change in Δ%SW and electrode position in a longitudinal direction or RVp-LVs. A combined GEE model of QLV/QRSd and electrode position in the circumferential direction showed a significant association of QLV/QRSd with change in Δ%SW, but no significant association of the electrode position.

Results for the individual patient

Despite the significant relation between QLV/QRSd and Δ%SW at the group level described above, there was considerable heterogeneity in this relation in individual patients. The association between Δ%SW and QLV/QRSd had a direct relation (i.e. positive slope) for 24 patients but an inverse relation (i.e. negative slope) for the remaining 24 patients (figure 5).

Table 3. Prediction of change in %-change in stroke work

Single variable models (GEE) – electrical delays			
	B	SE (95% CI)	p-value
QLV	0.579	0.193 (0.202-0.956)	**0.003**
QLV/QRSd	0.934	0.332 (0.283-1.586)	**0.005**
RVp-LVs	0.076	0.245 (-0.404-0.556)	0.756
Combined model (GEE) – anatomical position			
Longitudinal position			
Basal	-0.226	8.755 (-17.386-16.935)	0.979
Mid	4.157	7.109 (-9.776-18.090)	0.559
Apical	0*	-	-
Circumferential position			
Anterolateral	11.619	5.682 (0.483-22.755)	**0.041**
Lateral	9.068	4.543 (0.226-17.909)	**0.044**
Posterolateral or posterior	0*	-	-
Combined model (GEE) – significant predictors			
	B	SE (95% CI)	p-value
QLV/QRSd	0.809	0.351 (0.121-1.497)	**0.021**
Circumferential position			
Anterolateral	4.527	5.704 (-6.651-15.706)	0.427
Lateral	4.916	4.520 (-3.944-13.776)	0.227
Posterolateral or posterior	0*	-	-

Single variable models show the results of the generalized estimated equation (GEE) of each parameter. The parameters with p-values <0.10 were combined in a final model (i.e. GEE). The categories posterolateral and posterior were combined, as there were only three electrodes positioned posterior. B: beta-coefficient. SE: standard error, CI: confidence interval. For other abbreviations: see table 1. *: set to zero because the parameter is redundant.

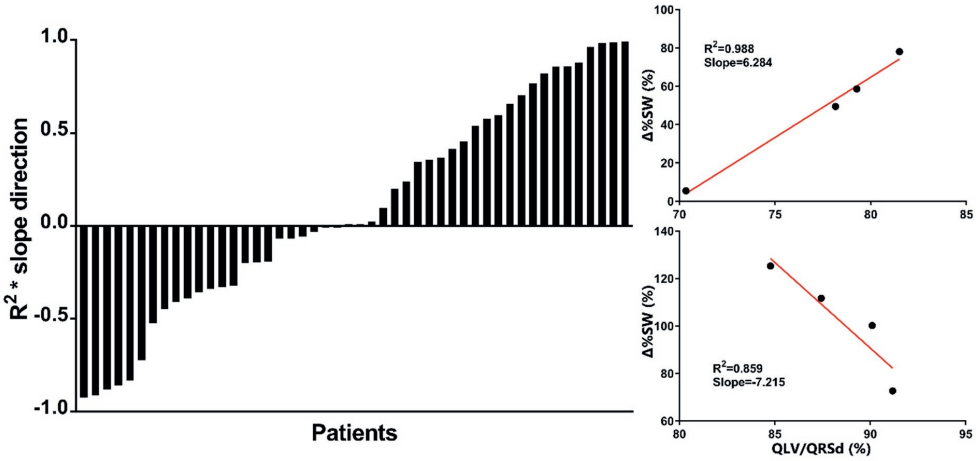


Figure 5: Distribution of the slope and coefficient of determination for Δ%SW and QLV/QRSd. The slope direction multiplied by the coefficient of determination (R^2) of the trendline fitted to QLV/QRSd and Δ%SW for each patient. Values are arranged from lowest to highest value. There are 24 patients with a direct relation (positive slope) and 24 with an invert relation (negative slope). Examples of a direct relation (upper right panel) and an inverse relation (lower right panel) are shown on the right.

The R^2 tended to be higher in patients with a direct relation (0.570±0.319), while it was lower for the patients with an inverse relation (0.377±0.320, p=0.05). These poorer correlations in case of an inverse relation may be explained by the smaller variation in Δ%SW in the patients with inverse versus those with a direct relation (26.8±20.0 vs. 50.8±44.7 Δ%SW, p=0.02 (figure 4)). However mean Δ%SW did not differ between patients with a direct (67.8Δ%SW) or inverse relation (70.6Δ%SW, p=0.87). Comparing baseline characteristics of patients with a direct and inverse QLV/QRSd-Δ%SW relation revealed no significant differences (table 1). However, QLV and QLV/QRSd values tended to be lower, while LV end-diastolic and end-systolic volumes tended to be larger for patients with a direct relation. Accordingly, LV ejection fraction tended to be lower in patients with a direct QLV/QRSd-%SW relation. There tended to be more electrodes positioned in a posterolateral or posterior position in patients with a direct relation, while there was a trend towards more apically positioned electrodes in patients with an inverse QLV/QRSd-%SW relation.

DISCUSSION

The present study showed a statistically significant relation between intrinsic ventricular conduction time (QLV/QRSd) and acute hemodynamic response (Δ%SW) at group level. However, only half of the patients showed a direct relation between QLV/QRSd and Δ%SW, while the other half had an inverse relation. Therefore, QLV or QLV/QRSd may not predict the electrode of a quadripolar LV lead that provides the largest hemodynamic response at the individual level. There was also no association between the paced interventricular conduction time (RVp-LVs) and Δ%SW. Nevertheless, anatomical position did reveal favorable sites for LV pacing, namely in the anterolateral or lateral position. Moreover, optimization of CRT with a quadripolar LV lead is important, as there was a large intra-individual variation in the acute hemodynamic response of the four electrodes.

The optimal pacing site

Our results indicate a discrepancy between the optimal pacing site for the entire cohort and for the individual patient. While a longer QLV was significantly associated with a better hemodynamic response at group level, the relation between QLV and response ranged from strongly positive to inverse between individual patients. This discrepancy may be explained by several factors. Most leads were positioned in an area of pronounced delayed activation, with high QLV/QRSd values. Also, the variation in QLV between the four electrodes was relatively small. In animal studies it has been shown that, especially in a model of non-ischemic heart failure, there is a large region within the LV wall that, when paced, provides a significant hemodynamic effect.(18) Therefore QLV/QRSd seems not predictive for the hemodynamic response within late activated areas, especially since some measurement variability has to be taken into account. In line with this idea is the observation that, patients with a direct relation tended to have lower QLV/QRSd values, potentially caused by suboptimally placed LV leads. This may imply that suboptimally placed leads may benefit more from selection of the pacing site with highest change in Δ%SW. The weak but significant association between QLV/QRSd and acute hemodynamic response on group level is of interest. The association indicates that pacing in a region with prolonged QLV/QRSd benefits acute hemodynamic response. However, it does not imply that increase in QLV/QRSd will automatically lead to an increase in

stroke work in each patient. In contrast to our results, Zanon et al. found a strong direct relation between QLV and hemodynamic response, which was apparent in each patient.(19) However, there are four main differences between their study and ours. Firstly, we used stroke work instead of dP/dt_{max}. While dP/dt_{max} is limited to pressure changes in the isovolumetric contraction phase, stroke work incorporates pressure and volume changes of the entire cardiac cycle.(20) Secondly, we only included patients with LBBB, as opposed to including also patients with intraventricular conduction delay and right bundle branch block.(19) The latter had lower QLV values and a less favorable substrate for CRT response. Thirdly, we optimized the AV delay at each pacing configuration and programmed the interventricular pacing delay to 40ms LV first. A study of our own group showed that pacing the LV 40ms before the RV improved CRT response in 80% of all patients.(16) Fourth and perhaps most important, while we only tested the four electrodes of a single quadripolar lead at a single target vein, Zanon et al. tested up to eleven pacing sites per patient in multiple cardiac veins, thereby including suboptimal sites with a short QLV. Thereby a large range of QLV values was obtained, larger than what is present in a single vein. The correlation between QLV and acute hemodynamic response seems driven by the shorter QLV values (<95ms), which are below the cut-off value for CRT response defined by Gold et al.(11) The lack of correlation between QLV/QRSd and hemodynamic response in a single vein is in line with results from the iSPOT study.(21) QLV and QLV/QRSd may therefore be suitable parameters for lead placement in general, indicating the overall expected benefit, as it is a predictor for acute hemodynamic and long-term CRT response.(11,19) However, the QLV or QLV/QRSd cannot be used for selection of the optimal electrode of a quadripolar LV lead after lead placement in an already optimal area (i.e. anterolateral or lateral).

It could be argued that the lack of a clear QLV-Δ%SW relation is due to the fact that not the delay during intrinsic activation, but that during RV pacing (a component of biventricular pacing) matters. Since the location of latest activated region often differs between RV pacing and LBBB activation,(22) we also investigated the relation RVp-LVs delay with Δ%SW. As the highest RVp-LVs value was frequently seen at the proximal electrodes, while the electrode with highest change in acute hemodynamic response was heterogeneously distributed between patients, RVp-LVs is also not suitable for optimization. Therefore,

optimization of the pacing location within a quadripolar lead seems more complicated than merely selecting the latest activated site during LBBB or RV pacing. A rather good effect is already achieved when pacing at a relatively late activated region. An alternative hypothesis would be that the optimal LV pacing site is located at a region with fast LV free wall depolarization.(23) Such regions proved to be especially located at anterolateral or lateral sites, as has been shown previously.(24,25) These regions may overlap with areas which are late activated during intrinsic conduction, with prolonged QLV or QLV/QRSd. However, the actual 'hotspot' may differ, as the sites with largest QLV/QRSd values did not always produce the highest increase in Δ%SW.

Acute hemodynamic effect

The effect of CRT on increase in stroke work was relatively large, however the findings are in line with results from earlier studies.(9;26) The relatively high Δ%SW may be ascribed to patient selection (i.e. strict LBBB and relative low percentage of patients with ischemic cardiomyopathy) and optimization of the pacing configuration and AV delay, recruiting more of the potential substrate. The inter-individual difference in the benefit of CRT was large in our study population, which is in line with recent findings.(21) Previous studies found more variation in dP/dt_{max} between patients or between different veins than pacing sites of a multipolar lead within a single vein.(21,27) However, our study showed a large intra-individual variation in Δ%SW change of the four electrodes. Selecting the pacing site of a quadripolar lead is therefore important for acute hemodynamic response in a subset of patients. Optimization of CRT with a quadripolar LV lead using stroke work from PV-loops, would result a favorable long-term response in most patients.(20) The 20% increase in Δ%SW cut-off value for response, defined by De Roest et al,(20) may result in nine (18%) non-responders for biventricular pacing with the distal electrode (i.e. conventional CRT) compared to only four patients (8%) for biventricular pacing with the optimal pacing configuration. Multi-point pacing may result in an even greater benefit,(28,29) which will be addressed in future work. QLV has also been associated with reverse remodeling and volumetric response to CRT.(11) The association of QLV/QRSd, SW and dP/dt_{max} with volumetric response in this patient cohort is of interest and will be investigated.

Clinical application

Lead positioning is important for CRT response, as anterolateral and lateral positions resulted in relatively better response compared to posterolateral and posterior positions. The LV lead may preferable be placed in such a region, accompanied by considerable electrical delay, seen in high QLV/QRSd values. However, as QLV/QRSd (or RVp-LVs) is not capable of predicting the optimal electrode of a quadripolar lead after lead positioning in each individual patient, it should not be used for this purpose. The QLV/QRSd may therefore be used to select a vein for quadripolar LV lead placement, after which optimization of the pacing electrode should be dependent on functional assessment of CRT response. As not all clinicians have access to PV-loop measurements, future studies on alternative and preferably non-invasive methods to optimize CRT response are of interest.

Limitations

Although the sample size is relatively large for an invasive study and conducted in multiple centers, it is limited by the number of patients included. The strict inclusion criteria also reduced the number of eligible patients and prolonged the time period of inclusion. Three patients with underestimation of baseline function were excluded, as they showed PV-loops with crossing lines. Some of the patients that were included in the final analysis experienced underestimation of baseline stroke work, due to the fact that the shape of the loops was not rectangular but tailed, thereby reducing the area of the loop. This is a known phenomenon in conductance measurements for PV-loops in heart failure patients. Therefore, the absolute value of Δ%SW increase may be overestimated, but due to the repeated measurement design (i.e. each patient serves as its own control), it is possible to compare different settings within each patient. Although the study methodology was complex and the distribution of patients over the three centers was uneven, baseline characteristics were comparable between centers, as well as the relationship between QLV/QRSd and Δ%SW. Our methods may have a different result in patients with intraventricular conduction delay, as optimization may have a bigger impact in patients with a less favorable substrate for CRT. The current protocol with various AV-delays and pacing settings was time-consuming. Therefore, the interventricular delay was fixed at an offset of 40ms LV first, because such an

offset is favorable in most CRT patients.(16) Whether the acute hemodynamic response obtained in each patient correlates to an improved long-term prognosis is debatable. However, changes in dP/dt_{max} are unable to predict reverse remodeling,(30) while changes in SW are associated with favorable volumetric response.(20)

CONCLUSION

There are large intra-individual variations in acute hemodynamic CRT response between electrodes of a quadripolar LV lead, indicating the benefit of patient specific optimization. Although QLV/QRSd had a significant association with acute hemodynamic CRT response at group level, QLV/QRSd was not usable to predict the electrode of a quadripolar LV lead with highest hemodynamic response for the individual patient. Therefore, optimization of the pacing configuration of CRT with a quadripolar LV lead should rely on functional assessment of cardiac function, instead of local electrical delay.

REFERENCES

1. Russo AM, Stainback RF, Bailey SR, Epstein AE, Heidenreich PA, Jessup M, Kapa S, Kremers MS, Lindsay BD, Stevenson LW. ACCF/HRS/AHA/ASE/HFSA/SCAI/SCCT/SCMR 2013 appropriate use criteria for implantable cardioverter-defibrillators and cardiac resynchronization therapy: a report of the American College of Cardiology Foundation appropriate use criteria task force, Heart Rhythm Society, American Heart Association, American Society of Echocardiography, Heart Failure Society of America, Society for Cardiovascular Angiography and Interventions, Society of Cardiovascular Computed Tomography, and Society for Cardiovascular Magnetic Resonance. J Am Coll Cardiol. 2013;61:1318-68.
2. Cleland JG, Daubert JC, Erdmann E, Freemantle N, Gras D, Kappenberger L, Tavazzi L. The effect of cardiac resynchronization on morbidity and mortality in heart failure. N Engl J Med. 2005;352:1539-49.
3. Ghio S, Freemantle N, Scelsi L, Serio A, Magrini G, Pasotti M, Shankar A, Cleland JG, Tavazzi L. Long-term left ventricular reverse remodelling with cardiac resynchronization therapy: results from the CARE-HF trial. Eur J Heart Fail. 2009;11:480-8.
4. Wilkoff BL, Fauchier L, Stiles MK, Morillo CA, Al-Khatib SM, Almendral J, Aguinaga L, Berger RD, Cuesta A, Daubert JP, Dubner S, Ellenbogen KA, Estes NA, 3rd, Fenelon G, Garcia FC, Gasparini M, Haines DE, Healey JS, Hurtwitz JL, Keegan R, Kolb C, Kuck KH, Marinskis G, Martinelli M, McGuire M, Molina LG, Okumura K, Proclemer A, Russo AM, Singh JP, Swerdlow CD, Teo WS, Uribe W, Viskin S, Wang CC, Zhang S, Document R. 2015 HRS/EHRA/APHRS/SOLAECE expert consensus statement on optimal implantable cardioverter-defibrillator programming and testing. Europace. 2016;18:159-83.
5. Khan FZ, Virdee MS, Palmer CR, Pugh PJ, O'Halloran D, Elsik M, Read PA, Begley D, Fynn SP, Dutka DP. Targeted left ventricular lead placement to guide cardiac resynchronization therapy: the TARGET study: a randomized, controlled trial. J Am Coll Cardiol. 2012;59:1509-1518.
6. Abu Daya H, Alam MB, Adelstein E, Schwartzman D, Jain S, Marek J, Gorcsan J, Saba S. Echocardiography-guided left ventricular lead placement for cardiac resynchronization therapy in ischemic vs nonischemic cardiomyopathy patients. Heart Rhythm. 2014;11:614-9.
7. Bogaard MD, Doevendans PA, Leenders GE, Loh P, Hauer RN, van Wessel H, Meine M. Can optimization of pacing settings compensate for a non-optimal left ventricular pacing site? Europace. 2010;12:1262-9.
8. van Everdingen WM, Cramer MJ, Doevendans PA, Meine M. Quadripolar Leads in Cardiac Resynchronization Therapy. J Am Coll EP. 2015:225-237.
9. Pappone C, Calovic Z, Vicedomini G, Cuko A, McSpadden LC, Ryu K, Romano E, Saviano M, Baldi M, Pappone A, Ciaccio C, Giannelli L, Ionescu B, Petretta A, Vitale R, Fundaliotis A, Tavazzi L, Santinelli V. Multipoint left ventricular pacing improves acute hemodynamic response assessed with pressure-volume loops in cardiac resynchronization therapy patients. Heart Rhythm. 2014;11:394-401.
10. Thibault B, Dubuc M, Khairy P, Guerra PG, Macle L, Rivard L, Roy D, Talajic M, Karst E, Ryu K, Paiement P, Farazi TG. Acute haemodynamic comparison of multisite and biventricular pacing with a quadripolar left ventricular lead. Europace. 2013;15:984-91.

11. Gold MR, Birgersdotter-Green U, Singh JP, Ellenbogen KA, Yu Y, Meyer TE, Seth M, Tchou PJ. The relationship between ventricular electrical delay and left ventricular remodelling with cardiac resynchronization therapy. Eur Heart J. 2011;32:2516-2524.
12. Singh JP, Fan D, Heist EK, Alabiad CR, Taub C, Reddy V, Mansour M, Picard MH, Ruskin JN, Mela T. Left ventricular lead electrical delay predicts response to cardiac resynchronization therapy. Heart Rhythm. 2006;3:1285-92.
13. Singh JP, Klein HU, Huang DT, Reek S, Kuniss M, Quesada A, Barsheshet A, Cannom D, Goldenberg I, McNitt S, Daubert JP, Zareba W, Moss AJ. Left ventricular lead position and clinical outcome in the multicenter automatic defibrillator implantation trial-cardiac resynchronization therapy (MADIT-CRT) trial. Circulation. 2011;123:1159-66.
14. Kronborg MB, Johansen JB, Riahi S, Petersen HH, Haarbo J, Jorgensen OD, Nielsen JC. An anterior left ventricular lead position is associated with increased mortality and non-response in cardiac resynchronization therapy. Int J Cardiol. 2016;222:157-62.
15. Strauss DG, Selvester RH, Wagner GS. Defining left bundle branch block in the era of cardiac resynchronization therapy. Am J Cardiol. 2011;107:927-34.
16. Bogaard MD, Meine M, Tuinenburg AE, Maskara B, Loh P, Doevendans PA. Cardiac resynchronization therapy beyond nominal settings: who needs individual programming of the atrioventricular and interventricular delay? Europace. 2012;14:1746-53.
17. Sohaib SM, Whinnett ZI, Ellenbogen KA, Stellbrink C, Quinn TA, Bogaard MD, Bordachar P, van Gelder BM, van Geldorp IE, Linde C, Meine M, Prinzen FW, Turcott RG, Spotnitz HM, Wichterle D, Francis DP. Cardiac resynchronisation therapy optimisation strategies: systematic classification, detailed analysis, minimum standards and a roadmap for development and testing. Int J Cardiol. 2013;170:118-31.
18. Helm RH, Byrne M, Helm PA, Daya SK, Osman NF, Tunin R, Halperin HR, Berger RD, Kass DA, Lardo AC. Three-dimensional mapping of optimal left ventricular pacing site for cardiac resynchronization. Circulation. 2007;115:953-61.
19. Zanon F, Baracca E, Pastore G, Fraccaro C, Roncon L, Aggio S, Noventa F, Mazza A, Prinzen F. Determination of the longest intrapatient left ventricular electrical delay may predict acute hemodynamic improvement in patients after cardiac resynchronization therapy. Circ Arrhythm Electrophysiol. 2014;7:377-83.
20. de Roest GJ, Allaart CP, Kleijn SA, Delnoy PP, Wu L, Hendriks ML, Bronzwaer JG, van Rossum AC, de Cock CC. Prediction of long-term outcome of cardiac resynchronization therapy by acute pressure-volume loop measurements. Eur J Heart Fail. 2013;15:299-307.
21. Sterlinski M, Sokal A, Lenarczyk R, Van Heuverswyn F, Rinaldi CA, Vanderheyden M, Khalameizer V, Francis D, Heynens J, Stegemann B, Cornelussen R. In Heart Failure Patients with Left Bundle Branch Block Single Lead MultiSpot Left Ventricular Pacing Does Not Improve Acute Hemodynamic Response To Conventional Biventricular Pacing. A Multicenter Prospective, Interventional, Non-Randomized Study. PloS one. 2016;11:e0154024.
22. Mafi Rad M, Blaauw Y, Dinh T, Pison L, Crijns HJ, Prinzen FW, Vernooy K. Different regions of latest electrical activation during left bundle-branch block and right ventricular pacing in cardiac resynchronization therapy patients determined by coronary venous electro-anatomic mapping. Eur J Heart Fail. 2014;16:1214-22.

23. Pluijmert M, Bovendeerd PH, Lumens J, Vernooy K, Prinzen FW, Delhaas T. New insights from a computational model on the relation between pacing site and CRT response. Europace. 2016;18:iv94-iv103.
24. Saxon LA, Olshansky B, Volosin K, Steinberg JS, Lee BK, Tomassoni G, Guarnieri T, Rao A, Yong P, Galle E, Leigh J, Ecklund F, Bristow MR. Influence of left ventricular lead location on outcomes in the COMPANION study. J Cardiovasc Electrophysiol. 2009;20:764-8.
25. Thebault C, Donal E, Meunier C, Gervais R, Gerritse B, Gold MR, Abraham WT, Linde C, Daubert JC, group Rs. Sites of left and right ventricular lead implantation and response to cardiac resynchronization therapy observations from the REVERSE trial. Eur Heart J. 2012;33:2662-71.
26. de Roest GJ, Wu L, de Cock CC, Delnoy PP, Hendriks ML, van Rossum AC, Allaart CP. Bifocal left ventricular stimulation or the optimal left ventricular stimulation site in cardiac resynchronization therapy: a pressure-volume loop study. Europace. 2016;18:1030-7.
27. Shetty AK, Duckett SG, Ma YL, Kapetanakis S, Ginks M, Bostock J, Carr-White G, Rhode K, Razavi R, Rinaldi CA. The acute hemodynamic response to LV pacing within individual branches of the coronary sinus using a quadripolar lead. Pacing Clin Electrophysiol. 2012;35:196-203.
28. Pappone C, Calovic Z, Vicedomini G, Cuko A, McSpadden LC, Ryu K, Jordan CD, Romano E, Baldi M, Saviano M, Pappone A, Vitale R, Catalano C, Ciaccio C, Giannelli L, Ionescu B, Petretta A, Fragakis N, Fundaliotis A, Tavazzi L, Santinelli V. Improving cardiac resynchronization therapy response with multipoint left ventricular pacing: Twelve-month follow-up study. Heart Rhythm. 2015;12:1250-8.
29. Zanon F, Marcantoni L, Baracca E, Pastore G, Lanza D, Fraccaro C, Picariello C, Conte L, Aggio S, Roncon L, Pacetta D, Badie N, Noventa F, Prinzen FW. Optimization of left ventricular pacing site plus multipoint pacing improves remodeling and clinical response to cardiac resynchronization therapy at 1 year. Heart Rhythm. 2016;13:1644-51.
30. Bogaard MD, Houthuizen P, Bracke FA, Doevendans PA, Prinzen FW, Meine M, van Gelder BM. Baseline left ventricular dP/dtmax rather than the acute improvement in dP/dtmax predicts clinical outcome in patients with cardiac resynchronization therapy. Eur J Heart Fail. 2011;13:1126-32.

SUPPLEMENTAL MATERIAL

Results for dP/dtmax

Δ%dP/dtmax had a variation between electrodes of 4.9±2.9% (supplementary figure 1). In the GEE, higher QLV/QRSd values were not associated with changes in Δ%dP/dtmax. There was also no significant association of QLV or RVp-LVs with $\Delta\%dP/dt_{max}$. Neither was there an association with the electrode position in either the longitudinal or circumferential direction (supplementary table 1).

Supplementary table 1. Prediction of change in %-change in dP/dt_{max}

Single variable models (GEE)			
	B	SE (95% CI)	p-value
QLV	-0.075	0.045 (-0.163-0.014)	0.100
QLV/QRSd	-0.003	0.030 (-0.061-0.014)	0.906
RVp-LVs	-0.001	0.016 (-0.033-0.002)	0.961
Combined model (GEE) anatomical position			
Longitudinal position			
Basal	0.925	0.734 (-0.525-2.375)	0.211
Mid	0.456	0.587 (-0.694-1.605)	0.437
Apical	0*	-	-
Circumferential position			
Anterolateral	-1.196	1.297 (-3.838-1.247)	0.318
Lateral	-0.735	0.738 (-2.183-0.712)	0.319
Posterolateral or posterior	0*	-	-

The single variable models depict the results of the generalized estimated equation of separate each parameter. B: beta-coefficient. SE: standard error, CI: confidence interval. For other abbreviations: see table 1. *: set to zero because the parameter is redundant.

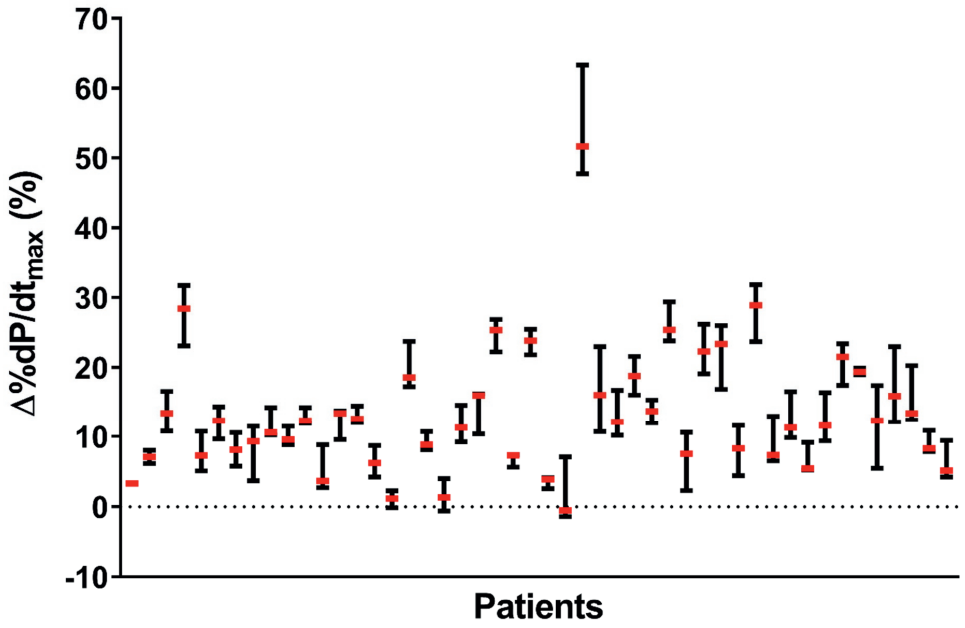


Figure S1: Acute hemodynamic response (dP/dtmax) per patient. Smallest, largest and median %-change in dP/dtmax (Δ%dP/dtmax) per patient. The red dashes depict the median, upper and lower bars the smallest and largest value obtained with one of the four electrodes of the quadripolar LV lead. Patients are ranked in the same order as figure 4 and 5.

Chapter 11

Hemodynamic Optimization in Cardiac Resynchronization Therapy: Should We Aim For dP/dt_{max} or Stroke Work?

JACC Clinical Electrophysiology; 2019;5:1013-1025

Alwin Zweerink
Odette A.E. Salden
Wouter M. van Everdingen
Gerben J. de Roest
Peter M. van de Ven
Maarten J. Cramer
Pieter A. Doevendans
Albert C. van Rossum
Kevin Vernooy
Frits W. Prinzen
Mathias Meine
Cornelis P. Allaart

ABSTRACT

Background: Hemodynamic optimization may increase benefit from cardiac resynchronization therapy (CRT). Typically, maximal LV pressure rise dP/dt_{max} is used as an index of ventricular performance. Alternatively, stroke work (SW) can be derived from pressure-volume (PV) loops. This study (i) evaluates the acute effect of dP/dt_{max} versus SW guided CRT optimization, and (ii) relates acute hemodynamic changes to long-term CRT response.

Methods: Forty-one patients underwent CRT implantation followed by invasive PV loop measurements. The stimulation protocol included sixteen LV pacing configurations using each individual electrode of the quadripolar lead with four atrioventricular (AV) delays. Conventional CRT was defined as pacing from the distal electrode with an AV delay of ~120ms.

Results: Compared to conventional CRT, dP/dt_{max} guided optimization resulted in one-third additional dP/dt_{max} increase (17±11% vs. 12±9%; p<0.001). Similarly, SW guided optimization resulted in one-third additional SW increase (80±55% vs. 53±48%; p<0.001). Comparing both optimization strategies, dP/dt_{max} favored contractility (8±12% vs. 5±10%; p=0.015) whereas SW optimization improved ventricular-arterial (VA) coupling (45% vs. 32%; p<0.001). After six months, mean LV ejection fraction (LVEF) change was 10±9% with 23 (56%) patients becoming CRT (super)responders (≥10% LVEF improvement). Whereas acute changes in SW were predictive for long-term CRT response (AUC 0.78; p=0.002), changes in dP/dt_{max} were not (AUC 0.65; p=0.112).

Conclusions: Pressure-volume guided hemodynamic optimization in CRT results in approximately one-third SW improvement on top of conventional CRT, caused by a mechanism of enhanced ventricular-arterial coupling. dP/dt_{max} optimization, on the other hand, favored LV contractility. Ultimately, acute changes in SW showed larger predictive value for long-term CRT response compared to dP/dt_{max}.

BACKGROUND

Optimization of cardiac resynchronization therapy (CRT) after implantation includes individualized programming of the atrioventricular (AV) and interventricular (VV) delay, selection of the most beneficial LV pacing electrode, or stimulation by multiple electrodes (i.e. multipoint pacing). Multiple optimization strategies are presently available and the best method remains to be established. Electrical (e.g. QRS duration/area; Q on surface ECG to LV sensing interval , QLV) and echocardiographic (e.g. stroke volume; mitral flow) parameters are most widely used in clinical practice although convincing scientific evidence for these methods is lacking. Alternatively, acute CRT response can be assessed by invasive hemodynamic testing in order to optimize device settings.(1) Typically, the maximum rate of LV pressure rise (dP/dt_{max}) is used as an index of ventricular performance.(2) To this purpose, a pressure guidewire is inserted in the LV cavity to perform measurements in a relatively easy and reliable manner. Alternatively, pressure-volume (PV) loops can be obtained by the use of a conductance catheter. A major advantage of the PV approach is that functional measures are provided with information on preload, afterload and contractility allowing to assess underlying physiological mechanisms. Stroke work (SW) incorporates all pressure and volume changes throughout the cardiac cycle and provides a comprehensive appraisal of LV pump function.(1,2)

At present, a direct comparison between invasive CRT optimization strategies is lacking. This study aims to (i) evaluate the acute effect of dP/dt_{max} versus SW guided CRT optimization, and (ii) relate acute changes in hemodynamic parameters to long-term CRT response.

METHODS

Study population

This study is part of the OPTICARE-QLV (Optimization of Cardiac Resynchronization Therapy with a Quadripolar Left Ventricular Lead) study, a multicenter, prospective, observational study. The main aim of the OPTICARE-QLV study was to relate electrical parameters (Q on surface ECG to LV sensing interval, QLV) to acute hemodynamic response in CRT with quadripolar LV leads, using conductance catheter measurements.(3) Inclusion criteria were moderate

to severe heart failure (NYHA class II or III) despite optimal medical therapy, LV ejection fraction ≤35%, sinus rhythm, and left bundle branch block (LBBB) according to the Strauss criteria. The study was performed according to the Declaration of Helsinki and in agreement with the local medical ethics committees. All subjects gave written informed consent.

Baseline procedures

All patients underwent ECG-, echocardiographic-, and cardiac magnetic resonance imaging (CMR) examination prior to device implantation. CRT implantation was performed under local anesthesia following standard procedures. Right ventricular (RV) and right atrial (RA) leads were placed at conventional positions. The quadripolar LV lead (Quartet 1458Q, St. Jude Medical, Saint Paul, Minnesota, United States) was targeted at an anterolateral, lateral, or posterolateral position using the tributaries of the coronary sinus. After lead placement, fluoroscopy images were made in the left anterior oblique (LAO) 40° and in the in the right anterior oblique (RAO) 30° angle to determine the specific position of each quadripolar LV lead electrode.

Stimulation protocol

Immediately after device implantation, a dedicated 7F conductance catheter (12 electrodes; 8, 10 or 12mm spacing; CD Leycom, Zoetermeer, The Netherlands) was inserted via the femoral artery and placed in a stable position in the LV apex. PV loops were recorded during each run of biventricular pacing in-between of baseline recordings with intrinsic conduction (i.e. LBBB). To ensure a stable rhythm, RA pacing with 5-10 bpm above the intrinsic heart rate was maintained throughout the stimulation protocol. The stimulation protocol included four LV pacing configurations using each individual electrode of the quadripolar lead (i.e. D1: distal electrode; M2: mid-distal electrode; M3: mid-proximal electrode; P4: proximal electrode) as cathode and the RV shock-coil as anode. Per pacing configuration, four AV-delays of approximately 80%, 60%, 40% and 20% of the intrinsic AV conduction (RA pacing to RV sensing interval) were programmed, resulting in a total of 16 “pacing runs” (figure 1). The order in which the electrodes were tested was randomized between patients. The VV-delay was fixed at 40ms LV pre-activation.(4)

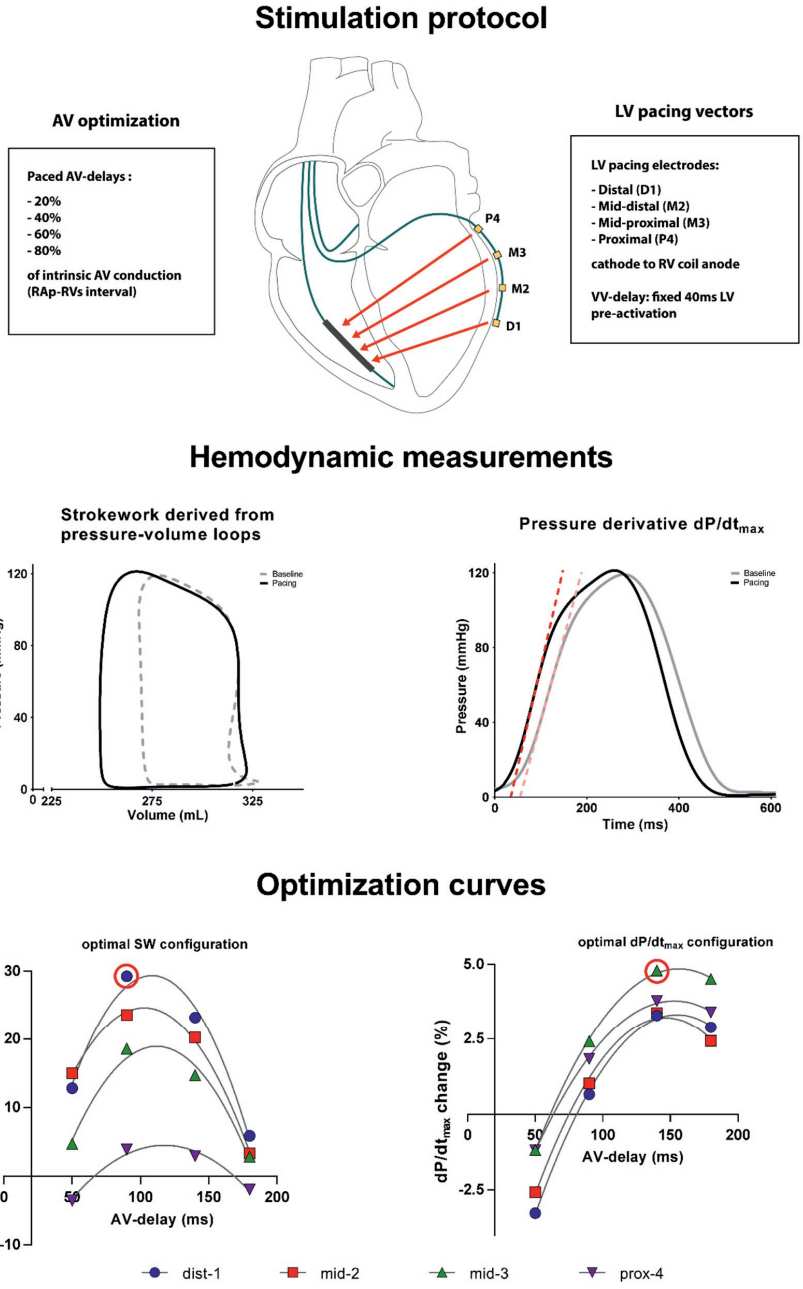


Figure 1: Hemodynamic optimization protocol. The stimulation protocol included four LV pacing configurations using each individual electrode of the quadripolar lead (D1: distal; M2: mid-distal; M3: mid-proximal; P4: proximal electrode). Per electrode, four AV-delays were programmed of approximately 80%, 60%, 40% and 20% of the intrinsic AV conduction. Per setting, acute response to CRT was measured by change in SW and dP/dtmax. The pacing configuration with the highest increase in SW and dP/dtmax was used for comparison.

Hemodynamic measurements

PV loops were constructed using Conduct NT software (version 2.8.1). Approximately 60 representative cardiac cycles per pacing run were averaged, disregarding all inappropriate beats. Baseline-loops were averaged from 30 beats recorded prior and afterwards each pacing run. Subsequently, baseline-loops were calibrated by CMR-derived LV volumes. Patients were excluded if the baseline-loop showed non-physiological characteristics (volume changes during the isovolumic phases) resulting in a hourglass-shaped baseline loop, as judged by two independent experts. LV pump function was quantified by both SW derived from PV loops and the pressure derivative dP/dt_{max}. To account for baseline drift, the effect of each biventricular pacing setting was calculated as the relative change in LV pump function compared with the mean of the two flanking baseline measurements. Optimization curves were used to identify the pacing configurations with the highest increase in SW and dP/dt_{max}, respectively (figure 1). PV indices were compared between the optimal SW and dP/dt_{max} configuration, as well as the conventional CRT configuration. Conventional CRT was defined as pacing the distal electrode with an AV delay of ~120ms. dP/dt_{max} was calculated as the maximum rate of LV pressure rise and SW was directly calculated as the area of the PV loop. In addition, maximal pressure (P_{max}), minimal pressure (P_{min}), pressure rise ($dP_{max-min}$), end-diastolic volume (EDV), end-systolic volume (ESV), stroke-volume (SV), and ejection fraction (EF) were measured. For volumetric measurements, end-diastole was defined at the time of dP/dt_{max} and end-systole was defined at the time of dP/dt_{min}. Effective arterial elastance (E_A) was calculated as end-systolic pressure divided by SV. LV end-systolic elastance (E_{ES}) was estimated by end-systolic pressure divided by end-systolic volume.(5) The specific end-systolic PV point for these measurements was defined as the maximum ratio of LV pressure to volume. Ventricular-arterial (VA) coupling was quantified as E_A/E_{ES}, and mechanical efficiency was calculated as the ratio of SW to the pressure-volume area (PVA) where PVA is the sum of SW and potential energy (PE).(6) The setting programmed in the device before discharge was left to the discretion of the operator. Typically, this was the optimal SW electrode with an adequate sensing signal and capture threshold without evidence of phrenic nerve stimulation.

Echocardiography

Echocardiography was performed before, and six months after CRT implantation. Echocardiographic images were analyzed by a dedicated core lab (University Medical Center Utrecht). LV volumes were measured using the biplane Simpson's method by two experienced observers and calculated as averages of multiple (2-3) consequent beats. Long-term CRT response was calculated as the absolute percent change in LVEF between baseline and follow-up. Patients with ≥10% increase in LVEF were classified as CRT super-responders as this cut-off value is widely used.

Statistical analysis

Continuous variables are expressed as mean ± standard deviation (SD) in case of normal distribution or otherwise as median and interquartile range. Categorical variables are presented as absolute numbers and percentages. Pearson's and Spearman correlations were calculated depending on whether distribution was normal or not. The paired t-test or Wilcoxon signed rank test was used to compare hemodynamic variables between the optimal SW, optimal dP/dt$_{max,}$ and conventional CRT settings. Cohen's Kappa (κ) coefficient was calculated as the level of agreement between the optimal LV lead pacing electrode and electrode position between groups. Receiver operating characteristics (ROC) curve analysis was used to determine the predictive value of hemodynamic parameters for long-term CRT response. The commercially available Statistical Package for Social Sciences software (IBM SPSS Statistics for Windows, Version 22.0, Armonk, NY, USA) was used for statistical analysis. A p-value of <0.05 was considered statistically significant.

RESULTS

Patient population

A total of fifty-one patients were enrolled in the main study, of whom ten were excluded from this analysis. Nine patients were excluded because of unreliable baseline PV loops and one patient was lost to follow-up due to a psychiatric disorder. Patients with unreliable baseline-loops demonstrated larger LVEDV (396±96ml vs. 287±82ms; p=0.002) and lower LVEF (16±2% vs. 26±8%; p=0.001) on CMR compared to patients included in the study. Patient characteristics of the remaining forty-one patients are presented in table 1.

Acute changes in hemodynamic parameters

During conventional CRT (D1 electrode; AV delay ~120ms), dP/dt_{max} increased by 12±9% and SW improved by 53±48% (table 2; figure 2). Compared to conventional CRT, dP/dt_{max} guided optimization (i.e. the setting that resulted in best dP/dt_{max}) resulted in one-third additional dP/dt_{max} change (17±11%; p<0.001), but with a similar SW change (52±45%; p=0.754). The highest dP/dt_{max} was achieved with electrode D1 in twelve (29%), M2 in twelve (29%), M3 in eight (20%) and P4 in nine (22%) patients, (table S1 of the supplemental material). The AV-delay that resulted in optimal dP/dt_{max} was longer compared to conventional CRT (165±41ms vs. 119±13ms; p<0.001).

Compared to conventional CRT, SW guided optimization (i.e. the setting that resulted in best SW) resulted in comparable dP/dt_{max} changes (12±10%; p=0.679), but one-third additional SW increase (80±55%; p<0.001). The largest SW was achieved with electrode D1 in twenty-two (54%), M2 in five (12%), M3 in five (12%) and P4 in nine (22%) patients. On average, the optimal SW AV-delay did not significantly differ from conventional CRT (132±58ms vs. 119±13ms; p=0.191).

Table 1. Patient characteristics at baseline and echocardiographic changes after six months

Variable	Total group (n=41)	Super-responders (n=23)	Others (n=18)	P-value
Age (years)	67 ± 9	65 ± 9	69 ± 8	0.184
Gender (n, % male)	25 (61%)	12 (52%)	13 (72%)	0.192
Etiology (n, % ICMP)	8 (20%)	7 (30%)	1 (6%)	0.046
NYHA class (n, %)				
Class II	29 (71%)	16 (70%)	13 (72%)	
Class III	12 (29%)	7 (30%)	5 (28%)	0.853
Medical history (n, %)				
Diabetes	5 (12%)	1 (4%)	4 (22%)	0.083
Hypertension	15 (37%)	7 (30%)	8 (44%)	0.355
Atrial fibrillation	4 (10%)	2 (9%)	2 (11%)	0.796
Medication (n, %)				
Beta-blocker	31 (76%)	18 (78%)	13 (72%)	0.655
Diuretics	29 (71%)	16 (70%)	13 (72%)	0.853
ACE / ATII inhibitors	40 (98%)	23 (100%)	17 (94%)	0.252
Aldosterone antagonist	26 (63%)	17 (74%)	9 (50%)	0.115
Lab – eGFR (ml/min/1.73m^2)	69 ± 15	73 ± 14	64 ± 16	0.069
Lab – NT-pro BNP (pmol/L)	57 (28 – 134)	51 (28 – 101)	62 (28 – 307)	0.511
ECG – PR duration (ms)	179 ± 30	170 ± 20	190 ± 37	0.029
ECG – QRS width (ms)	167 ± 14	169 ± 15	164 ± 13	0.244
EP – intrinsic AV interval (ms)*	271 ± 53	254 ± 36	293 ± 64	0.020
CMR – LVEDV (ml)	286 ± 83	303 ± 75	265 ± 90	0.148
CMR – LVESV (ml)	216 ± 80	231 ± 66	197 ± 94	0.179
CMR – LVEF (%)	25 ± 8	24 ± 6	28 ± 10	0.141
CMR – Scar on LGE images (n, %)	7 (18%)	2 (9%)	5 (31%)	0.082
CMR – Scar size (% LV mass)**	5 (3 – 16)	2 (1-2)	12 (5-19)	0.095
Follow-up				
Echo – Change in LVEF after six months (%)***	+10 ± 9	+16 ± 6	+2 ± 2	<0.001
Echo – Change in LVESV after six months (%)	-33 ± 18	-41 ± 16	-23 ± 15	<0.001

ICMP, ischemic cardiomyopathy; NYHA class, New York Heart Association functional class; ACE, angiotensin converter enzyme; ATII, angiotensin receptor II; eGFR, estimated glomerular filtration rate; NT-pro BNP, N-terminal prohormone brain natriuretic peptide; AV, atrioventricular; LVEDV, left ventricular end-diastolic volume; LVESV, left ventricular end-systolic volume; LVEF, left ventricular ejection fraction; LGE, late gadolinium enhancement; * intrinsic AV interval measured as right atrial pacing to right ventricular sensing interval **scar size in patients with presence of scar; ***absolute changes in % LVEF

Table 2. Acute hemodynamic changes during conventional CRT and after hemodynamic optimization by dP/dt_{max} and strokework

Variable	Conventional CRT	dP/dt_{max} optimization	SW optimization	P-value conventional vs. dP/dt_{max}	P-value conventional vs. SW	P-value dP/dt_{max} vs. SW
Δ dP/dt_{max} (%)	+12 ± 9	+17 ± 11	+12 ± 10	<0.001	0.679	<0.001
Δ P_{max} (%)	+1 ± 4	+4 ± 4	+1 ± 4	<0.001	0.913	<0.001
Δ P_{min} (%)	-25 ± 15	-26 ± 38	-25 ± 15	0.901	0.949	0.930
Δ $dP_{max-min}$ (%)	+3 ± 5	+6 ± 4	+3 ± 5	<0.001	0.993	<0.001
Δ EDV (%)	+3 ± 10	+4 ± 9	+5 ± 9	0.079	0.017	0.159
Δ ESV (%)	-10 ± 9	-7 ± 9	-12 ± 10	0.013	0.017	<0.001
Δ SV (%)	+52 ± 61	+51 ± 56	+85 ± 70	0.961	<0.001	<0.001
Δ EF (%)*	+9 ± 8	+8 ± 8	+13 ± 8	0.330	<0.001	<0.001
Δ SW (%)	+53 ± 48	+52 ± 45	+80 ± 55	0.754	<0.001	<0.001

dP/dt_{max}, maximum rate of pressure rise; P_{max}, maximal pressure; P_{min}, minimal pressure; $dP_{max-min}$, pressure rise; EDV, end-diastolic volume; ESV, end-systolic volume; SV, stroke volume; EF, ejection fraction; SW, stroke work; *absolute changes in % EF

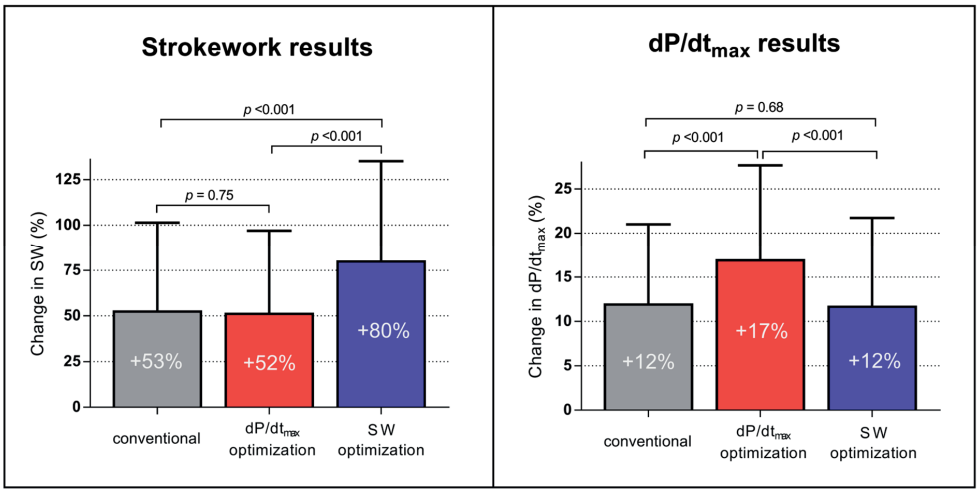


Figure 2: The effect of hemodynamic optimization on acute CRT response. The effect of hemodynamic optimization is illustrated for SW results (left diagram) and dP/dt$_{max}$ results (right diagram). SW guided optimization resulted in one-third additional SW increase compared to conventional CRT without additional dP/dt$_{max}$ changes. dP/dt$_{max}$ guided optimization resulted in one-third additional dP/dt$_{max}$ increase without additional SW benefit.

Comparing both optimization strategies, the optimal dP/dt$_{max}$ configuration differed from the optimal SW configurations by a lack of agreement in pacing electrode (κ -0.3) and a significant difference in AV delay (165±41ms vs. 132±58ms; p=0.001). When evaluating the relation between acute changes in SW and dP/dt$_{max}$ for all pacing configurations of the entire population (n=635), a weak correlation was found (R 0.24; p<0.001), illustrated in figure S1 of the supplemental material. Comparing SW and dP/dt$_{max}$ changes in a per-patient analysis, only nine (22%) patients demonstrated a positive correlation with a correlation coefficient ≥0.5 (figure S2). Comparing changes in hemodynamic parameters between dP/dt$_{max}$ and SW guided strategies, the former showed a larger pressure increase (6±4% vs. 3±5%; p<0.001) whereas SW optimization resulted in a larger SV augmentation (85±70% vs. 51±56%; p<0.001), see figure 3.

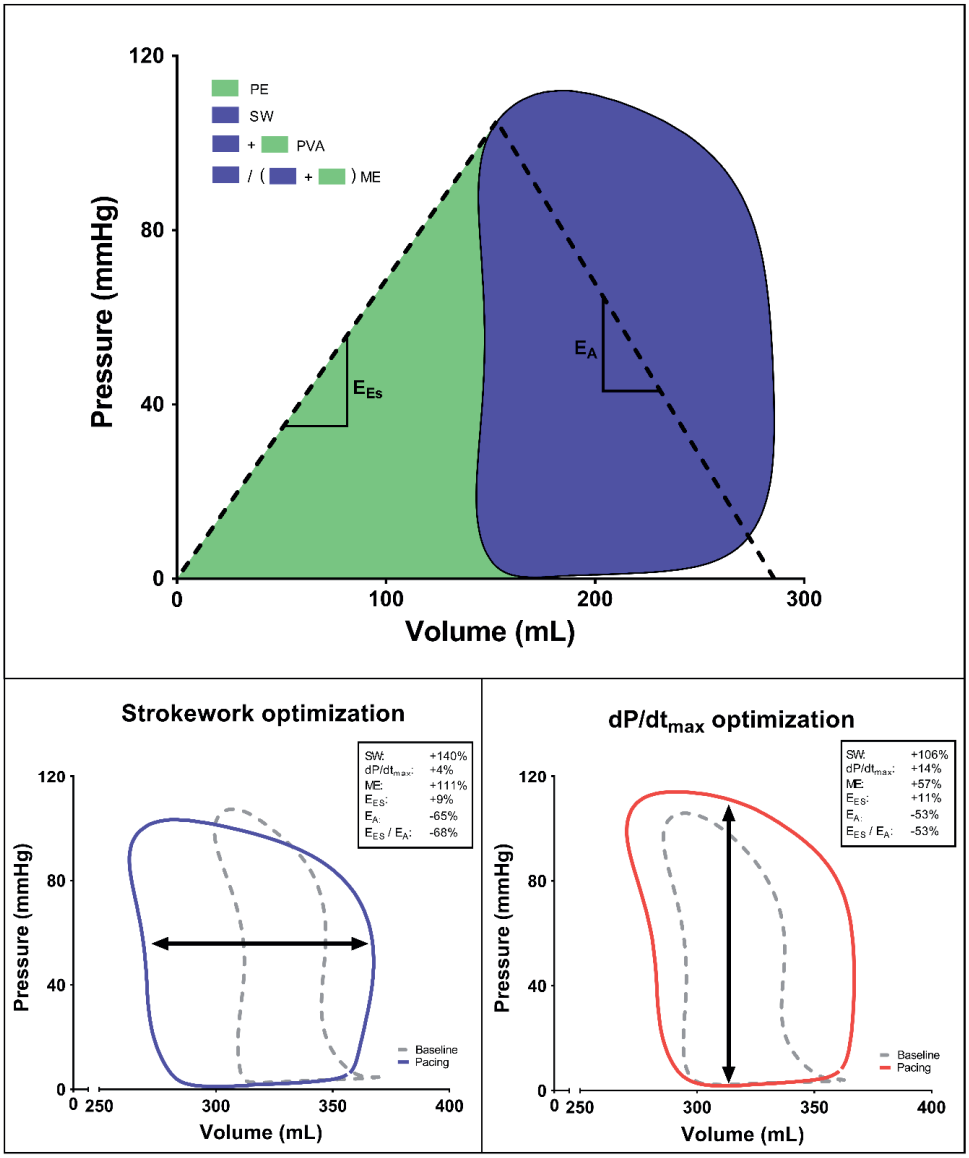


Figure 3: Ventricular-arterial coupling between optimization strategies. Schematic illustration of a PV-loop (top diagram). Typical example of PV-loops in a CRT patient illustrating the effects of SW guided optimization (bottom left diagram) and dP/dt_{max} guided optimization (bottom right diagram). SW optimization results in widening of the PV loop (i.e. SV augmentation) whereas dP/dt_{max} guided optimization results in lengthening of the PV loop (i.e. LV pressure rise increase). The optimal dP/dt_{max} configuration demonstrates highest contractility whereas optimal SW is achieved at lowered arterial load, resulting in improved VA coupling and higher mechanical efficiency.

To study interactions between the LV and the arterial system, table 3 summarizes changes in VA coupling between optimization strategies. Whereas dP/dt_{max} optimization was associated with larger E_{ES} increase compared to SW optimization (8±12% vs. 5±10%; p=0.015), SW optimization showed relatively larger reduction in E_A (44±44% vs. 26±35%; p<0.001). VA coupling at baseline was very unbalanced with E_A/E_{ES} ranging between 4.6 and 4.9. Improvement in E_A/E_{ES} was most pronounced for SW optimization (45±39% vs. 32±32%; p<0.001). Mechanical efficiency was depressed at baseline (SW/PVA: 0.31) with SW optimization resulting in highest mechanical efficiency (39±23% vs. 26±23%; p<0.001) compared to dP/dt_{max} optimization.

Acute changes in hemodynamic parameters in relation to long-term CRT response

Echocardiographic measurements showed high reproducibility with intra-class correlations (ICC) values of 0.95 (EDV); 0.96 (ESV) and 0.93 (EF) for intra-observer variability and ICC values of 0.92 (EDV); 0.95 (ESV) and 0.91 (EF) for inter-observer variability. Absolute LVEF change after six months was 10±9%, with 23 (56%) patients showing ≥10% increase in LVEF (CRT super-responders). For prediction of long-term CRT (super)response, change in SW showed an AUC of 0.78 (p=0.002) as demonstrated in table 4 and figure S3, whereas change in dP/dt_{max} revealed a non-significant AUC of 0.65 (p=0.112). To predict long-term CRT (super)response, an optimal cut-off value of 40% increase in SW change yielded a sensitivity of 96%, specificity of 50%, and positive and negative predictive values of 71% and 90%, respectively. Using this cut-off value, thirty-one (76%) patients were categorized having ≥40% increase in SW and ten (24%) patients with <40% increase, or an decrease in SW. Patients with ≥40% SW increase showed larger improvement in absolute LVEF (13±8% vs. 2±7%; p<0.001) and larger reduction in LVESV (-36±17% vs. -23±16%; p=0.041) at follow-up compared to patients without, illustrated in figure 4. The optimal cut-off value to predict long-term CRT response by change in dP/dt_{max} was 9%. Twenty-one (51%) patients with ≥9% dP/dt_{max} change were compared with twenty (49%) patients without, but no differences in absolute LVEF change (10±10% vs. 10±8%; p=0.939) or LVESV change (-32±21% vs. -34±14%; p=0.704) were found between groups.

Table 3. Acute changes in VA coupling during conventional CRT and after hemodynamic optimization by dP/dt_{max} and strokework

	Baseline	Pacing	Δ (%)	
Arterial load (E_A)				
Conventional CRT	2.6 ± 2.0	1.9 ± 1.2	-26 ± 42	
dP/dt_{max} optimization	2.6 ± 1.9	1.9 ± 1.3	-26 ± 35	
SW optimization	2.7 ± 2.1	1.6 ± 1.1	-44 ± 44	*
Contractility (E_{ES})				
Conventional CRT	0.60 ± 0.25	0.62 ± 0.27	+5 ± 12	
dP/dt_{max} optimization	0.60 ± 0.25	0.65 ± 0.28	+8 ± 12	*
SW optimization	0.60 ± 0.25	0.63 ± 0.26	+5 ± 10	*
VA coupling (E_A/E_{ES})				
Conventional CRT	4.6 ± 2.4	3.3 ± 1.9	-28 ± 37	
dP/dt_{max} optimization	4.7 ± 2.4	3.2 ± 1.6	-32 ± 32	
SW optimization	4.9 ± 2.7	2.7 ± 1.3	-45 ± 39	*
Mechanical efficiency (SW/PVA)				
Conventional CRT	0.31 ± 0.10	0.40 ± 0.13	+29 ± 26	*
dP/dt_{max} optimization	0.31 ± 0.10	0.39 ± 0.13	+26 ± 23	
SW optimization	0.31 ± 0.10	0.42 ± 0.12	+39 ± 23	*

E_A, arterial elastance; dP/dt_{max}, maximum rate of pressure rise; SW, stroke work; E_{ES}, end-systolic elastance; VA, ventricular-arterial; PVA, pressure-volume area. Statistical differences between optimization strategies are marked with an asterisk.

Table 4. Predictive value of hemodynamic parameters for long-term CRT response

Variable	AUC	P-value	Cut-off (%)	Sensitivity (%)	Specificity (%)	PPV (%)	NPV (%)
Δ dP/dt$_{max}$	**0.65**	0.112	≥ +9	65	67	71	60
Δ P$_{max}$	**0.60**	0.297	≤ +1	63	44	64	50
Δ P$_{min}$	**0.69**	0.035	≤ -26	54	72	72	54
Δ dP$_{max-min}$	**0.58**	0.374	≤ +3	58	56	64	50
Δ EDV	**0.51**	0.916	≥ +4	63	44	60	47
Δ ESV	**0.70**	0.031	≤ -12	58	78	78	58
Δ SV	**0.72**	0.015	≥ +45	83	61	74	73
Δ EF	**0.73**	0.010	≥ +9*	71	61	71	61
Δ SW	**0.78**	0.002	≥ +40	96	50	71	90

For abbreviations, see table 2; *absolute changes in % EF

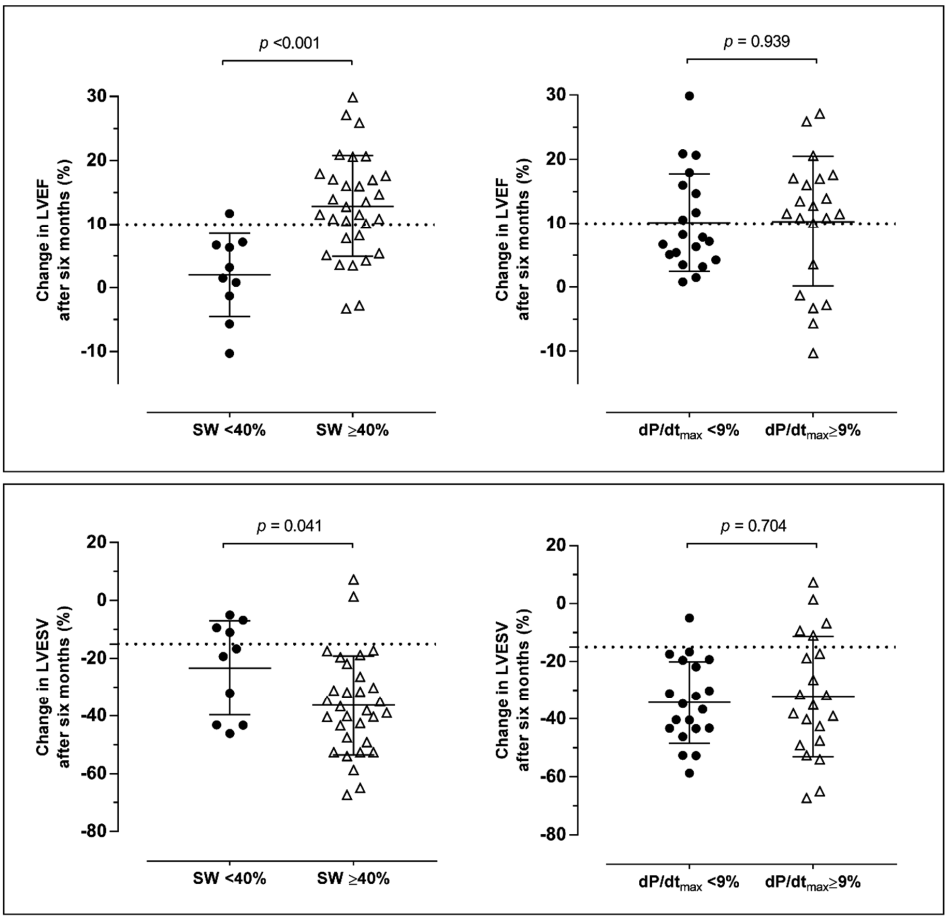


Figure 4: Acute CRT response and echocardiographic changes after six months. Scatter plots illustrating long-term echocardiographic absolute changes in LVEF (upper panel) and LVESV (lower panel) for patient stratification by SW changes (left diagrams) and dP/dt_{max} changes (right diagrams).

DISCUSSION

The present study demonstrates that PV guided hemodynamic optimization of the LV pacing electrode and AV delay in CRT with quadripolar leads results in approximately one-third additional SW improvement on top of conventional CRT. Hemodynamic optimization by the pressure derivate dP/dt_{max} also showed one-third additional dP/dt_{max} improvement compared to conventional CRT. Improvement in one parameter, however, did not coincide with the other indicating two different mechanisms. Whereas dP/dt_{max} optimization favored LV

contractility (expressed as E_{ES}), SW optimization improved ventricular-arterial coupling leading to higher stroke volume and ejection. Acute changes in SW showed higher predictive value for long-term CRT response compared to change in dP/dt_{max}.

Hemodynamic optimization strategies

Previous studies showed that invasive hemodynamic optimization in CRT can be used to guide LV lead placement,(3,7-12) find the optimal AV- and VV-delay,(4,13,14) and evaluate benefit from multi-site stimulation.(12,15-17) A standardized approach for invasive optimization, however, is lacking as part of these studies used dP/dt_{max},(4,7,10-14,16) while others used SW as optimization parameter.(3,8,9,14-17) Although the two strategies have been used interchangeably in literature, previous work from our group showed a discordant relationship between dP/dt_{max} and SW improvement among CRT candidates.(18) Pappone et al. found that even within an individual patient, changes in the two parameters were often poorly correlated.(16) The present study confirms previous findings, and extends these by evaluating the effect of invasive hemodynamic optimization by dP/dt_{max} versus SW on cardiac performance in CRT with quadripolar LV leads. Each optimization strategy resulted in approximately 1/3 additional improvement in the parameter used for optimization. Improvement in one parameter, however, did not coincide with the other (figure 2). These findings indicate that although CRT with quadripolar LV leads provides substantial room for hemodynamic optimization, results differ significantly between optimization strategies. Interestingly, dP/dt_{max} guided optimization resulted in longer AV-delays (165ms, 63% of intrinsic AV interval) compared to SW guided optimization (132ms, 49% of intrinsic AV interval). Possibly, these longer AV-delays allow for fusion of the intrinsic AV conduction and LV capture (i.e. fusion pacing) which has been shown to favor dP/dtmax.(19) Comparing hemodynamic effects, marked differences were observed in LV pressure rise and stroke volume between optimization strategies. Whereas dP/dt_{max} optimization favored LV pressure rise (i.e. height increase of the PV loop), SW optimization rather showed SV augmentation (i.e. widening of the PV loop), see figure 3. Increases in SV involved small changes in EDV and large ESV reduction. These changes can be explained by different interactions between the LV and the arterial system influencing ventricular performance by alterations in

cardiac afterload (i.e. VA coupling). Under normal conditions, the VA system is closely coupled with an E_A/E_{ES} ratio of 0.6-1.2 to achieve optimal work and mechanical efficiency.(20) In chronic HF, however, depressed systolic function (low E_{ES}) coupled to a high arterial impedance (high E_A) will result in a state of afterload mismatch with severely elevated E_A/E_{ES}.(21) Previous studies showed that CRT directly improves VA coupling by enhancing LV systolic performance (E_{ES}) and reducing net arterial load (E_A).(22,23) The immediate reduction in afterload has been ascribed to acute effects of CRT on the sympathetic nerve activity.(24,25) Our results are in line with previous findings, demonstrating enhanced VA coupling during biventricular pacing as a result of beneficial changes in both determinants (i.e. E_{ES} increase and E_A reduction). When comparing VA coupling between optimization strategies, dP/dt_{max} optimization resulted in highest E_{ES} rise whereas SW optimization showed most reduction in E_A. Net changes in VA coupling were most pronounced for SW optimization with 45% reduction in E_A/E_{ES}.

One must consider that LV systolic function is affected by changes in preload, afterload and contractility. Since additional increases in SW are achieved under conditions of equal contractility (defined as E_{ES}) and comparable preload (defined as EDV), enhanced VA coupling may be considered an important mechanism of CRT response (i.e. SW optimization ≈ VA optimization). Interestingly, it has been described that improvements in cardiac function during CRT are obtained at diminished energy cost indicating enhanced mechanical efficiency.(26) Mechanical efficiency can be calculated from the PV loop by the ratio of SW (i.e. external work) to the pressure-volume area (PVA). The latter reflects the total mechanical energy that is generated by the LV.(27) SW optimization demonstrated highest improvement in mechanical efficiency (39%) relative to dP/dt_{max} optimization (26%) and conventional CRT (29%). These differences may be important since therapeutic interventions that enhance mechanical efficiency have proven to be beneficial with respect to outcome.(28)

Acute hemodynamic changes and long-term CRT response

Previous studies that examined the predictive value of dP/dt$_{max}$ changes for long-term CRT response yielded conflicting results. Duckett et al. showed that the rise in dP/dt$_{max}$ accurately predicted reverse remodeling after CRT at a cut-off value of 10%.(29) However, their results are not supported by several other studies. Two studies (one of our group in a different population) found dP/dt$_{max}$ changes to be unrelated to reverse remodeling after CRT.(30,31) In addition, two more studies found no relationship between acute change in dP/dt$_{max}$ and cardiac morbidity or survival.(32,33) Results of the present study add to the accumulating evidence opposing a relationship between acute changes in dP/dt$_{max}$ and long-term CRT outcome. Although the optimal cut-off value that we found is similar to the one found by Duckett et al., patients with acute dP/dt$_{max}$ increase ≥9% lacked favorable long-term CRT response compared to patient with <9% (figure 4).

Acute changes in SW, on the other hand, accurately predicted long-term CRT response with an optimal cut-off value of 40%. Recently, our group was the first to demonstrate a clear association between acute SW increase and reverse remodeling after six months of CRT.(30) Acute SW response accurately predicted ≥15% reduction in LV end-systolic volume (LVESV) at an optimal cut-off value of 20% in a mixed population of wide- and narrow QRS complex patients. The present study, however, included only patients with strict LBBB (Strauss definition). The presence of favorable patient characteristics associated with large CRT benefit, combined with the PV-guided hemodynamic optimization protocol resulted in almost every patient becoming a CRT responder following the ≥15% LVESV reduction definition (6 non-responders). Therefore, we used the alternative definition of ≥10% absolute LVEF increase to identify “super-responders” resulting in a lower response rate (18 non-responders). The stricter definition of CRT response explains the higher cut-off value of 40% SW change that we found in the present study. Still, acute changes in SW showed high sensitivity for prediction of long-term CRT response, similar to previous findings.(30) In other words, patients lacking acute SW response are unlikely to become responders at the long-term. This was underlined by ten SW non-responders, of which only one became a long-term responder (figure 4).

Limitations

Some limitations need to be taken into consideration. Due to the invasive nature of the study protocol, the sample size may be considered relatively small. Furthermore, we only included patients with strict LBBB (Strauss criterion) resulting in a homogenous population with a low number of ischemic cardiomyopathy and transmural scar. Moreover, a relatively large part of patients was excluded from the present analysis because of unreliable baseline PV loops. These patients demonstrated severe LV dilation with low ejection fractions on CMR. As a result, electrical conductance is measured in a large blood-pool with minimal volume changes throughout the cardiac cycle, resulting in a low signal-to-noise ratio. Baseline PV-loops showed large volume changes during the isovolumic phases, resulting in a hourglass-shaped loop. Underestimation of the baseline loop results in excessive SW changes during biventricular pacing, overestimating LV pump function changes. Although these measurements can still be used to determine the optimal pacing configuration (the patient serves as its own control), absolute changes in SW do not adequately reflect benefit from CRT. Lastly, the effect of hemodynamic optimization on long-term CRT response was not investigated in comparison with a control group. Since the optimal SW setting was typically used for programming, this may have introduced bias.

Clinical application

The development of quadripolar leads offers new possibilities and challenges in the field of CRT. Multiple stimulation sites are now offered from a single lead, increasing opportunities for CRT optimization strategies.(34) Hemodynamic optimization showed to be highly rewarding with an additional one-third increase in acute CRT response. Although non-invasive methods are searched to optimize settings, previous findings of the OPTICARE-QLV demonstrated that (i) electrical (QLV) parameters were unable to identify the most beneficial pacing electrode of a quadripolar lead,(3) (ii) optimal AV-delays varied substantially between patients,(35) and (iii) benefit from multipoint pacing was hard to predict from baseline parameters.(17) The use of other non-invasive methods such as echocardiography or electrocardiographic markers also remain to be proven. For now, invasive hemodynamic optimization strategies may therefore be considered the gold standard approach to optimize benefit from CRT.(1)

However, the conductance technique is invasive, limited available in clinical practice, and not suitable for all patients. The additional time duration of the stimulation protocol was about 60 minutes but because the protocol was performed after wound closure (using the programmer), there was no additional risk of device infection. There was one complication of ventricular fibrillation (on entering the LV with the guidewire) that was successfully treated by cardiac defibrillation. No perforation, stroke or bleeding was observed. Although invasive hemodynamic optimization is unfeasible in clinical practice, the concept of volume-based optimization may guide future implementation of non-invasive surrogates of LV volume changes such as changes in intra-cardiac impedance, or stimulation in the CMR environment. It should be noted, however, that non-invasive surrogates do not always translate to direct hemodynamic measurements.

CONCLUSION

Pressure-volume guided hemodynamic optimization in CRT results in approximately one-third additional SW improvement on top of conventional CRT. Hemodynamic optimization by the pressure derivate dP/dt_{max} showed a similar one-third additional dP/dt_{max} improvement compared to conventional CRT. Improvement in one parameter, however, did not coincide with the other indicating different mechanisms. Whereas dP/dt_{max} optimization favored LV contractility (expressed as Ees), SW optimization improved ventricular-arterial coupling leading to higher stroke volume and ejection. Ultimately, acute changes in SW showed larger predictive value for long-term CRT response compared to dP/dt_{max}. Pressure-volume guided hemodynamic optimization may therefore be considered a potential strategy to use the full potential of CRT with quadripolar leads.

REFERENCES

1. Burkhoff D. Pressure-volume loops in clinical research: a contemporary view. J Am Coll Cardiol 2013;62:1173-6.
2. Kass DA, Maughan WL, Guo ZM, Kono A, Sunagawa K, Sagawa K. Comparative influence of load versus inotropic states on indexes of ventricular contractility: experimental and theoretical analysis based on pressure-volume relationships. Circulation 1987;76:1422-36.
3. van Everdingen WM, Zweerink A, Cramer MJ et al. Can We Use the Intrinsic Left Ventricular Delay (QLV) to Optimize the Pacing Configuration for Cardiac Resynchronization Therapy With a Quadripolar Left Ventricular Lead? Circulation: Arrhythmia and Electrophysiology 2018;11.
4. Bogaard MD, Meine M, Tuinenburg AE, Maskara B, Loh P, Doevendans PA. Cardiac resynchronization therapy beyond nominal settings: who needs individual programming of the atrioventricular and interventricular delay? Europace 2012;14:1746-53.
5. Steendijk P, Tulner SA, Bax JJ et al. Hemodynamic effects of long-term cardiac resynchronization therapy: analysis by pressure-volume loops. Circulation 2006;113:1295-304.
6. Nozawa T, Yasumura Y, Futaki S, Tanaka N, Uenishi M, Suga H. Efficiency of energy transfer from pressure-volume area to external mechanical work increases with contractile state and decreases with afterload in the left ventricle of the anesthetized closed-chest dog. Circulation 1988;77:1116-24.
7. Butter C, Auricchio A, Stellbrink C et al. Effect of resynchronization therapy stimulation site on the systolic function of heart failure patients. Circulation 2001;104:3026-9.
8. Dekker AL, Phelps B, Dijkman B et al. Epicardial left ventricular lead placement for cardiac resynchronization therapy: optimal pace site selection with pressure-volume loops. J Thorac Cardiovasc Surg 2004;127:1641-7.
9. Delnoy PP, Ottervanger JP, Luttikhuis HO et al. Pressure-volume loop analysis during implantation of biventricular pacemaker/cardiac resynchronization therapy device to optimize right and left ventricular pacing sites. Eur Heart J 2009;30:797-804.
10. Gold MR, Auricchio A, Hummel JD et al. Comparison of stimulation sites within left ventricular veins on the acute hemodynamic effects of cardiac resynchronization therapy. Heart Rhythm 2005;2:376-81.
11. Kass DA, Chen CH, Curry C et al. Improved left ventricular mechanics from acute VDD pacing in patients with dilated cardiomyopathy and ventricular conduction delay. Circulation 1999;99:1567-73.
12. Zanon F, Baracca E, Pastore G et al. Multipoint pacing by a left ventricular quadripolar lead improves the acute hemodynamic response to CRT compared with conventional biventricular pacing at any site. Heart Rhythm 2015;12:975-81.
13. Auricchio A, Stellbrink C, Block M et al. Effect of pacing chamber and atrioventricular delay on acute systolic function of paced patients with congestive heart failure. The Pacing Therapies for Congestive Heart Failure Study Group. The Guidant Congestive Heart Failure Research Group. Circulation 1999;99:2993-3001.
14. Verbeek XA, Vernooy K, Peschar M, Cornelussen RN, Prinzen FW. Intra-ventricular resynchronization for optimal left ventricular function during pacing in experimental left bundle branch block. J Am Coll Cardiol 2003;42:558-67.

15. de Roest GJ, Wu L, de Cock CC et al. Bifocal left ventricular stimulation or the optimal left ventricular stimulation site in cardiac resynchronization therapy: a pressure-volume loop study. Europace 2016;18:1030-7.
16. Pappone C, Calovic Z, Vicedomini G et al. Multipoint left ventricular pacing improves acute hemodynamic response assessed with pressure-volume loops in cardiac resynchronization therapy patients. Heart Rhythm 2014;11:394-401.
17. van Everdingen WM, Zweerink A, Salden OAE et al. Pressure-Volume Loop Analysis of Multipoint Pacing With a Quadripolar Left Ventricular Lead in Cardiac Resynchronization Therapy. JACC: Clinical Electrophysiology 2018.
18. de Roest G, Knaapen P, Gotte M et al. Stroke work or systolic dP/dtmax to evaluate acute response to cardiac resynchronization therapy: are they interchangeable? Eur J Heart Fail 2009;11:706-8.
19. van Gelder BM, Bracke FA, Meijer A, Pijls NH. The hemodynamic effect of intrinsic conduction during left ventricular pacing as compared to biventricular pacing. J Am Coll Cardiol 2005;46:2305-10.
20. De Tombe PP, Jones S, Burkhoff D, Hunter WC, Kass DA. Ventricular stroke work and efficiency both remain nearly optimal despite altered vascular loading. Am J Physiol 1993;264:H1817-24.
21. Borlaug BA, Kass DA. Ventricular-vascular interaction in heart failure. Cardiol Clin 2011;29:447-59.
22. Pieragnoli P, Perego GB, Ricciardi G et al. Cardiac resynchronization therapy acutely improves ventricular-arterial coupling by reducing the arterial load: assessment by pressure-volume loops. Pacing Clin Electrophysiol 2015;38:431-7.
23. Zocalo Y, Bia D, Armentano RL et al. Resynchronization improves heart-arterial coupling reducing arterial load determinants. Europace 2013;15:554-65.
24. Hamdan MH, Barbera S, Kowal RC et al. Effects of resynchronization therapy on sympathetic activity in patients with depressed ejection fraction and intraventricular conduction delay due to ischemic or idiopathic dilated cardiomyopathy. Am J Cardiol 2002;89:1047-51.
25. Gademan MG, van Bommel RJ, Ypenburg C et al. Biventricular pacing in chronic heart failure acutely facilitates the arterial baroreflex. Am J Physiol Heart Circ Physiol 2008;295:H755-60.
26. Ukkonen H, Beanlands RS, Burwash IG et al. Effect of cardiac resynchronization on myocardial efficiency and regional oxidative metabolism. Circulation 2003;107:28-31.
27. Takaoka H, Takeuchi M, Odake M, Yokoyama M. Assessment of myocardial oxygen consumption (Vo2) and systolic pressure-volume area (PVA) in human hearts. Eur Heart J 1992;13 Suppl E:85-90.
28. Knaapen P, Germans T, Knuuti J et al. Myocardial energetics and efficiency: current status of the noninvasive approach. Circulation 2007;115:918-27.
29. Duckett SG, Ginks M, Shetty AK et al. Invasive acute hemodynamic response to guide left ventricular lead implantation predicts chronic remodeling in patients undergoing cardiac resynchronization therapy. J Am Coll Cardiol 2011;58:1128-36.
30. de Roest GJ, Allaart CP, Kleijn SA et al. Prediction of long-term outcome of cardiac resynchronization therapy by acute pressure-volume loop measurements. Eur J Heart Fail 2013;15:299-307.

31. Stellbrink C, Breithardt OA, Franke A et al. Impact of cardiac resynchronization therapy using hemodynamically optimized pacing on left ventricular remodeling in patients with congestive heart failure and ventricular conduction disturbances. J Am Coll Cardiol 2001;38:1957-65.
32. Bogaard MD, Houthuizen P, Bracke FA et al. Baseline left ventricular dP/dtmax rather than the acute improvement in dP/dtmax predicts clinical outcome in patients with cardiac resynchronization therapy. Eur J Heart Fail 2011;13:1126-32.
33. Suzuki H, Shimano M, Yoshida Y et al. Maximum derivative of left ventricular pressure predicts cardiac mortality after cardiac resynchronization therapy. Clin Cardiol 2010;33:E18-23.
34. van Everdingen WM, Cramer MJ, Doevendans PA, Meine M. Quadripolar Leads in Cardiac Resynchronization Therapy. JACC Clin Electrophysiol 2015;1:225-237.
35. van Everdingen WM, Zweerink A, Salden OAE et al. Atrioventricular optimization in cardiac resynchronization therapy with quadripolar leads: should we optimize every pacing configuration including multi-point pacing? Europace 2018.

SUPPLEMENTAL MATERIAL

Table S1. Device programming during conventional CRT and after hemodynamic optimization by dP/dt_{max} and strokework

Variable	Conventional CRT	dP/dt_{max} optimization	SW optimization	Kappa / P-value conventional vs. dP/dt_{max}	Kappa / P-value conventional vs. SW	Kappa / P-value dP/dt_{max} vs. SW
Electrode (n, %)						
D1	41 (100%)	12 (29%)	22 (54%)			
M2	0	12 (29%)	5 (12%)	Κ 0.0 (0.0 – 0.0)	Κ 0.0 (0.0 – 0.0)	Κ -0.3 (-0.2 – 0.2)
M3	0	8 (20%)	5 (12%)			
P4	0	9 (22%)	9 (22%)			
Circumferential position (n, %)						
Anterior	0	0	0			
Anterolateral	4 (10%)	7 (17%)	7 (17%)	Κ 0.5 (0.2 – 0.7)	Κ 0.5 (0.3 – 0.8)	Κ 0.5 (0.3 – 0.8)
Lateral	23 (56%)	26 (63%)	26 (63%)			
Posterolateral	14 (34%)	8 (20%)	8 (20%)			
Posterior	0	0	0			
Longitudinal position (n, %)						
Basal	0	13 (32%)	11 (27%)	Κ 0.3 (0.0 – 0.5)	Κ 0.5 (0.3 – 0.7)	Κ 0.2 (-0.1 – 0.4)
Mid	29 (71%)	21 (51%)	19 (46%)			
Apical	12 (29%)	7 (17%)	11 (27%)			
Paced AV delay (ms)	119 ± 13	165 ± 41	132 ± 58	p<0.001	p=0.191	p=0.001
Paced AV delay (% intrinsic AV interval)*	45 ± 9	63 ± 14	49 ± 19	p<0.001	p=0.352	p<0.001

*intrinsic AV interval measured as right atrial pacing to right ventricular sensing interval

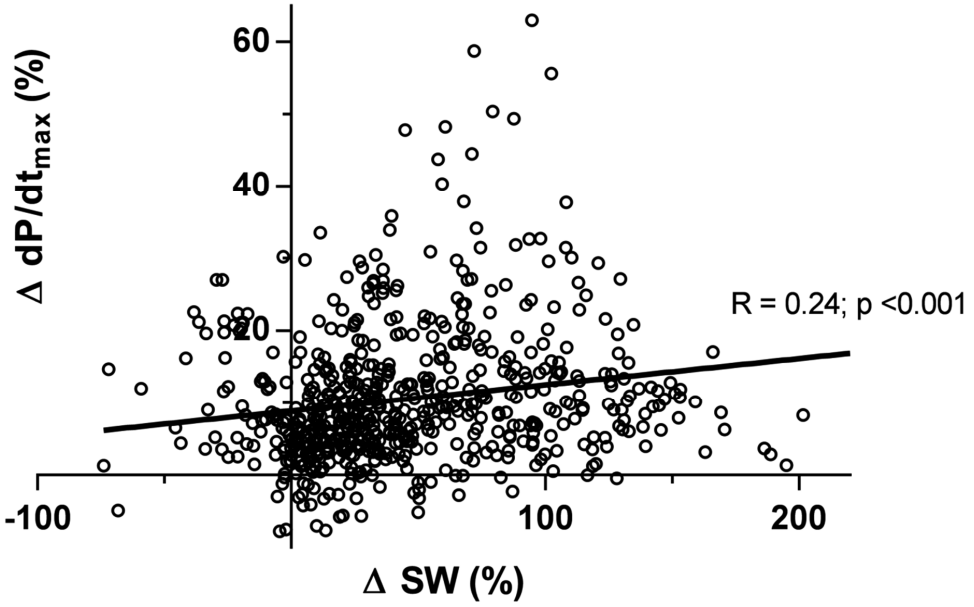


Figure S1: Relation between changes in SW and dP/dt_{max} for the total group. The relation between change in SW (x-axis) and change in dP/dt_{max} (y-axis) per pacing configuration is illustrated for the total group.

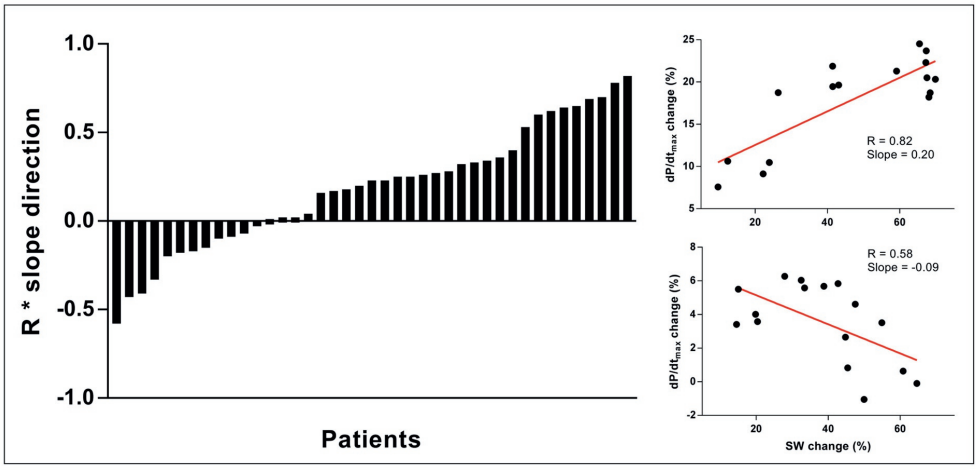


Figure S2: Relation between changes in SW and dP/dt_{max} per patient analysis. The relation between changes in SW and dP/dt_{max} per individual is illustrated by the slope direction multiplied by the correlation coefficient (R) of the trend line. Twenty-nine patients demonstrated a positive slope (patient example in upper right corner) whereas twelve patients demonstrated a negative slope (patient example in lower right corner). Only nine patients demonstrated a positive correlation with R ≥0.5.

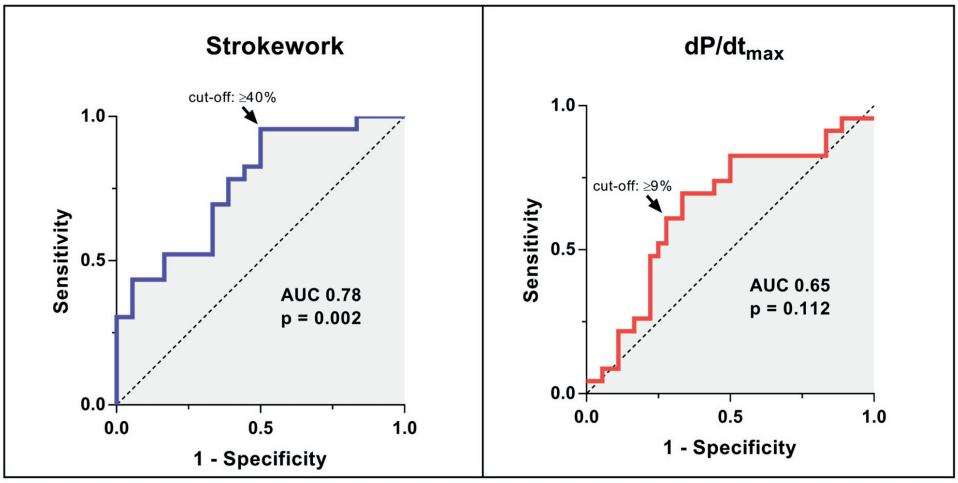


Figure S3: Predictive value of SW and dP/dt$_{max}$ for long-term CRT response. ROC curve analysis for predicting long-term CRT response by changes in SW (left diagram) and by changes in dP/dt$_{max}$ (right diagram).

Chapter 12

Chronotropic Incompetence in Chronic Heart Failure: A State-of-the-Art Review

Circ Heart Failure 2018;11:e004969

Alwin Zweerink
Anne-Lotte C.J. van der Lingen
M. Louis Handoko
Albert C. van Rossum
Cornelis P. Allaart

ABSTRACT

Chronotropic incompetence (CI) is generally defined as the inability to increase the heart rate (HR) adequately during exercise to match cardiac output (CO) to metabolic demands. In patients with heart failure (HF), however, this definition is unsuitable since metabolic demands are unmatched to CO in both conditions. Moreover, HR dynamics in HF patients differ from those in healthy subjects and may be affected by beta-blocking medication. Nevertheless, it has been demonstrated that CI in HF is associated with reduced functional capacity and poor survival. During exercise the normal heart increases both stroke volume and HR, whereas in the failing heart contractility reserve is lost thus rendering increases in CO primarily dependent on cardio-acceleration. Consequently, insufficient cardio-acceleration due to CI may be considered a major limiting factor in the exercise capacity of HF patients. Despite the profound effects of CI in this specific population, the issue has drawn limited attention over the past years and is often overlooked in clinical practice. This might partly be caused by a lack of standardized approach to diagnose the disease, further complicated by changes in HR dynamics in the HF population which render reference values derived from a normal population invalid. Cardiac implantable electronic devices (ICD; CRT) now offer a unique opportunity to study HR dynamics and provide treatment options for CI by rate-adaptive pacing using an incorporated sensor that measures physical activity. This review provides an overview of disease mechanisms, diagnostic strategies, clinical consequences and state-of-the-art device therapy for CI in HF.

INTRODUCTION

The term chronotropic incompetence (CI) was introduced in 1975 by M.H. Ellestad and M.K. Wan in a paper describing a high incidence of coronary events observed after a reduced heart rate (HR) response during treadmill stress testing.(1) Shortly after this observation it was found that a substantial part of the heart failure (HF) population had impaired chronotropic response during exercise testing.(2,3) Subsequently, in the 1980's, pacemakers were equipped with sensors of physical activity and rate-responsive pacing emerged as a therapeutic option for patients with CI. Despite interest on this topic in the ensuing years, scientific focus in the field of HF shifted towards the other component of cardiac output - stroke volume (or ejection fraction). Currently, implantable cardiac device technology is widely applied in the HF population, with modern implantable cardioverter defibrillators (ICD) and cardiac resynchronization therapy (CRT) devices offering the option for CI detection and treatment using physiological sensors that measure metabolic need during physical activity. Despite the high prevalence and significant impact of CI in the HF population, it remains unrecognized in clinical practice. Device-based treatment options for the large proportion of the HF population implanted with a cardiac device, might renew interest in the topic of CI.

HEART RATE DYNAMICS

In the normal heart, spontaneous depolarization of specialized pacemaker cells in the sinoatrial node drives intrinsic HR which is approximately 100 beats per minute (bpm). Modulation of the intrinsic HR by the autonomic nervous system is the result of dynamic balance of sympathetic- and parasympathetic influences.(4) While the parasympathetic nervous system predominates at rest, slowing the HR to 70 bpm on average, exercise results in withdrawal of parasympathetic and increase of sympathetic activity causing the heart to accelerate. After termination of exercise, sympathetic withdrawal and increased parasympathetic tone normally result in a rapid HR decline. During adult life, the maximum achievable HR drops with age which is partly due to a reduced ß-adrenergic responsiveness decreasing the ability to augment the HR above the intrinsic HR. However, the decline in peak HR mainly depends on a gradual decline of the intrinsic HR.(5) The intrinsic HR can be assessed by autonomic

denervation induced by dual pharmacological blockade of both the sympathetic and parasympathetic pathways. Jose and Collison showed the intrinsic HR to decrease approximately 0.5 bpm per year, a rate similar to the decrease of maximum HR.(6)

CI is defined as the inability of the heart to increase its rate appropriate to increased activity or demand.(7) In the dynamic process of HR regulation during exercise, incompetence of heart rate response may either present as a delayed heart rate increase, submaximal peak heart rate, heart rate instability during exercise, or an inadequate heart rate recovery (figure 1).



Figure 1: Types of chronotropic incompetence during exercise testing. During cardiopulmonary exercise testing, chronotropic incompetence may present as a submaximal peak heart rate (A), delayed heart rate response (B), heart rate instability during the test (C), or an inadequate heart rate recovery afterwards (D). Control curves and curves of chronotropic incompetence (CI) are normalized for exercise time. Figure adapted from reference 4 with permission.

Traditionally, however, CI is diagnosed when a person reaches a significantly lower maximum HR during maximal exertion in comparison with a group of age-matched controls. The reference value, the Age Predicted Maximal HR (APMHR), is classically described by the equation of Astrand et al: [220 – age].(8) Several cut-off values have been proposed to define a pathological chronotropic response, of which 80% of the APMHR (%pHR) is typically used. Although still widely accepted, Astrand's formula has been shown to overestimate maximal HR in younger subjects, while underestimating it in older persons.(9) The exact mechanisms of CI have not been elucidated, although factors contributing to CI include sinus node dysfunction, ischemic heart disease, autonomic dysfunction and LV dysfunction as will be discussed later.(10) Since the introduction of the term CI in 1975, this phenomenon has repeatedly proved to be an independent predictor of mortality in the general population,(1,11-14)

CHRONOTROPIC INCOMPETENCE IN CHRONIC HEART FAILURE

Exercise capacity in heart failure

Heart failure is characterized by the inability of the heart to maintain or increase cardiac output (CO) during exercise to meet aerobic requirements. In chronic HF, decreased CO leads to peripheral skeletal muscle wasting (catabolic state) and worsening symptoms of early muscular fatigue and dyspnea during physical activity.(15) The 'gold standard' for assessment of functional capacity is cardiopulmonary exercise testing (CPET) with measurement of peak oxygen consumption (pVO_2).(16) pVO_2 is calculated using Fick's laws of diffusion and is the product of CO and the arteriovenous oxygen difference (AO_2 - VO_2). Acute changes in oxygen consumption during physical activity are mainly dependent on an increase in CO which is the product of HR and stroke volume (SV). Comparing 237 chronic HF patients to 118 healthy age-matched controls, Witte and colleagues demonstrated that exercise capacity was markedly reduced in HF, with a pVO_2 difference of approximately 40% (HF: 20.1 vs. control: 34.4 mL/kg/min).(17) A similar shortfall in pVO_2 is reported comparing healthy controls and HF patients with preserved EF (HFpEF).(18-22)

Whereas the normal heart increases both SV and HR during exercise, contractility reserve is depressed in the failing heart thus rendering increases in CO primarily dependent on cardio-acceleration. Consequently, insufficient cardio-acceleration (i.e. CI) may be a major limiting factor in the exercise capacity

of heart failure patients. Witte et al. found a linear correlation between change in HR and pVO_2 as illustrated in figure 2. This link between chronotropic response and exercise capacity was confirmed by later studies.(23-26)

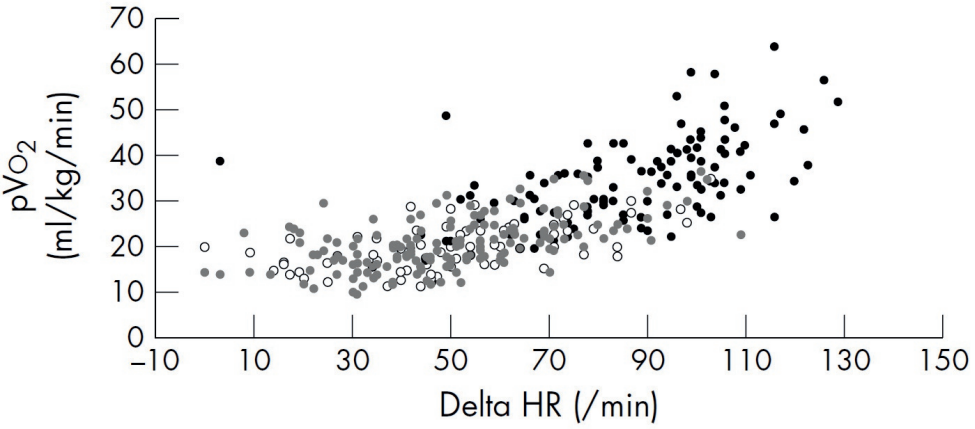


Figure 2: Relation between change in heart rate and exercise capacity. Relation between change in HR and peak oxygen consumption (pVO2) in HF patients with (grey circles) and without (open circles) beta blocking medication, and non-HF control subjects (black circles). Similar correlations were demonstrated between HR change and pVO2 for each group (R 0.56, p<0.001; R 0.60, p<0.001; R 0.53, p<0.001, respectively). However, whether CI is cause or consequence of a limited exercise capacity cannot be distinguished. Figure reproduced from reference 17 with permission.

Key studies investigating the effects of CI on exercise capacity in HF patients show 12-23% lower pVO_2 values for CI patients compared to non-CI HF patients as summarized in table 1. Despite the clear association between CI and impaired exercise capacity in HF patients, causality is debated. Moreover, the definition of CI overlaps with the definition of HF, and it may be hard to distinguish between the two. CI could also be considered a logical consequence of the reduced exercise performance in advanced stages of HF. Whether CI is the cause or the consequence of impaired exercise capacity is important, as CI now serves as a potential therapeutic target for implantable cardiac device technology in HF patients.

Table 1. Key studies investigating the effects of CI on the exercise capacity in heart failure patients

Study	Sample size (n)	Age (years)	BB (%)	LV dysf.	CI criteria	CI present (%)	pVO_2 no CI (mL/kg/min)	pVO_2 CI (mL/kg/min)	Δ pVO_2 CI vs no CI (%)
***Witte et al.*(17) 2006**	237	67 ± 11	69%	mean EF 32%	<80% APMHR	43%	21.2 ± 5.5	18.6 ± 5.3	-12% (p<0.001)
					<80% HRR	72%	22.4 ± 4.8	17.8 ± 4.8	-21% (p<0.001)
***Brubraker et al.*(24) 2006**	102	69 ± 6	N/A	57% EF ≤35%	<85% APMHR or <0.8 chronotropic index	23%	14.6 ± 0.4	12.4 ± 0.8	-15% (p=0.01)
***Jorde et al.*(41) 2008**	278	51 ± 10	72%	77% EF <30%	<80% APMHR	46%	19.9 ± 5.8	15.4 ± 4.7	-23% (p<0.001)
***Al Naijar et al.*(23) 2012**	411	65 ± 11	66%	16% mild 47% mod 36% sev	<80% APMHR	42%	21.1 ± 6.0	18.0 ± 5.6	-15% (p<0.001)
***Magri et al.*(26) 2012**	549	62 ± 11	100%	mean EF 36%	<80% APMHR	61%	17.4 ± 4.8	14.4 ± 3.8	-17% (p<0.001)
					<80% HRR	84%	18.2 ± 5.1	15.1 ± 4.2	-17% p<0.001
***Magri et al.*(42) 2014**	1045	58 ± 12	82%	mean EF 28%	<70% APMHR	32%	17.5 ± 4.4	14.9 ± 4.1	-15% (p<0.001)
					<65% HRR	69%	17.1 ± 4.4	14.8 ± 4.1	-13% (p<0.001)
Jamil et al.(25) 2016	147	74 (66-78) mild-mod 72 (63-80) sev	92%	39% mild-mod 61% sev	<0.8 chronotropic index	73%	17.6 ± 6.0	15.0 ± 5.2	-15% (p<0.001)

BB, beta blocker; LV dysf, left ventricular dysfunction; CI, chronotropic incompetence; pVO_2, peak oxygen consumption; EF, ejection fraction; APMHR, age predicted maximal heart rate; HRR, heart rate reserve; chronotropic index = HRR / metabolic reserve; N/A, not available

Pathophysiology of chronotropic incompetence

The modern pathophysiologic approach towards heart failure is based on the 'neurohormonal model'.(27) This model describes activation of physiological compensatory mechanisms after the initial decline of left ventricular (LV) pump function in an attempt to maintain functional capacity. Increased myocardial stretch of the failing heart induces release of natriuretic peptides, an initial regulatory mechanism, followed by activation of the adrenergic (i.e. sympathetic) signaling pathway and the renin-angiotensin-aldosterone system. Natriuretic peptides increase HR directly by stimulating ionic currents of the sinoatrial node myocytes.(28) Subsequently, increased cardiac filling pressures lead to HR augmentation by activation of the cardiopulmonary baroreceptors stimulating the adrenergic pathway.(29) Despite initially compensating for the reduced cardiac output, this increases myocardial oxygen demand, ischemia and oxidative stress. Moreover, high catecholamine levels induce peripheral vasoconstriction and increase both pre- and afterload, generating additional stress to the cardiac muscle. As HF progresses, this compensatory mechanism gets increasingly activated for further support to the failing heart. Increased catecholamines such as norepinephrine (NE) increase contractile function, induce cardiac myocyte hypertrophy, and further increase HR. Concurrently, chronic sympathetic over-activation leads to downregulation and desensitization of cardiac β-receptors which is thought to be the main mechanism of CI in HF patients.(30) This was illustrated for the first time by Colluci et al.(31) In their study, HF subjects demonstrated NE peak levels during exercise comparable to normal subjects, but the increase in HR for any given increase in NE was markedly reduced. In addition, HR response after NE infusion was markedly reduced in HF patients suggesting decreased β-adrenergic sensitivity of the sinoatrial node. This was confirmed by a later study in which the ΔHR/ΔlogNE ratio, used as an index of sinoatrial node sympathetic responsiveness, was shown to decrease progressively from mild chronic heart failure to severe chronic heart failure.(30) Other studies by Bristow and colleagues demonstrated that chronic adrenergic over-activation in HF patients leads to downregulation of β-adrenergic receptor density in the myocardium.(32-35) Furthermore, heart failure is a state of increased sympathetic tone and decreased vagal activity, which may lead to a phenomenon of "accentuated antagonism". This describes an interplay of

sympathetic and parasympathetic effects where the impact of sympathetic activation on HR decreases with increasing parasympathetic tone and knowledge of both is essential to interpretation of HR responses.(36)

Recently, a pathophysiologic distinction was made between increased resting HR and attenuated exercise HR response found in HF patients.(37) Benes et al. studied the neurohormonal profiles in a group of 81 patients with advanced systolic HF and 25 age-, sex, and body-size matched controls. Resting HR correlated with markers of myocardial stress and inflammation, while HR response during exercise was correlated with levels of NE and copeptin reflecting neurohormonal overstimulation. In line with previous reports, sinus node responsiveness to NE was diminished in the HF patients compared to the healthy subjects. In summary, an imbalanced autonomic nervous system is mainly accountable for limited HR modulation in HF patients. However, slowing of the intrinsic HR by sinus node remodeling during the HF process might contribute to the reduction in maximal HR, although this has not been scientifically proven.(38)

Diagnosis of CI

A standardized approach to diagnosis of CI in HF is currently lacking. Instead, multiple approaches have been proposed, each with associated advantages and disadvantages. Traditionally, CI is diagnosed when a person reaches a significantly lower maximum HR during exertion in comparison with a group of age-matched controls. However, the traditional [220 – age] formula for APMHR, derived from a healthy population, does not apply to patients with cardiovascular diseases (CVD) taking associated medications, as demonstrated by Brawner et al.(39) In a cross-validation group of patients with CVD, they showed the [220-age] equation to overestimate the maximal HR by 40±19 bpm. Based on a sub-study of the HF-ACTION trial with 767 symptomatic HF patients on beta-blocking medication, Keteyian et al. formulated a two-variable equation for estimation of the APMHR in HF: [119 + 0.5(resting HR) – 0.5(age)]. This formula was superior to the standard [220 - age] equation although a standard error of approximately 18 bpm remained present reflecting a substantial amount of individual variation. Refining the APMHR formula improved prediction of peak HR in the HF population and might be used in clinical practice as a reference value during exercise testing. However, since most HF studies investigating

clinical consequences of CI used the traditional [220 - age] formula, cut-off values to diagnose CI using alternative equations are unknown. New studies are needed to define equation-specific cut-off values for assessment of CI.

An alternative approach to evaluate chronotropic response is to relate peak achievable HR to resting HR, the so-called HR response, which is defined as the difference between resting HR and peak HR at maximal exertion. Subsequently, HR reserve (HRR) can be calculated by dividing HR response by the difference between resting HR and APMHR: HRR = [(peak HR – resting HR) / (APMHR – resting HR) * 100]. Usually a cut-off value of 80% of the age-predicted heart rate reserve (%pHRR) is used to determine CI. The advantage of HRR is that it measures HR dynamics rather than a static peak HR value during exercise. In patients with severely elevated resting HR, however, HRR is decreased while peak HR might be normal.

For each diagnostic approach to detect CI, the patient must reach maximal exertion during the exercise test. Other reasons for test termination like chest pain or orthopedic concerns render the result invalid. Since maximal exertion in HF patients may be blunted by co-morbidities, deconditioning, medication, or by heart failure itself, it can be difficult to factor in exactly how much true limitations in achievable HR play a role in this phenomenon. To quantify patient effort in an objective way, respiratory gas exchange analysis can be used to assess the respiratory exchange ratio (RER). This ratio, defined as VCO2/VO2, increases during graded exercise until maximal exertion. Presently a cut-off value of ≥1.05 is generally accepted to ensure maximal exertion. In case of an RER value of <1.05, an alternative approach to evaluate chronotropic response has been proposed by Wilkoff and Miller.(40) They relate chronotropic response to work rate (i.e. HRR / metabolic reserve = chronotropic index) during different grades of exercise testing. The metabolic reserve is measured by metabolic equivalents (METS) and is defined as ($METS_{stage}$ – $METS_{rest}$) / ($METS_{peak}$ – $METS_{rest}$). A chronotropic index <0.8 usually defines CI. Although this method has the advantage of correction for physical fitness, it is not routinely used.

Prevalence rates

Prevalence rates of CI in the HF population vary substantially dependent on definition and cut-off value used.(17,23-26,41,42) Furthermore, prevalence rates might be influenced by medication as will be discussed later. Most studies determined CI by using either 80% of the APMHR or 80% of the HRR as a cut-off during cardiopulmonary exercise testing. Prevalence rates using APMHR vary from 42% to 61% whereas rates are higher using HRR (72% to 84%, see table 1). Recently, a large multicenter study examined 1045 HF patients and used several APMHR and HRR cut-off values to define CI.(42) Although patient characteristics in this study are comparable to those mentioned above, reported prevalence rates of CI are slightly higher with 64% using <80% APMHR and 88% using <80% HRR. The effects of different cut-off values for APMHR and HRR to calculate the prevalence of CI are illustrated in figure 3. However, as stated earlier, reference values used for APMHR of HRR pertain to the healthy population which may lead to overestimation in the HF population.

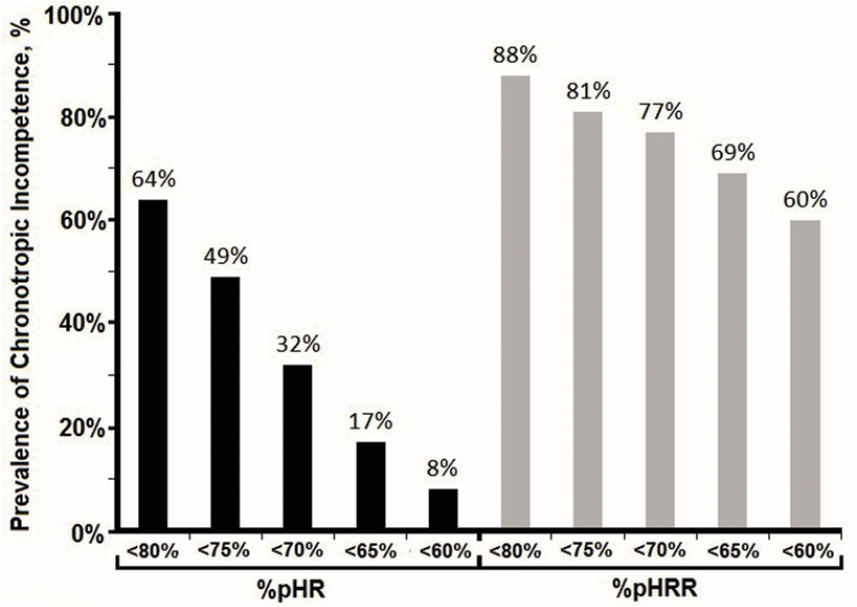


Figure 3: Prevalence of chronotropic incompetence by measured peak heart rate and heart rate reserve at different cut-off values. Prevalence of chronotropic incompetence in the heart failure population may vary dependent on the definition and cut-off value used. %pHR: percentage age-predicted peak heart rate; %pHRR: percentage age-predicted heart rate reserve. Figure reproduced from reference 42 with permission.

Prognosis

Several studies proved the presence of CI in the HF population to be a prognostic marker of adverse events.(37,42,43) Dobre et al. performed a sub-study in 1118 HF patients of the HF-ACTION trial and found a HRR <60% during exercise testing to be associated with increased all-cause mortality and all-cause hospitalization.(43) Magri et al. investigated multiple definitions of CI in a cohort of 1045 HF patients (figure 4).(42) The prognostic values of either percentage APMHR (%pHR) or percentage HRR (%pHRR) were found to be highly dependent on the cut-off value used. A cut-off value of 65% for %pHR and 70% for %pHRR showed optimal results with each parameter being independently related to cardiovascular mortality with a hazard ratio of 2.04 and 1.77, respectively. Kaplan-Meier curves for both definitions of CI are presented in figure 3. However, the prevalence of CI was low for the %pHR <65% definition (17% CI) whereas prevalence was high using the %pHRR <70% definition (77% CI). Despite the clear association, no causal relationship has been proven between CI and mortality in HF patients.

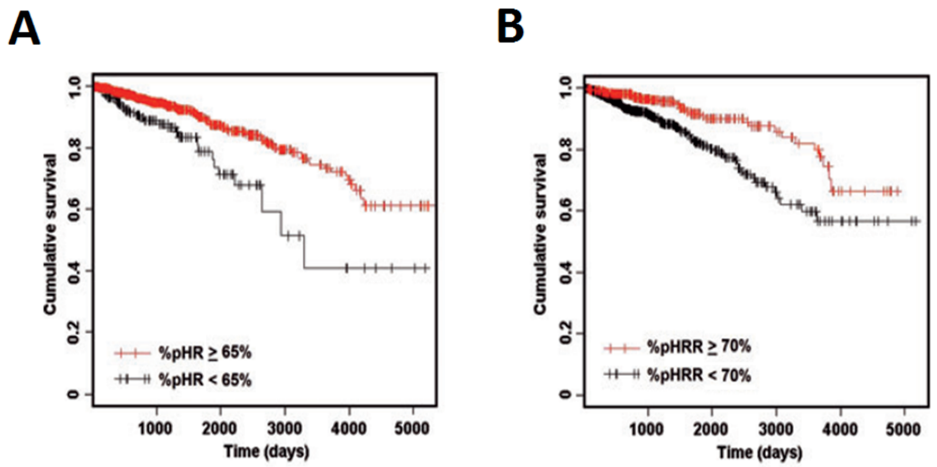


Figure 4: Survival of heart failure patients with and without chronotropic incompetence. Kaplan-Meier curves comparing cardiovascular mortality of heart failure patients with (black line) and without (red line) chronotropic incompetence using cut-off values of (A) 65% age-predicted peak heart rate (%pHR) and (B) 70% age-predicted heart rate reserve (%pHRR). Each variable was found to be an independent predictor of cardiovascular mortality (hazard ratio 2.04 and 1.77, respectively). Figure adapted from reference 42 with permission.

Alternatively, delayed heart rate recovery after cessation of exercise can be used as a prognostic marker although this measure not necessarily reflects CI. Several studies showed that HR recovery after CPET can be used as a prognostic marker for mortality in HF patients.(44,45) The optimal cut-off values found in these studies, however, are inconsistent ranging from a decline of 4 to 12 bpm.(44-46) Moreover, resting HR itself can be used to predict adverse events.(47-49) In chronic HF patients of the CHARM study, baseline resting HR in those with sinus rhythm was associated with increased mortality, with every 10 bpm increase associated with increases of 8% in all-cause mortality.(50) A recent study by Vazir et al. in a cohort of chronic HF patients showed that changes in resting HR over time can predict adverse outcome, such that a rise in HR was found to be associated with elevated risk and a drop in HR with reduced risk.(51) Given these findings, HR dynamics (i.e. peak HR, HR recovery, resting HR) might be used for risk stratification of HF patients in current practice.

Medication effects

Drug therapies are the cornerstone of treatment in chronic HF. Multiple types of HF medication can potentially confound assessment of CI, including beta blockers, selective sinoatrial node inhibitors and anti-arrhythmic drugs. Effects of beta blocking medication have received most scientific interest over the years.(52) Several large-scale studies showed that the use of beta blocking therapy is associated with CI in the HF population(17,23,53), irrespective of medication dosage.(26) Cessation of beta blocking therapy subsequently increases peak HR during exercise but does not fully normalize chronotropic response as shown by Hirsh et al.(54) In contrast with these findings, a study by Jorde et al. could not demonstrate a difference in beta-blocking therapy usage between CI and non-CI patients with severe HF.(41) It could be speculated that the beta-blocking effect on CI becomes less pronounced in advanced stages of the disease. In line with this concept, a relatively large medication effect was observed in healthy subjects after administration of beta blockers, with a 16-25% reduction in peak HR during exercise.(55)

Although CI is linked to poor clinical outcome, reducing HR by therapeutic agents shows a paradoxical beneficial effect on survival. Underlying mechanisms for these contrasting results are only partially understood. Beta blockers which antagonize the activated sympathetic system reduce both resting- and peak HR.

Slowing resting HR reduces mortality in patients with heart failure. In a meta-analysis of 23 beta-blocker HF trials including a total of 19.000 patients, mortality benefit was related to the magnitude of resting HR reduction.(56) In contrast, lowering peak HR (i.e. induction of CI) is associated with unfavorable outcome. Hung and colleagues demonstrated in a large population of 64.549 patients that %pHR was inversely associated with all-cause mortality, but beta-blocker treatment significantly attenuated this relation.(53) Patients on beta-blocking therapy who achieved 65% pHR showed a similar adjusted mortality rate as those not on beta-blocking therapy who achieved 85% pHR. Accordingly, CI in a patient taking beta-blocking medication may not reflect the same hazard as in one without, because of the cardio-protective role of beta-blockers.

The relatively new therapeutic agent ivabradine, a selective sinoatrial node inhibitor, proved to be beneficial for HF patients in the landmark SHIFT trial.(57) This double-blind randomized controlled trial included 6505 patients with a resting HR over 70 bpm despite optimal medical therapy (90% on beta-blockers) and showed the addition of ivabradine to reduce resting HR as well as the risk of cardiovascular events. In a 24-h holter ECG sub-study among 602 patients, a significant improvement in HR variability and various parameters of parasympathetic activity was demonstrated after 8 months of additional treatment of ivabradine compared to placebo.(58) Another sub-study with 275 patients undergoing echocardiography demonstrated reduced effective arterial elastance (i.e. cardiac afterload) as an underlying hemodynamic mechanism of isolated HR reduction which may contribute to the beneficial outcome of ivabradine-treated patients with heart failure.(59) Scientific data assessing the effect of ivabradine on peak HR during exercise are scarce. Two small-scale studies found ivabradine treatment to be beneficial for the exercise capacity of HF patients,(60,61) but one of them found peak HR during exercise to increase after ivabradine therapy(60) whereas peak HR was decreased in the other.(61) A recent publication by Jamil et al. presented a series of investigations including an interventional randomized crossover study investigating the effects of ivabradine on exercise capacity in chronic HF patients.(25) In twenty-six patients with sinus rhythm, a single-dose of ivabradine 7.5 mg reduced resting HR and peak HR during exercise, without affecting the HR rise or exercise capacity. The effect of ivabradine on chronotropic response is therefore uncertain. Lastly, exercise capacity can be improved by the combination of beta-blockers and

ivabradine in comparison to beta-blockers alone. In the CARVIVA HF trial with 131 HF patients, ivabradine as well as the combination of carvedilol plus ivabradine after 12 weeks of treatment improved exercise capacity and quality of life, but carvedilol alone did not.(62)

Heart failure with preserved ejection fraction

HFpEF is characterized by increased LV filling pressures due to diastolic dysfunction which becomes especially overt during exercise.(63) Increased filling pressures lead to activation of the sympathetic pathway, similar to the pathophysiology of HF with reduced ejection fraction (HFrEF). Borlaug et al. compared exercise capacity of HFpEF patients and hypertensive cardiac hypertrophy matched controls.(18) Their results indicate that exercise capacity was more depressed in HFpEF patients which could not be ascribed to relaxation abnormalities. Significant differences in chronotropic response and vasodilator reserve were found indicating autonomic dysfunction in HFpEF patients. In agreement with these findings, a recent paper by Kosmala et al. showed chronotropic responses to be gradually impaired during progressive stages of HFpEF.(64) Whether reversal of the CI improves exercise capacity in HFpEF patients is uncertain, as increases in HR may compromise LV filling in these patients with prolonged relaxation. It could be speculated that CI functions more as a compensatory protective mechanism in HFpEF patients. The RESET study was designed to evaluate the effect of HR augmentation by rate-adaptive pacing in patients with mild to moderate HFpEF, but unfortunately this trial was suspended due to lack of enrollment.(65)

Heart transplant recipients

Iatrogenic CI in heart transplant recipients, as a result of autonomic denervation, is considered to be an important determinant of a limited exercise capacity following heart transplantation. However, HR dynamics tend to improve over the first post-operative year by a concomitant decrease of resting HR and increase of peak HR together with an increase of $pVO_{2.(66)}$ This partial reversal of CI may be due to increased sensibility of the graft sinus node to circulating catecholamines, or by sympathetic re-innervation of the graft.(67) When resting HR remains higher than 100 bpm, these patients are at higher risk for mortality compared to those with resting HR lower than 100 bpm.(68) Endurance training as well as rate-adaptive pacing may improve chronotropy and physical fitness level in heart transplant recipients as will be discussed below.(69,70)

THERAPIES FOR CHRONOTROPIC INCOMPETENCE IN HEART FAILURE

Exercise training

Exercise training improves cardiorespiratory fitness in HF patients with both reduced and preserved EF.(71) Improvements in fitness level are associated with changes in markers of autonomic function including HR variability and HR recovery.(72,73) In a study by Keteyian and colleagues, a total of 51 HF patients were randomized to an exercise program of approximately 72 half-hour training sessions over 24 weeks, or control group.(74) Seventy-eight percent of the patients in the exercise group tested positive for CI (%pHR <85%) during baseline testing. In the exercise group, peak HR increased ~7% whereas it remained unchanged in the control group. Comparing CI and non-CI patients in the exercise group, the former achieved a ~10% increase in peak HR and a ~14% increase in pVO_2 after the training program whereas peak HR and pVO_2 were relatively unchanged in non-CI patients. Changes in HR reserve were strongly correlated to changes in pVO_2 (R 0.75). On the other hand, no changes were found in the ratio of HR reserve to norepinephrine reserve, suggesting sinoatrial node sympathetic responsiveness to be unaltered. These results indicate that exercise training improves chronotropic responsiveness in HF patients with CI, but specific mechanisms remain unclear.

Detection of Chronotropic Incompetence by implantable electronic devices

Technological advances in sensor technology and pacing algorithms for conventional bradycardia-pacemakers have now been integrated into implantable electronic devices for the HF population, such as ICD and CRT devices. In line with international guidelines, a substantial part of the HFrEF population is currently equipped with these devices, which offers the unique opportunity to study HR dynamics. Recently, the group of Wilkoff introduced the Heart Rate Score (HRSc), a novel device histogram-based marker of chronotropic performance.(75,76) The HRSc is defined as the percentage of all sensed and paced atrial events in the single tallest 10 bpm histogram bin. For example, when all events occur in the 60-70 bpm bin, the HRSc is 100%. When events are distributed over a wider range with rates below 60 bpm and over 70 bpm, the HRSc becomes lower. Using a cut-off value of 70%, Wilkoff et al. demonstrated that the HRSc independently predicted 5-year mortality in a large population of 57.893 ICD and 67.929 CRT-D patients.(76) These findings do not necessarily indicate a causal relationship between reduced HR dynamics and poor prognosis, as reduced HRSc may also reflect decreased levels of physical activity in sicker patients. As a measure for CI, HRSc has not been compared to regularly used measures such as %pHR and HRR. In contrast with previously discussed measures for CI, however, HRSc assessment does not require maximal exertion and might provide an alternative for the diagnosis of CI. In patients without an implanted device, the HRSc can be obtained using holter monitoring.

Rate-adaptive pacing using activity sensors

In 1967, rate-adaptive pacing was introduced as a pacemaker feature for patients with CI to restore “physiological” HR response to daily physical activities.(77) Rate-adaptive pacemakers control HR using a single activity sensor, or a combination of sensors. The accelerometer (XL) is the oldest and most widely used sensor that measures postural changes and body movements during physical activity. The XL offers rapid response to exercise with high sensor reliability, but specificity is low and the sensor is relatively unresponsive to forms of exercise where the upper body remains in a static state, such as cycling. Also, exercise intensity might be under- or overestimated, as walking down the stairs generates similar HR increases as walking up the stairs. Other sensors use more physiological surrogates of physical exercise such as shortening of the QT interval

or changes in right ventricular impedance during the cardiac cycle (CLS, closed loop stimulation).(78) These measures are surrogates for the inotropic state and offer high specificity for physical exertion and good sensor reliability, but with moderate speed of response and moderate proportionally to metabolic needs.(79) Another physiological approach to measure metabolic activity is by measuring respiratory minute ventilation (MV) which offers high specificity, good proportionality to metabolic needs, high sensor reliability, but with moderate speed of response.(79) Since no single sensor is flawless in the imitation of sinus node behavior, different sensors with complementary characteristics may be combined. The most common combination includes an activity sensor to induce a rapid response to exercise, and a metabolic sensor (i.e. QT interval, CLS, or MV) that provides a delayed but proportional and stable acceleration to sustained exercise and deceleration during recovery. A combined approach with blended XL and MV sensors restored chronotropic response more favorably than a XL sensor alone in CI pacemaker patients in the LIFE study.(80)

Rate-adaptive pacing and prognosis

When applying rate adaptive pacemaker therapy to a patient, a clear distinction should be made between ventricular stimulation and atrial stimulation. It is well known that right ventricular pacing results in ventricular desynchronization which reduces LV stroke volume, therefore increases in HR by ventricular pacing do not necessarily translate to an increase in CO.(81) Wilkoff et al. showed in the Dual Chamber and VVI Implantable Defibrillator (DAVID) trial that programming dual chamber rate-adaptive (DDDR) pacing with an atrioventricular interval ~180ms resulted in nearly 60% ventricular pacing.(82) This was associated with a significant increase in adverse events compared to ventricular backup pacing and the trial was prematurely stopped. Atrial pacing, on the other hand, maintains physiological ventricular activation and preserves mechanical synchrony. In the DAVID II trial, fixed-rate atrial (AAI-70) pacing resulted in similar survival compared to ventricular backup-only pacing and was considered a safe therapy.(83) A recent study among 1.154 CRT-D patients with HRSc ≥70% from the ALTITUDE population showed that rate-responsive pacing (DDDR) using an accelerometer lowered the HRSc from 88% to 78%.(75) This decrease in HRSc was associated with a significant survival benefit compared to a group of matched patients without rate-adaptive pacing (DDD), see figure 5. In non-CI

patients with HRSc <70%, on the other hand, there was no survival benefit of the DDDR over DDD pacing. Despite these promising results, further validation in a randomized controlled trial setting is needed. These findings indicate that appropriate (i.e. CI) patient selection is important for rate-adaptive pacing therapy to be a potential successful therapy. It might also explain why Martin et al. found no benefit in all-cause mortality and heart failure morbidity of DDDR pacing compared to DDD mode in an unselected population of 1.433 CRT patients in the multi-center PEGASUS CRT trial.(84)

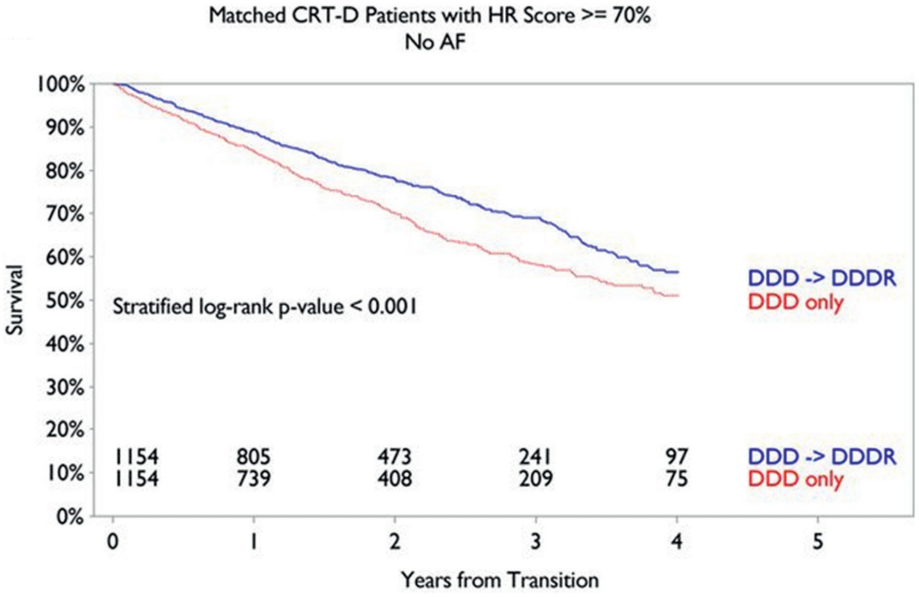


Figure 5: Rate-adaptive pacing improves survival in heart failure patients with chronotropic incompetence diagnosed using a heart rate score. In CRT patients with chronotropic incompetence measured by a heart rate score (HRSc) ≥70%, reprogramming the device from DDD mode to DDDR mode (i.e. rate-adaptive pacing on) improved (i.e. lowered) the HRSc and was associated with improved survival (Hazard Ratio 0.74, p<0.001). AF: atrial fibrillation. Figure reproduced from reference 75 with permission.

Rate-adaptive pacing and exercise capacity

Assuming a causal link between CI and the limitation in exercise capacity in HF patients, reversal of CI by rate-adaptive pacing should increase exercise capacity. Conflicting results exist on this topic. Studies investigating effects of rate-adaptive pacing on exercise capacity in HF patients with CI are summarized in table 2. Tse and colleagues were the first to report a small interventional study providing rate adaptive pacing to 20 HF patients with CRT who tested positive for CI (APMHR <85%).(85) Eleven patients with severe CI, reflected by APMHR <70%, achieved significantly higher peak HR and pVO_2 during exercise with rate-adaptive pacing on compared to off, whereas patients 70-85% APMHR did not (Figure 6). The authors conclude that in HF patients with severe CI, rate-adaptive pacing using CRT provides incremental benefit on exercise capacity. Recently, these findings were confirmed in a study by Palmisano et al. investigating effects of rate-responsive pacing in 60 HF patients with CRT who underwent atrioventricular junction ablation because of permanent refractory atrial fibrillation.(86) These patients with iatrogenic CI demonstrated an acute improvement in walking distance during 6MWT when rate-responsive pacing was applied using an accelerometer. Walking distance improved linearly in relation to the increases in HR during rate-responsive pacing. Contradictory results were found by Sims and colleagues who studied 13 HF patients with CRT and severe CI (<70% APMHR) in a randomized double-blind crossover pilot study.(87) In nine patients, peak HR increased by approximately 20% and was associated with a 5% improvement of 6MWT distance. However, pVO2 did not differ between DDDR and DDD mode. In the remaining four (31%) patients, the DDDR mode using default settings did not result in rate-adaptive pacing. Other studies investigating the effects of rate-adaptive pacing in less severe stages of CI showed disappointing effects on exercise capacity in HF patients. Thielen et al. performed a small-scale study investigating the effects of rate-adaptive pacing in 14 CRT patients with CI (<85% APMHR) and performed echocardiographic examination during CPET.(88)

Table 2. Studies investigating the effects of rate-adaptive pacing on exercise capacity in heart failure patients with CI

Study	Sample size (n)	Age (years)	Rhythm	LV dysf.	CI criteria	device type	activity sensor / pacemaker mode	endpoints	results
Tse et al.(85) 2005	20	65 ± 3	sinus rhythm	mean EF 28%	<70% APMHR (n = 11)	CRT	accelerometer DDDR mode	CPET	~20% increase pVO_2 (p<0.05)
					70-85% APMHR (n = 9)				unchanged pVO_2 (p=ns)
***Thielen et al.*(88) 2008**	14	62 ± 3	sinus rhythm	mean EF 31%	<85% APMHR	CRT	unknown sensor DDDR mode	Doppler echocardiography / CPET	~15% increase CO (p=0.001) unchanged pVO_2 (p=ns)
***Passman et al.*(89) 2009**	10	57 ± 14	sinus rhythm	mean EF 24%	no CI criteria	dual chamber ICD	accelerometer AAIR mode	CPET	unchanged pVO_2 (p=ns)
***Sims et al.*(87) 2011**	13	59 ± 16	sinus rhythm	mean EF 17%	<70% APMHR	CRT	unknown sensor DDDR mode	6MWT / CPET	~5% increase 6MWT distance (p=0.05) unchanged pVO_2 (p=ns)
***Jamil et al.*(25) 2016**	79	74 ± 8	sinus rhythm (n=53)	mean EF 33%	no CI criteria	various	unknown sensor unknown mode	CPET	unchanged pVO_2 (p=ns)
			atrial fibrillation (n=26)						unchanged pVO_2 (p=ns)
Palmisano et al.(86) 2017	60	70 ± 12	biv. pacing	mean EF 40%	100% 'iatrogenic' CI after AV nodal ablation	CRT	accelerometer VVIR mode	6MWT	~8% increase 6MWT distance (p<0.001)

LV dysf, left ventricular dysfunction; CI, chronotropic incompetence; EF, ejection fraction; APMHR, age predicted maximal heart rate; CRT, cardiac resynchronization therapy; pVO2, peak oxygen consumption; CPET, cardiopulmonary exercise testing; CO, cardiac output; ICD, implantable cardiac defibrillator; 6MWT, six minute walking test; biv, biventricular; AV, atrioventricular

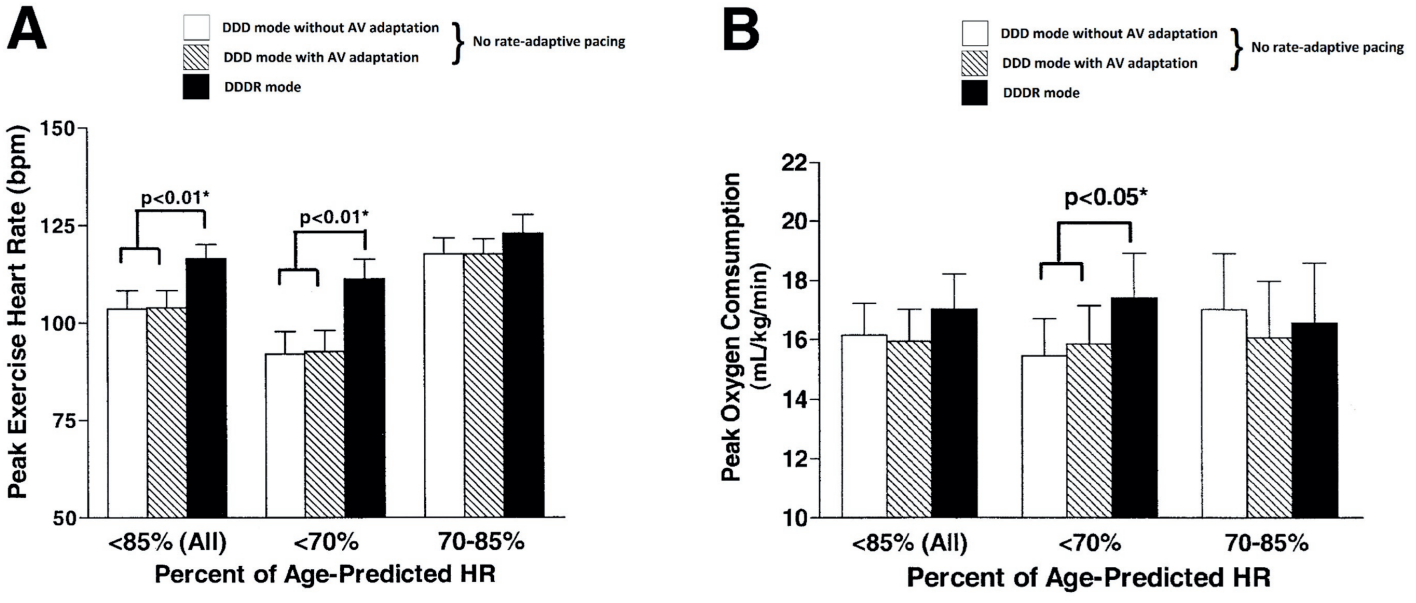


Figure 6: Rate-adaptive pacing restores chronotropic response and exercise capacity in heart failure patients with severe chronotropic incompetence. Rate-adaptive pacing in CRT patients with CI (age-predicted peak heart rate <85%) increased peak HR during exercise (A), but did not have any incremental benefit on exercise capacity (B). In patients with severe CI (age-predicted peak heart rate <70%), rate-adaptive pacing increased both peak HR (A) and exercise capacity (B). White and ruled bars represent DDD mode without and with atrioventricular interval adaptation, respectively (i.e. no rate-adaptive pacing); black bars represent DDDR mode (i.e. rate-adaptive pacing). Figure adapted from reference 85 with permission.

First, patients underwent CPET in DDD mode for baseline measurements and after an interval of at least 24 hours this was repeated in DDDR mode. It was demonstrated that rate-adaptive pacing increased peak HR and CO during exercise, however, acute increases in cardiac performance had no direct effect on exercise capacity (i.e. pVO2). These findings suggest that peripheral muscle adaptations are needed to utilize the additional oxygen supply and underline the importance of a time interval between CPETs sufficient to facilitate adaptation (the so-called “training effect”). In another small-scale study by Passman and colleagues, 10 patients with HF and dual-chamber ICDs underwent a single-cross-over study protocol with randomization to atrial rate adaptive (AAIR) pacing or ventricular backup (VVI) pacing.(89) In this study, CI was not part of the inclusion criteria and peak HR at baseline was found to be relatively high - 130 bpm on average. During AAIR stimulation, peak HR was significantly increased but no significant difference in pVO2 was observed. Recently, Jamil et al. published on the effects of CI on exercise capacity in an observational study, followed by an interventional study examining the effects of HR augmentation using rate-adaptive pacing.(25) In this randomized crossover study, 79 patients were enrolled with symptomatic HF and moderate-to-severe LV dysfunction (EF ≤45%) implanted with various cardiac devices. Of these patients, 53 were in sinus rhythm and 26 had atrial fibrillation (AF). The presence of CI was not required for participation in the study but using the <0.8 cut-off for chronotropic index (HRR / metabolic reserve), 84% of the patients tested positive for CI during CPET. Subjects were tested on 2 occasions, 1 week apart, and were randomly assigned to rate-adaptive pacing mode on or off. The authors do not state the type of activity sensor used or the pacemaker mode programmed. Sensor sensitivity was set to maximum, and the upper rate during rate-adaptive pacing was set to APMHR [220 – age]. Peak HR demonstrated a significant increase during rate adaptive pacing in both the sinus rhythm and AF group. In the AF group, there was a trend towards improving pVO2 (p=0.058), but in the sinus rhythm group pVO2 remained unchanged (p=0.350). The authors conclude that CI seems to be a bystander rather than a contributor to exercise intolerance in this group of unselected patients with CHF. However, there are several limitations in this study. A proportion of patients that participated in the study lacked CI and the percentage of right ventricular pacing during rate-adaptive pacing is unknown. Moreover, rate-adaptive pacing settings might have been too aggressive by

using an upper rate of [220 - age]. Kindermann et al. elegantly demonstrated that restoring chronotropic response to the APMHR [220 - age] reference value yields suboptimal effects on both cardiac performance and exercise capacity.(90) In this study, the optimal upper rate limit was determined in 49 pacemaker patients using CPET and Doppler echocardiography. It was shown that the optimal upper rate limit in HF patients (EF ≤45%) was approximately 75% of APMHR. Finally, the time interval of 1 week between CPET might have been too short in the Jamil study to enable a training effect, as discussed previously. Future studies should address the following: (i) appropriate (i.e. CI) patient selection; (ii) use of the most accurate available activity sensors; (iii) optimal rate-adaptive pacing settings (sensor sensitivity, upper rate limit); and (iv) recognition of the time period necessary to facilitate peripheral adaptation after changes in device settings (the training effect).

ONGOING STUDIES

Ongoing trials in the field of CI focus primarily on effects of rate-adaptive pacing on exercise capacity in HF patients. In their study, Zhang and colleagues aim to assess the effect of rate-adaptive atrial (AAIR) pacing treatment for patients with HF and CI on exercise tolerance and quality of life.(91) Another prospective, randomized, single-blind cross-over study by Hsu et al. investigates effects of rate-adaptive pacing using an accelerometer compared to the CLS activity sensor in CRT-D patients.(92) In the Rate-Adaptive Atrial Pacing In Diastolic Heart Failure (RAPID-HF) trial, the effects of rate-adaptive pacing using a dual-chamber pacemaker will be assessed in HFpEF patients.(93) Lastly, the Rate Adaptive Atrial Pacing in Heart Failure Patients with Chronotropic Incompetence (ADAPTION) trial conducted by our group aims to assess the ability of minute ventilation (MV) sensor driven rate-adaptive pacing to restore functional capacity and quality of life in HF patients with CI.(94) Patients implanted with a dual-chamber ICD are tested for CI based on the HRSc provided by the device. Sixty-five patients diagnosed with CI will enter a double blind randomized cross-over study and will be randomized in a 1:1 fashion to either AAIR pacing function on or off (DDI-50). After 3 months, the pacing mode will be switched to the opposite mode for another time period of 3 months. Both quality-of-life scores and six-minute walk distances will be compared between the groups.

SUMMARY

Chronotropic incompetence is defined as the inability of the heart rate to increase adequately in response to exercise. CI has a high prevalence in the HF population and is associated with reduced functional capacity and poor survival. Although the underlying mechanisms for CI in HF are not fully understood, the imbalanced autonomic nervous system that is chronically shifted towards the sympathetic pathway has been shown to reduce β-adrenergic responsiveness, resulting in a reduced heart rate response to exercise. Since contractility reserve is lost in the failing heart, insufficient cardio-acceleration (i.e. CI) may be a limiting factor in the exercise capacity of HF patients. Despite the potential importance of CI in this population, the issue has drawn limited attention and is often unrecognized in clinical practice. This is in part due to the lack of a standardized approach to diagnose CI. Chronotropic response can either be analyzed by assessment of peak HR or HR reserve (i.e. the change from resting HR to peak HR) using a maximal exercise test, preferably in combination with respiratory gas exchange analysis to ensure maximal exertion. While HR reserve reflects HR dynamics in contrast to static peak HR measurement, both markers yield similar prognostic value. To define an abnormal response (i.e. CI), peak HR should be compared to a HF population specific APMHR reference value. Specific formulas to calculate APMHR for the HF population have been derived, but are rarely used and may require further refinement with respect to HF severity. Consequently, a 'gold-standard' approach for diagnosis of CI in heart failure is still lacking. Despite the clear association between CI and impaired exercise capacity in HF patients, causality is uncertain. Whether CI is the cause or the consequence of impaired exercise capacity is important, as CI now serves as a potential therapeutic target using implantable cardiac device technology in HF patients. A substantial part of the HF population is presently equipped with an implanted device offering the unique opportunity to study HR dynamics and deliver pacemaker therapy. Rate-adaptive pacing has shown favorable effects on both exercise capacity and survival in a well selected subset of HF patients with manifest CI. Advances in device technology by incorporating additional physiological activity sensors and the detection of CI using a device histogram-based (HRSc) score might improve future treatment of CI in the HF population. To improve understanding of CI, future experimental studies in a randomized controlled setting should be encouraged.

REFERENCES

1. Ellestad MH, Wan MK. Predictive implications of stress testing. Follow-up of 2700 subjects after maximum treadmill stress testing. Circulation. 1975;51(2):363-9.
2. Higginbotham MB, Morris KG, Conn EH, Coleman RE, Cobb FR. Determinants of variable exercise performance among patients with severe left ventricular dysfunction. Am J Cardiol. 1983;51(1):52-60.
3. Weber KT, Kinasewitz GT, Janicki JS, Fishman AP. Oxygen utilization and ventilation during exercise in patients with chronic cardiac failure. Circulation. 1982;65(6):1213-23.
4. Camm AJ, Fei L. Chronotropic incompetence--Part I: Normal regulation of the heart rate. Clin Cardiol. 1996;19(5):424-8.
5. Christou DD, Seals DR. Decreased maximal heart rate with aging is related to reduced {beta}-adrenergic responsiveness but is largely explained by a reduction in intrinsic heart rate. J Appl Physiol (1985). 2008;105(1):24-9.
6. Jose AD, Collison D. The normal range and determinants of the intrinsic heart rate in man. Cardiovasc Res. 1970;4(2):160-7.
7. Brubaker PH, Kitzman DW. Chronotropic incompetence: causes, consequences, and management. Circulation. 2011;123(9):1010-20.
8. Astrand PO. Physical performance as a function of age. JAMA. 1968;205(11):729-33.
9. Tanaka H, Monahan KD, Seals DR. Age-predicted maximal heart rate revisited. J Am Coll Cardiol. 2001;37(1):153-6.
10. Camm AJ, Fei L. Chronotropic incompetence--Part II: Clinical implications. Clin Cardiol. 1996;19(6):503-8.
11. Hinkle LE, Jr., Carver ST, Plakun A. Slow heart rates and increased risk of cardiac death in middle-aged men. Arch Intern Med. 1972;129(5):732-48.
12. Elhendy A, Mahoney DW, Khandheria BK, Burger K, Pellikka PA. Prognostic significance of impairment of heart rate response to exercise: impact of left ventricular function and myocardial ischemia. J Am Coll Cardiol. 2003;42(5):823-30.
13. Lauer MS, Francis GS, Okin PM, Pashkow FJ, Snader CE, Marwick TH. Impaired chronotropic response to exercise stress testing as a predictor of mortality. JAMA. 1999;281(6):524-9.
14. Azarbal B, Hayes SW, Lewin HC, Hachamovitch R, Cohen I, Berman DS. The incremental prognostic value of percentage of heart rate reserve achieved over myocardial perfusion single-photon emission computed tomography in the prediction of cardiac death and all-cause mortality: superiority over 85% of maximal age-predicted heart rate. J Am Coll Cardiol. 2004;44(2):423-30.
15. Tzanis G, Dimopoulos S, Agapitou V, Nanas S. Exercise intolerance in chronic heart failure: the role of cortisol and the catabolic state. Curr Heart Fail Rep. 2014;11(1):70-9.
16. Fleg JL, Pina IL, Balady GJ, Chaitman BR, Fletcher B, Lavie C, et al. Assessment of functional capacity in clinical and research applications: An advisory from the Committee on Exercise, Rehabilitation, and Prevention, Council on Clinical Cardiology, American Heart Association. Circulation. 2000;102(13):1591-7.
17. Witte KK, Cleland JG, Clark AL. Chronic heart failure, chronotropic incompetence, and the effects of beta blockade. Heart. 2006;92(4):481-6.

18. Borlaug BA, Melenovsky V, Russell SD, Kessler K, Pacak K, Becker LC, et al. Impaired chronotropic and vasodilator reserves limit exercise capacity in patients with heart failure and a preserved ejection fraction. Circulation. 2006;114(20):2138-47.
19. Borlaug BA, Olson TP, Lam CS, Flood KS, Lerman A, Johnson BD, et al. Global cardiovascular reserve dysfunction in heart failure with preserved ejection fraction. J Am Coll Cardiol. 2010;56(11):845-54.
20. Haykowsky MJ, Brubaker PH, John JM, Stewart KP, Morgan TM, Kitzman DW. Determinants of exercise intolerance in elderly heart failure patients with preserved ejection fraction. J Am Coll Cardiol. 2011;58(3):265-74.
21. Phan TT, Shivu GN, Abozguia K, Davies C, Nassimizadeh M, Jimenez D, et al. Impaired heart rate recovery and chronotropic incompetence in patients with heart failure with preserved ejection fraction. Circ Heart Fail. 2010;3(1):29-34.
22. Topilsky Y, Rozenbaum Z, Khoury S, Pressman GS, Gura Y, Sherez J, et al. Mechanisms of Effort Intolerance in Patients With Heart Failure and Borderline Ejection Fraction. Am J Cardiol. 2017;119(3):416-22.
23. Al-Najjar Y, Witte KK, Clark AL. Chronotropic incompetence and survival in chronic heart failure. Int J Cardiol. 2012;157(1):48-52.
24. Brubaker PH, Joo KC, Stewart KP, Fray B, Moore B, Kitzman DW. Chronotropic incompetence and its contribution to exercise intolerance in older heart failure patients. J Cardiopulm Rehabil. 2006;26(2):86-9.
25. Jamil HA, Gierula J, Paton MF, Byrom R, Lowry JE, Cubbon RM, et al. Chronotropic Incompetence Does Not Limit Exercise Capacity in Chronic Heart Failure. J Am Coll Cardiol. 2016;67(16):1885-96.
26. Magri D, Palermo P, Cauti FM, Contini M, Farina S, Cattadori G, et al. Chronotropic incompentence and functional capacity in chronic heart failure: no role of beta-blockers and beta-blocker dose. Cardiovasc Ther. 2012;30(2):100-8.
27. Mann DL, Bristow MR. Mechanisms and models in heart failure: the biomechanical model and beyond. Circulation. 2005;111(21):2837-49.
28. Springer J, Azer J, Hua R, Robbins C, Adamczyk A, McBoyle S, et al. The natriuretic peptides BNP and CNP increase heart rate and electrical conduction by stimulating ionic currents in the sinoatrial node and atrial myocardium following activation of guanylyl cyclase-linked natriuretic peptide receptors. J Mol Cell Cardiol. 2012;52(5):1122-34.
29. Kaye DM, Jennings GL, Dart AM, Esler MD. Differential effect of acute baroreceptor unloading on cardiac and systemic sympathetic tone in congestive heart failure. J Am Coll Cardiol. 1998;31(3):583-7.
30. Samejima H, Omiya K, Uno M, Inoue K, Tamura M, Itoh K, et al. Relationship between impaired chronotropic response, cardiac output during exercise, and exercise tolerance in patients with chronic heart failure. Jpn Heart J. 2003;44(4):515-25.
31. Colucci WS, Ribeiro JP, Rocco MB, Quigg RJ, Creager MA, Marsh JD, et al. Impaired chronotropic response to exercise in patients with congestive heart failure. Role of postsynaptic beta-adrenergic desensitization. Circulation. 1989;80(2):314-23.
32. Bristow MR, Ginsburg R, Umans V, Fowler M, Minobe W, Rasmussen R, et al. Beta 1- and beta 2-adrenergic-receptor subpopulations in nonfailing and failing human ventricular myocardium: coupling of both receptor subtypes to muscle contraction and selective beta 1-receptor down-regulation in heart failure. Circ Res. 1986;59(3):297-309.

33. Bristow MR, Hershberger RE, Port JD, Gilbert EM, Sandoval A, Rasmussen R, et al. Beta-adrenergic pathways in nonfailing and failing human ventricular myocardium. Circulation. 1990;82(2 Suppl):I12-I25.
34. Bristow MR, Anderson FL, Port JD, Skerl L, Hershberger RE, Larrabee P, et al. Differences in beta-adrenergic neuroeffector mechanisms in ischemic versus idiopathic dilated cardiomyopathy. Circulation. 1991;84(3):1024-39.
35. Bristow MR, Minobe W, Rasmussen R, Larrabee P, Skerl L, Klein JW, et al. Beta-adrenergic neuroeffector abnormalities in the failing human heart are produced by local rather than systemic mechanisms. J Clin Invest. 1992;89(3):803-15.
36. Uijtdehaage SH, Thayer JF. Accentuated antagonism in the control of human heart rate. Clin Auton Res. 2000;10(3):107-10.
37. Benes J, Kotrc M, Borlaug BA, Lefflerova K, Jarolim P, Bendlova B, et al. Resting heart rate and heart rate reserve in advanced heart failure have distinct pathophysiologic correlates and prognostic impact: a prospective pilot study. JACC Heart Fail. 2013;1(3):259-66.
38. Sanders P, Kistler PM, Morton JB, Spence SJ, Kalman JM. Remodeling of sinus node function in patients with congestive heart failure: reduction in sinus node reserve. Circulation. 2004;110(8):897-903.
39. Brawner CA, Ehrman JK, Schairer JR, Cao JJ, Keteyian SJ. Predicting maximum heart rate among patients with coronary heart disease receiving beta-adrenergic blockade therapy. Am Heart J. 2004;148(5):910-4.
40. Wilkoff BL, Miller RE. Exercise testing for chronotropic assessment. Cardiol Clin. 1992;10(4):705-17.
41. Jorde UP, Vittorio TJ, Kasper ME, Arezzi E, Colombo PC, Goldsmith RL, et al. Chronotropic incompetence, beta-blockers, and functional capacity in advanced congestive heart failure: time to pace? Eur J Heart Fail. 2008;10(1):96-101.
42. Magri D, Corra U, Di LA, Cattadori G, Maruotti A, Iorio A, et al. Cardiovascular mortality and chronotropic incompetence in systolic heart failure: the importance of a reappraisal of current cut-off criteria. Eur J Heart Fail. 2014;16(2):201-9.
43. Dobre D, Zannad F, Keteyian SJ, Stevens SR, Rossignol P, Kitzman DW, et al. Association between resting heart rate, chronotropic index, and long-term outcomes in patients with heart failure receiving beta-blocker therapy: data from the HF-ACTION trial. Eur Heart J. 2013;34(29):2271-80.
44. Arena R, Guazzi M, Myers J, Peberdy MA. Prognostic value of heart rate recovery in patients with heart failure. Am Heart J. 2006;151(4):851-13.
45. Nanas S, Anastasiou-Nana M, Dimopoulos S, Sakellariou D, Alexopoulos G, Kapsimalakou S, et al. Early heart rate recovery after exercise predicts mortality in patients with chronic heart failure. Int J Cardiol. 2006;110(3):393-400.
46. Kubrychtova V, Olson TP, Bailey KR, Thapa P, Allison TG, Johnson BD. Heart rate recovery and prognosis in heart failure patients. Eur J Appl Physiol. 2009;105(1):37-45.
47. Bohm M, Swedberg K, Komajda M, Borer JS, Ford I, Dubost-Brama A, et al. Heart rate as a risk factor in chronic heart failure (SHIFT): the association between heart rate and outcomes in a randomised placebo-controlled trial. Lancet. 2010;376(9744):886-94.
48. Fox K, Borer JS, Camm AJ, Danchin N, Ferrari R, Lopez Sendon JL, et al. Resting heart rate in cardiovascular disease. J Am Coll Cardiol. 2007;50(9):823-30.
49. Palatini P, Julius S. Elevated heart rate: a major risk factor for cardiovascular disease. Clin Exp Hypertens. 2004;26(7-8):637-44.

50. Castagno D, Skali H, Takeuchi M, Swedberg K, Yusuf S, Granger CB, et al. Association of heart rate and outcomes in a broad spectrum of patients with chronic heart failure: results from the CHARM (Candesartan in Heart Failure: Assessment of Reduction in Mortality and morbidity) program. J Am Coll Cardiol. 2012;59(20):1785-95.
51. Vazir A, Claggett B, Jhund P, Castagno D, Skali H, Yusuf S, et al. Prognostic importance of temporal changes in resting heart rate in heart failure patients: an analysis of the CHARM program. Eur Heart J. 2015;36(11):669-75.
52. Hjalmarson A, Goldstein S, Fagerberg B, Wedel H, Waagstein F, Kjekshus J, et al. Effects of controlled-release metoprolol on total mortality, hospitalizations, and well-being in patients with heart failure: the Metoprolol CR/XL Randomized Intervention Trial in congestive heart failure (MERIT-HF). MERIT-HF Study Group. JAMA. 2000;283(10):1295-302.
53. Hung RK, Al-Mallah MH, Whelton SP, Michos ED, Blumenthal RS, Ehrman JK, et al. Effect of Beta-Blocker Therapy, Maximal Heart Rate, and Exercise Capacity During Stress Testing on Long-Term Survival (from The Henry Ford Exercise Testing Project). Am J Cardiol. 2016;118(11):1751-7.
54. Hirsh BJ, Mignatti A, Garan AR, Uriel N, Colombo P, Sims DB, et al. Effect of beta-blocker cessation on chronotropic incompetence and exercise tolerance in patients with advanced heart failure. Circ Heart Fail. 2012;5(5):560-5.
55. Stoschitzky K, Koshucharova G, Zweiker R, Maier R, Watzinger N, Fruhwald FM, et al. Differing beta-blocking effects of carvedilol and metoprolol. Eur J Heart Fail. 2001;3(3):343-9.
56. McAlister FA, Wiebe N, Ezekowitz JA, Leung AA, Armstrong PW. Meta-analysis: beta-blocker dose, heart rate reduction, and death in patients with heart failure. Ann Intern Med. 2009;150(11):784-94.
57. Swedberg K, Komajda M, Bohm M, Borer JS, Ford I, Dubost-Brama A, et al. Ivabradine and outcomes in chronic heart failure (SHIFT): a randomised placebo-controlled study. Lancet. 2010;376(9744):875-85.
58. Bohm M, Borer JS, Camm J, Ford I, Lloyd SM, Komajda M, et al. Twenty-four-hour heart rate lowering with ivabradine in chronic heart failure: insights from the SHIFT Holter substudy. Eur J Heart Fail. 2015;17(5):518-26.
59. Reil JC, Tardif JC, Ford I, Lloyd SM, O'Meara E, Komajda M, et al. Selective heart rate reduction with ivabradine unloads the left ventricle in heart failure patients. J Am Coll Cardiol. 2013;62(21):1977-85.
60. Amosova E, Andrejev E, Zaderey I, Rudenko U, Ceconi C, Ferrari R. Efficacy of ivabradine in combination with Beta-blocker versus uptitration of Beta-blocker in patients with stable angina. Cardiovasc Drugs Ther. 2011;25(6):531-7.
61. Sarullo FM, Fazio G, Puccio D, Fasullo S, Paterna S, Novo S, et al. Impact of ''off-label'' use of ivabradine on exercise capacity, gas exchange, functional class, quality of life, and neurohormonal modulation in patients with ischemic chronic heart failure. J Cardiovasc Pharmacol Ther. 2010;15(4):349-55.
62. Volterrani M, Cice G, Caminiti G, Vitale C, D'Isa S, Perrone Filardi P, et al. Effect of Carvedilol, Ivabradine or their combination on exercise capacity in patients with Heart Failure (the CARVIVA HF trial). Int J Cardiol. 2011;151(2):218-24.
63. Borlaug BA. The pathophysiology of heart failure with preserved ejection fraction. Nat Rev Cardiol. 2014;11(9):507-15.

64. Kosmala W, Rojek A, Przewlocka-Kosmala M, Mysiak A, Karolko B, Marwick TH. Contributions of Nondiastolic Factors to Exercise Intolerance in Heart Failure With Preserved Ejection Fraction. J Am Coll Cardiol. 2016;67(6):659-70.
65. Kass DA, Kitzman DW, Alvarez GE. The restoration of chronotropic competence in heart failure patients with normal ejection fraction (RESET) study: rationale and design. J Card Fail. 2010;16(1):17-24.
66. Givertz MM, Hartley LH, Colucci WS. Long-term sequential changes in exercise capacity and chronotropic responsiveness after cardiac transplantation. Circulation. 1997;96(1):232-7.
67. Mettauer B, Levy F, Richard R, Roth O, Zoll J, Lampert E, et al. Exercising with a denervated heart after cardiac transplantation. Ann Transplant. 2005;10(4):35-42.
68. Wachter SB, McCandless SP, Gilbert EM, Stoddard GJ, Kfoury AG, Reid BB, et al. Elevated resting heart rate in heart transplant recipients: innocent bystander or adverse prognostic indicator? Clin Transplant. 2015;29(9):829-34.
69. Richard R, Verdier JC, Duvallet A, Rosier SP, Leger P, Nignan A, et al. Chronotropic competence in endurance trained heart transplant recipients: heart rate is not a limiting factor for exercise capacity. J Am Coll Cardiol. 1999;33(1):192-7.
70. Melton IC, Gilligan DM, Wood MA, Ellenbogen KA. Optimal cardiac pacing after heart transplantation. Pacing Clin Electrophysiol. 1999;22(10):1510-27.
71. Pandey A, Parashar A, Kumbhani DJ, Agarwal S, Garg J, Kitzman D, et al. Exercise training in patients with heart failure and preserved ejection fraction: meta-analysis of randomized control trials. Circ Heart Fail. 2015;8(1):33-40.
72. Kiilavuori K, Toivonen L, Naveri H, Leinonen H. Reversal of autonomic derangements by physical training in chronic heart failure assessed by heart rate variability. Eur Heart J. 1995;16(4):490-5.
73. Myers J, Hadley D, Oswald U, Bruner K, Kottman W, Hsu L, et al. Effects of exercise training on heart rate recovery in patients with chronic heart failure. Am Heart J. 2007;153(6):1056-63.
74. Keteyian SJ, Brawner CA, Schairer JR, Levine TB, Levine AB, Rogers FJ, et al. Effects of exercise training on chronotropic incompetence in patients with heart failure. Am Heart J. 1999;138(2 Pt 1):233-40.
75. Olshansky B, Richards M, Sharma A, Wold N, Jones P, Perschbacher D, et al. Survival After Rate-Responsive Programming in Patients With Cardiac Resynchronization Therapy-Defibrillator Implants Is Associated With a Novel Parameter: The Heart Rate Score. Circ Arrhythm Electrophysiol. 2016;9(8).
76. Wilkoff BL, Richards M, Sharma A, Wold N, Jones P, Perschbacher D, et al. A Device Histogram-Based Simple Predictor of Mortality Risk in ICD and CRT-D Patients: The Heart Rate Score. Pacing Clin Electrophysiol. 2017;40(4):333-43.
77. Voukydis PC, Krasner JL. A physiologically regulated cardiac pacemaker. Br J Exp Pathol. 1967;48(1):118-23.
78. Dell'Orto S, Valli P, Greco EM. Sensors for rate responsive pacing. Indian Pacing Electrophysiol J. 2004;4(3):137-45.
79. Katritsis D, Shakespeare CF, Camm AJ. New and combined sensors for adaptive-rate pacing. Clin Cardiol. 1993;16(3):240-8.
80. Coman J, Freedman R, Koplan BA, Reeves R, Santucci P, Stolen KQ, et al. A blended sensor restores chronotropic response more favorably than an accelerometer alone in

pacemaker patients: the LIFE study results. Pacing Clin Electrophysiol. 2008;31(11):1433-42.
81. Nagele H, Rodiger W, Castel MA. Rate-responsive pacing in patients with heart failure: long-term results of a randomized study. Europace. 2008;10(10):1182-8.
82. Wilkoff BL, Cook JR, Epstein AE, Greene HL, Hallstrom AP, Hsia H, et al. Dual-chamber pacing or ventricular backup pacing in patients with an implantable defibrillator: the Dual Chamber and VVI Implantable Defibrillator (DAVID) Trial. JAMA. 2002;288(24):3115-23.
83. Wilkoff BL, Kudenchuk PJ, Buxton AE, Sharma A, Cook JR, Bhandari AK, et al. The DAVID (Dual Chamber and VVI Implantable Defibrillator) II trial. J Am Coll Cardiol. 2009;53(10):872-80.
84. Martin DO, Day JD, Lai PY, Murphy AL, Nayak HM, Villareal RP, et al. Atrial support pacing in heart failure: results from the multicenter PEGASUS CRT trial. J Cardiovasc Electrophysiol. 2012;23(12):1317-25.
85. Tse HF, Siu CW, Lee KL, Fan K, Chan HW, Tang MO, et al. The incremental benefit of rate-adaptive pacing on exercise performance during cardiac resynchronization therapy. J Am Coll Cardiol. 2005;46(12):2292-7.
86. Palmisano P, Aspromonte V, Ammendola E, Dell'era G, Ziacchi M, Guerra F, et al. Effect of fixed-rate vs. rate-RESPONSIve pacing on exercise capacity in patients with permanent, refractory atrial fibrillation and left ventricular dysfunction treated with atrioventricular junction aBLation and bivEntricular pacing (RESPONSIBLE): a prospective, multicentre, randomized, single-blind study. Europace. 2017;19(3):414-20.
87. Sims DB, Mignatti A, Colombo PC, Uriel N, Garcia LI, Ehlert FA, et al. Rate responsive pacing using cardiac resynchronization therapy in patients with chronotropic incompetence and chronic heart failure. Europace. 2011;13(10):1459-63.
88. Van Thielen G, Paelinck BP, Beckers P, Vrints CJ, Conraads VM. Rate response and cardiac resynchronisation therapy in chronic heart failure: higher cardiac output does not acutely improve exercise performance: a pilot trial. Eur J Cardiovasc Prev Rehabil. 2008;15(2):197-202.
89. Passman R, Banthia S, Galvez D, Sheldon T, Kadish A. The effects of rate-adaptive atrial pacing versus ventricular backup pacing on exercise capacity in patients with left ventricular dysfunction. Pacing Clin Electrophysiol. 2009;32(1):1-6.
90. Kindermann M, Schwaab B, Finkler N, Schaller S, Bohm M, Frohlig G. Defining the optimum upper heart rate limit during exercise: a study in pacemaker patients with heart failure. Eur Heart J. 2002;23(16):1301-8.
91. ClinicalTrials.gov. Assessment of AAIR Pacing Treatment for Heart Failure Patients With Chronotropic Incompetence. Available at: https://www.clinicaltrials.gov/ct2/show/NCT03071952
92. ClinicalTrials.gov. Rate Response With CLS Versus Accelerometer and Effect on Both Subjective Symptoms and Objective Outcomes in a Heart Failure Population Implanted With Cardiac Resynchronization With Defibrillator Device: The CLASS Trial. Available at: https://www.clinicaltrials.gov/ct2/show/NCT02693262
93. ClinicalTrials.gov. Rate-Adaptive Atrial Pacing In Diastolic Heart Failure (RAPID-HF). Available at: https://www.clinicaltrials.gov/ct2/show/NCT02145351
94. ClinicalTrials.gov. Rate Adaptive Atrial Pacing in Heart Failure (ADAPTION). Available at: https://clinicaltrials.gov/ct2/show/NCT03235843

Chapter 13

Summary and Future Perspectives

Selection criteria for Cardiac Resynchronization Therapy (CRT) are mainly based on the morphology and time duration of the QRS complex. Following guideline criteria, however, approximately one-third of the patients implanted with CRT will not respond favorably. Over the last two decades, numerous studies have sought to determine variables associated with improved CRT response. It is now widely accepted that these factors include strict left bundle branch block (LBBB) morphology, longer QRS duration (QRSd), sinus rhythm, non-ischemic etiology, younger age and female gender. On the other hand, consensus has still not been reached on the predictive value of cardiac imaging techniques in CRT candidates. On this matter, the role of myocardial strain parameters is especially debated. After the decision to implant CRT has been made, the question arises if device optimization strategies increases benefit from the therapy. This, again, is topic of significant debate and requires further research. The present thesis aims to investigate two strategies that can potentially increase effectiveness of CRT: (i) improved selection of potential responders prior to implantation using cardiac imaging techniques and (ii) optimized device settings afterwards in order to maximize hemodynamic benefits. Both strategies will be discussed below in part one (patient selection) and part two (device optimization), respectively.

Part IA Normalization of QRS duration to LV dimension

CRT provides electrical therapy for heart failure in the form of pacing pulses that resynchronize the ventricular contraction sequence affected by distorted electrical conduction. Being an electrical therapy for an electrical disease, it is not surprising that patient selection for CRT is guided by the electrical parameter QRSd. Increased QRSd, however, may arise from slow cell-to-cell conduction (i.e. true LBBB), or by increased conduction path length (dilation of the failing heart). Part IA of the thesis evaluates the theoretical concept that incorporation of left ventricular (LV) structural measurements in the assessment of electrical delay,

by normalizing QRSd to LV size, improves prediction of CRT response. **Chapter two** provides a proof-of-principle study amongst thirty-two patients who underwent CMR imaging before CRT implantation followed by invasive pressure-volume loop measurements to obtain acute LV pump function changes during CRT. Normalization of QRSd to LV dimension (i.e. QRSd divided by LV dimension) improved correlation with acute LV pump function improvement by CRT. Different metrics of LV size (volumes; diameter; length; mass) all showed similar results in relation to QRSd and CRT response. In addition, women achieved more pump function improvement during CRT compared to men. This sex-specific difference in CRT outcome may be partly ascribed to differences in LV size between both sexes. As the female heart is generally smaller, women have shorter QRSd compared to men. In order to reach the cut-off QRSd value for CRT (guidelines are identical for men and women), female hearts will have more conduction delay compared to male hearts and might therefore be more amenable for successful treatment with CRT. These results were confirmed by Varma et al. who showed in a subsequent study that sex-specific differences in the QRSd-response relationship resolved after QRSd normalization to LV dimension.(1) Subsequently, **chapter three** extends the role of QRSd normalization to the prediction of clinical endpoints in a large population of two-hundred-fifty patients eligible for CRT. QRSd normalization improved prediction of survival after CRT implantation. Moreover, normalized QRSd yielded prognostic value in a prediction model together with age, atrial fibrillation, renal function and heart failure etiology. These findings indicate that a multi-modality approach including electrical, structural and clinical parameters could potentially improve patient selection for CRT.

Part IB Myocardial strain imaging

In CRT, electrical resynchronization leads to LV pump function improvement by mechanical re-coordination of contraction between different regions of the LV walls, especially between the septum and lateral wall. A more homogenous work distribution increases LV pump function efficiency and results in larger external work to eject blood.(2) Therefore, the purpose of CRT may be referred to as mechanical re-coordination rather than electrical resynchronization therapy. This concept is supported by results from the PROSPECT trial where numerous dyssynchrony parameters were unable to predict CRT outcome.(3) Whether

detection of mechanical discoordination (systolic stretching of segments) rather than dyssynchrony (regional timing differences between segments) yields additional value in the prediction of LV pump function improvement after CRT remains to be proven. Part 1B of this thesis evaluates the role of myocardial strain imaging to improve patient selection for CRT. In **chapter four** regional strain measurements are combined with LV pressure curves to calculate myocardial work distribution.(4) Contribution of the septum to total LV work varies widely in CRT candidates with LBBB, and the lower the septal contribution to total myocardial work (or the higher the septal waste) at baseline the higher the acute improvement in pump function that can be achieved during CRT. These results are confirmed in a subsequent study by Vecera et al. who showed that wasted septal work strongly predicted CRT response after one year.(5) Myocardial strain imaging therefore provides an insight in the negative effect of LBBB on myocardial work and energy utilization, and reflects the potential benefit that can be achieved by CRT. In our small-scale study, all patients underwent CMR tagging (CMR-TAG) to obtain high-quality regional strain curves. Availability of CMR-TAG, however, is very limited in clinical practice. Therefore, the role of other non-invasive imaging techniques such as CMR feature tracking (CMR-FT) and speckle tracking echocardiography (STE) is of interest. **Chapter five** provides a comparison of strain values obtained with CMR-FT and STE versus 'gold standard' CMR-TAG. Twenty-seven CRT-candidates, prospectively included in the Markers And Response to CRT (MARC) study, underwent CMR imaging and echocardiographic examination. Both CMR-FT and STE techniques showed to be potentially valuable alternatives for CMR-TAG, especially in the evaluation of mechanical discoordination. Subsequently, **chapter six** provides echocardiographic follow-up data in these patients allowing to compare predictive value for CRT response of different strain parameters using multiple imaging techniques. Of all strain parameters, measuring end-systolic septal strain (ESS_{sep}) showed strongest relation with CRT response after one year, irrespective of imaging technique. ESS_{sep} reflects fiber length change of the septum throughout systole. Detection of septal discoordination with higher ESS_{sep} values (i.e. septal stretching instead of contraction) at baseline was associated with more extensive reverse remodeling after CRT. Moreover, measuring ESS_{sep} by any available imaging technique showed to be additive to present guideline criteria (QRS morphology; QRSd). The application of strain

imaging has yet not been included in daily practice, but it is likely to become a useful application when evaluating heart failure patients for CRT implantation. This may be of particular interest in CRT candidates with unfavorable patient characteristics (non-strict LBBB morphology, shorter QRSd), in whom benefit from CRT is doubted. Subsequently, the novel segment length in cine (SLICE) strain technique is introduced. The purpose of SLICE is to provide the clinician a simplified strain analysis technique to estimate benefit from CRT by analyzing standard CMR cine images, based on previous findings. More specifically, SLICE consists of a series of manual frame-to-frame segment length measurements between anatomic landmarks on standard short-axis CMR cines. In a first step, SLICE was validated to 'gold standard' CMR tagging in twenty-seven patients of the MARC population (**chapter seven**). SLICE-derived strain values showed good agreement with CMR-TAG and good-to-excellent reproducibility. An advantage of the SLICE technique is that it obviates the need for additional CMR scanning sequences (i.e. CMR-TAG) or commercial post-processing software tools (i.e. CMR-FT). However, strain parameters that require SLICE analysis of the entire strain curve may take a long processing time (up to 60 minutes). Subsequently, SLICE analysis was performed in fifty-seven MARC patients who underwent standard CMR examination in **chapter eight**. Predictive value of different SLICE-derived strain parameters were compared with ESS_{sep} showing the strongest relation to reverse remodeling after CRT. These results are in line with earlier CMR-TAG, CMR-FT and STE findings, indicating that ESS_{sep} is a robust predictor of CRT response. In a multivariable analysis, ESS_{sep} showed to be an independent predictor of CRT response together with age at implant and QRS_{AREA} derived by vector-loop ECG analysis. A great advantage of the ESS_{sep} parameter is that it requires only two (end-systolic and end-diastolic) segment length measurements and can be performed in under ten minutes, making this a fast and straightforward technique. Lastly, the role of the SLICE-ESS_{sep} measurement was extended to the prediction of clinical outcome after CRT in a large population of CRT candidates. **Chapter nine** presents a two-center study including two-hundred-eighteen patients who underwent CMR imaging including late gadolinium enhancement (LGE) prior to CRT implantation. The main findings of this study were that a positive ESS_{sep} at baseline was associated with two- to three-fold lower rate of all-cause mortality and HF events after CRT implantation. However, predictive value ESS_{sep} was confounded by regional

scarring of the septum, indicating that SLICE should be combined with LGE to exclude septal scarring as the cause of septal stretching. In clinical practice, CMR imaging is increasingly used to screen candidates by measuring LVEF combined with LGE imaging to guide LV lead placement.(6) Additional SLICE analysis of the septum could potentially improve diagnostic yield of CMR and guide future patient selection for CRT.

Part II Device optimization

In part two of this thesis several CRT optimization strategies are evaluated. The first two chapters are part of the OPTICARE-QLV (Optimization of Cardiac Resynchronization Therapy with a Quadripolar Left Ventricular Lead) study. The main aim of the OPTICARE-QLV study was to relate electrical parameters (Q on surface ECG to LV sensing interval, QLV) to acute hemodynamic response in CRT using quadripolar LV leads as described in **chapter ten**. Forty-eight heart failure patients with LBBB were prospectively enrolled and underwent both electrical and invasive pressure-volume loop measurements directly after CRT implantation. Although there was a large variation in acute hemodynamic CRT response between different electrodes of the quadripolar lead, electrical parameters (QLV; QLV/QRSd) were unable to identify the most beneficial pacing electrode of a quadripolar lead. Therefore, optimization of the pacing configuration of CRT with a quadripolar LV lead should rely on functional assessment of cardiac function, instead of local electrical delay. Acute CRT response can be assessed by invasive hemodynamic testing in order to optimize device settings. Typically, the maximum rate of LV pressure rise (dP/dt_{max}) is used as an index of ventricular performance. Alternatively, stroke work (SW) can be measured from pressure-volume loops. **Chapter eleven** evaluates the acute effect of dP/dt_{max} versus SW guided CRT optimization, and relates acute hemodynamic changes to long-term CRT response. It was demonstrated that hemodynamic optimization of the LV pacing electrode and AV delay in CRT with quadripolar leads result in approximately one-third additional improvement in the parameter used for optimization (either dP/dt_{max} or SW). Improvement in one parameter, however, did not coincide with the other indicating two different mechanisms. Whereas dP/dt_{max} optimization favored LV contractility, SW optimization improved ventricular-arterial coupling leading to higher stroke volume and ejection. Acute changes in SW showed high predictive value for

prediction of long-term CRT response, whereas predictive value of dP/dt_{max} change was non-significant. Pressure-volume guided hemodynamic optimization may therefore be considered a potential strategy to use the full potential of CRT with quadripolar leads. Lastly, **chapter twelve** summarizes recent literature on the role of cardiac implantable electronic devices (ICD; CRT) for treatment of chronotropic incompetence (CI) in HF patients. A substantial part of the HF population is presently equipped with an implanted device offering the unique opportunity to study HR dynamics and deliver pacemaker therapy. Rate-adaptive pacing has shown favorable effects on both exercise capacity and survival in a well selected subset of HF patients with manifest CI. Advances in device technology by incorporating additional physiological activity sensors and the detection of CI using a device histogram-based heart rate score might improve future treatment of CI in the HF population.

Clinical implications

Patients with HF, reduced ejection fraction and wide QRS on the electrocardiogram are recommended for CRT by the present guidelines. Electrical resynchronization typically results in narrowing of the QRS complex and leads to LV pump function improvement by mechanical re-coordination of LV contraction. Previous studies showed that CRT candidates with narrow QRS complexes yield no benefit (or derived harm) from CRT.(7) On the other hand, not every patient with wide QRS complex benefits from the therapy. Therefore additional selection criterion are needed to reduce the rate of non-response. Current guidelines on CRT justify the use of cardiac imaging only to estimate LV ejection fraction. However, information on cardiac dimensions could potentially add to the predictive value of QRS duration as demonstrated in the first part of the thesis (QRSd normalization). In addition, assessment of cardiac mechanics may also be used to further improve patient selection for CRT. Although parameters of mechanical dyssynchrony (regional timing differences) showed inconsistent results, mechanical discoordination (systolic stretching) of the septum provides added value to guideline parameters in the prediction of LV pump function improvement after CRT, irrespective of imaging technique. When comparing different imaging techniques, CMR has unique advantages over echocardiography in accurately and reproducibly quantifying LV size and function and by enabling the detection of myocardial scar tissue. Additional

SLICE analysis of the septum further increases diagnostic yield of CMR and may therefore be considered the first-choice imaging modality in the work-up of CRT candidates. Performing CMR imaging is in particular of interest in patients in whom benefit from CRT is doubted (old age, ischemic cardiomyopathy, non-strict LBBB morphology). In case CMR imaging shows severe LV dilatation (low QRSd/LVEDV ratio), lack of septal discoordination (negative SLICE-ESS_{sep}), and extensive myocardial scarring (especially of the septum), CRT may be withheld in these patients. Because different types of parameters yielded predictive value in multivariable analysis, a multimodality work-up including clinical parameters, electrical (ECG) assessment and mechanical (CMR) analysis seems legitimate before undergoing invasive CRT implantation. After the decision has been made for CRT implantation, device optimization strategies may be considered to use the full potential of CRT with quadripolar leads. Electrical (i.e. QRS duration; QLV) and echocardiographic (i.e. stroke volume; mitral flow) parameters are most widely used in clinical practice although convincing scientific evidence for these methods is lacking. Pressure-volume guided hemodynamic optimization in CRT using a conductance catheter results in approximately one-third additional LV pump function improvement on top of conventional CRT. Although invasive hemodynamic optimization is unfeasible in clinical practice, the concept of volume (instead of pressure) -based optimization may guide future implementation of non-invasive surrogates such as intra-cardiac impedance measured between leads, or CRT stimulation in the CMR environment (see future perspectives). Lastly, reversal of CI by rate-adaptive pacing algorithms may increase clinical benefit from device implantation. Strategies to improve CRT as investigated in the thesis are summarized in figure 1.

Pre-implantation: patient selection

- Clinical factors: age ; renal function ; etiology ; atrial fibrillation
- Electrocardiogram: QRSd ; QRS morphology ; QRS_{AREA}
- CMR imaging: LVEDV (QRSd/LVEDV) ; LVEF ; LGE ; $SLICE\text{-}ESS_{SEP}$

Peri-implantation: LV lead placement

- Lead: Quadripolar LV lead
- Location: Lateral area outside scar, away from phrenic nerve

Post-implantation: device optimization

- Optimization of LV pacing electrode and AV- / VV-delays by volumetric parameters (stroke work or stroke volume)
- Optimization of heart rate profile by detection of CI and treatment by rate-adaptive pacing during exercise

Figure 1: Strategies to improve Cardiac Resynchronization Therapy: QRSd, QRS duration; LVEDV, LV end-diastolic volume; LVEF, LV ejection fraction; LGE, late gadolinium enhancement; $SLICE\text{-}ESS_{SEP}$; end-systolic septum strain derived by segment length in cine analysis; QLV, atrioventricular; VV, interventricular; CI, chronotropic incompetence

FUTURE PERSPECTIVES

Electrocardiography

Using guideline recommendations for CRT based on standard ECG parameters (QRS morphology and QRSd) results in a large proportion of patients becoming non-responders.(8) Recent studies suggest that vectorcardiography may identify LV lateral wall delayed activation better than conventional ECG parameters.(9) $QRS_{AREA,}$ obtained from a 3d vector loop synthesized from a digital 12-lead ECG, showed predictive value for CRT response over standard ECG parameters in the MARC study including 240 patients.(10) In addition, QRS_{AREA} showed improved prediction of clinical outcome in other studies.(11,12) The latest development in non-invasive ECG imaging is body surface mapping. A MRI or CT scan is performed with up to 224 unipolar electrodes placed on the patient's chest and subsequently these electrodes are used to obtain a 224 lead ECG. Subsequently, a 3-dimensional mesh of the ventricles is constructed, and isochronal maps are superimposed to display detailed electrical wave propagation. Body surface mapping reliably and accurately detects electrical dyssynchrony, the site of latest activation, and electrical resynchronization during biventricular pacing.(13) Advanced electrical mapping, however, does not obviate the need for cardiac imaging to assess the mechanical consequences arising from the electrical conduction disorder.

Cardiac imaging before and after CRT implantation

A promising strategy to increase benefit from CRT is targeted LV lead delivery by multi-modality imaging. Optimal pacing sites can be determined by CMR imaging (i.e. segment with late contraction outside scar area) and CT scans (i.e. anatomy of coronary sinus and phrenic nerve) and fused with live fluoroscopic projections during implantation.(14,15) Of note, CMR is also capable of visualization of the coronary venous anatomy, enabling a single-modality work-up for CRT candidates.(16) Moreover, CMR can now be used for follow-up of CRT patients as CE-marked CMR-compatible CRT devices have recently been launched for clinical applications. Theoretically, these novel devices allow for evaluation of pacing effects on the myocardium using CMR, providing new opportunities to individualize CRT settings. However, due to their metal composition these devices cause various types of artifacts within CMR images. Therefore, we initiated the PICARIA-CRT trial (Pacing in Cardiac Magnetic Resonance Imaging,

a CRT Trial) at our center. The objective of this pilot study is to assess the feasibility of CMR imaging in patients implanted with a CMR compatible CRT-D, and to evaluate the effect of biventricular pacing on LV functional measurements. The first cases showed promising results with sufficient image quality for LV volume quantification as illustrated in figure 2.

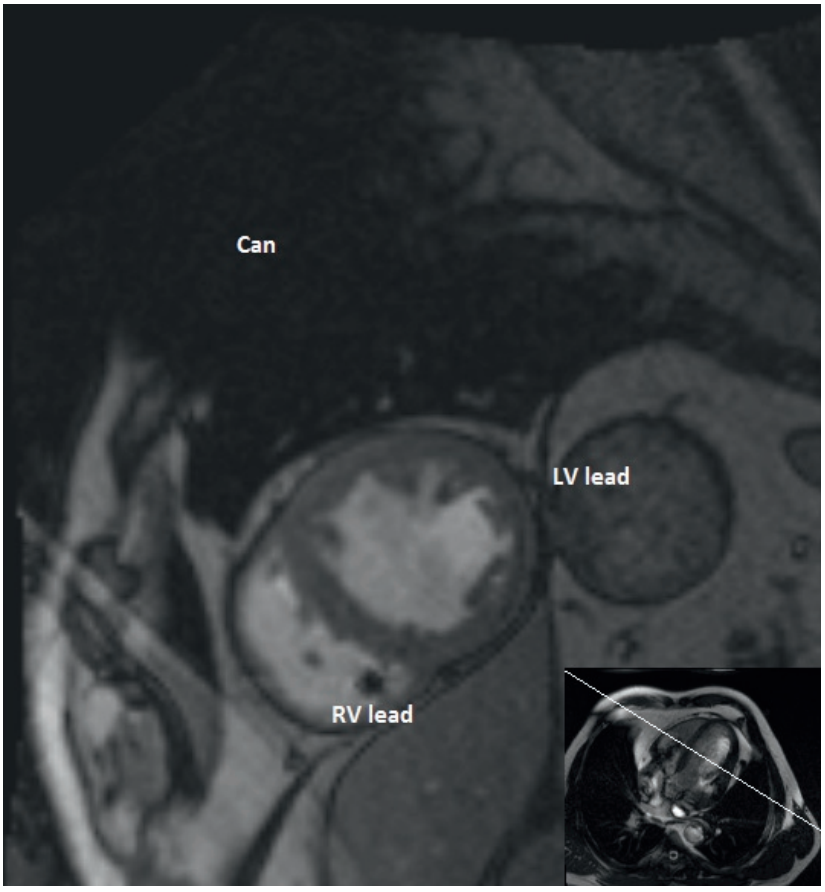


Figure 2: CMR imaging in a patient implanted with a CRT-D: Short-axis cine image in a patient implanted with a CMR-compatible CRT device demonstrating good image quality using a retrospectively ECG-gated spoiled gradient echo (SPGR) sequence.

Measuring LV stroke volume during different pacing configurations allows for a volume-based optimization strategy similar to the invasive pressure-volume loop approach. Moreover, CMR volumes may be combined with brachial pressure measurements to obtain completely non-invasive pressure-volume loops as recently demonstrated by Seemann et al.(17) Non-invasive pressure-volume loop optimization could potentially result in a similar one-third additional LV pump function improvement on top of conventional CRT, but without the risks of an invasive procedure.

Intra-cardiac conductance optimization

As the heart undergoes functional and structural changes during the process of reverse remodeling after CRT, optimal device settings may vary over time. Continuous assessment of LV pump performance enables non-stop optimization of LV pump function during real-life. Surrogate parameters of LV pump function can be derived by the device itself using the same principle as the (invasive) conductance catheter. LV conductance is measured between standard ventricular leads by applying a current between the RV coil and one of the LV electrodes and measuring the returning voltage between the RV ring and one of the LV electrodes, see figure 3. This technique enables real-time optimization of CRT by maximizing the amplitude of the conductance signal, resembling LV stroke volume.(18) Furthermore, this method may be used for remote home monitoring to timely detect heart failure progression and prevent heart failure hospitalization. Lastly, the conductance technique may be used to detect hemodynamic unstable arrhythmias and provide appropriate ICD therapy. Taken together, intra-cardiac conductance measurements may have large implications for patients with HF implanted with a biventricular device. Since validation studies showed promising results with accurate and robust assessment of LV volume changes,(18-20) future studies in a clinical trial setting are awaited.

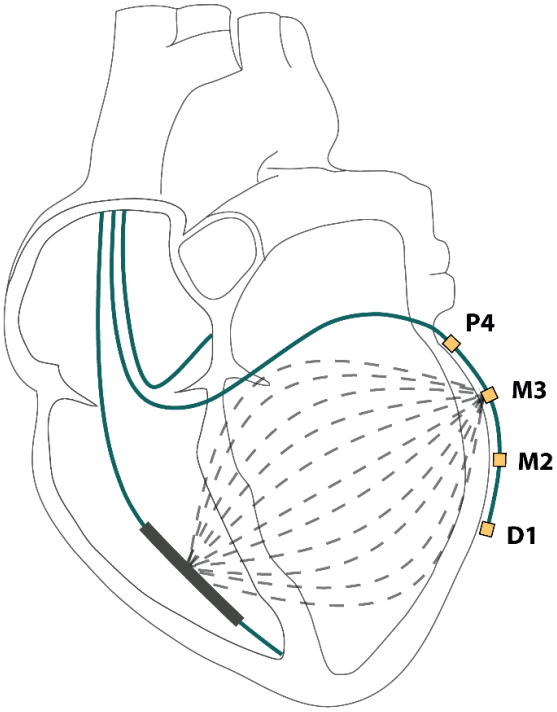


Figure 3: Intra-cardiac conductance measurements: Intra-cardiac conductance is measured by applying a current between the RV coil and one of the LV electrodes (in this example M3) and measuring the returning voltage between the RV ring and one of the LV electrodes (D1 or M2 or P4).

Heart rate optimization

Cardiac output is the product of stroke volume and heart rate. In addition to strategies that optimize LV stroke volume (as previously discussed), improving HR responsiveness during exercise may further improve exercise capacity in patients with HF and CI. The ADAPTION (Rate Adaptive Atrial Pacing in Heart Failure Patients with Chronotropic Incompetence) trial led by our group aims to assess the ability of minute ventilation sensor driven rate-adaptive pacing to restore functional capacity and quality of life in HF patients with CI. It is hypothesized that CI is common in the heart failure population and that reversal of CI by rate adaptive pacing using physiological (minute ventilation) activity sensors could potentially add to the benefit of cardiac implantable electronic devices such as CRT.

New cardiac pacing techniques

Recently, His bundle pacing (HBP) has gained interest as an alternative to biventricular pacing (CRT). By stimulating native conduction tissue distal to the conduction block causing LBBB, normal conduction pathways are recruited and relatively normal electrical activation of the ventricles is accomplished (figure 4). HBP might overcome pump function deterioration induced by conventional right ventricular pacing, and several studies have shown HBP to achieve greater electrical resynchronization compared to conventional CRT.(21) Further pump function improvement might even be achieved by His-Optimized CRT (HOT-CRT) in which His bundle pacing is combined with biventricular pacing or univentricular pacing to further improve synchrony.

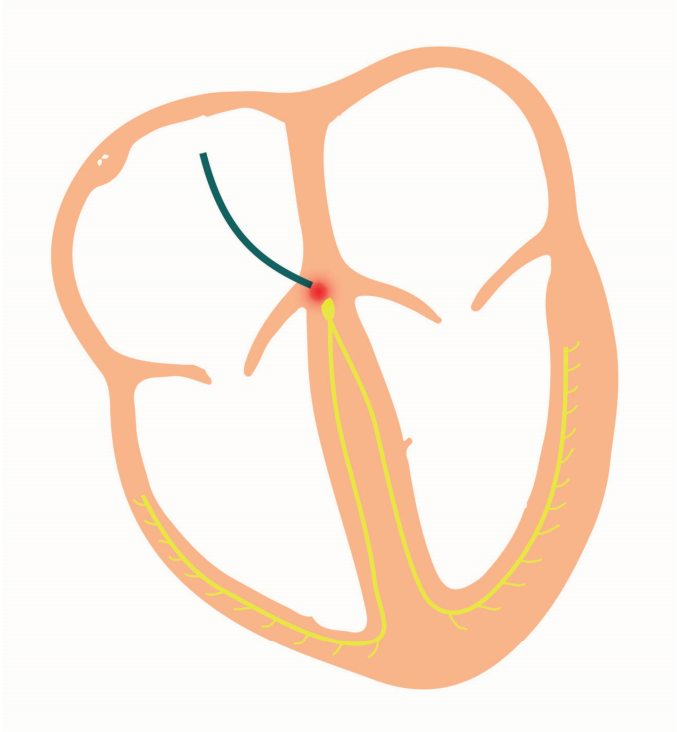


Figure 4: His Bundle Pacing: His Bundle Pacing engages the His bundle-Purkinje conduction system (in yellow) and can restore physiological activation of the ventricles with correction of (proximally located) bundle branch block.

Recently, a feasibility study showed that HOT-CRT was successfully achieved in 25 of 27 patients.(22) QRS duration at baseline was 183±27 ms and significantly narrowed to 162±17 ms with CRT, to 151±24 ms during HBP, and further to 120±16 ms during HOT-CRT. However, electrical resynchronization with HOT-CRT has never been evaluated in greater detail than by simply measuring QRS duration. Currently the HOT-CRT study is conducted at the University Hospital of Geneva which aims an in-depth electrical characterization of HOT-CRT using ECG imaging. Other new LV pacing approaches include endocardial pacing as well as leadless LV pacing.(23) In endocardial pacing, the LV lead is placed in the LV endocardium through a trans-septal atrial or ventricular approach. Although the operator will be able to reach all regions off the LV and endocardial pacing results in fast LV depolarization, this technique is hampered by an increased risk of thrombo-embolic events.(24,25) In contrast, the use of a leadless endocardial LV lead electrode avoids thrombo-embolic risks.(26) Leadless pacemakers could be the future of cardiac pacing.

REFERENCES

1. Varma N, Lappe J, He J, Niebauer M, Manne M, Tchou P. Sex-Specific Response to Cardiac Resynchronization Therapy: Effect of Left Ventricular Size and QRS Duration in Left Bundle Branch Block. JACC Clin Electrophysiol. 2017;3(8):844-53.
2. Prinzen FW, Vernooy K, De Boeck BW, Delhaas T. Mechano-energetics of the asynchronous and resynchronized heart. Heart Fail Rev. 2011;16(3):215-24.
3. Chung ES, Leon AR, Tavazzi L, Sun JP, Nihoyannopoulos P, Merlino J, et al. Results of the Predictors of Response to CRT (PROSPECT) trial. Circulation. 2008;117(20):2608-16.
4. Russell K, Eriksen M, Aaberge L, Wilhelmsen N, Skulstad H, Gjesdal O, et al. Assessment of wasted myocardial work: a novel method to quantify energy loss due to uncoordinated left ventricular contractions. Am J Physiol Heart Circ Physiol. 2013;305(7):H996-1003.
5. Vecera J, Penicka M, Eriksen M, Russell K, Bartunek J, Vanderheyden M, et al. Wasted septal work in left ventricular dyssynchrony: a novel principle to predict response to cardiac resynchronization therapy. Eur Heart J Cardiovasc Imaging. 2016;17(6):624-32.
6. Leyva F, Foley PW, Chalil S, Ratib K, Smith RE, Prinzen F, et al. Cardiac resynchronization therapy guided by late gadolinium-enhancement cardiovascular magnetic resonance. J Cardiovasc Magn Reson. 2011;13:29.
7. Holzmeister J, Gorcsan J, 3rd, Ruschitzka F. Cardiac-resynchronization therapy in heart failure with a narrow QRS complex. N Engl J Med. 2014;370(6):580-1.
8. Daubert C, Behar N, Martins RP, Mabo P, Leclercq C. Avoiding non-responders to cardiac resynchronization therapy: a practical guide. Eur Heart J. 2017;38(19):1463-72.
9. Mafi Rad M, Wijntjens GW, Engels EB, Blaauw Y, Luermans JG, Pison L, et al. Vectorcardiographic QRS area identifies delayed left ventricular lateral wall activation determined by electroanatomic mapping in candidates for cardiac resynchronization therapy. Heart Rhythm. 2016;13(1):217-25.
10. Maass AH, Vernooy K, Wijers SC, van 't Sant J, Cramer MJ, Meine M, et al. Refining success of cardiac resynchronization therapy using a simple score predicting the amount of reverse ventricular remodelling: results from the Markers and Response to CRT (MARC) study. Europace. 2018;20(2):e1-e10.
11. Emerek K, Friedman DJ, Sorensen PL, Hansen SM, Larsen JM, Risum N, et al. Vectorcardiographic QRS area is associated with long-term outcome after cardiac resynchronization therapy. Heart Rhythm. 2019;16(2):213-9.
12. van Stipdonk AMW, Ter Horst I, Kloosterman M, Engels EB, Rienstra M, Crijns H, et al. QRS Area Is a Strong Determinant of Outcome in Cardiac Resynchronization Therapy. Circ Arrhythm Electrophysiol. 2018;11(12):e006497.
13. Bear LR, Huntjens PR, Walton RD, Bernus O, Coronel R, Dubois R. Cardiac electrical dyssynchrony is accurately detected by noninvasive electrocardiographic imaging. Heart Rhythm. 2018;15(7):1058-69.
14. Salden OAE, van den Broek HT, van Everdingen WM, Mohamed Hoesein FAA, Velthuis BK, Doevendans PA, et al. Multimodality imaging for real-time image-guided left ventricular lead placement during cardiac resynchronization therapy implantations. Int J Cardiovasc Imaging. 2019.

15. Nguyen UC, Cluitmans MJM, Luermans J, Strik M, de Vos CB, Kietselaer B, et al. Visualisation of coronary venous anatomy by computed tomography angiography prior to cardiac resynchronisation therapy implantation. Neth Heart J. 2018;26(9):433-44.
16. Bhagirath P, Zweerink A, Allaart C, Gotte M. Imaging for cardiac resynchronisation therapy requires cardiac magnetic resonance. Neth Heart J. 2018;26(12):640.
17. Seemann F, Arvidsson P, Nordlund D, Kopic S, Carlsson M, Arheden H, et al. Noninvasive Quantification of Pressure-Volume Loops From Brachial Pressure and Cardiovascular Magnetic Resonance. Circ Cardiovasc Imaging. 2019;12(1):e008493.
18. Larson ER, Porterfield JE, Sagar S, Marmol-Velez J, Panday M, Escobedo D, et al. Admittance to detect alterations in left ventricular stroke volume. Heart Rhythm. 2014;11(11):2075-83.
19. Ginks MR, Sciaraffia E, Karlsson A, Gustafsson J, Hamid S, Bostock J, et al. Relationship between intracardiac impedance and left ventricular contractility in patients undergoing cardiac resynchronization therapy. Europace. 2011;13(7):984-91.
20. Zima E, Lippert M, Czygan G, Merkely B. Determination of left ventricular volume changes by intracardiac conductance using a biventricular electrode configuration. Europace. 2006;8(7):537-44.
21. Arnold AD, Shun-Shin MJ, Keene D, Howard JP, Sohaib SMA, Wright IJ, et al. His Resynchronization Versus Biventricular Pacing in Patients With Heart Failure and Left Bundle Branch Block. J Am Coll Cardiol. 2018;72(24):3112-22.
22. Vijayaraman P, Herweg B, Ellenbogen KA, Gajek J. His-Optimized Cardiac Resynchronization Therapy to Maximize Electrical Resynchronization. Circ Arrhythm Electrophysiol. 2019;12(2):e006934.
23. Galand V, Singh JP, Leclercq C. Alternative left ventricular pacing approaches for an optimal cardiac resynchronization therapy. Heart Rhythm. 2019.
24. Gamble JHP, Herring N, Ginks M, Rajappan K, Bashir Y, Betts TR. Endocardial left ventricular pacing for cardiac resynchronization: systematic review and meta-analysis. Europace. 2018;20(1):73-81.
25. Morgan JM, Biffi M, Geller L, Leclercq C, Ruffa F, Tung S, et al. ALternate Site Cardiac ResYNChronization (ALSYNC): a prospective and multicentre study of left ventricular endocardial pacing for cardiac resynchronization therapy. Eur Heart J. 2016;37(27):2118-27.
26. Reddy VY, Miller MA, Neuzil P, Sogaard P, Butter C, Seifert M, et al. Cardiac Resynchronization Therapy With Wireless Left Ventricular Endocardial Pacing: The SELECT-LV Study. J Am Coll Cardiol. 2017;69(17):2119-29.

Appendix

Appendix I

Nederlandse Samenvatting

Hartfalen is een klinisch syndroom dat gekenmerkt wordt door een afwijking van de cardiale structuur of functie die leidt tot het falen van het hart om de benodigde zuurstof te leveren aan de weefsels en organen. In praktijk zal dit zich uiten door snelle vermoeidheid en kortademigheid bij geringe inspanning. Hartfalen komt frequent voor in de westerse landen en zal in de loop der jaren steeds vaker voorkomen door de toenemende vergrijzing. De overlevingskans na de diagnose bedraagt ongeveer 50% na vijf jaar en 10% na tien jaar. Een kwart van de patiënten die zich presenteren met hartfalen heeft een geleidingsstoornis in het hart met een verlengde QRS-duur op het elektrocardiogram (ECG). In de meerderheid van de gevallen betreft het een linkerbundeltakblok (LBTB). Deze geleidingsvertraging heeft ten gevolge dat verschillende delen van het hart zich op verschillende tijdsmomenten samentrekken. Deze ongecoördineerde en ondoeltreffende werking van het hart zorgt voor verdere daling van de linkerventrikel pompfunctie en een toename van het hartfalen.

Cardiale Resynchronisatietherapie (CRT), een pacemakertherapie waarbij men beoogt door middel van biventriculaire hartspier-stimulatie de linkerventrikel weer synchroon te laten contraheren, heeft een bewezen gunstig effect op de kwaliteit van leven en overleving van patiënten met hartfalen en een LBTB. Bij CRT worden drie draden geïmplanteerd: één in het rechteratrium, één in de rechterventrikel en één draad op de laterale wand van de linkerventrikel. Met deze drie draden kan de ventriculaire op de atriale activatie worden afgestemd maar ook de binnen de linkerventrikel activatie van het septum en de laterale wand. De belangrijkst criteria om in aanmerking te komen voor CRT zijn: linkerventrikeldysfunctie met een ejectiefractie ≤35%, een verlengde QRS-duur op het ECG ≥130ms en aanhoudende hartfalen klachten ondanks maximale medicamenteuze therapie. Er is echter gebleken dat de CRT-behandeling niet altijd het gewenste effect sorteert. Bij een-derde van de patiënten treedt geen verbetering op van de klachten of in inspanningstolerantie, de zogenaamde “non-responders”. Onderzoek binnen CRT richt zich met name op twee pijlers

om de effectiviteit van deze therapie te vergroten: (i) het vooraf selecteren van potentiële “responders” door middel van beeldvormende technieken en (ii) het optimaliseren van de CRT instellingen na implantatie om een zo groot mogelijke toename in pumpfunctieverbetering te bewerkstelligen.

Deel IA Normaliseren van QRS-duur ten opzichte van linkerventrikel grootte

Bij CRT wordt een elektrische ziekte (LBTB) behandeld door middel van een elektrische therapie (hartspier-stimulatie). Het is dan ook voor de hand liggend dat de patiënten-selectie voor CRT is gebaseerd op een elektrische maat, namelijk QRS-duur. Hoewel een toename in QRS-duur het gevolg kan zijn van trage cel-tot-cel geleiding (het ware LBTB), kan deze ook het gevolg zijn van een toename in geleidingsafstand door dilatatie van het falende hart. Het eerste deel van dit proefschrift introduceert een nieuw concept waarbij structurele eigenschappen van het hart worden meegewogen in de bepaling van de elektrische geleidingvertraging, namelijk door QRS-duur te corrigeren voor de grootte van het hart. De hypothese is dat deze gecombineerde maat sterker voorspellend is voor de effecten van CRT dan QRS-duur alleen. In **hoofdstuk 2** wordt dit concept getest in een groep van tweeëndertig patiënten die voorafgaand aan CRT implantatie een MRI onderzoek ondergingen. Na implantatie werd het acute effect van CRT op de linkerventrikel pompfunctie gemeten door invasieve druk-volume lussen. Het normaliseren van de QRS-duur voor de hartgrootte (op MRI gemeten) verbeterde de relatie met acute pompfunctie veranderingen tijdens CRT. Tevens werd aangetoond dat vrouwen beter reageren op CRT dan mannen. Dit verschil is mogelijk toe te schrijven aan het verschil in hartgrootte tussen beide seksen. Aangezien het vrouwenhart kleiner is dan dat van de man zal de QRS-duur hierdoor korter zijn. Om de vereiste QRS-duur te bereiken voor CRT (de richtlijnen zijn gelijk voor mannen en vrouwen), heeft het vrouwenhart relatief meer geleidingsvertraging en zal daardoor potentieel beter reageren op CRT.

Hoofdstuk 3 vertaalt de rol van QRS-duur normalisatie naar het voorspellen van klinische eindpunten in een grote populatie van tweehonderdvijftig patiënten die in aanmerking kwamen voor CRT. Het normaliseren van QRS-duur voor de hartgrootte verbeterde de voorspellende waarde voor de overlevingsduur na CRT implantatie. Daarnaast had de genormaliseerde QRS-duur toegevoegde waarde in een predictiemodel samen met leeftijd, atriumfibrilleren, nierfunctie

en hartfalen etiologie. Deze bevindingen wijzen erop dat een multimodaliteit benadering met zowel elektrische, structurele alsook klinische parameters de patiënten-selectie voor CRT zou kunnen verbeteren.

Deel IB Beeldvorming van de ongecoördineerde contractie van het hart

De verbetering in linkerventrikel pompfunctie tijdens CRT is niet gebaseerd op de elektrische resynchronisatie zelf, maar komt voort uit het re-coördineren van de mechanische contractie tussen verschillende delen van het hart, met name tussen het septum en de laterale wand. Vanuit deze gedachte lijkt het zinvol om vooraf te kijken of het substraat van ongecoördineerde contractie aanwezig is, om zo de gunstige effecten van CRT op de linkerventrikel functie te voorspellen. Deel twee van het proefschrift onderzoekt de potentiële rol van beeldvormende technieken die de myocardiale contractie visualiseren en kwantificeren om zodoende de patiënten-selectie voor CRT te verbeteren. In **hoofdstuk vier** worden regionale contractie waarden gecombineerd met linkerventrikel druk curves om de myocardiale arbeidsverdeling te berekenen. Allereerst werd gezien dat de bijdrage van het septum aan de totale arbeidsproductie sterk varieert tussen hartfalen patiënten met een LBTB. Ten tweede bleek dat een lage arbeidsbijdrage (hoge arbeidsverspilling) van het septum gerelateerd was aan een grotere pompfunctieverbetering tijdens CRT. Beeldvormende technieken die de ongecoördineerde contractie van het hart kwantificeren kunnen zodoende een indruk geven van de negatieve effecten van het LBTB op de mechanische efficiëntie van het hart, en daarmee iets zeggen over de potentiële ruimte voor verbetering tijdens CRT. In deze kleinschalige studie ondergingen de proefpersonen cardiale MRI met aanvullende ‘tagging’ opnames (CMR-TAG) om hoge kwaliteitsmetingen van regionale contracties te verkrijgen. In de klinische praktijk is deze gespecialiseerde techniek echter zeer beperkt beschikbaar. Derhalve is het nuttig om ook de rol van alternatieve beeldvormende technieken zoals MRI feature tracking (CMR-FT) en speckle tracking echocardiografie (STE) te onderzoeken. In **hoofdstuk vijf** worden regionale contractiewaarden gemeten met CMR-FT en STE en vergeleken met CMR-TAG (gouden standaard). Zevenentwintig patiënten die een CRT apparaat kregen in het kader van de Markers And Response to CRT (MARC) studie, ondergingen vooraf MRI beeldvorming alsook een echocardiografisch onderzoek. Zowel CMR-FT als STE bleken geschikte alternatieven voor CMR-TAG, met name in het kwantificeren

van een ongecoördineerde contractie van het hart. **Hoofdstuk zes** voorziet in de echocardiografische vervolggegevens van deze patiënten na 1 jaar, om zodoende de voorspellende waarde van verschillende parameters gemeten met verschillende technieken te vergelijken. We vonden dat de eind-systolische septum lengteverandering (ESS_{sep}) het sterkst gerelateerd was aan echocardiografische verbetering in pompfunctie na CRT, onafhankelijk van de beeldvormende techniek die werd gebruikt. Het detecteren van een ongecoördineerde septumbeweging met veel systolische rek (hoge ESS_{sep}) tijdens LBTB was geassocieerd met een grote verbetering in pompfunctie na 1 jaar. Het meten van ESS_{sep} door welke beschikbare techniek dan ook had bewezen toegevoegde waarde in het voorspellen van de effecten van CRT bovenop de criteria in de huidige richtlijnen (QRS-duur en morfologie). Hoewel deze beeldvormende technieken nog niet dagelijks worden gebruikt in het selecteren van patiënten voor CRT, zou dit in de toekomst mogelijk een toegevoegde waarde kunnen hebben. Dit onderzoek zou met name nuttig bijdragend zijn in patiënten waarbij getwijfeld word aan het nut van CRT (ischemische hartziekten, niet-typisch LBTB, korte QRS-duur). In het daaropvolgende deel van het proefschrift wordt een nieuwe techniek geïntroduceerd: de segment lengte in cine (SLICE) analyse. Het doel van SLICE is om de arts een simpele meettechniek te bieden om het effect van CRT te voorspellen op basis van standaard MRI beelden, gebaseerd op eerdere bevindingen. SLICE bestaat uit een serie handmatige metingen van een bepaalde segment lengte (septum of laterale wand) tussen vaste anatomische herkenningspunten op standaard MRI korte-as cine beelden. De lengte-verandering van het segment door de cardiale cyclus heen kan worden omgezet in een contractiecurve. Als eerste stap werd SLICE gevalideerd tegen ‘gouden standaard’ CMR-TAG (**hoofdstuk 7**). Contractiewaarden verkregen met SLICE hadden een goede overeenkomst met CMR-TAG en bleken reproduceerbaar bij herhaalde metingen. Een voordeel van de SLICE techniek is het ontbreken van de noodzaak tot aanvullende CMR scan-sequenties (zoals bij CMR-TAG) of gespecialiseerde nabewerkingssoftware (zoals bij CMR-FT). Het meten van een parameter die de volledige SLICE contractiecurve omvat bleek echter tijdrovend (tot 60 minuten). Bij de vervolgstudie werd SLICE analyse verricht bij zevenenvijftig MARC patiënten die een standaard MRI onderzoek ondergingen alvorens CRT implantatie zoals beschreven in **hoofdstuk acht**. De voorspellende

waarde van verschillende SLICE contractie parameters werd onderling vergeleken waarbij ESS_{sep} de sterkste relatie liet zien met pompfunctieverbetering na CRT. Deze resultaten komen overeen met de voorgaande bevindingen middels CMR-TAG, CMR-FT en STE, daarmee lijkt ESS_{sep} een robuuste voorspeller voor CRT response te zijn. Het voordeel van de ESS_{sep} parameter is dat deze slechts twee (eind-diastolische en eind-systolische) segment lengte metingen vereist en binnen 10 minuten kan worden verricht, resulterend in een snelle en eenvoudige meettechniek. Ten slotte werd de rol van de veelbelovende SLICE-ESS_{sep} meting uitgebreid naar het voorspellen van klinische eindpunten in een grote populatie van CRT patiënten. **Hoofdstuk negen** presenteert een studie met tweehonderdachttien patiënten die een MRI onderzoek inclusief late-contrast-aankleuring (LGE) ondergingen alvorens CRT implantatie. De belangrijkste bevindingen van deze studie waren dat een positieve ESS_{sep} waarde in de uitgangssituatie gerelateerd was aan een twee-tot-drie maal lager optreden van overlijden en hartfalen opnames na CRT implantatie. De voorspellende waarde van ESS_{sep} werd verminderd bij aanwezigheid van littekenweefsel in het septum, hetgeen erop wijst dat aanvullende LGE opnames nodig zijn om verlittekening als oorzaak van septale oprekking uit te sluiten. In de klinische praktijk wordt MRI beeldvorming in toenemende mate gebruikt om patiënten te screenen voor CRT door het meten van de linkerventrikel ejectiefractie gecombineerd met LGE beeldvorming om de linkerventrikel-draad buiten een gebied met littekenweefsel te plaatsen. Aanvullende SLICE analyse van het septum zou de diagnostische opbrengst van het MRI onderzoek verder kunnen vergroten en de patiënten-selectie voor CRT kunnen verbeteren.

Deel II Optimaliseren van CRT instellingen

In deel twee van het proefschrift worden verschillende strategieën beschreven om CRT instellingen te individualiseren en zodoende de gegeven therapie te optimaliseren. De eerste twee hoofdstukken zijn onderdeel van de OPTICARE-QLV (optimalisatie van CRT met een quadripolaire linkerventrikel draad) studie. Het hoofddoel van de OPTICARE-QLV studie was om elektrische parameters (Q op het ECG tot linkerventrikel sensing interval, QLV) te relateren aan acute hemodynamische response tijdens CRT met een quadripolaire linkerventrikel draad zoals beschreven in **hoofdstuk tien.** Achtenveertig patiënten met

hartfalen en een LBTB werden prospectief geïncludeerd en ondergingen zowel elektrische als invasieve druk-volume lus metingen direct na CRT implantatie. Alhoewel er een grote variatie was in acute hemodynamische CRT response tussen verschillende electroden van de quadripolaire linkerventrikel draad, bleken elektrische parameters (QLV; QLV/QRS-duur) niet in staat de beste stimulatie electrode te identificeren. Derhalve zal optimalisatie van de stimulatie configuratie moeten plaatsvinden op basis van andere parameters. Het effect van CRT kan bijvoorbeeld gemeten worden door middel van invasieve hemodynamische metingen. Van oudsher wordt de maximale snelheid van linkerventrikel druktoename (dP/dt_{max}) gebruikt als surrogaat voor linkerventrikelfunctie. Als alternatief kan de slagarbeid (SW) bepaald worden op basis van druk-volume lussen. **Hoofdstuk elf** onderzoekt de acute effecten van dP/dt_{max} versus SW optimalisatie, en relateert directe hemodynamische veranderingen aan lange termijn respons. Hierbij werd aangetoond dat hemodynamische optimalisatie resulteert in een-derde additionele verbetering in de parameter gebruikt voor optimalisatie (zowel dP/dt_{max} alsook SW). Een verbetering in de ene parameter ging echter niet gepaard met een verbetering in de andere hetgeen wijst op verschillende onderliggende mechanismen. Waar dP/dt_{max} optimalisatie resulteerde in de grootste toename in linkerventrikel contractiliteit, leidde SW optimalisatie tot een betere ventriculo-arteriële koppeling met een hoger slagvolume. In tegenstelling tot acute veranderingen in SW die duidelijk gerelateerd waren aan CRT response op lange termijn, bleken acute veranderingen in dP/dt_{max} geen voorspellende waarde te hebben. Zodoende vormt hemodynamische optimalisatie middels druk-volume lussen een potentiële strategie om een maximale toename in pumpfunctieverbetering te behalen in CRT patiënten met een quadripolaire linkerventrikel draad. Ten slotte geeft **hoofdstuk twaalf** een literatuuroverzicht aangaande de rol van cardiale geïmplanteerde elektronische apparaten (ICD; CRT) voor de behandeling van chronotrope incompetentie (CI) in hartfalen. Een aanzienlijk deel van de hartfalen patiënten is tegenwoordig geïmplanteerd met een elektronisch device dat ons in staat stelt om de hartfrequentie te bestuderen en zo nodig ondersteunende pacemaker therapie te bieden. Frequentie-adaptieve pacemakertherapie lijkt gunstige effecten te sorteren op de inspanningstolerantie en overleving van patiënten met manifeste CI. Ontwikkelingen in de device technologie waarbij fysiologische sensoren worden

gebruikt om fysieke inspanning te detecteren zullen mogelijk de toekomstige behandeling van CI in hartfalen patiënten verbeteren.

Klinische implicaties

Patiënten met hartfalen, een verminderde ejectiefractie en een breed QRS complex op het ECG hebben een indicatie voor CRT volgens de huidige richtlijnen. Electrische resynchronisatie resulteert in versmalling van het QRS complex en leidt tot linkerventrikel pompfunctie verbetering door mechanische re-coördinatie van de linkerventrikel contractie. Voorgaande studies hebben laten zien dat CRT kandidaten met een smal QRS complex geen voordeel ontlenen aan CRT. Anderzijds heeft niet iedere patiënt met een breed QRS complex baat van de therapie. Derhalve zijn additionele selectiecriteria nodig om het aantal non-responders te reduceren. De huidige richtlijnen voor CRT rechtvaardigen het gebruik van cardiale beeldvorming enkel om de linkerventrikel ejectie fractie te meten. Informatie over de hartgrootte kan echter de voorspellende waarde van QRS-duur vergroten zoals aangetoond in het eerste deel van het proefschrift (QRS-duur normalisatie). Daarnaast kan het inzichtelijk maken van myocardiale contractie patronen de patiënten-selectie voor CRT potentieel verbeteren. Het constateren van een ongecoördineerde beweging (oprekken) van het septum had toegevoegde waarde in het voorspellen van pompfunctieverbetering na CRT bovenop de huidige richtlijnen, ongeacht de beeldvormende techniek die werd gebruikt. Wanneer verschillende technieken vergeleken worden heeft cardiale MRI unieke voordelen ten opzichte van echocardiografie in het nauwkeurig meten van hartgrootte en functie en het detecteren van littekenweefsel. Aanvullende SLICE analyse van het septum vergroot de diagnostische opbrengst van het MRI onderzoek dat daardoor als eerste-keuze techniek geldt voor CRT kandidaten. Het verrichten van MRI onderzoek is met name interessant in patiënten bij wie een gunstig effect van CRT onzeker is (hoge leeftijd, eerder hartinfarct, niet-typisch LBTB op het ECG). Wanneer er bij de MRI sprake is van ernstige dilatatie van de linkerventrikel (laag genormaliseerd QRSd), gebrek aan ongecoördineerde beweging van het septum (negatieve SLICE-ESS_{sep}), en uitgebreid littekenvorming (met name van het septum), kan CRT mogelijk achterwege worden gelaten. Aangezien verschillende typen parameters toegevoegde waarde lieten zien in predictiemodellen valt een multimodaliteit selectie met klinische, elektrische (ECG) en mechanische (MRI)

parameters te overwegen alvorens over te gaan tot CRT implantatie. Na het besluit tot CRT implantatie kan optimalisatie van de instellingen overwogen worden om het volledige rendement uit de quadripolaire linkerventrikel draad te behalen. Elektrische en echocardiografische parameters worden hiervoor het meest gebruikt hoewel hier geen overtuigend wetenschappelijk bewijs voor bestaat. Hemodynamische optimalisatie middels druk-volume lussen resulteerde in een-derde additionele pompfunctie verbetering bovenop de standaard therapie. Deze invasieve optimalisatie techniek is misschien niet geschikt voor de klinische praktijk, maar het concept van volume (in plaats van druk) geleide optimalisatie vormt de basis voor niet-invasieve surrogaten zoals intra-cardiale impedantie tussen draden, of CRT stimulatie in de MRI. Ten slotte kan behandeling van CI middels frequentie modulerende algoritmes de klinische opbrengt van CRT vergroten.

Appendix II

Dankwoord

Promoveren is een bijzondere vorm van duursport. Het tijdsbestek tussen onderzoeksvoorstel en publicatie loopt in de jaren en vraagt volharding. Anderzijds is de beloning groot als je 'jouw' bevindingen mag presenteren op congres, het manuscript gepubliceerd wordt in een wetenschappelijk tijdschrift, en uiteindelijk het proefschrift vormt zoals deze. Promoveren doe je echter niet alleen. In de eerste plaats wil ik dit dankwoord richten aan alle patiënten die hebben deelgenomen. Daarnaast wil ik alle collega's, familie en vrienden bedanken.

Copromotor **dr. C.P. Allaart**, beste Cor, jij bent de drijvende kracht achter dit proefschrift. In juni 2012 ben ik voor het eerst op gesprek geweest om als student extra onderzoek te doen naast de geneeskunde studie. Met veel enthousiasme tekende je een druk curve op het whiteboard en wist mij ervan te overtuigen om me volledig op een of andere parameter genaamd 'Tau' te storten. In de jaren daarna ben je altijd een voorbeeld geweest als wetenschapper pur sang (niet snel wel grondig). Buiten werktijd heb ik je ook altijd sterk weten te waarderen en ik hoop dat er nog vele borrels, etentjes, Z4 ritten (kap open) en whiskeys mogen volgen!

Copromotor **prof.dr. R. Nijveldt**, beste Robin, ik bewonder jouw tomeloze energie en enthousiasme. Jij hebt mij geleerd om niet in problemen te denken maar om er vol voor te gaan. Als MRI specialist heb je een flinke stempel op het proefschrift weten te drukken. Mijn verblijf in Duke University Hospital was de kers op de taart waar ik je bijzonder dankbaar voor ben. Hoewel je bent overgelopen naar Radboud UMC onderhouden we goed contact en ik kijk erg uit naar je oratie als professor.

Promotor **prof.dr. A.C. van Rossum**, beste Bert, dank voor het gestelde vertrouwen in mij als promovendus. Hoewel cardiale stimulatie enigszins buiten jouw onderzoeksgebied valt hebben we elkaar op het gebied van cardiale MRI goed kunnen vinden. Tevens wil ik je bedanken voor het steunen mijn huidige onderzoeks-avontuur in Genève. Als afdelingshoofd heb ik altijd veel respect gehad voor je verbindende rol binnen de afdeling.

Tevens wil ik de leden van de leescommissie, **prof.dr. C. Boer, prof.dr. M.J. Schalij, prof. dr. H. Burri, dr. M.J.W. Götte, prof.dr. J. Stoker** bedanken voor hun bereidwilligheid en inzet voor de beoordeling van dit proefschrift. Daarnaast speciale dank aan **prof.dr. F.W. Prinzen** voor zijn rol als gast-opponent.

Mijn voorgangers **Gerben Jan de Roest** en **LiNa Wu** hebben ervoor gezorgd dat ik aan boord van een rijdende trein stapte. LiNa jouw inspanningen voor de MARC studie hebben belangrijk bijgedragen aan dit proefschrift. Hoewel jouw toekomst niet meer bij de cardiologie ligt wens ik je het allerbeste toe. Gerben Jan, kortweg Gerjan, jij was mijn directe begeleider toen ik begon als student-onderzoeker en ik had mij er geen betere kunnen wensen. Met kritische blik en verstand van zaken heb je mij een stoomcursus ‘promoveren op CRT’ gegeven en hebben we gezamenlijk mijn eerste publicatie geschreven. We zijn later nog vaak bij elkaar over de vloer geweest voor het beruchte “research-avondje” onder genot van hapje en drankje(s). Ik weet zeker dat je een uitstekende device-cardioloog zult worden!

Vervolgens gaat mijn dank uit naar het ritmeteam met o.a. **Cor Allaart, Michiel Kemme, Vokko van Halm, Carel de Cock, Giovanni Tahapary, Herbert Hauer, Thijs Hendriks, Freek Hörters, Stefan Timmer** en **Lourens Robbers.** De ritmeteambespreking was, ondanks haar variabele tijdstippen en locaties, een vast ijkpunt in de week waar ik veel geleerd heb over de indicatiestelling bij device patiënten en waar studiekandidaten werden gescreend. Andere betrokkenen bij studieprocedures waren de ICD technici **Noortje, Marjolein, Mindel, Eva, Mariska, Kyle** en **Joran**; alle HCK personeel met speciale vermelding van **Leon** op HCK1 en planners **Karolien, Nicole, Karin, Els**; ondersteuning van St. Jude (nu Abbott) voor OPTICARE procedures door **Jos, Anna** en **Rob**; ondersteuning van CD Leycom door **Jan Schreuder**; gespecialiseerd

verpleegkundige **Saskia Elshout** met wie ik een hoop een-tweetjes heb gedaan (jij de voorzet tijdens het voorlichtingsgesprek en ik vervolgens studiedeelname van de patiënt binnenschieten); research verpleegkundigen **Debby, Ellen, Yvonne, Mineke, Britt, Hanneke**; gespecialiseerd hartfalen verpleegkundigen **Ron, Mireille, Irene**; afdelingssecretaressen **Gaby** en **Sandra**; statisticus **Peter vd Ven** en ten slotte (emeritus) systeembeheerder **Johan Karreman**. Allen bedankt!

Studies met cardiale beeldvorming (MARC; OPTICARE) zijn mogelijk gemaakt door de MRI cardiologen **Robin Nijveldt, Ramon van Loon, Marco Götte, Aernout Beek, Tjeerd Germans, Jasper Selder, Lisah Wong,** diverse MRI fellows, laboranten en technisch genie **Joost Kuijer**. **Mary Belderok** bedankt voor het plannen van de MRI onderzoeken (uiteraard pas nadat ik lengte en gewicht had nagevraagd). Verder wil ik de cardiologen **Thelma Konings, Karin de Boer, Otto Kamp, Louis Handoko** en echolaboranten **Vidya, Arnoud, Linda, Marian** ontzettend bedanken voor het vervaardigen en beoordelen van alle studie echo's.

De overige cardiologen **Yolande Appelman, Paul Knaapen, Jorrit Lemkes, Koen Marques, Niels van Royen, Alex Nap, Gerrit Veen, Niels Verouden**, hebben bijgedragen aan een leerzame tijd in de kliniek waarbij ook regelmatig gelachen mocht worden (met name tijdens de overdracht en de IC visite met dr. Veen). Tevens wil ik alle fellows en arts-assistenten bedanken voor de prettige samenwerken onder diensttijd maar ook daarbuiten (lees: borrels, wintersport!).

Dan is het nu de beurt aan vruchtbare samenwerkingen die met andere Nederlandse ziekenhuizen zijn ontstaan. Als eerste wil ik het Universitair Medisch Centrum Utrecht noemen waarmee wij intensief hebben samengewerkt tijdens de OPTICARE studie. Deze studie, uitgevoerd door **Wouter van Everdingen** onder bezielende leiding van der große **Mathias Meine**, heeft flink wat gezamenlijke publicaties opgeleverd. Wouter wij hebben intensief samengewerkt en het was dan ook een eer om jouw paranymf te mogen zijn. Ik bewonder je sportieve prestaties (bijna dagelijks op Strava) ondanks je drukke carrière binnen de radiologie en het starten van een gezinnetje in Arnhem. Het ga je goed en ik hoop dat we contact houden. Jouw

(wan)gedrag tijdens ACC Orlando zullen we voor het gemak maar even vergeten. De samenwerking met opvolgster **Odette Salden** verliep ook soepel, zij zal binnenkort zelf ook promoveren. Ten slotte wil ik de bijzonder sympathieke **Maarten-Jan Cramer** noemen als expert op het gebied van echocardiografie. Na Utrecht en Amsterdam volgde ook deelname van het Maastricht Universitair Medisch Centrum. Het was een waar genoegen om op bezoek te gaan bij de hoge heren uit het zuiden waaronder **Frits Prinzen** (fysiologie) en **Kevin Vernooy** (cardiologie). Maar ook de betrokken onderzoekers **Uyen Chau Nguyen** en **Floor Salden** zijn prettige en succesvolle (recente publicatie JACC) collega's gebleken. Ten slotte wil ik het gehele MARC studieteam bedanken met o.a. **Isabelle van Gelder, Alexander Maass, Frederik de Lange, Marc Vos, Michiel Rienstra** en mijn penvriend **Bastiaan Geelhoed** (goed voor honderden mails).

The following international collaborations are greatly acknowledged. First I want to thank my friends from Duke University Hospital (Durham, USA) for being their guest during my research scholarship. Special thanks to **Michele Parker** who helped me (a lot) with all the paperwork to get the J1 Visa and permission from the hospital for the SLICE project. The project was made possible by **Igor Klem** and **Raymond Kim** from the Duke CMR Center and **Brett Atwater** and **Daniel Friedman** from the electrophysiology department. Igor you were extremely friendly to me and I will never forget the boat trip that we made in Wilmington! Also many thanks to Daniel who proved to be a true wizard with Excel sheets.
Secondly, I want to thank my current colleagues at the University Hospital of Geneva. Although the NHI grant was granted to others, we found alternative ways to realize this one-year research fellowship. **Professor Burri**, dear Haran, after my arrival we went straight to the cathlab for a His implantation. Despite your busy days and crazy international flying schemes you always make time for our research projects. **Professor Mach**, dear François, thank you for having me at the cardiology department and inviting us for diner. **Carine Stettler** you are a great research nurse, without you I would not have survived. Also I was pleasantly surprised to find the Flemish (Nederlandstalige) device fellow **Elise Bakelants** sitting next to me. Elise I am looking forward to climbing the Col des Glières together! Furthermore I want to thank **Florence, Beatrice, Nicole, Nerea and Carine** for helping me out many times. Lastly I'd like to say thanks to my new Russian friend **Stepan Zubarev** for all HOT-CRT electrical imaging studies.

Dan is het nu de beurt aan mijn collega-onderzoekers in het VUmc. Allereerst een ode aan mijn kamergenoten **Raquel, Rahana** en **Stefan** met wie ik talloze uren heb doorgebracht in kamer ZH 4D38. Raquel, 1m60 pure dynamiet, jij hebt VUmc dikwijls op zijn grondvesten laten schudden met je woede-uitbarstingen. Daartegenover kon je op feestjes dan weer zomaar in slaap vallen. Dankzij jouw vlijmscherpe gevoel voor humor konden we vaak weer lachen om vlak daarvoor nog ondragelijke situaties. Heel veel succes met het afronden van de hart-brein studie! Rahana jij was regelmatig te vinden aan “de overkant”, een mysterieuze plek waar het basale onderzoek naar HCM plaatsvond. Ik wens je veel succes met het afronden van je promotie en de opleiding tot radioloog. Stefan Biesbroek, kortweg Bies, dat je het kleinste bureau had weerhield je er niet van om enorme stapels papier te verzamelen tussen een wildgroei van koffiebekertje waarbij om onduidelijke reden de laatste slok niet werd opgedronken. Je wisselde non-invasief MRI onderzoek af met weerzinwekkende beenspierbiopten. Ondanks de talloze REJECTS die we samen moesten doorstaan zijn er toch nog aardig wat meesterwerken op onze `wall of fame` belandt. Het traditionele vrijdagmiddag biertje uit de illegale koelkast met uiteenlopende muziek variërend van Simple Minds tot de Vengaboys vormde een goede afsluiter van de werkweek. **Anne-lotte, Marthe, Amaya, Mark** en **Luuk**, dankzij jullie floreert het ritmeonderzoek als nooit tevoren. Ik kijk er erg naar uit om jullie allemaal terug te zien op het EHRA congres in Wenen. Mark (om exacte te zijn M.Mulder2) wij hebben op het einde ook tijd doorgebracht als kamergenoten en jij bleek echt een mooi vent (….. -vrije zone!). Anne-lotte jij nam vaak het voortouw met het regelen van allerlei zaken waarvoor hulde. Marthe verraste vriend en vijand met haar haar directe uitspraken. Amaya organiseerde een mooi uitstapje naar de kust. Luuk je bent een waardige opvolger en ik wens je heel veel succes met het afronden van de PICARIA studie (gas erop!). Binnen de groep was ook een sportieve club van fietsers met o.a. **Moniek, Michiel, Roel, Hendryk-Jan, Misha** en **Pepijn**. De Amstel gold rit bleek een ware afvalrace met onafgebroken regen, vergeten voorwielen en niet nader te noemen personen die na de eerste heuvel alweer huiswaarts keerden. Verder bestond de gevestigde orde uit **Nina, Gladys, Pien, Maurits, Arno, Ahmet, Wynand, Paul, Sebastiaan, Ahmet, Henk, Guus, Matthijs** en is er inmiddels alweer een nieuwe lichting met **Yve, Klaske, Eva, Beau, Ruben** en **Soufiane**. De groep van onderzoekers is altijd hecht gebleken met ontelbare kopjes koffie, verjaardagstaarten, Basket biertjes, huisfeestjes, de Hut spareribs,

congresreizen en als klap de vuurpijl het jaarlijkse “wintersymposium”. Houdt dit in stand! Ten slotte wil ik de student-onderzoekers Caitlin en Natalia bedanken voor hun inzet en eindeloze lijntje-streepje MRI analyses.

Met het opgroeien in de achterhoek hadden mijn jeugdvrienden **Jesse, Jelle, Ties, Reinoud** en ik één ding gemeen: alles wat op benzine loopt is mooi! Dit resulteerde in een crossbaan door het bos met uiteenlopend materieel variërend van omgebouwde crossbrommers tot opgevoerde grasmaaitrekker en de legendarische crossauto. Later werden dit levensgevaarlijke supersportmotoren, off-the-road ritten en snelle vierwielers. Onaangepast gedrag wordt nog steeds voortgezet in de vorm van carbit schieten op oudejaarsdag en weekendjes Nürburgring. Daarnaast zijn er de middelbare school vrienden **Moniek, Marleen, Erik, Eddie, Karel** en **Matthijs** met wie we nog altijd jaarlijks samenkomen. Ik denk niet dat we voorbeeldige scholieren waren maar het is toch nog goed gekomen met iedereen. Dan alle dispuutsgenoten van het H.D. FURIOSUS met mijn jaargenoten **Maarten, Rens, Hugo, Etienne,** en daarboven **Jan, Chris, Johan, Ben** en **Frederick**. Toen ik vanuit de achterhoek naar Amsterdam kwam was ik wat wereldvreemd maar daar hebben jullie mij in korte tijd overheen geholpen. De avonturen die wij hebben beleeft zouden nog wel eens schadelijk kunnen zijn voor een ieders carrière en zal ik derhalve hier niet noemen. Ik vond het prachtig dat jullie zijn komen skiën in Chamonix! Tevens wil ik de jongerejaars noemen o.a. **Lucas, Rogier, Ralph, Melle, Jan, Bart, Erwin, Ralph, Coen, Rafael, Bas, Lodewijk** (et cetera). Ten slotte een speciale vermelding voor onze huisvriendin **Evelien**, jij komt al sinds jaar en dag met enige regelmaat over de vloer en hebt met veel belangstelling het hele proces rondom dit proefschrift gevolgd.

Dan volgt nu een eervolle vermelding van mijn paranimfen **Johan Lim** en **Stefan Biesbroek**. Johan, als dispuutsgenoot en mede geneeskunde-student hadden we veel gemeenschappelijke delers en we konden direct goed met elkaar overweg. Tijdens ons bestuurs-jaar “Puur Bestuur” hebben we vele mooie ervaringen gedeeld waar we later met veel plezier op terug kunnen kijken (wat mij betreft staat de deal om naar hetzelfde bejaardentehuis te gaan nog steeds). Het leven als promovendus is jou ook niet vreemd en ik hoop dat je binnenkort je eigen onderzoek binnen de Neurologie mag afronden. Stefan we hebben elkaar al

leren kennen toen we nog student waren tijdens de wetenschappelijke stage. Onze promotie-tijd heeft veel overlap gekend en in de tijd dat we op dezelfde kamer zaten hebben we als mannelijke bondgenoten weerstand geboden tegen dreigende vrouwelijke overheersende invloeden. Ook buiten werktijd hebben we tijd doorgebracht op de racefiets en met dubbelen op de tennisbaan (waarbij na verloop van tijd de bal alleen nog maar heen en weer ging tussen Lotte en Mathilde). Het is een eer dat jullie beiden mij zullen bijstaan!

Lieve **pap en mam**, dankzij jullie liefdevolle zorgen kijk ik terug op een fijne jeugd. Het was heerlijk om buitenaf op te groeien en zoveel tijd door te brengen met 'buiten spelen'. De verre vakanties naar Zuid-Frankrijk met overbeladen caravan (voldoende aardappels mee) zijn mij dierbaar. Als oudste kind was de opvoeding vast niet altijd gemakkelijk maar jullie hebben mij altijd gestimuleerd om me verder te ontwikkelen (ook als hier een half jaar huisarrest voor nodig was). **Winand** jij hebt bepaald geen gemakkelijke jeugd gehad maar op keiharde doorzettingsvermogen heb jij al zoveel beperkingen overwonnen. Ik ben trots dat je het zo ver hebt weten te schoppen! **Maikel** jij bent altijd de jongste van het stel geweest maar inmiddels heb jij ook een grote-mensen baan binnen de IT en een vriendin. Ik vond het leuk om uitstapjes te maken zoals driften in Lelystad en jullie jaarlijkse bezoekje aan Amsterdam. **Opa's en oma's** (opa Zweerink en oma Jannie still going strong) jullie kwamen altijd gezamenlijk op visite voor mijn verjaardag, dat zal ik niet vergeten. Dank voor alle vijf-guldens!

Dan rest nu nog de belangrijkste persoon in mijn leven, Mathilde. De laatste woorden in dit dankwoord zijn voor jou, maar niet nadat ik mijn schoonfamilie(s) heb genoemd. **Petra en Jan**, jullie hebben mij ontzettend hartelijk ontvangen en meegenomen op verre reizen. Nog altijd mag ik het voorgerecht bij kerst bepalen (Gravlax graag!). Als huis/kader-arts hebben jullie veel interesse getoond in mijn onderzoek en dikwijls namen jullie uitgeknipte artikelen mee. **Martin en Elke**, jullie hebben mij ook bijzonder welkom geheten. Ondanks jullie drukke bestaan aan het hoofd van het familiebedrijf zien wij elkaar altijd op vaste momenten. De organisatie rondom kerstavond in Knokke neemt grootse (lees: André Rieu - achtige) vormen aan. Martin wij delen de passie voor auto's, veel dank dat wij op de m535i mogen passen! Dan zus en (half)broers. **Hielkje en Tom**, jullie nemen regelmatig cadeaus voor ons mee maar hetmooiste cadeau is toch wel

de kleine **Isolde** zijn die onze harten heeft gestolen (voorheen had ik niet veel met kinderen). Zij heeft sinds kort te duchten van kleine zus **Fië**. Dan **Anton,** met jou valt altijd wel iets te beleven. Veel succes met je avontuur in Korea en zorg dat je **Deborah** binnenboord houdt (she is a catch!). **Mathieu en Axelle**, wij kijken erg uit naar jullie trouw in de Florence! **Mikhaël en Charlotte**, jullie vormen ook een prachtig stel. Tot snel!

Dan volgt nu toch echt het slotpleidooi. **Lieve Mathilde**, na tien jaar weten we inmiddels wel wat we aan elkaar hebben. We kunnen op elkaar rekenen, als alles goed gaat maar ook als het even tegenzit. Toen ik je voor het eerst zag was je een stralende verschijning en daarna ben ik hopeloos gevallen voor je mooie pure karakter. Je hebt mijn promotietijd van het begin tot het einde meegemaakt en bent inmiddels zelf in staat om het linkerbundeltakblok te herkennen. Je hebt mij in die tijd altijd gesteund hoewel dit heus niet altijd gemakkelijk was. Samen zijn we ons avontuur in Frankrijk aangegaan en ik geniet nog iedere dag van jou en **Sammie** in onze berghut. Mathilde, ik zeg het misschien niet vaak maar ik houd van jou.

Appendix III

Curriculum Vitae



Alwin Zweerink was born on March 24th 1988 in Steenderen, the Netherlands. After finishing pre-university education, he left the region “Achterhoek” and moved to Amsterdam to study medicine (Vrije Universiteit, Amsterdam). During his study he joined a student’s fraternity where he was a board member for one year (H.D. FURIOSUS) and where he met Mathilde Verbrugge who soon became his girlfriend. Early clinical internships sparked a special interest in Cardiology and the topic of his research internship became hemodynamics in Cardiac Resynchronization Therapy (VU University Medical Center). After graduation he started his clinical career as a resident at the cardiology department of the Northwest Clinics, Alkmaar. Subsequently, research on the topic of Cardiac Resynchronization Therapy was continued in the form of a PhD course under supervision of dr. C.P. Allaart, prof. dr. R. Nijveldt (co-promotors) and prof. dr. A.C. van Rossum (promotor) which resulted in this thesis. The year after he worked as a resident at the cardiology department of the Amsterdam University Medical Centers, location VU University Medical Center. Currently he is working as a research fellow on the topic of His Bundle Pacing at the University Hospital of Geneva under supervision of professor Burri. After one year he will return to Amsterdam to start the Speciality Training Program in Cardiology.

Appendix IV

List of Publications

- **Zweerink A,** Friedman DJ, Klem I, van de Ven PM, Vink C, Biesbroek PS, Hansen SM, Kim RJ, van Rossum AC, Atwater BD, Allaart CP and Nijveldt R. Septal Mechanics by Segment Length in Cine (SLICE) Strain Analysis Predicts Clinical Outcome After Cardiac Resynchronization Therapy. *Submitted.*
- **Zweerink A**, Nijveldt R, Braams NJ, Maass AH, Vernooy K, de Lange FJ, Meine M, Geelhoed B, Rienstra M, van Gelder IC, Vos MA, van Rossum AC and Allaart CP. Segment Length in Cine (SLICE) Strain Analysis: a Practical Approach to Estimate Potential Benefit from Cardiac Resynchronization Therapy. *Submitted.*
- **Zweerink A**, Allaart CP and Burri H. Shifting Diastolic Filling from Right to Left in Non-Obstructive Hypertrophic Cardiomyopathy: Exploring New Indications for Biventricular Pacing. *European Journal of Heart Failure. 2020.*
- Becker MAJ, Allaart CP, **Zweerink A**, Cornel JH, van de Ven PM, van Rossum AC and Germans T. Correlation between septal midwall late gadolinium enhancement on CMR and conduction delay on ECG in patients with nonischemic dilated cardiomyopathy. *International Journal of Cardiology Heart&Vasculature. 2020.*
- **Zweerink A**, Hopman LHGA and Allaart CP. Efficiency is key. *Eur Heart J Cardiovasc Imaging. 2020;21:154-156.*
- **Zweerink A**, Salden OAE, van Everdingen WM, de Roest GJ, van de Ven PM, Cramer MJ, Doevendans PA, van Rossum AC, Vernooy K, Prinzen FW, Meine M and Allaart CP. Hemodynamic Optimization in Cardiac Resynchronization Therapy. *JACC: Clinical Electrophysiology. 2019;5:1013-1025.*

- van Everdingen WM, **Zweerink A**, Salden OAE, Cramer MJ, Doevendans PA, van Rossum AC, Prinzen FW, Vernooy K, Allaart CP and Meine M. Atrioventricular optimization in cardiac resynchronization therapy with quadripolar leads: should we optimize every pacing configuration including multi-point pacing? *Europace. 2019;21:e11-e19.*
- Parbhudayal RY, Guclu A, **Zweerink A**, Biesbroek PS, Croisille P, Clarysse P, Michels M, Stooker W, Vonk ABA, van der Ven PM, van Rossum AC, van der Velden J and Nijveldt R. Myocardial adaptation after surgical therapy differs for aortic valve stenosis and hypertrophic obstructive cardiomyopathy. *Int J Cardiovasc Imaging. 2019;35:1089-1100.*
- **Zweerink A**, van Everdingen WM, Nijveldt R, Salden OAE, Meine M, Maass AH, Vernooy K, de Lange FJ, Vos MA, Croisille P, Clarysse P, Geelhoed B, Rienstra M, van Gelder IC, van Rossum AC, Cramer MJ and Allaart CP. Strain imaging to predict response to cardiac resynchronization therapy: a systematic comparison of strain parameters using multiple imaging techniques. *ESC Heart Fail. 2018;5:1130-1140.*
- van Everdingen WM, **Zweerink A**, Salden OAE, Cramer MJ, Doevendans PA, Engels EB, van Rossum AC, Prinzen FW, Vernooy K, Allaart CP and Meine M. Pressure-Volume Loop Analysis of Multipoint Pacing With a Quadripolar Left Ventricular Lead in Cardiac Resynchronization Therapy. *JACC Clin Electrophysiol. 2018;4:881-889.*
- Biesbroek PS, Hirsch A, **Zweerink A**, van de Ven PM, Beek AM, Groenink M, Windhausen F, Planken RN, van Rossum AC and Nijveldt R. Additional diagnostic value of CMR to the European Society of Cardiology (ESC) position statement criteria in a large clinical population of patients with suspected myocarditis. *Eur Heart J Cardiovasc Imaging. 2018;19:1397-1407.*
- **Zweerink A**, van der Lingen ACJ, Handoko ML, van Rossum AC and Allaart CP. Chronotropic Incompetence in Chronic Heart Failure. *Circ Heart Fail. 2018;11:e004969.*

- van Everdingen WM, **Zweerink A**, Nijveldt R, Salden OAE, Meine M, Maass AH, Vernooy K, De Lange FJ, van Rossum AC, Croisille P, Clarysse P, Geelhoed B, Rienstra M, Van Gelder IC, Vos MA, Allaart CP and Cramer MJ. Comparison of strain imaging techniques in CRT candidates: CMR tagging, CMR feature tracking and speckle tracking echocardiography. *Int J Cardiovasc Imaging. 2018;34:443-456.*
- Bhagirath P, **Zweerink A**, Allaart CP and Gotte M. Imaging for cardiac resynchronisation therapy requires cardiac magnetic resonance. *Neth Heart J. 2018;26:640.*
- **Zweerink A**, Friedman DJ, Klem I, van de Ven PM, Vink C, Biesbroek PS, Hansen SM, Emerek K, Kim RJ, van Rossum AC, Atwater BD, Nijveldt R and Allaart CP. Size Matters: Normalization of QRS Duration to Left Ventricular Dimension Improves Prediction of Long-Term Cardiac Resynchronization Therapy Outcome. *Circ Arrhythm Electrophysiol. 2018;11:e006767.*
- Amier RP, Smulders MW, van der Flier WM, Bekkers S, **Zweerink A**, Allaart CP, Demirkiran A, Roos ST, Teunissen PFA, Appelman Y, van Royen N, Kim RJ, van Rossum AC and Nijveldt R. Long-Term Prognostic Implications of Previous Silent Myocardial Infarction in Patients Presenting With Acute Myocardial Infarction. *JACC Cardiovasc Imaging. 2018;11:1773-1781.*
- van Everdingen WM, **Zweerink A**, Cramer MJ, Doevendans PA, Nguyen UC, van Rossum AC, Prinzen FW, Vernooy K, Allaart CP and Meine M. Can We Use the Intrinsic Left Ventricular Delay (QLV) to Optimize the Pacing Configuration for Cardiac Resynchronization Therapy With a Quadripolar Left Ventricular Lead? *Circ Arrhythm Electrophysiol. 2018;11:e005912.*
- **Zweerink A**, Wu L, de Roest GJ, Nijveldt R, de Cock CC, van Rossum AC and Allaart CP. Improved patient selection for cardiac resynchronization therapy by normalization of QRS duration to left ventricular dimension. *Europace. 2017;19:1508-1513.*
- **Zweerink A**, Leusveld E, Allaart CP and Kemme MJ. Unexpected rhythm regularity in a patient with atrial fibrillation and a changing frontal plane axis over time. *Neth Heart J. 2017;25:278-279; 282-285.*

- **Zweerink A**, Allaart CP, Kuijer JPA, Wu L, Beek AM, van de Ven PM, Meine M, Croisille P, Clarysse P, van Rossum AC and Nijveldt R. Strain analysis in CRT candidates using the novel segment length in cine (SLICE) post-processing technique on standard CMR cine images. *Eur Radiol. 2017;27:5158-5168.*
- **Zweerink A**, de Roest GJ, Wu L, Nijveldt R, de Cock CC, van Rossum AC and Allaart CP. Prediction of Acute Response to Cardiac Resynchronization Therapy by Means of the Misbalance in Regional Left Ventricular Myocardial Work. *J Card Fail. 2016;22:133-42.*